Western Graduate&PostdoctoralStudies

Western University
Scholarship@Western

Electronic Thesis and Dissertation Repository

8-1-2014 12:00 AM

Synthesis, Properties, and Applications of Carboxylic Acid Functionalized Polyisobutylene

Inderpreet Sran
The University of Western Ontario

Supervisor
Dr. Elizabeth Gillies
The University of Western Ontario

Graduate Program in Chemical and Biochemical Engineering
A thesis submitted in partial fulfillment of the requirements for the degree in Master of Engineering Science
© Inderpreet Sran 2014

Follow this and additional works at: https://ir.lib.uwo.ca/etd

 Part of the Polymer Science Commons

Recommended Citation

Sran, Inderpreet, "Synthesis, Properties, and Applications of Carboxylic Acid Functionalized Polyisobutylene" (2014). *Electronic Thesis and Dissertation Repository*. 2412.
https://ir.lib.uwo.ca/etd/2412

This Dissertation/Thesis is brought to you for free and open access by Scholarship@Western. It has been accepted for inclusion in Electronic Thesis and Dissertation Repository by an authorized administrator of Scholarship@Western. For more information, please contact wlswadmin@uwo.ca.

SYNTHESIS, PROPERTIES, AND APPLICATIONS OF CARBOXYLIC ACID FUNCTIONALIZED POLYISOBUTYLENE

(Thesis format: Integrated Article)

by

Inderpreet Sran

Graduate Program in Chemical and Biochemical Engineering

A thesis submitted in partial fulfillment
of the requirements for the degree of
Master of Engineering Science

The School of Graduate and Postdoctoral Studies
The University of Western Ontario
London, Ontario, Canada

© Inderpreet Sran, 2014

Abstract

Polyisobutylene (PIB) and its copolymers are used in a wide range of commercial products owing to their high chemical stability, impermeability, elasticity, and biocompatibility. In this thesis, linear and arborescent PIB containing small percentages of isoprene (IP) were functionalized to provide epoxide, allylic alcohol, and carboxylic acid derivatives of PIB. These carboxylic acid derivatives were subsequently used to conjugate the antiproliferative agent paclitaxel (PTX) for investigation as a potential vascular stent coating. The PTX release rates were compared with those of physical mixtures of PTX with carboxylic-acid-functionalized PIB and with the triblock copolymer PS-*b*-PIB-*b*-PS. Covalent conjugation led to significantly slower drug release. AFM imaging of films of the materials suggested that the physical mixtures exhibited multiple domains at the surface, while the materials in which PTX was covalently conjugated appeared very uniform. Coatings of the conjugated materials on a stainless steel surface suffered less surface degradation than the physically mixed materials, remained intact, and adhered well to the surface throughout the thirty-five day study. Tensile testing and rheological studies showed that the incorporation of carboxylic acids or PTX into the polymer introduced significant changes to PIB's mechanical and rheological properties. Cytotoxicity assays showed that the coatings did not release toxic levels of PTX or other species into a cell culture medium over a 24 hour period, yet the levels of PTX in the materials were sufficient to prevent C2C12 cells from adhering to and proliferating on them. Overall, these results suggest that covalent PIB-PTX conjugates have promise as coatings for vascular stents.

Keywords

Polyisobutylene, paclitaxel, arborescent, isoprene, drug release, stent coating, tensile testing, rheological study,

Co-Authorship statement

The work described in this thesis contains contributions from the author as well as coworkers from Western, LANXESS Inc. and supervisor Dr. Elizabeth Gillies. The exact contributions to each project are described below.

Chapter 1 was written by the author and was edited by supervisor Dr. Gillies.

The work described in Chapter 2 was collaboration between the author and other members of the Gillies group and LANXESS Inc. Initial experimental work corresponding to the synthesis of polymers was carried out by Matthew McEachran. The author was responsible for scaling up of the synthesis and for tensile testing under the supervision of Dr. Gillies. Measurements of the rheological properties were performed by the author under the supervision of Dr. John R. de Bruyn. The adhesion experiments were carried out by Brianna Binder from LANXESS Inc. Dr. John F. Trant, a postdoctoral fellow under the supervision of Dr. Gillies provided general assistant in the laboratory and in the analysis of the results. The manuscript draft was also written collaboratively with the author preparing a draft of the sections on tensile testing and rheology and Matthew McEachran preparing the section on the synthesis. The manuscript was edited by Dr. Trant, Dr. de Bruyn, and Dr. Gillies.

Chapter 3 was collaboration between the author and other members of the Gillies group and LANXESS Inc. The synthetic method was initially developed by Matthew McEachran but all of the experimental work corresponding to the synthesis and preparation of the polymeric surfaces described in this chapter were carried out by the author under the supervision and guidance of Dr. Gillies.. Dr. John F. Trant, a postdoctoral fellow under the supervision of Dr. Gillies provided general assistance in the laboratory and with the interpretation of the results. HPLC measurements and cell studies were performed with the help of the Gillies group's lab technician, Aneta Borecki. Dr. Heng-Yong Nie assisted the author with AFM measurements. A draft of a manuscript was written collaboratively by the author and Dr. Trant and was edited by Dr. Gillies and Dr. de Bruyn.

For Chapter 4, all the described synthesis, film preparation, and characterization work was performed by the author under the supervision of Dr. Gillies. Dr. John F. Trant, a postdoctoral fellow under the supervision of Dr. Gillies provided general assistant in the laboratory and in the interpretation of the results. HPLC measurements and cell studies were performed with the help of the Gillies lab technician, Aneta Borecki. A draft of a manuscript was written by the author and Dr. Trant and was edited by Dr. Gillies and Dr. de Bruyn.

Table of Contents

Table of Tables

Table of Schemes

Table of Figures

List of Abbreviations

AFM	atomic force microscopy
Arb	arborescent
BMS	bare metal stents
d	doublet
DES	drug eluting stent
DMAP	4-dimethylaminopyridine
DSC	differential scanning calorimetry
FDA	food and drug administration
HPLC	high performance liquid chromatography
IB	isobutylene
IP	isoprene
IR	infrared spectroscopy
m	multiplet
m-CPBA	meta-chloroperoxybenzoic acid
MeCl	methyl chloride
M_n	number average molecular weight
MW	molecular weight
M_w	weight average molecular weight
NMR	nuclear magnetic resonance
PDI	polydispersity index

PEG	poly(ethylene glycol)
PIB	poly(isobutylene)
PMMA	poly(methyl methacrylate)
PS	polystyrene
PTX	paclitaxel
RB	butyl rubber/ poly(isobutylene-co-isoprene)
ROP	ring-opening polymerization
s	singlet
SIBS	poly(styrene-*b*-isobutylene-*b*-styrene)
tBMA	*tert*-butyl methacrylate
Tg	glass transition temperature
TGA	thermal gravimetric analysis
THF	tetrahydrofuran
UV	ultraviolet
wt%	weight percentage

Chapter 1

1 Introduction

1.1 General Introduction

Biomaterials are a vast and continuously evolving field that encompasses the enhancement and extension of life through materials. There are many different classifications of biomaterials, however a common theme is the use of materials to enhance or substitute function within a biological system. Biomaterials are used widely in a variety of applications, including cardiovascular, dental and neural implants, orthopaedic prosthetics and drug delivery systems. Biomaterials can be both medical and non-medical and they can be natural or synthetic. For clarity, biomaterials can be separated into two sub-categories, which are not mutually exclusive - structural and functional biomaterials. Examples of structural biomaterials include glass eyes and artificial limbs. Their purpose is to provide structural support without interacting with the biological system. Functional biomaterials on the other hand interact with the biological system to replace or enhance biological function; examples of functional biomaterials are artificial organs, pacemakers and controlled release implants. Most biomaterials are still being optimized to tackle some common issues, including improved biocompatibility, mechanical properties and degradation. These issues are critical to the enhancement and development of biomaterials for explicit applications. Thus this thesis will look at improvement of a one such potential biomaterial. Specifically, linear butyl rubber and arborescent polyisobutylene (PIB) will be fictionalized with carboxylic acid moieties and paclitaxel (PTX). The resultant changes in the physical properties of these polymers will be examined via tensile and rheological experiment. A release and preliminary biological study of these polymers will be carried out to evaluate the potential application of these polymers for stent coating.

1.2 Butyl rubber

1.2.1 Historical development of butyl rubber

Butyl rubber (RB) is a synthetic copolymer with unique physical and chemical properties. RB is a copolymer of isobutylene (IB) and a small amount of isoprene (IP). The IP units are added to provide an olefinic handle for cross-linking, most commonly performed using sulfur. The cross-linking improves mechanical properties as well as abrasion resistance. RB has numerous attractive properties including low permeability to air, gases and moisture, excellent aging, thermal and chemical stability, resistance to ultraviolet (UV) degradation, oxidation and ozone, electrical insulation properties, good adhesion to other types of rubber and biocompatibility.[1, 2]

PIB was first polymerized in 1873, but had a low molecular weight (MW). I. G. Farben was subsequently able to synthesize a higher MW PIB by decreasing the polymerization temperature in 1931.[3] Their process used boron trifluoride as a catalyst at -75 °C. In 1937 William Joseph Sparks and Robert McKee Thomas of Standard Oil and Development Company (Exxon) were able to synthesize poly(isobutylene-*co*-isoprene), commonly referred to as RB. They first used 1,3-butadiene as the co-monomer but found that 2-methyl-1,3-butadiene (isoprene, IP) was a better co-monomer. RB became more prominent in World War II due to the shortage in the supply of natural rubber. The desire to make PIB into a rubbery copolymer with low functionality, resulted in the production of a low-modulus vulcanized networks that resisted ozonolysis and oxidation.[4] Furthermore, due to its oxidative, enzymatic and hydrolytic resistance, it is also biocompatible for long-term applications.[10]

1.2.2 Synthesis of butyl rubber

RB is currently synthesized by cationic polymerization of isobutylene (IB) (2-methylpropene) and IP at -78°C in methyl chloride (MeCl) (Scheme 1.1). High purity monomers are required for this process. They are purified via flashing and stripping. The polymerization is performed using a Lewis acid catalyst system (co-initiator and initiator). Some common Lewis acid co-initiators include alkylaluminum dichloride, tin tetrachloride, aluminum trichloride, titanium tetrachloride and boron trifluoride. Typical initiators include hydrochloric acid, organic acids, and Brønsted acids such as water. Alkyl halides can also be used. The polymerization is initiated by reacting IB with a Lewis acid to produce a carbenium ion (Scheme 1.2). The polymerization is

propagated by the addition of IB and IP to the carbenium ions. This reaction is highly exothermic, thus it can be manipulated by decreasing the temperature. The rate of propagation is limited by diffusion and can be tuned by manipulating temperature, solvent polarity and the presence of counterions, and has been determined to be around 108 L/(mol*s). The polymers propagate until chain transfer or termination occurs.[6, 7] The polymerization of IB and IP occurs head-to-tail resulting in a predominantly 1,4-addition (90-95%) . Chemical analysis has shown little evidence for the presence of 1, 2 and 3, 4 modes of entry.[8] The amount of IP can be tuned from 0.5% to 7.0%. The IP is distributed randomly throughout RB, due to the low percentage and similar reactivity ratios between IP and IB.[3]

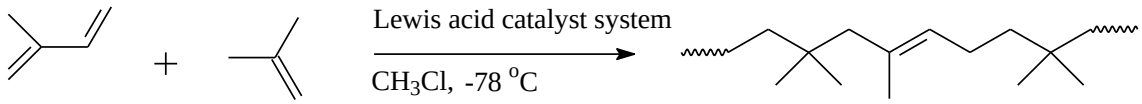

Scheme 1.1. General scheme for the cationic polymerization of butyl rubber

Initiation

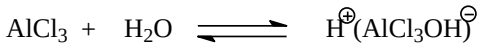

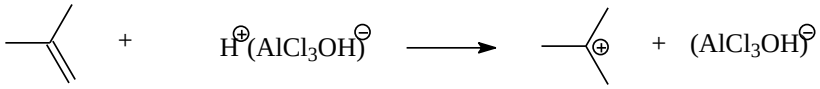

Propagation

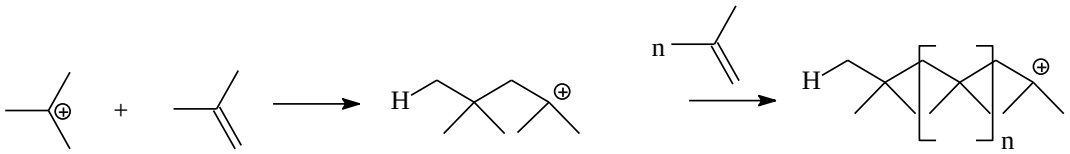

Termination and Chain Transfer

Chain Transfer

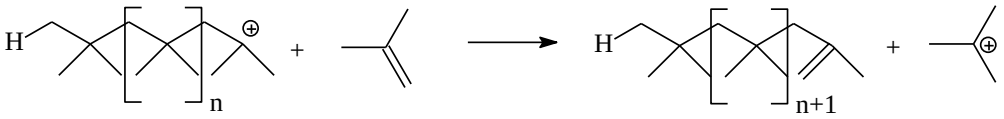

Chain Termination via "proton abstraction"

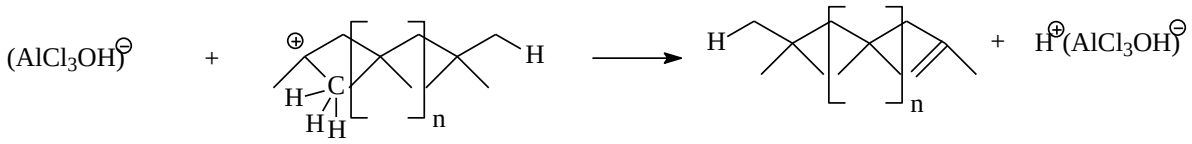

Scheme 1.2. Cationic polymerization of RB showing initiation, propagation and termination steps.

Chain transfer occurs when a monomer abstracts a proton from the growing polymer chain. The polymer chain is subsequently terminated and the monomeric carbocation propagates a new chain. The chain transfer can also occur with solvent, another polymer chain or impurities. The MW of the polymer is strongly influenced by the temperature of the polymerization because the activation energy of the chain transfer is higher than for propagation. This issue is more prominent in the synthesis of RB containing higher IP content. By increasing the IP percentage, lower MW copolymers are observed due to the co-monomer's affinity to chain transfer.[4] Chain termination occurs by unimolecular rearrangement of the ion pair, where the 2nd last carbon of the chain releases a proton and forms a terminal alkene bond. Chain termination can also happen

through formation of stable allylic carbenium ions or via carbocation reaction with nucleophilic species like amines or alcohols. The control of the termination step is important because it allows for production of RB with various MWs and which is capable of further modification.

1.2.3 Chemical and physical properties

RB exhibits high hydrolytic, oxidative and enzymatic resistance .[1,3,10] The saturated segments of PIB impart RB with physical properties including low permeability to both gases and liquids, thermal stability, weathering, chemical and moisture resistance as well as vibration damping.[13] RB has a T_g of about -65 °C.[15] Some important physical properties of RB are summarized in Table 1.1.

Table 1.1. Physical properties of RB.[19]

Property	Value
Density (g/cm^3)	0.917
Glass Transition, T_g (°C)	-75 to -67
Heat Capacity, C_p (kJ/kgK)[b]	1.95
Refractive Index, n_p	1.5081

RB and its derivatives are readily soluble in nonpolar solvents. Owing to the hydrophobic nature of RB, it has excellent stability, especially to UV degradation and oxidation. However RB can be degraded by atmospheric ozone over extended periods of time. This can be prevented by the introduction of antioxidants.[14] RB has shown air retention within tires to be at least 8 times better than that of natural rubber.[11] This is attributed to the efficient intermolecular packing resulting in relatively high density and low permeability to small molecule diffusants such as N_2, CO_2, He, H_2, and O_2.[16-18] Table 1.2 compares the diffusivity of several gases in RB and natural rubber.

Table 1.2.1.2 Diffusivity of gases in butyl rubber and natural rubber at 25 °C.

Gas	Diffusivity (cm^2/s) x 10^6	
	Butyl Rubber	**Natural Rubber**
N_2	0.045	1.1
CO_2	0.058	1.1
O_2	0.081	1.6
H_2	1.52	10.2
He	5.93	21.6

1.2.4 Properties and biomedical applications of polyisobutylene and butyl rubber

The favorable properties of PIB-based materials allow them to be used in diverse array of products such as automobile tires, sporting equipment, adhesive sealants, viscosity modifiers, chewing gum, and drug eluting stents.[1,2] The major use of PIB-based materials is in the automotive industry, involving tires (tire innerliner, innertubes) and other automotive parts (sidewalls and hosing).[12-14, 19] PIB based materials have also been used in pharmaceutical applications such as RB-stoppers and have been approved by the food and drug administration (FDA) for chewing gum because of their biological inertness.[11] The excellent biocompatibility of PIB-based material makes them ideal for other biomedical applications as well. For example, PIB-based materials are being investigated as corneal shunts for the treatment of glaucoma,[20] as well as in synthetic aortic valves.[21] There has also been some research showing PIB-poly(methyl methacrylate) (PMMA) composites have good properties relative to commercial bone cements, because of the incorporation of the elastomeric PIB into the glassy PMMA material.[23, 24] However, there were limitations in this application because of void formation throughout the material. This led to inconsistencies in the material itself, rendering it unsuitable for clinical use in bone cements. Multi-arm copolymers of PIB-cyanoacrylates have been reported as promising materials for intervertebral disk replacement.[25, 26]

In the Taxus™ vascular stent, a linear triblock copolymer of polystyrene (PS)-PIB-PS (SIBS) is used in the drug-eluting coating.[10, 28] The PS blocks impart thermoplastic properties to the rubber, allowing it to behave as a cross-linked rubber at physiological temperature and also making it readily processable at higher temperatures or in solution. Moreover, copolymers of PIB and hydrophilic polymers for example poly(*N*,*N*-dimethylacrylamide) or poly(ethylene

glycol) (PEG) have been used to develop membranes that can encapsulate cells while allowing the exchange of oxygen, nutrients, and secreted proteins such as insulin across the membrane.[5] PEG incorporation into RB materials is also of interest because of PEG's characteristic nature to exhibit protein resistance.[29] PIB-PEG copolymers could therefore be used to protect against biofouling.[4] There are also many other examples involving the functionalization of PIB for its incorporation into polymer networks[31-34] as well as linear,[35-39] star,[40-42] miktoarm,[43-45] and graft copolymers. [45-51] With these systems, interesting functions such as stimuli-responsive network swelling, [31, 33] templating of inorganic materials,[35,45] cell encapsulation,[5] controlled drug release,[52] and protein patterning and resistance[45,46] have been achieved.

1.3 Arborescent polyisobutylene

1.3.1 Historical development of arborescent polyisobutylene

The development of several new living polymerization techniques during recent decades has provided the opportunity to make a wide variety of branched polymers. These include dendritic (hyperbranched and arborescent) structures, [53, 54] star-like structures, [55] graft copolymers, [56] and others. There has been significant interest in branched polymers due their significantly lower viscosity and less shear sensitivity than their linear counterparts.[58] Dendritic structures have shown a great deal of potential, because of their spherical symmetry comprising a central core surrounded by a regular branching pattern.[59] Monodisperse dendritic polymers (dendrimers) were first synthesized by Fritz Vögtle in 1978 using the divergent approach.[65] Since their first synthesis, many other groups including Denkewalter, Tomalia, Newkome, and Fréchet have worked in this area, developing divergent and convergent strategies for their synthesis.[60,61] Dendrimers have very narrow molecular weight distributions and have a controlled and symmetric structure. However dendrimers have a major drawback, which is their complicated and time-consuming synthesis process.

Hyperbranched polymers are another class of branched polymers that have less symmetrical architectures and lower branching frequencies. The history of hyperbranched polymers can be dated back to the end of 19th century, when Berzelius described the formation of a resin from tartaric acid and glycerol. In 1901 Smith reported the reaction between phthalic

anhydride or phthalic acid and glycerol to prepare a polymer.[62] In the 1940s Flory outlined an route that relied on "one-pot polycondensation" to synthesize hyperbranched polymers.[63] The one pot polycondensation is simple compared to dendrimer synthesis, however the reaction time is often very long (10-100 h). In the 1990s, Fréchet[57, 64, 65] developed a novel approach for the synthesis of hyperbranched polymers called "Self-Condensing Vinyl Polymerization" (SCVP). This method allowed for the synthesis of hyperbranched structures using "inimers". The inimers have the features of both a monomer and an initiator. In SCVP the initiator component of the inimer reacts with the monomer component of another inimer, forming a dimerthat has two active sites. (Scheme 1.3)

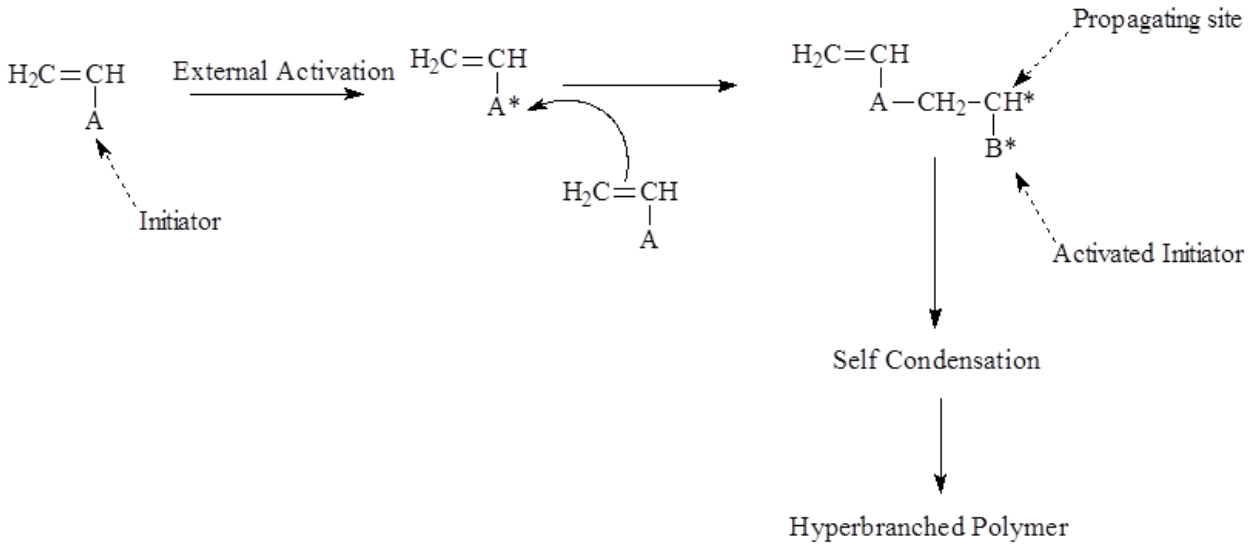

Scheme 1.3. Self-condensing vinyl polymerization

Arborescent polymers combine the features of both dendrimers and hyperbranched polymers, with longer polymer chains between the branching points. The concept of arborescent polymers dates back to 1991, where two papers were published almost simultaneous by Gauthier[76] on arborescent polymers and Tomalia[61] on comb-burst polymers. These syntheses relied on grafting onto procedures, where side chains were synthesized separately and then reacted with substrates bearing suitable coupling sites. Since then, high MW arborescent polystyrenes and polyisoprenes have been prepared by this method, but this synthetic route is rather time-consuming and difficult. In 1996 Puskas and coworkers developed an alternative and commercially feasible method using a small quantity of an inimer copolymerized with an

olefin.[65-67] In 1998 Puskas and coworkers were able to synthesize high MW arborescent polyisobutylene (arb-PIB) (Figure 1.1) in a one-pot living-type polymerization process using 4-(2-hydroxyisopropy)styrene or 4-(2-methoxyisopropyl)styrene as the inimer.[69, 70] This living polymerization requires that the chain transfer side reactions and irreversible termination should be absent. Another requirement is that the initiating and propagating sites on the inimer have comparable reactivity. In 2008 the same group was able to develop high MW arborescent polymers comprising a PIB core and an outer shell composed of IB and IP, *p*-methyl styrene or cyclopentadiene.[71]

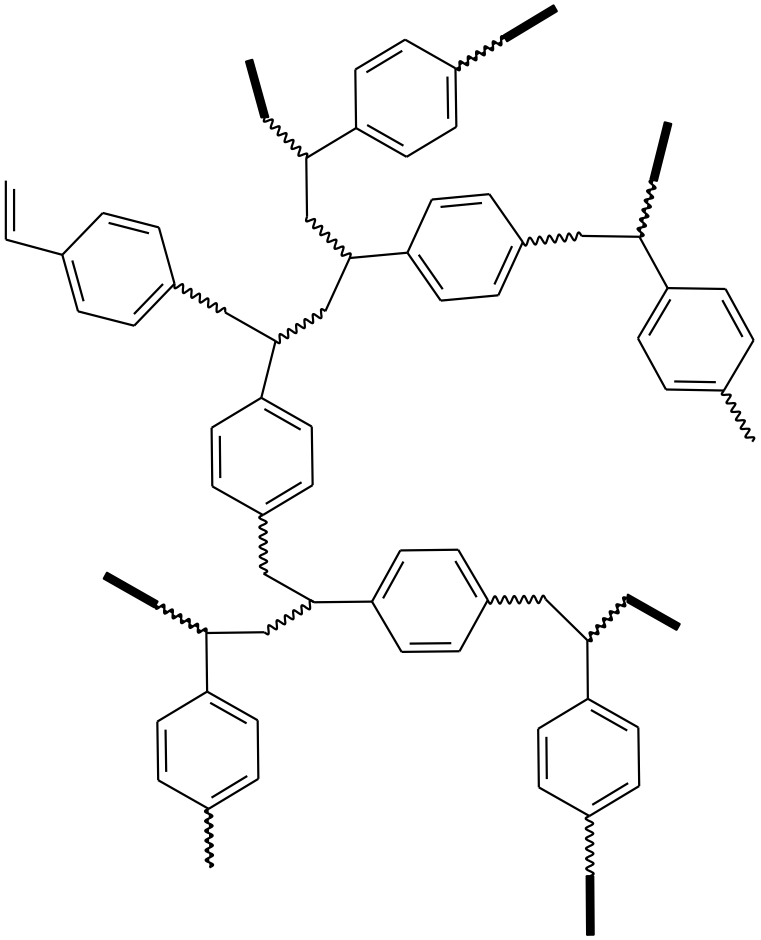

Figure 1.1. Cartoon of arb-PIB prepared using the 4-(2-methoxy-isopropyl)styrene inimer.

1.3.2 Synthesis of arborescent polyisobutylene and its copolymers

Arb-PIBs with outer blocks are prepared by first polymerizing IB in the presence of the inimer and then adding the next monomer to complete the polymerization. For example, Scheme 1.4 shows the polymerization of arb-PIB-*co*-IP. The core was synthesized by living carbocationic

polymerization of IB using 4-(2-methoxy-isopropyl)styrene as the inimer and $TiCl_4$ as the initiator.[69] The polymerization was carried out at -95 ^oC in methylcyclohexane (MeCHx) and MeCl at 60/40 vol/vol. The reaction order was determined to be close to one. The IP was added to this mixture after complete conversion of IB. To improve the incorporation *N*, *N*-dimethylacetamide (DMA) was also added. The polymerization was terminated by addition of NaOH in methanol.

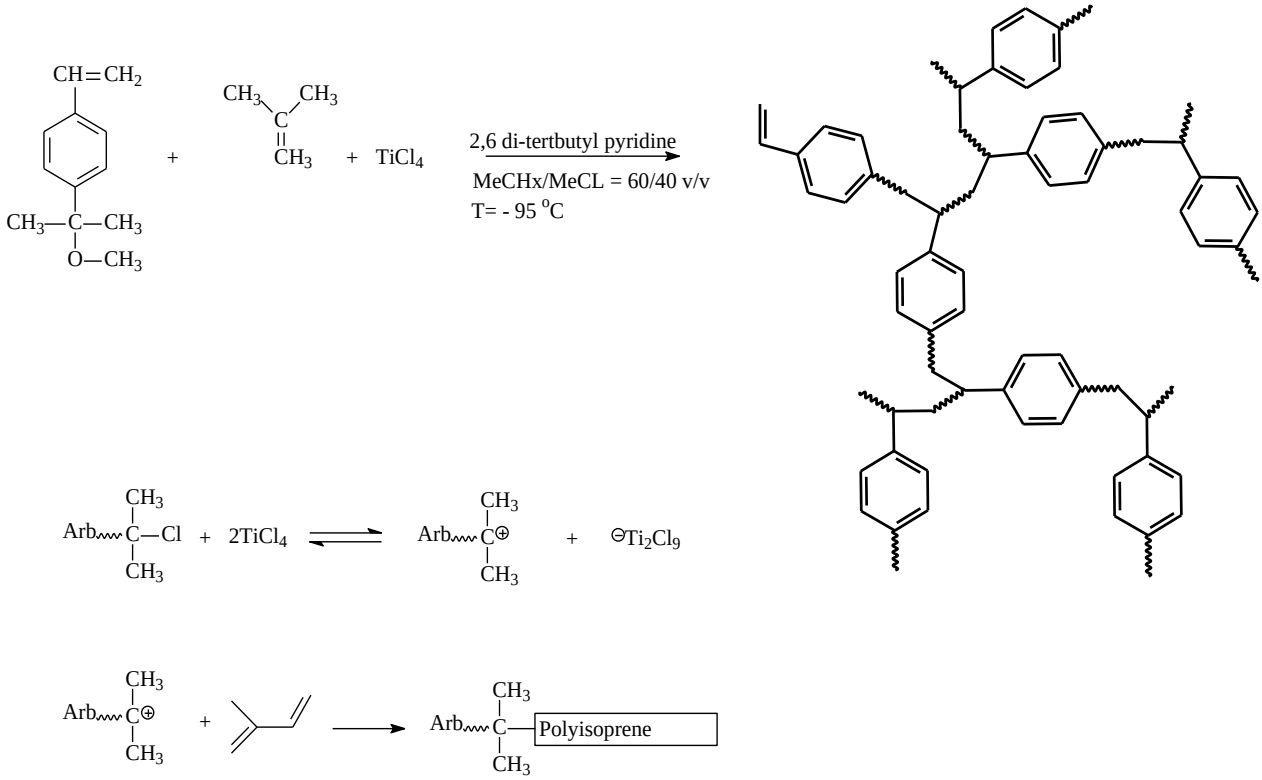

Scheme 1.4. Cationic polymerization of arborescent polyisobutylene

1.3.3 Properties of arborescent polyisobutylene

The initial studies have shown many possibilities for arb-PIB materials becoming an excellent substitute to the linear SIBS material in biomedical applications like stent coating.[73] Also arb-PIBs have better combinations of properties such as improved fatigue life and lower creep in comparison to the linear counterparts. This is due to a "double network" structure with a covalently branched core embedded into a self-assembling thermolabile network.[71,74] Arb-PIB typically retains the properties of its linear counterparts including good thermal, environmental

and chemical resistance, coupled with processability, excellent barrier properties, and outstanding biostability and biocompatibility.[72,75] The arb-PIB-*co*-IP with terminal IP-rich sequences exhibits thermoplastic elastomer properties unlike RB.[53] The Gillies group has recently prepared arb-PIB grafted with PEG chains and compared them with the linear PIB-PEG graft copolymers.[68] It was found that the arborescent materials exhibited similar resistance to protein adsorption as the linear analogues when cast as films, but different tensile properties and self-assembly behaviour in aqueous solution and in the solid state. Overall, this work reinforces the importance in polymer architecture in imparting specific properties to materials.

1.4 Vascular stents

Cardiovascular diseases (heart disease) have been one of the major causes of death in modern society. Cardiovascular diseases are a class of diseases caused by disorder of the heart and the blood vessels. The causes of cardiovascular diseases are diverse but atherosclerosis and hypertension are the most common. The atherosclerosis process includes a number of problems that result in the thickening of artery walls. It can be caused by the accumulation of lipid deposition and lipid-laden macrophages in atherosclerotic plaques. The rupture of these plaques is the prime reason behind arterial thrombosis, the changes in the artery wall that interfere with the blood flow and increase the chance of heart attack.[77] Thrombosis is the formation of a blood clot in the artery which blocks the flow of the blood in the vessel. It occurs because of an immune system response involving platelets and fibrin which form a blood clot to prevent blood loss. This can result in too much clotting which can reduce the blood flow to a tissue causing hypoxia. In turn, this can result in accumulation of lactic acid in the oxygen-deprived tissue. The clot can also break free, resulting in the formation of a embolus, which is capable of clogging arterial capillary beds at a site distant from its origin. The use of vascular stents to treat these conditions has been one of the most effective and rapidly adopted medical interventions. The vascular stents are made of small expandable tubes which are mounted onto a balloon catheter and inserted into the narrow section of the vessel and then expanded. (Figure 1.2) A vascular stent acts as a stabilizing framework for the blood vessel and thus maintains its patency (a non-obstructed state).[78] Initially, only balloon inflations were used to reduce coronary lesions but this only served as a temporary solution.[79] The rates of restenosis were very high after balloon

angioplasty because of recoil effect of the vessels and constrictive remodeling. Restenosis is re-narrowing of the blood vessel leading to restricted blood flow. It occurs after angioplasty or insertion of a stent as new tissue grows inside the stent, covering the struts of the stent. These new tissue consists of healthy cells from the lining of the arterial wall. This is a favorable effect because development of normal lining over the stent allows blood to flow smoothly over the stented area without clotting. However, scar tissue may later form underneath the new healthy lining. The growth of these scar tissues underneath the lining of the artery may cause the artery to be become narrow, thus obstructing blood flow. Restenosis is typically seen 3 to 6 months after the insertion of stent.[82]

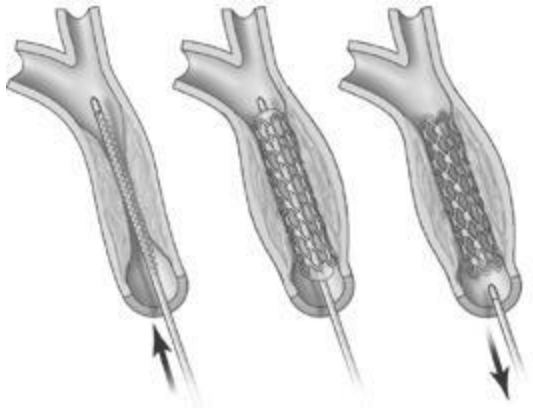

Figure 1.2. Implantation of a stent into blood vessel[80]

In 1987, Sigwart[81] adopted intravascular stents to combat this problem; the stent was able to reduce the recoil phenomenon at both acute and chronic levels. This first generation of stent was named the bare metal stent (BMS). However there have been numerous reports suggesting that the BMS causes unavoidable vessel damage due to the pathological biological cascade, which causes thickening of the blood vessel (Figure 1.3b).[82] The late luminal damage restricts the lasting effectiveness of the BMS, potentially leading to thrombosis and blood clotting. The restenosis rates for the BMS are between 20 to 40%, which is an improvement from 40 to 60% for arteries not stented.[83] These rates are very reliant on the patient and their current/previous medical conditions such as diabetes. There are currently dozens of BMS available in the market and they are usually made of 316L stainless steel (316L SS), cobalt-chromium (Co-Cr) alloy or

titanium and its alloy (e.g. Nitinol). 316L stainless steel is the most common used metal for stents.[84]

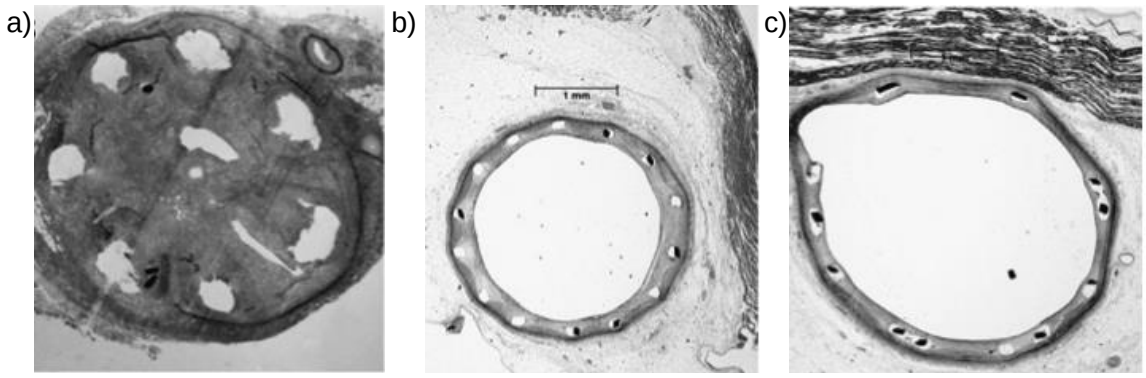

Figure 1.3. Cross-sectional images of porcine coronary arteries with stent explants, a) a poly(carbonate urethane)-coated stent exhibiting substantial inflammation and proliferation (2 months), b) a bare metal stent at 3 months showing some restenosis and c) poly(styrene)-co-poly(isobutylene)-co-poly(styrene) (SIBS)-coated stent at 180 days showing resilience[84].

The development of the drug eluting stent (DES) is considered to be the most successful improvement to stents in the history of their development. It uses polymers containing drugs coated on metal stents to help with the treatment of cardiovascular diseases.[85] The DES provides mechanical support to the artery and also inhibits in-stent restenosis response as well as early thrombosis by means of pharmacotherapy (Figure 1.3c). A decade of clinical use of the first generation DES has shown overwhelming support of its benefits over BMS counterparts [85, 86]. The first generation of DES that received regulatory approval from both European Union Conformiteé Européenne (CE) and FDA are Cypher™ (Cordis, Warren, New Jersey, USA) and Taxus™ (Boston Scientific, Natick, Massachusetts, USA). The Cypher™ is made of 316L SS platform and has a coating of poly(ethelene-*co*-vinyl acetate) and poly(*n*-butyl methacrylate) carrying sirolimus[87]. The Taxus™ also uses a 316L SS substrate, but it has a single layer of SIBS coating containing 1 μg/mm^2 paclitaxel (PTX).[88] Even though the first generation of DES represent a marked improvement over the BMS, there are still concerns. Restenosis has still been observed, along with poor re-endothelialization,[89] delayed healing[89] and tissue growth[90] behind the polymeric film, causing thrombosis. While the cause of these phenomena are still not fully understood, multiple factors including toxic effects from the entrapped drug and/or an acute or delayed hypersensitivity reaction from the polymer and/or drug could be involved.[85] The second

generation of DES incudes Endeavor^{TM} (Medtronic vascular, Santa Rosa, CA, USA) and Xience V^{TM} (Abbott Vascular, CA, USA)[91]The substrate for these stents is Co-Cr. Endeavor has a coating of zotarolimus and an anti-fouling phospholipid-based copolymer,[92] while Xience V has a coating of poly(*n*-butyl methacrylate) and poly(vinylidenefluoro-*co*-hexafluoropropylene) acting as an intermediate layer and drug carrier layer respectively.[93] There is no convincing evidence that the 2nd generation of DES are superior to 1st, as the problems like restenosis and impaired endothelial healing are still being reported for these devices. However the Co-Cr substrate in the 2nd generation DES is more flexible with higher radial strength allowing for thinner strut design than stainless steel 316L SS [94].

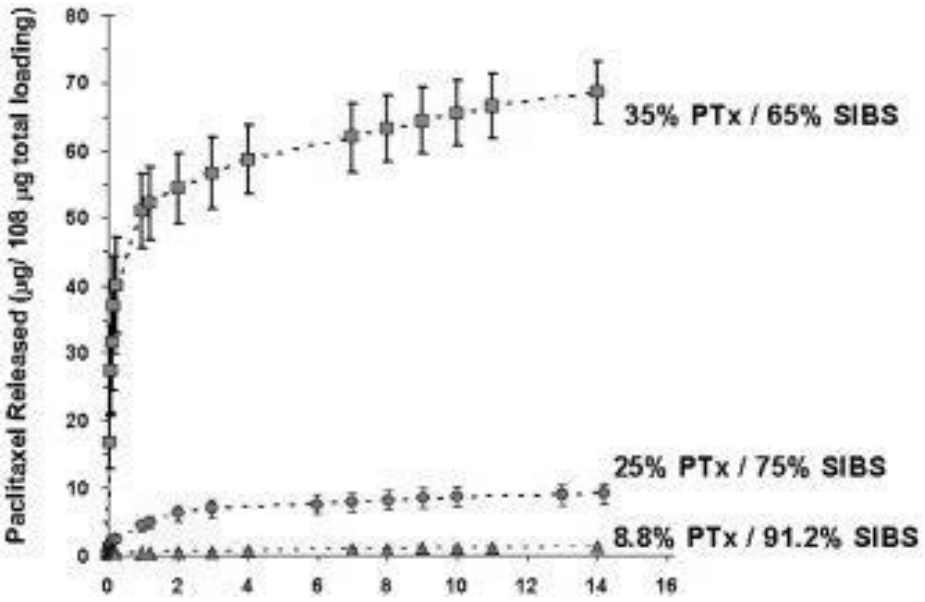

Figure 1.4. Drug release profile via control of wt % of drug to polymer.[99]

The polymers used for DES are known to be durable, but they are limited by low adhesion to the metal, which can result in delamination of the polymers from the substrate, causing thrombosis.[95, 96] These polymers have also been shown to exhibit erratic release profiles.[97, 98] The DES drug release profiles have been studied extensively and the release of the drug can be controlled to some degree, by using different weight percentages [99] (wt. %) of drugs and modifications of the carrier. [100, 101] The release profile of SIBS and PTX has been tuned by

changing the wt. % of the mixture (Figure 1.4). [99] The release rate of PTX can be increased by the addition of more hydrophilicity, by using of poly(styrene-*co*-maleic anhydride) (SMA) as part of the polymer mixture. [101] There has also been research done on using biodegradable stents (BDS), which can be prepared from both polymers (e.g., poly(lactic acid), poly(glycolic acid), polycaprolactone) and metals (Mg-based or Fe-based alloys).[102] The BDS are designed to temporarily support the artery for about 3-6 months.[85] The polymer most commonly used in biodegradable stents is poly(L-lactic acid) (PLLA), which is metabolized into lactic acid, carbon dioxide and water.[103] Metals with low toxicity like pure magnesium, iron and their alloys can be applied in designs of BDS.[104] The BDS have several advantages but also have several limitations. For example, ester hydrolysis can cleave random sites and will result in a burst release of drug. In addition, accumulated acidity caused by the degradation can lead to local chronic inflammation and hypersensitivity. Once the polymer has been degraded, the substrate can have the same problem as BMS. Moreover these biodegradable polymers do not have the ideal mechanical properties needed for the constant wear *in vivo*[107] and have similar rates of restenosis as DES.[105, 106] The limitation with using a biodegradable metallic stent made of Mg or its alloys is that Mg corrodes into soluble $Mg(OH)_2$, $MgCl_2$ and H_2 at a fast rate.[108] The released Mg ions, together with the formation of hydrogen bubbles will increase local pH values, which again can cause chronic inflammatory reactions and blood disorders.[109, 110] Also the metal-based BMS becomes thinner during the process of corrosion, resulting in the loss of strength of the scaffolding. The BMS made of pure Fe and its alloys are still under evaluation concerning the biocompatibility and toxicity of the degradable products.[111, 112]

The DES has three major components - the drug, polymer, and scaffold. The two drugs approved for clinical use are sirolimus and PTX. These drugs have very different mechanisms of action, but yield a similar result of inhibition of cell proliferation. Sirolimus (rapamycin) is a natural macrocyclic, lipophilic lactone with immunosuppressive activity. Sirolimus was first isolated in 1970's from bacteria Streptomyces hygroscopicus found in soil samples from the Easter Islands. [113] It has excellent antimicrobial, antifungal and immunosuppressive properties, and is also used to prevent rejection in organ transplantation. Sirolimus binds to a specific class of cytosolic proteins called FK binding protein 12 (FKBP12), which results in inhibition of regulatory signal transduction kinase.[114-116] On the other hand, PTX inhibits cell proliferation by stabilizing microtubules. It interferes with the normal breakdown of microtubules during cell

division. PTX has shown a remarkable reduction in neointimal hyperplasia in animal studies, thus leading to its use in DES.[118, 119]

The development of DES is multi-faceted and complicated in terms of polymer and drug selection, every decision can change the way the stent affects the therapeutics of the DES. The current approaches of optimizing the DES are focused on preparing new platforms, new coatings and new techniques of elution.[120] There has been far more focus on methods used to combine drug and stent. For example, the use of different drug loading methods can influence the release kinetics and stent-blood interface.[121] The current commercial DES has disadvantages such as delamination and burst release, but these problems can be fixed through optimization. Therefore it should be possible to capitalize on the excellent mechanical properties of the DES.

1.5 Paclitaxel

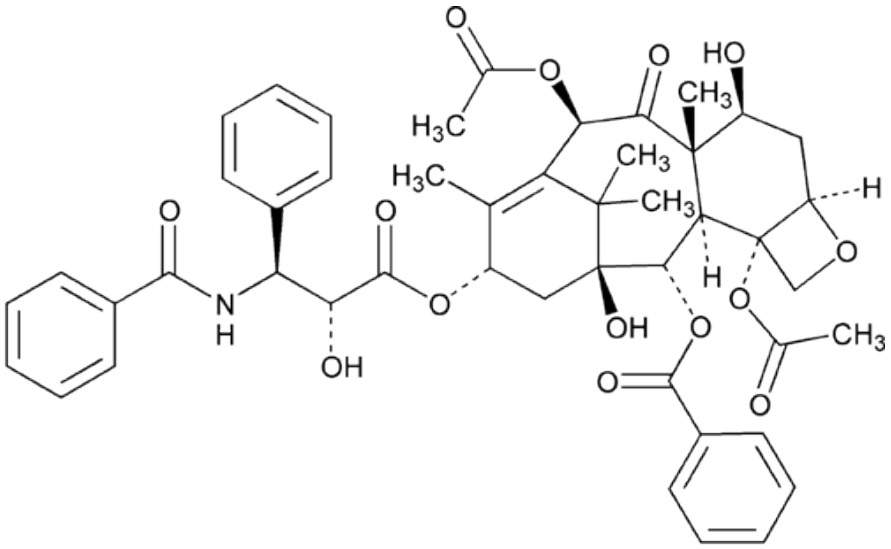

Figure 1.5. Structure of paclitaxel

PTX (Figure 1.5) is one of the most effective chemotherapy drugs used to inhibit cell division. It is used in the treatment of a broad range of cancers including lung, ovarian, and breast cancer.[122] PTX is also used to prevent restenosis, which is the recurrence of abnormal narrowing of an artery or valve after corrective surgery. First isolated in 1967 by Wall and Wani from the bark of *Taxus brevifolia* while working at Research Triangle Institute, it was named as Taxol. It was discovered later that entophytic fungi living in the bark synthesize PTX.[123] PTX was first commercially developed by Bristol-Myers Squibb Company and sold under generic name of Paclitaxel with the trademark of Taxol. PTX is a crystalline powder with the empirical formula

of $C_{47}H_{51}NO_{14}$. It has a molecular weight of 853.9 g/mol and the melting point is about 216 ^{o}C.[123] PTX is very lipophilic, and therefore has very poor aqueous solubility (~0.4 μg/mL). PTX solubility is increased by using Cremophor EL (CrEL) (polyoxyethylated castor oil) as an excipient. However, CrEL is known to have many serious side effects, such as hypersensitivity reactions.[125] Extensive research is been done to find other ways of administrating PTX to mitigate these side effects. This research is largely based on using nanoparticle assisted chemotherapeutic drug delivery.[126-128] The use of nanoparticles for drug delivery has other advantages such as slower clearance and improvement of accuracy in target delivery.[124]

Paclitaxel targets tubulin. It has been observed that PTX treated cells have difficulty with cell division, spindle assembly and chromosome segregation.[123] PTX stabilizes and protects microtubules against disassembly. At higher doses it can block microtubule detachment from the centrosomes.[123] Because of its biological properties, PTX is also being used as an antiproliferative agent to prevent restenosis of coronary stents and is one of two drugs most commonly found in drug-eluting stents, the other being Sirolimus.

1.6 Evaluation of polymers

1.6.1 Physical characterization

1.6.1.1 Tensile testing

Tensile tests are among the most common mechanical tests that can be performed on materials. They are usually simple, relatively inexpensive and fully standardized, where the sample of specific material is exposed to controlled tension until failure. Tensile test results are very important in the selection of materials for any application. They show how a material will behave under force and are used to create stress (σ) versus strain (ε) curves of the material. Figure 1.6 shows stress versus strain curves for some typical polymeric materials. Tensile testing is used to provide information about the material's ultimate tensile strength (UTS),[129] Figure 1.7 Shows some important parameters gotten from a stress versus strain curve.

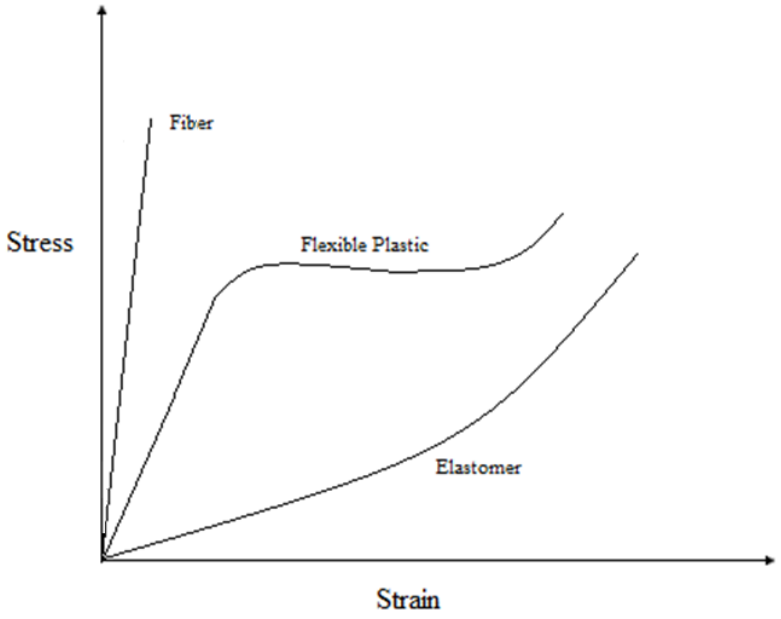

Figure 1.6. Stress – strain plot for typical polymeric materials.

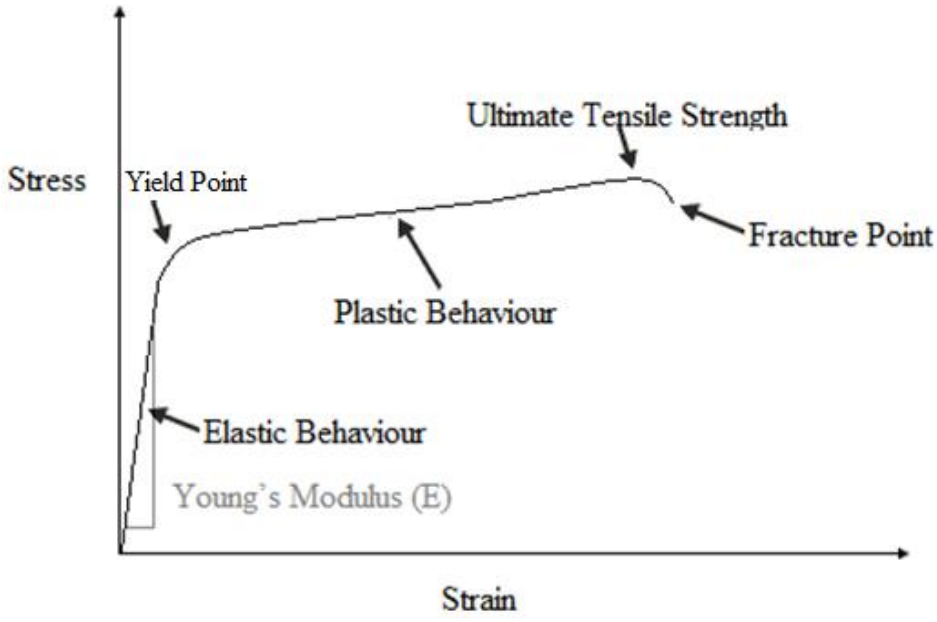

Figure 1.7. A stress – strain curve showing important parameters.

A universal testing machine is the most common type of testing machine used for tensile tests. It uses two self-aligning grips where the sample is positioned and secured. The alignment of the sample is crucial, because if there is misalignment either due to an angle or offset to one

side the sample will undergo a bending force. This can be very bad for a brittle material and dramatically skew the results, causing the initial potion of the stress-strain curve to be non-linear.[132] The samples for tensile testing are aligned with the direction of the pull and stretched uniaxally until failure (breakage) by slowly increasing the tensile load. Tensile testing machines need to stretch the sample at a constant rate while at the same time measuring the instantaneous applied load and resulting displacement. The load (F) and the displacement (Δ) are used to determine the stress (σ) and strain (ε) by using the initial cross-sectional area A_0 and length L_0 by the following equation.[129]

$$\sigma = \frac{F}{A_0} \qquad \varepsilon = \frac{\Delta}{L_0} = \frac{L - L_0}{L_0} \qquad 1$$

In the initial portions of the stress versus strain curve, most materials obey Hooke's law to reasonable approximation. Therefore, the relationship between stress versus strain is linear. The slope of this region is known as modulus of elasticity or Young's modulus (E).

$$E = \frac{\sigma}{\varepsilon} \qquad 2$$

The Young's modulus is the measurement of the stiffness or resistance to elastic deformation of the material. In this region the material behaves elastically and will return to its initial shape after the applied stress is removed. Stiffer materials exhibit higher Young's modulus.[129] Once the stress versus strain deviates from the straight-line relationship and Hooke's Law no longer applies, some permanent deformation will result in the material. This point is called the elastic or proportional limit (yield point) and the material will plastically deform upon any further increase in load.[131] The material will not return back to its initial shape under relaxed conditions (no load). However the elastic limit is not always well defined, so the yield strength is used. The yield strength is the stress required to produce a minor amount of plastic deformation.

In the plastic portion of the curve the material undergoes a rearrangement of its internal molecular or microscopic structure, wherein atoms are moved to new equilibrium positions.

The plasticity is the result of molecular mobility of a material; However for crystalline materials it can result from dislocation motion.[133] Materials missing this mobility, for example by having internal microstructures which block dislocation motion, are usually brittle rather than ductile. This stress versus strain curve of brittle materials is usually linear over the full range of strain and terminates in fracture without noticeable plastic flow.[132] Another important point from the stress versus stain curve is the ultimate tensile strength (UTS). This is the maximum stress the material can sustain during the test. The UTS for brittle materials is at the end of the linear-elastic portion of the stress-strain curve or close to the elastic limit. However for ductile materials the UTS is typically in the plastic portion of the stress-strain curve. The UTS is the highest point in the stress vs stain curve.

A polymer usually follows Hooke's law at lower strain, therefore enabling the calculation of Young's modulus.[130] However, for many elastomers and semi-crystalline polymers, the linear portion of the curve is difficult to define. Because of this, moduli may be determined by secant or tangent methods. In the secant method the curve is bisected and the slope (E) is determined from the bisecting line.[131] In the tangent method the value of E is determined at any point in linear section of the curve. E for elastomers is normally very low, in the range of 0.5 – 1 MPa,[129] while semicrystalline polymers exhibit higher values for E and UTS. Elastomers usually have higher strain at yield point (yield strain) than other materials, in the range of 1 to 10.[132] The yield strain is important, because a larger yield strain corresponds to resistance to brittle fracture, which is very important for many biomedical applications.

The necking and drawing are important concepts in tensile testing. They show the behavior of the material and its fracturing. Necking occurs once the yield point is reached; there will be a site on the sample where the local stress is maximum, due to perhaps a nick or some other defect at the surface. The localized flow at this site cannot be compensated by further strain hardening, so the area at this site will be reduced.[129] This will increase the local stress even more and thus accelerate the flow further. This localized and increasing flow will lead to necking in the material. Before the necking, the deformation of a material is usually uniform throughout the specimen, but after necking all subsequent deformation happens in the neck.[135] The neck can become smaller and smaller until fracture. This is the fracturing process of most brittle

materials.[136] However in the ductile material, once the necking is formed it does not continue to shrink but stretches to a "natural draw ratio" which is a function of temperature and specimen processing. The drawing is observed after this ratio. Drawing occurs when the material at the neck shoulder is pulled down. Through the drawing process the neck propagates until it is the full length of the sample.[132] However not all polymers are able to withstand the drawing process and drawing will only happen when the necking process produces a strengthened microstructure whose breaking load is higher than the load needed to induce necking in the material just outside the neck area. Figure 1.8 shows the necking and drawing process of a polymer.

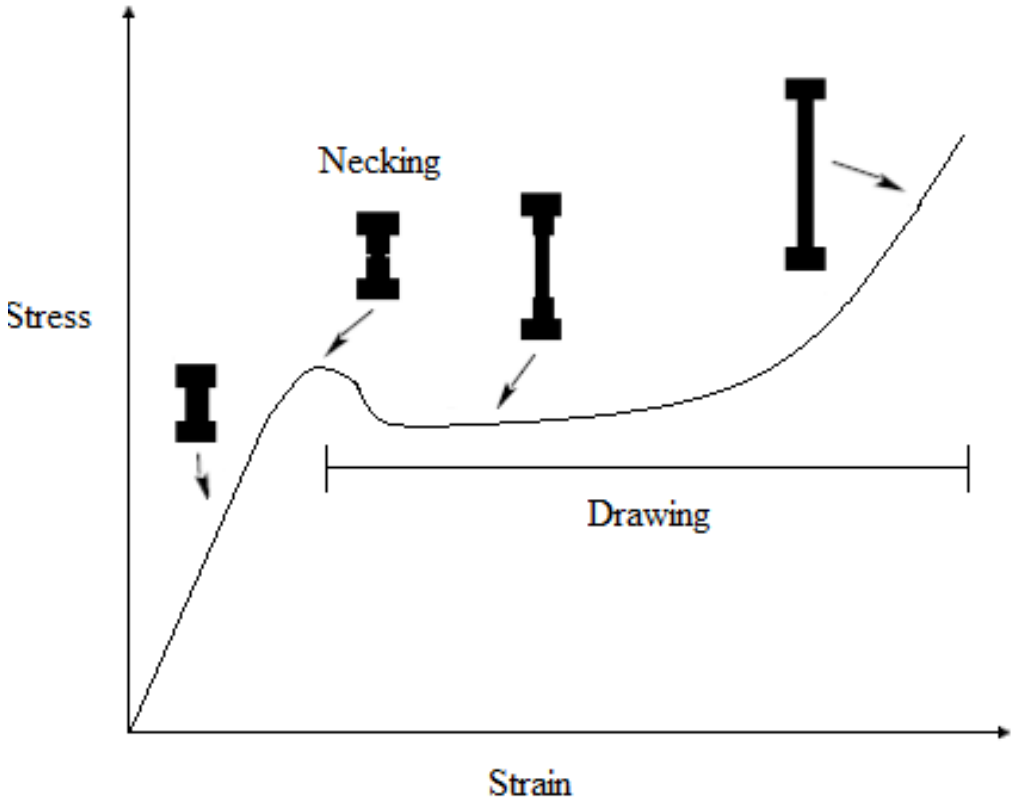

Figure 1.8. Necking and drawing

1.6.1.2 **Rheology**

Rheology is the study of the deformation and flow of a material. It is used to study the deformation of materials whose behaviour falls between solids and fluids (i.e., viscoelastic materials).[136] Rheological studies are used to determine the intrinsic properties of a material,

including its viscosity and elasticity. Viscosity (η) is the property of a fluids resistance to flow or deformation and is the relationship between shear rate and shear stress that causes the movement of a fluid (equation 5)[137]. Rheology functions on the principle that an external force exerted on a material will result in the particles undergoing displacement relative to each other. This displacement of the particles is known as strain. An ideally viscous material will undergo irreversible strain after an external anisotropic force is exerted on it. An ideally elastic material on the other hand will undergo elastic strain once an external anisotropic force is exerted on the sample. The energy needed for this strain is stored, and after the force is released an elastic material will spontaneously fully recover to its original form. There are only a small number of materials with any importance which show ideally viscous behaviour. Most materials are neither ideally viscous nor ideally elastic, but rather exhibit behaviour between these two ideal conditions.[138] These materials are called viscoelastic materials. Viscoelastic materials exhibit a time dependent elastic response. Once the force is removed, part of the deformation recovers instantly. More force is recovered with time and in some materials there will be a permanent deformation. Rheology was first coined in 1920 by Eugene Bingham a professor at Lehigh University.[134] Rheological studies can be utilized to analyze substances with complex microstructure, for example muds, sludge, suspensions, polymers, bodily fluids and other biological materials or other materials which belong to the class of soft matter.[140]

Rheology studies are performed using a rheometer. This instrument imposes a specific stress to the fluid, and monitors the resultant deformation. The rheometer has the ability to provide a steady shear rate that enables it to be used as a viscometer to measure steady shear or bulk viscosity.[135] It is also able to apply very small amounts of rotation or deformation in a dynamic or oscillatory fashion. This dynamic shear testing can be visualized as if the sample were being "vibrated" between parallel plates or concentric cylinders, as opposed to being sheared in a continuous fashion. The rheometer enables this "vibratory" measurement to be applied to a sample in a controlled fashion while also controlling the sample temperature.[142] There are number of typical sample testing geometries, the most common type being parallel plates (Figure 1.9A), cone and plate (Figure 1.9B), concentric cylinder (Figure 1.9C), and solid or torsion rectangular (Figure 1.9D).[139] The parallel plate geometry is more commonly used for elastomers while concentric cylinder is more commonly used for fluids.

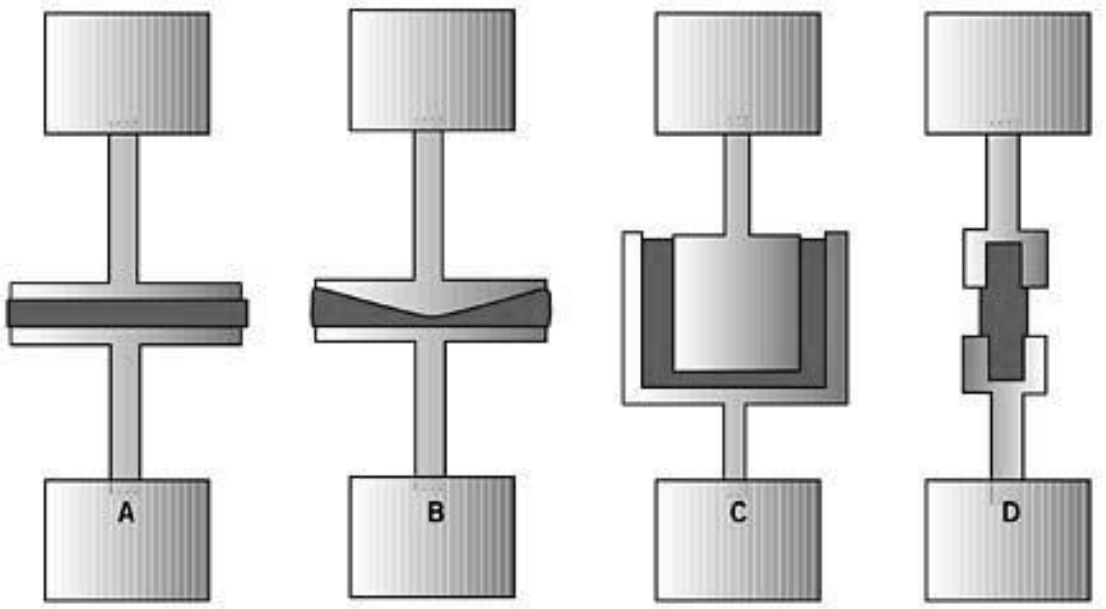

Figure 1.9. Common rheometer testing geometries: a) parallel plate, b) cone and plate c)concentric cylinder, d) solid or torsion rectangular.[139]

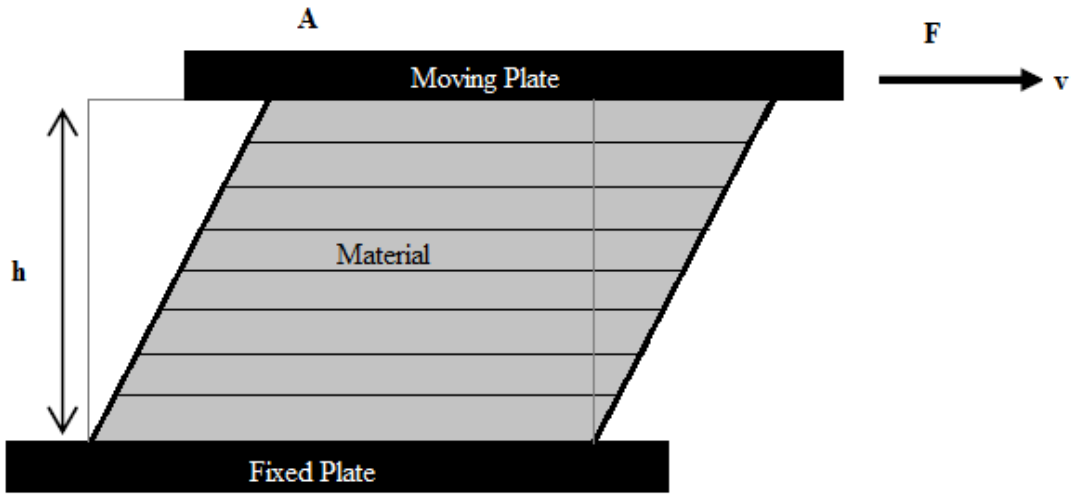

Figure 1.10. Illustration of the parallel plate model

In a typical measurement using the parallel plate configuration, the material is placed between two plates, a moving plate and a fixed plate (Figure 1.10). The top plate (moving plate) with a known surface area of A [m^2], is moved by force F [$N=kgm/s^2$] at the speed of v [m/s].

The bottom plate (fixed plate) will remain at rest and can be used to provide heat to the material. The height of the material is known as h [m].[138] The change in the position of the moving plate will result in the thinnest element of the material undergoing displacement between the plates. It is fundamentally important for rheological studies that displacement is laminar. If it is turbulent, the flow resistance will be increases, and material will show false rheological properties. The rheological properties that can be determined from this test are shear rate (D), shear stress (τ), viscosity (η) and strain (γ). Shear rate (equation 3) or the velocity gradient is the rate at which shear deformation occurs and it has the units of s^{-1}.[135]

$$D = \frac{v}{h} \qquad 3$$

Shear stress (equation 4) is a parallel-acting force, where two layers inside the fluid slide against each other. This is in contrast to compression (perpendicular-acting force), tension (stretching force), and torsion (twisting force). Shear stress has the units of Pascal.

$$\tau = \frac{F}{A} \qquad 4$$

Viscosity of a fluid is the ratio of the shear stress to shear rate. Viscosity has the units of Pascal-sec.

$$\eta = \frac{\tau}{D} \qquad 5$$

Strain is ratio of displacement and gap and thus is dimensionless.

$$\gamma = \frac{dx}{h} \qquad 6$$

Hooke's law is used to give the relationship between force and deformation. Hooke's law states that the force is proportional to deformation. The elastic modulus (G) is the constant of proportionality and it is an intrinsic property of a solid.

$$\tau = G\gamma \qquad 7$$

Rheological properties of viscoelastic materials can be determined by running a sinusoidal oscillations experiment. The basic principle of this experiment is to induce a

sinusoidal shear deformation into the material and measure the resultant stress response. The frequency of oscillation (ω) of the shear deformation is used to determine the time scale. In this experiment one plate is kept stationary (bottom plate) while the other plate (top plate) is rotated by motor, thus imposing a time dependent strain on the sample.

$$\gamma(t) = \gamma * \sin(\omega t) \qquad 8$$

The time dependent stress τ (t) is determined by measuring the torque imposed by the sample onto the rotating plate. The time dependent stress response at a single frequency reveals key differences between materials. Ideally an elastic material will exhibit stress in phase with the applied sinusoidal strain deformation. Therefore sample stress is proportional to the strain deformation, and the proportionality constant is the shear modulus of the material. However in an ideally viscous material, applied strain and the measured stress are out of phase, with a phase angle of $\alpha = \pi/2$. Again sample stress is proportional to the rate of strain deformation and proportionality constant for ideally viscous material is the viscosity of the fluid. Viscoelastic materials have a response that is both in-phase and out-of-phase. This response shows the solid like (in-phase) and liquid like (out-of-phase) behaviour of the material. The phase shift of α of viscoelastic materials lies between that of solids and liquids, $0 < \alpha < \pi/2$. The data for viscoelastic materials is analyzed by decomposing the stress wave into two waves of the same frequency, one in phase (sin ωt) with strain wave and one out of phase(cos ωt), described by equation 9

$$\tau = \tau' + \tau'' = \tau_0' \sin(\omega t) + \tau_0'' \cos(\omega t) \qquad 9$$

The viscoelastic behaviour of a material at ω can be characterized by the storage modulus (in-phase), G' (ω), and the loss modulus (out-of-phase), G'' (ω)

$$G' = \frac{\tau_0'}{\gamma_0}\text{, storage or elastic moduli} \qquad 10$$

$$G'' = \frac{\tau_0''}{\gamma_0}\text{, viscous or loss moduli} \qquad 11$$

Oscillatory experiments are typically performed to measure G'(ω) and G''(ω). These measurements are made as a function of ω, because these material properties are dependent on

the time scale over which it is deformed. Figure 1.11 shows a typical example of G'(ω) and G''(ω) plot.[140] Figure 1.11a displays a plot for hydrogel particles suspended in a liquid?. At low ω the response is viscous-like, where G" is larger than the G'. However at the higher ω the G' dominates the response, indicating solid-like behaviour. Figure 1.11b show the response of an elastomer which is dominated by a solid like behaviour over full range of available ω.

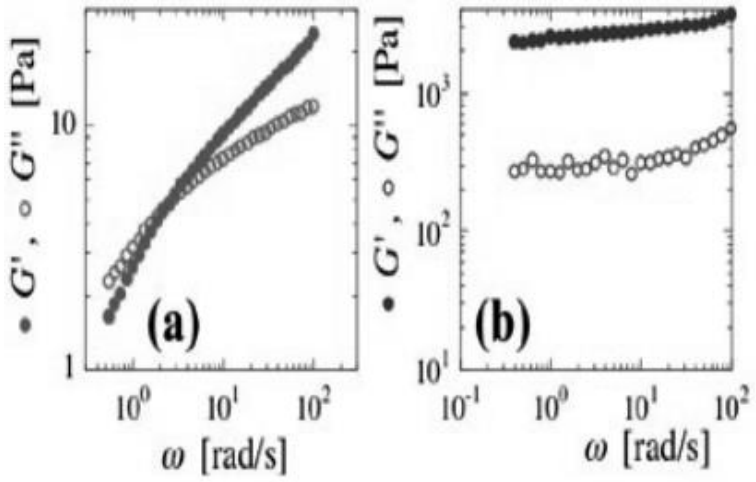

Figure 1.11. Frequency dependence of G' and G'' for (a) a suspension of hydrogel and (b) for the elastomer blend DC-9040 (Dow Corning), a typical additive in cosmetic and pharmaceutical formulations.[140]

Another important parameter from this test is the loss tangent, which is the ratio of viscous modulus over elastic modulus. It indicates the behaviour of viscoelastic material. A loss tangent less than one is indicative of a solid-like matrial, while higher than one indicates a more viscous material.

$$Loss\ tangent = \frac{G''}{G'} \qquad 12$$

Another experiment that can be done using the rheometer is the creep and recovery test. In the creep section of this experiment the stress is increased instantly from 0 to τ_0 and the strain is recorded against time. The material will react to this stress by deforming. In the recovery section of this experiment the stress is removed and the elastic response of the material is measured.

When creep and recovery tests are combined they enable the measurement of elasticity of the sample, because an elastic material will recoil and attempt to recover its original shape. In an ideal elastic material, as long as the stress is applied, a constant strain will be observed. 100 % of the strain energy is stored and once the stress is removed the material will display immediate recovery to original shape. In an ideal viscous material the constant stress will result in the strain increasing linearly over time. The input stress is used up for flowing process and once the stress is removed the strain obtained by the material will be maintained, thus there will be no recovery. The viscoelastic material will show characteristics of both elastic and viscous strain. A partial recovery by the elastic portion will be observed, but the portion of viscous strain will remain. Viscoelastic materials which exhibit complete recovery after sufficient time following removal of load are called *anelastic*.

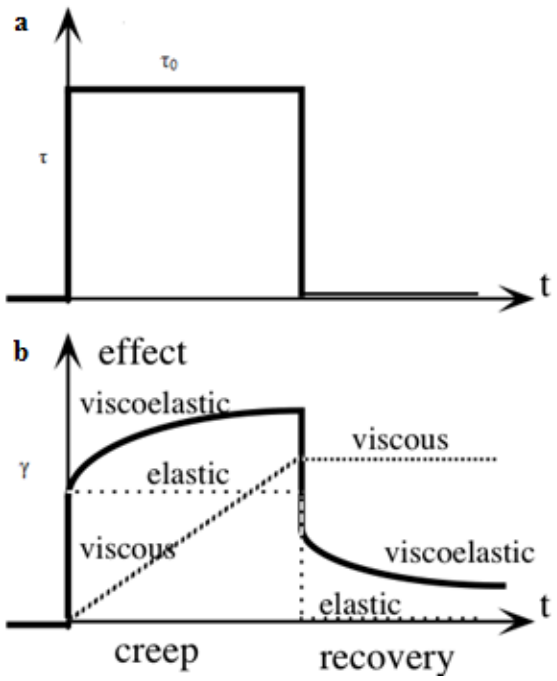

Figure 1.12. Creep and recovery a) stress applied to the polymer vs time, b) Resultant strain profile of the polymer.

Figure 1.12 shows an ideal creep and recovery of a material. The applied stress will lead to a spontaneous jump in strain, the strain rate will then decrease. During this time the macromolecules are reoriented and stretched. In the recovery phase two types of recoveries take

place, elastic and viscoelastic. The elastic recovery is the initial drop in strain. In the viscoelastic recovery stain is recovered over time. If the remaining strain is very small the material is called viscoelastic solid. If it is large, the material is considered as a viscoelastic liquid. Typically, creep and recovery data is expressed in term of compliance (J). Compliance is a material specific quantity and it measures the flexibility of a material. The greater the compliance the more a material can be strained under certain shear stress.

$$\gamma(t) = J(t) * \tau_0 \qquad 13$$

1.7 Motivation and Goals of Thesis

While much research has explored the optimization of RB and PIB for applications in the automobile industry, the promise of these polymers for biomedical applications has yet to be fulfilled. Due to the limited numbers of chemical functional groups on RB available for performing chemical reactions, the functionalization of these polymers has yet to be fully explored, especially in the areas of tuning their properties and functions for biomedical applications. In the area of DES, there are limitations to the current coating, including poor control over the drug release, and modest adhesion to the metal surface. The overall goal of this thesis was to develop new synthetic methods for functionalizing both linear RB and arb-PIB, especially with carboylic acid moieties, to study how these functional groups affect the physical properties of the rubber, and to apply them for the covalent conjugation of PTX to control its release. The physical properties of the materials will be examined, primarily by tensile and rheological experiments. A preliminary biological study of linear RB and arb-PIB will be carried out to look at the potential application of these polymers for stent coatings.

Chapter 2 describes the synthesis of carboxylic acid functionalized RB and studies of its properties. The starting material will be the allylic alcohol functionalized polymer previously developed in the Gillies group. Once the carboxylic acid functionalized RB is synthesized, its mechanical properties need to be examined and compared with RB and it derivatives. The mechanical properties will be examined by tensile testing and rheological studies. The introduction of chemical functionality, and in particular carboxylic acid moieties should improve the tensile properties, due to increasing number of electrostatic interactions and hydrogen

bonding. Additionally, RB containing lower (2.2) and higher (7) percent of IP will be compared to determine the effects of the density of pendant functional groups on the properties. It is hypothesized that the derivatives prepared from RB with higher IP containing should have better tensile and rheological properties due to the presence of more electrostatic and hydrogen bonding interactions.

Chapter 3 describes the synthesis and study of PTX functionalized linear RB for potential stent coating applications. The mechanical properties of the drug conjugate will be examined by tensile and rheological experiments and compared to carboxylic acid functionalized RBs and SIBS. It is hypothesized that the PTX functionalized RB should be more brittle then carboxylic acid functionalized RBs, due to introduction of crystallinity arising from the PTX. Additionally PTX release studies will be conducted to evaluate the effects of the covalent conjugation on the drug release rates. These materials will be compared with commercial SIBS. Also the toxicity and ability of films of these polymers to support the growth of cells will be evaluated.

Chapter 4 describes the application of the synthetic methods described in Chapters 2 and 3 to arb-PIB. The mechanical and rheological properties of the polymers are studied along with the drug release, film properties, and preliminary biological properties. The results will be compared to the SIBS and the linear analogues.

1.8 References

1. Puskas, J.; Chen, Y. *Biomacromolecules.* **2004**, *5*, 1141.
2. Puskas, J.; Chen, Y.; Dahman, Y.; Padavan, D. *Journal of Polymer Science Part A: Polymer Chemistry.* **2004**, *42*, 3091.
3. Morton, M.; Editor *Rubber Technology. 3rd Ed*; Van Nostrand Reinhold, **1987**.
4. American Chemical Society*; Advances in Chemistry Series*; American Chemical Society: Washington. **1962**, 34, 260.
5. Isayeva, I. S.; Kasibhatla, B. T.; Rosenthal, K. S.; Kennedy, J. P. *Biomaterials.* **2003**, *24*, 3483.
6. Roth, M.; Mayr, H. *Macromolecules.* **1996**, *29*, 6104.
7. Schlaad, H.; Kwon, Y.; Sipos, L.; Faust, R.; Charleux, B. *Macromolecules.* **2000**, *33*, 8225.
8. Cheng, D.; Gardner, I.; Wang, H.; Frederick, C.; Dekmezian, A.; Hous, P. *Rubber Chemistry & Technology.* **1990**, *63*, 265.
9. Thomas, M.; Sparks, W. J. *Synthetic Rubber*, Whitby, G. S. Ed., John Wiley & Sons,New York, **1963**.
10. Pinchuk, L.; Wilson, G. J.; Barry, J. J.; Schoephoersterd, R. T.; Parele, J. -M.;Kennedy, J. P. *Biomaterials.* **2008,** *29*, 448.
11. Wong, W. K. *Rubber World.* **2009**, *240*, 20.
12. Zhang, Y.; Chen, X.; Zhang, Y.; Zhang, Y. *Macromolecular Materials and Engineerin.* **2001**, *286*, 443.
13. Van Amerongen, G. J. *Journal of Applied Physics.* **1946**, *17*, 972.
14. Cadieux, P.; Watterson, J.; Denstedt, J.; Harbottle, R.; Puskas, J.; Howard, J.; Gan, B.; Reid, G. Colloids and Surfaces. **2003**, *28*, 95.
15. Rodgers, B. In *Rubber Compounding: Chemistry and Applications;* Marcel Dekker: New York, N.Y. **2004**, 645.
16. Pant, P.; Boyd, R. *Macromolecules.***1992**, *25*, 494.
17. Pant, P.; Boyd, R. *Macromolecules.***1993**, *26*, 679.
18. Boyd, R.; Pant, P. *Macromolecules.***1991**, *24*, 6325.
19. Mark, H. F.; Kroschwitz, J. I. In *Encyclopedia of Polymer Science and Engineering;* Wiley: New York.**1985**.

20. Acosta, A. C.; Espana, E. M.; Yamamoto, H.; Davis, S.; Pinchuk, L.; Weber, B. A.; Orozco, M.; Dubovy, S.; Fantes, F.; Parel, J. M. *Archives of Ophthalmology* **2006**, *124*, 1742.
21. Gallocher, S. L.; Aguirre, A. F.; Kasyanov, V.; Pinchuk, L.; Schoephoerster, R. T. *Journal of Biomedical Materials Research - Part B Applied Biomaterials* **2006**, *79*, 325.
22. Hopfenberg, H. B.; Stannett, V.; *Polymer Science and Technology*; Plenum Press: New York, **1974**, 6, 482.
23. Kennedy, J. P.; Richard, G. C. *Macromolecules.* **1993**, *26*, 567.
24. Kennedy, J. P.; Askew, M. J.; Richard, G. C. *Journal of Biomaterials Science. Polymer edition.* **1993**, *4*, 445.
25. Kennedy, J. P. *Macromolecular Symposia.* **2001**, *175*, 127.
26. Kennedy, J. P.; Midha, S.; Gadkari, A. *Journal of Macromolecular Science-Chemistry.* **1991**, *28*, 209.
27. Fonagy, T.; Ivan, B.; Szesztay, M. *Macromolecular Rapid Communications.* **1998**, *19*, 479.
28. Strickler, F.; Richard, R.; McFadden, S.; Lindquist, J.; Schwarz, M. C.; Faust, R.; Wilson, G. J.; Boden, M. *Journal of Biomedical Materials Research Part A.* **2010**, *92A*, 773.
29. Andrade, J. D.; Hlady, V.; Jeon, S. I. *Advances in Chemistry Series* **1996**, *248*, 57.
30. Yamashita, S.; Yamada, A.; Oohata, M.; Kohjiya, S. *Makromolekulare Chemie.* **1985**, *186*, 1373.
31. Kali, G.; Vavra, S.; Laszlo, K.; Ivan, B. *Macromolecules* **2013**, *46*, 5337.
32. Haraszti, M.; Toth, E.; Ivan, B. *Chemistry of Materials.* **2006**, *18*, 4952.
33. Kali, G.; Vavra, S.; Laszlo, K.; Ivan, B. *Macromolecules* **2013**, *46*, 5337.
34. Fodor, C.; Kali, G.; Iván, B., *Macromolecules* **2011**, 44, 4496.
35. Ivan, B.; Haraszti, M.; Erdodi, G.; Scherble, J.; Thomann, R.; Mulhaupt, R. *Macromolecular Symposia.* **2005**, *227*, 265.
36. Ivan, B.; Almdal, K.; Mortensen, K.; Johannsen, I.; Kops, J. *Macromolecules* **2001**, *34*, 1579.
37. Groenewolt, M.; Brezesinski, T.; Schlaad, H.; Antonietti, M.; Groh, P. W.; Ivan, B. *Advanced Materials.* **2005**, *17*, 1158.
38. Chen, X.; Ivan, B.; Kops, J.; Batsberg, W. *Macromolecular Rapid Communications.* **1998**, *19*, 585.
39. Jakubowski, W.; Tsarevsky, N. V.; Higashihara, T.; Faust, R.; Matyjaszewski, K. *Macromolecules.* **2008**, *41*, 2318.

40. Storey, R. F.; Scheuer, A. D.; Achord, B. C. *Polymer*. **2005**, *46*, 2141.
41. Kurian, P.; Zschoche, S.; Kennedy, J. P. *Journal of Polymer Science Part A: Polymer Chemistry*. **2000**, *38*, 3200.
42. Kali, G.; Szesztay, M.; Bodor, A.; Ivan, B. *Macromolecular Symposia*. **2013**, *323*, 37.
43. Feldthusen, J.; Ivan, B.; Mueller, A. H. E. *Macromolecules* **1998**, *31*, 578.
44. Keszler, B.; Fenyvesi, G. Y.; Kennedy, J. P. *Journal of Polymer Science Part A: Polymer Chemistry*. **2000**, *38*, 706.
45. Zhu, Y.; Storey, R. F. *Macromolecules* **2012**, *45*, 5347.
46. Breland, L. K.; Storey, R. F. *Polymer* **2008**, *49*, 1154.
47. Binder, W. H.; Sachsenhofer, R. *Macromolecular Rapid Communications*. **2008**, *29*, 1097.
48. Bonduelle, C. V.; Karamdoust, S.; Gillies, E. R. *Macromolecules* **2011**, *44*, 6405.
49. Bonduelle, C. V.; Gillies, E. R. *Macromolecules* **2010**, *43*, 9230.
50. Karamdoust, S.; Bonduelle, C. V.; Amos, R. C.; Turowec, B. A.; Guo, S.; Ferrari, L.; Gillies, E. R. *Journal of Polymer Science Part A: Polymer Chemistry*. **2013**, *51*, 3383.
51. Yamashita, S.; Kodama, K.; Ikeda, Y.; Kohjiya, S. *Journal of Polymer Science Part A: Polymer Chemistry*. **1993**, *31*, 2437.
52. Parent, J. S.; Malmberg, S.; McLean, J. K.; Whitney, R. A. *European Polymer Journal*. **2010**, *46*, 702.
53. Puskas, J. E.; Dos Santos, L. M.; Kaszas, G.; Kulbaba, K. *Journal of Polymer Science Part A: Polymer Chemistry*. **2009**, *47*, 1148.
54. Foreman, E. A.; Puskas, J. E.; Kaszas, G. *Journal of Polymer Science Part A: Polymer Chemistry*. **2007**, *45*, 5947.
55. Puskas, J. E.; Chen, Y.; Dahman, Y.; Padavan, D. *Journal of Polymer Science Part A: Polymer Chemistry*. **2004**, *42*, 3091.
56. Darling, S. B. *Prog. Polym. Sci.* **2007**, *32*, 1152.
57. Fre´chet, J. M. *Journal of Science*. **1994**, *263*, 170.
58. Puskas, J. E.; Kaszas, G. *Prog. Polym. Sci*. **2000**, *25*, 403.
59. Buhleier, E.; Wehner, W.; Vögtle, F. *Synthesis* **1978**, *1978*, 155.
60. Vögtle, F.; Weber, E. *Angew. Chem. Int. Ed.* **1979,** *18*, 753.
61. Tomalia, D. A.; Hedstrand, D. M.; Ferritto, M. S. *Macromolecules* **1991**, 24, 1435.

62. Puskas, J. E.; Antony, P.; Kwon, Y.; Kovar, M.; Norton, P. R., *Macromolecular Symposia*. **2002**, *183*, 191.
63. Flory, P. J. *J. Am. Chem. Soc.* **1941,** *63*, 3083.
64. Aoshima, S.; Fre´chet, J. M. J.; Grubbs, R. B.; Henmi, M.; Leluc, L. *Polym. Prepr.* **1995**, *36*, 531.
65. Fre´chet, J. M. J.; Henmi, M.; Gistov, I.; Aoshima, S.; Leluc, M. R.; Grubbs, R. B. *Science* **1995**, *29*, 1080.
66. Chilkoti, A.; Ratner, B. D.; Briggs, D. *Chemistry of Materials.* **1991,** *3*, 51.
67. Liu, Y.; Yang, D. Q.; Nie, H. -Y.; Lau, W. M.; Yang, J. *J. Chem. Phys.* **2011**, *134*, 074704
68. Karamdoust, S.; Crewdson, P.; Ingratta, M.; Gillies, E. R., *Submitted* **2014**.
69. Paulo, C.; Puskas, J. E. *Macromolecules* **2001**, *34*, 734.
70. Puskas, J. E.; Grasmuller, M. *Macromolecular Symposia.* **1998**, *132*, 117.
71. Holden, G. K., H. R.; Quirk, R. *In Thermoplastic Elastomers*, 3rd Ed. Hanser Publishers, Munich, **2004**.
72. Puskas, J. E.; Kwon, Y. C.; Antony, P.; Bhowmick, A. K. *Journal of Polymer Science Part A: Polymer Chemistry*. **2005**, *43*, 1811-1826.
73. Puskas, J. E.; Foreman-Orlowski, E. A.; Lim, G. T.; Porosky, S. E.; Evancho- Chapman, M. M.; Schmidt, S. P.; El Fray, M.; Piątek, M.; Prowans, P.; Lovejoy, K. *Biomaterials* **2010**, *31*, 2477.
74. Puskas, J. E.; Kwon, Y. *Polymers for Advanced Technologies.* **2006**, *17*, 615.
75. Puskas, J. E.; Antony, P.; Kwon, Y.; Paulo, C.; Kovar, M.; Norton, P. R.; Kaszas, G.; Altstädt, V. *Macromolecular Materials and Engineering.* **2001**, *286*, 565.
76. Gauthier, M.; Mo¨ller, M. *Macromolecules* **1991**, 24, 4548.
77. Mackman, N, *Nature.* **2008**, 451, 914.
78. Fontaine, B.; Fresno, C., *United States Patent*, **1994**.
79. Gruentzig, A.; King, S.; Schlumpf, M.; Siegenthaler, W. *N. The New England Journal of Medicine.* **1987**, *316*, 1127.
80. North Point Domain, *Carotid Stenting*, Sentara Vascular Specialists. **2014**.
81. Sigwart, U.; Puel, J.; Mirkovitch, V., *The New England Journal of Medicine*. **1987**, 316, 701.
82. Scott, N. *Adv. Drug Deliv. Rev.* **2006**, *58*, 358.

83. Abizaid, A.; Kornowski, R.; Mintz, G.; Hong, M.; Abizaid, A.; Mehran, R.; Pichard, A.; Kent, K.; Satler, L.; Wu, H.; Popma, J.; Leon, M. *J. Am. Coll. Cardiol.* **1998**, *32*, 584.
84. Pinchuk, L.; Wilson, G. J.; Barry, J. J.; Schoephoerster, R. T.; Parel, J.; Kennedy, J. P. *Biomaterials* **2008**, *29*, 448.
85. James, S. K.; Stenestrand, U.; Lindback, J.; Carlsson, J.; Schersten, F.; Nilsson, T.; Wallentin, L.; Lagerqvist, B. *The New England Journal of Medicine.* **2009**, *360*, 1933.
86. Moreno, R.; Fernandez, C.; Sanchez-Recalde, A.; Galeote, G.; Calvo, L.; Alfonso, F.; Hernandez, R.; Sanchez-Aquino, R.; Angiolillo, D. J.; Villarreal, S.; Macaya, C.; Lopez-Sendon, J. L. *European Heart Journal.* **2007**, *28*, 1583.
87. Wolf, K. V.; Zong, Z.; Meng, J.; *J Biomed Mater Res A.* **2008**, 87, 272.
88. Ranade, S. V.; Miller, K. M.; Richard, R. E.; *J Biomed Mater Res A.* 71, 625.
89. Jimenez-Valero, S.; Moreno, R.; Sanchez-Recalde, A. *J. Invasive Cardiol.* **2009**, *21*, 488.
90. Hong, M.; Mintz, G.; Lee, C.; Park, D.; Park, K.; Lee, B.; Kim, Y.; Song, J.; Han, K.; Kang, D.; Cheong, S.; Song, J.; Kim, J.; Park, S.; Park, S. *Circulation* **2006**, *113*, 414.
91. Khan, W.; Farah, S.; Domb, A. J., J *Control Release,* **2012**, 161, 703.
92. Burke, S. E.; Kuntz, R. E.; Schwartz, L. B.; *Adv Drug Deliv Rev*. **2006**, 58, 437.
93. Sheiban, I.; Villata, G.; Bollati, M., *Vasc Health Risk Manag.* **2008**, 4, 31.
94. Wykrzykowska, J. J; Onuma, Y.; Serruys, P. W., *Expert Opin Drug Deliv*. **2009**, 6, 113.
95. Levy, Y.; Mandler, D.; Weinberger, J.; Domb, A. J. *Journal of Biomedical Materials Research Part B: Applied Biomaterials.* **2009**, *91B*, 441.
96. Ormiston, J.; Currie, E.; Webster, M.; Kay, P.; Ruygrok, P.; Stewart, J.; Padgett, R.; Panther, M. *Catheter. Cardio. Inte.* **2004**, *63*, 332.
97. Yoo, H.; Oh, J.; Lee, K.; Park, T. *Pharm. Res.* **1999**, *16*, 1114.
98. Tong, R.; Cheng, J. *Angew. Chem. Int. Ed.* **2008**, *47*, 4830.
99. Ranade, S.; Miller, K.; Richard, R.; Chan, A.; Allen, M.; Helmus, M. *Journal of Biomedical Materials Research Part A.* **2004**, *71A*, 625.
100. Sipos, L.; Som, A.; Faust, R. *Biomacromolecules* **2005**, *6*, 2570.
101. Richard, R.; Schwarz, M.; Chan, K.; Teigen, N.; Boden, M. *Journal of Biomedical Materials Research Part A.* **2009**, *90A*, 522.
102. Bourantas, C. V.; Onuma, Y.; Farooq, V., *Int J Cardiol*, **2012**, 167, 11.
103. Nair, L. S.; Laurencin, C. T., *Polym Sci*. **2007**, 32, 762.

104. Moravej, M.; Mantovani, D.; *Int J Mol Sci.* **2011**, 12, 4250.
105. Grube, E.; Schofer, J.; Hauptmann, K. E.; Nickenig, G.; Curzen, N.; Allocco, D. J.; Dawkins, K. D. A. *JACC: Cardiovascular Interventions.* **2010**, *3*, 431.
106. Mehilli, J.; Byrne, R. A.; Wieczorek, A.; Iijima, R.; Schulz, S.; Bruskina, O.; Pache, J.; Wessely, R.; Schoemig, A.; Kastrati, A.; *European Heart Journal.* **2008**, *29*, 1975.
107. Papafaklis, M. I.; Chatzizisis, Y. S.; Naka, K. K.; Giannoglou, G. D.; Michalis, L. K. *Pharmacol. Ther.* **2012**, *134*, 43.
108. Yun, Y.; Dong, Z. Y.; Lee, N., *Mater Today*. **2009**, 12, 22.
109. Zberg, B.; Uggowitzer, P. J.; Loeffler, J. F., *Nat Mater*. **2009**, 8,887.
110. Gu, X. N.; Zheng, Y. F.; Cheng, Y., *Biomaterials*. **2009**, 30,484.
111. Mueller, P. P.; May, T.; Perz, A., *Biomaterials*. **2006**, 27, 2193.
112. Purnama, A.; Hermawan, H.; Champetier. S., *Acta Biomater*. **2013**, 9, 8746.
113. Teirstein, P. *Circulation.* **2001**, *104*, 1996.
114. Rogue, M.; Cordon-Cardo, C.; Fuster, V.; Reis, E.; Drobnjak, M.; Badimon, J. *Atherosclerosis* **2000**, *153*, 315.
115. Gallo, R.; Padurean, A.; Jayaraman, T.; Marx, S.; Rogue, M.; Adelman, S.; Chesebro, J.; Fallon, J.; Fuster, V.; Marks, A.; Badimon, J. *Circulation* **1999**, *99*, 2164.
116. Groth, C.; Backman, L.; Morales, J.; Calne, R.; Kreis, H.; Lang, P.; Touraine, J.; Claesson, K.; Campistol, J.; Durand, D.; Wramner, L.; Brattstrom, C.; Charpentier, B. *Transplantation* **1999**, *67*, 1036.
117. Heldman, A.; Cheng, L.; Jenkins, G.; Heller, P.; Kim, D.; Ware, M.; Nater, C.; Hruban, R.; Rezai, B.; Abella, B.; Bunge, K.; Kinsella, J.; Sollott, S.; Lakatta, E.; Brinker, J.; Hunter, W.; Froehlich, J. *Circulation* **2001**, *103*, 2289.
118. Hong, M.; Kornowski, R.; Bramwell, O.; Ragheb, A.; Leon, M. *Coron. Artery Dis.* **2001**, *12*, 513.
119. Strickler, F.; Richard, R.; McFadden, S.; Lindquist, J.; Schwarz, M. C.; Faust, R.; Wilson, G. J.; Boden, M. *Journal of Biomedical Materials Research Part A.* **2010**, *92A*, 773.
120. Kukreja, N.; Onuma, Y.; Daemen, J., *Pharmacol Res*. **2008**, 57, 171.
121. Schwartz, R. S., Edelman, E. R.; Carter, A., *Circulation*. **2002**, 106, 1867.
122. Jordan, M. A.; Wilson, L., *Nature Reviews Cancer*, **2004**, *4*, 253.
123. Priyadarshini, K.; Keerthi, A.U., *Med chem.* **2012**, 2, 139.

124. Park, S.; Kang.; S, Chen, X.; Kim, EJ.; Kim, J., *Biomaterials*. **2012**, 34, 598.
125. Gelderblom, H.; Verweij, J.; Nooter, K.; Sparreboom, A., *European Journal of Cancer*. **2001**, *37*, 1590.
126. Li, Y.; Bi, Y.; Xi, Y.; Li, L., *J Drug Target*. **2012**,21,188.
127. Zhang, J.; Zhao, J.; Zhang, W.; Liu, G.; Yin, D., *J Gynecol Cancer*. **2012**, 22, 1450.
128. Byron, S.A.; Loch, D.C.; Pollock, P.M., *J Gynecol Cancer*. **2012**, 22, 1517.
129. Callister, W. D., Jr. *Fundamentals of Materials Science and Engineering: An Interactive E-Text, 2nd Edition*; Wiley, **2004**.
130. Ashby, M. F.; Ferreira, P. J.; Schodek, D. L. *Nanomaterials, Nanotechnologies and Design*; Butterworth-Heinemann: Boston, **2009**.
131. Boyer, H.F., *Atlas of Stress-Strain Curves*, ASM International, Ohio, **1987**.
132. Courtney, T.H., *Mechanical Behavior of Materials*, McGraw-Hill, New York, **1990**.
133. Hayden, H.W., W.G. Moffatt and J. Wulff, *The Structure and Properties of Materials:Vol. III Mechanical Behavior*, Wiley, New York, **1965**.
134. Macosko, W. C., *Rheology: Principles, Measurements and Applications*, Wiley-VCH, New York, **1994**.
135. Larson, R.G., *The Structure and Rheology of Complex Fluids*, Oxford University Press, New York, **1999**.
136. Barnes, H.A.; Hutton, J.F.; Walters, K., *An Introduction to Rheology*. Elsevier Sci, Amsterdam, **2001**.
137. Cogswell, F. N., *Polymer Melt Rheology, a Guide for Industrial Practice*, George Godwin, London, **1981**.
138. Barnes, H. A., *A Handbook of Elementary Rheology*, The University of Wales, Institute of Non-Newtonian Fluid Mechanics, Aberystwyth, 2000.
139. Ceramic Industry, *Using Rheology to Improve Manufacturing*, **2002**.
140. Wyss, H. M.; Larsen, R. J.; Weitz, D. A., *G.I.T Laboratory Journal*. 2007, *3*, 68.

Chapter 2

2 Carboxylic acid functionalized butyl rubber: synthesis, characterization and physical properties

2.1 Introduction

Polyisobutylene (PIB)-based materials are widely used commercially in a diverse array of products such as automobile tires, sporting equipment, adhesive sealants, viscosity modifiers, chewing gum, and drug eluting stents.[1,2] The widespread use of these polymers can be attributed to their favorable properties, including but not limited to, exceptional thermal and chemical stability, impermeability to gas and water, high damping, high elasticity, and non-toxicity. While the simple, saturated hydrocarbon backbone is responsible for many of PIB's advantageous properties, it also limits the ability to modify and tune the properties of the polymer. For this reason, many applications of PIB have involved the introduction of chemical functionalities to the PIB backbone or terminus, or the incorporation of PIB into block copolymers. For example, isobutylene can be copolymerized with small amounts (i.e., < 8 mol%) of isoprene (IP) to produce a random copolymer commonly referred to as RB. These sites of unsaturation on the IP can be used to cross-link the rubber, providing the mechanical properties required for many applications. In the Taxus™ vascular stent, a linear triblock copolymer of polystyrene (PS)-PIB-PS (SIBS) is used in the drug-eluting coating.[3,4] The PS blocks impart thermoplastic properties to the rubber, not only allowing it to behave as a cross-linked rubber at physiological temperature, yet also making it readily processable at higher temperatures or in solution. There are also many other examples involving the functionalization of PIB for its incorporation into polymer networks[5-8] as well as linear,[9-13] star,[14-16] miktoarm,[17-19] and graft copolymers. [20-25] With these systems, interesting functions such as stimuli-responsive network swelling,[5,7] templating of inorganic materials,[9,19] cell encapsulation,[26] controlled drug release,[27] and protein patterning and resistance[20,22] have been achieved.

Of the various chemical functionalities that can be introduced to PIB, carboxylic acid moieties are of particular interest. First, they provide versatile functional handles that can be used for further functionalization with a wide range of nucleophiles such as amines and alcohols. Secondly, they provide sites for ion-pair or hydrogen-bond-mediated aggregation within the rubber. This can potentially alter the material properties such as mechanical strength and rheological behavior.[28-30] Thirdly, carboxylic acid moieties can enhance adhesion to metal surfaces.[31-33] This has the potential to reduce delamination from vascular stents, a challenge that has been previously reported for the SIBS material in the Taxus™ stent.[3]

There are several examples involving the functionalization of the PIB terminus with carboxylic acid moieties,[34,35] as well as the polymerization of poly(*t*-butylacrylate) and poly(*t*-butylmethacrylate) from atom transfer radical polymerization (ATRP) initiation sites at the terminus or in the middle of the PIB chain, followed by acidic or thermal deprotection to provide carboxylic acid moieties.[12,17,18,36] There are also examples involving the introduction of pendant carboxylic acids along the backbone of RB via the grafting of maleic anhydride, followed by the anhydride ring-opening with amines or alcohols.[37-40] However, there are still relatively few studies concerning the effects of these carboxylic acid moieties on the properties of these modified materials.[38,39,41,42]

The Gillies group has reported a simple and highly efficient epoxidation/elimination sequence to provide access to RB derivatives having allylic alcohol moieties along the polymer backbone. These hydroxyl groups have been activated and reacted with alcohol and amine functionalized PEG to provide RB-PEG graft copolymers.[20,21] They have also been further derivatized to undergo elimination to *exo*-dienes, which can undergo Diels Alder reactions to prepare graft copolymers with or without carboxylic acid moieties.[40] Presented here is an approach for the elaboration of the allylic alcohol moieties to introduce pendant carboxylic acid moieties via either the ring opening of cyclic anhydrides. The effects of the carboxylic acid moieties on the adhesion of the resulting materials to stainless steel surfaces, as well as their tensile and rheological properties are explored.

2.2 Experimental section

2.2.1 General procedures and materials

Two forms of RB, one with 2 mol% isoprene (IP), M_w = 400 kg/mol, PDI = 2.8 and the other having 7 mol% IP, M_w = 1050 kg/mol, PDI = 3.3 were provided by LANXESS Inc. (London, Canada). Polymer **2-*l*** was prepared as previously reported.[21] Solvents were purchased from Caledon Labs (Caledon, Ontario). All other chemicals were purchased from either Sigma-Aldrich or Alfa Aesar and were used without further purification unless otherwise noted. Dry toluene was obtained from an Innovative Technology (Newburyport, USA) solvent purification system based on aluminium oxide columns. Dichloromethane, pyridine and triethylamine were freshly distilled from CaH_2 prior to use. ^{1}H NMR spectra were obtained in $CDCl_3$ at 400 MHz or 600 MHz on Varian Inova instruments. NMR chemical shifts (δ) are reported in ppm and are calibrated against residual solvent signals of $CDCl_3$ (δ 7.26). Infrared spectra were obtained of films from CH_2Cl_2 on NaCl plates or as KBr pellets using a Bruker Tensor 27 instrument. Size exclusion chromatography (SEC) was performed on a Waters 2695 separations module equipped with a 2414 differential refractometer using THF or $CHCl_3$ as solvent and two Polymer Laboratories Resipore columns (300 mm x 7.5 mm) in series as the stationary phase. Molecular weight calibration was carried out using PS standards. Differential scanning calorimetry (DSC) and thermogravimetric analysis (TGA) were performed on a Mettler Toledo DSC 822e. For DSC, the heating/cooling rate was 10 °C/min between -120 to +150 °C. Glass transition temperatures were obtained from the second heating cycle.

2.2.2 Synthesis of polymer 4d-*l*

Allylic alcohol functionalized polymer **2-*l*** [21] (10 g, 3.9 mmol of hydroxyl groups) was dissolved in 350 mL of anhydrous toluene in a nitrogen purged flask containing a magnetic stir bar. The solution was heated to 70 °C prior to the addition of triethylamine (NEt_3) (11 mL, 78 mmol) and 4-(dimethylamino)pyridine (DMAP) (0.99 g, 7.8 mmol). Finally, a solution of diglycolic anhydride (4.5 g, 39 mmol) dissolved in anhydrous toluene (30 mL) was added via syringe and the reaction mixture was allowed to stir at 70 °C for 16 hours. The product was washed with distilled water then twice with 6M HCl before being concentrated under reduced pressure. The product was purified by precipitation (2:1 acetone/toluene) and then dried under high vacuum to

provide 9.1 g of polymer **4d-*l*** as off-white amorphous solid in 90 % yield. T_g= -61 °C; ^{1}H NMR (400 MHz, $CDCl_3$) δ_{ppm} 5.29 (br s, 1H), 5.12 (s, 1H), 4.95 (s, 1H), 4.20-4.40 (m, 4H), 1.42 (s, 145H), 1.12 (s, 431H); IR (KBr pellet): 1230, 1365, 1390, 1475, 1733, 1758, 2974 cm^{-1}; SEC ($CHCl_3$): M_w = 309 kg/mol, PDI = 2.5.

2.2.3 Synthesis of polymer 4d-*h*

Epoxidized RB derivative **1-*h***[22] (10 g, 12 mmol of epoxide) was dissolved in 350 mL of anhydrous toluene. To this solution was added one equivalent of HCl (1.0 mL, 12 mmol) and the reaction mixture was stirred at at room temperature for 1 hour. Due to solubility issues, **2-*h*** was not isolated. Instead, the HCl was neutralized with sodium carbonate and then the solution was dried with $MgSO_4$. The mixture was centrifuged and the solution of **2-*h*** decanted from the $MgSO_4$. The solution was then heated to 70 °C, then 20 equivalents of NEt_3 (33.7 mL, 242 mmol) were added followed by 2 equivalents of DMAP (3.1 g, 24.2 mmol). A solution of diglycolic anhydride (10 equivalents, 14.0 g, 121 mmol) dissolved in toluene was then added via syringe and the reaction mixture was stirred at 70 °C overnight. The product was then purified and isolated as described above for **4d-*h*** to provide 8.6 g of the polymer as a white amorphous solid in 86 % yield over the two steps.; T_g= -53 °C; ^{1}H NMR (400 MHz, $CDCl_3$) 5.29 (brs, 1H), 5.12 (s, 1H), 4.95 (s, 1H), 4.20-4.40 (m, 4H), 1.42 (s, 69H), 1.12 (s, 209H). IR (thin film from CH_2Cl_2): 1230, 1365. 1390, 1475, 1733, 1758, 2974 cm^{-1}.

2.2.4 Tensile testing

To make samples for tensile testing, 1.5 g of polymer was compressed into a 0.3 mm thick flat sheet using a hydraulic hot press (Carver Hydraulic Unit Model # 3851 OC). Samples 60 mm x 5 mm in size were cut from this sheet. The tensile test was performed at ambient (22 ± 1 ºC) temperature using an Instron 3300 Series Universal Testing Machine with a 1-kN load cell at an extension rate of 400mm/min, in accordance with ASTM D882 – 12.[43] Load and extension were calibrated prior to the test. To prevent slippage of the samples from the clamps of the testing machine, 10 mm of material was inserted into each clamp, leaving an effective sample length of 40 mm. At least six trials were performed for each polymer.

2.2.5 Adhesion tests

Rubber samples for adhesion tests were prepared by compressing the polymers into flat sheets 0.5 to 3.3mm thick between mylar and teflon using a hydraulic hot press (Carver Hydraulic Unit Model # 3851 OC) for 5 minutes at 100 °C. A 6.35 × 50.8 mm strip of material was cut from the sheet using a standard die. The test specimens were then placed in the apparatus at right angles to each other to define the area of contact. A 450 g weight was placed on the weight support, the dwell time was set to 60 seconds, and strips were died out with the Tel-Tak die. The stainless steel specimen was placed in the top platen. The Mylar was removed from the rubber surface and placed in the lower platen. The force gauge was zeroed. The lower platen was raised to make contact with the specimen in the upper platen. At the end of the dwell time period the drive motor began to pull the specimens apart and the force required for separation was recorded. The measurements were performed in triplicate for each sample.

2.2.6 Rheology

Rheological measurements were performed using a TA Instruments AR-1500ex stress-controlled rheometer with a 25 mm-diameter parallel-plate tool. Sandpaper was glued to both plates to prevent slip. Circular samples 25 mm in diameter were cut from a sheet prepared by compressing 1.5 g of polymer into a flat sheet using the hydraulic hot press. The sample thickness was measured at three different places, approximately 0.5 mm for all samples. The sample was then placed in the rheometer, the gap between the plates set to the lowest of these measurements, and the sample annealed at 100 ºC for 1 hour. Small-angle oscillatory shear and creep-recovery measurements were carried out on each sample. Oscillatory tests were performed at angular frequencies between 0.1 and 100 rad/s with the oscillating stress amplitude controlled at 100 Pa, which we confirmed was in the linear viscoelastic regime for our materials. All rheological measurements were done at 37 ºC. The data were averaged over at least three trials for each polymer.

2.3 Results and Discussion

The starting material for the synthesis was a previously reported epoxidized RB derivative.[21,22] This material was prepared from RB starting materials containing either low (2 mol%) or high (7 mol%) IP content, providing derivatives containing either 2 mol% (**1-*l***) or 7 mol% (**1-*h***) epoxidized monomers. **1-*l*** was reacted with aqueous HCl in toluene to provide the allylic alcohol derivative **2-*l*** (Scheme 2.1). For the initial synthetic studies, the reactivity of **2-*l*** with various cyclic anhydrides (**3a-d**) was investigated.

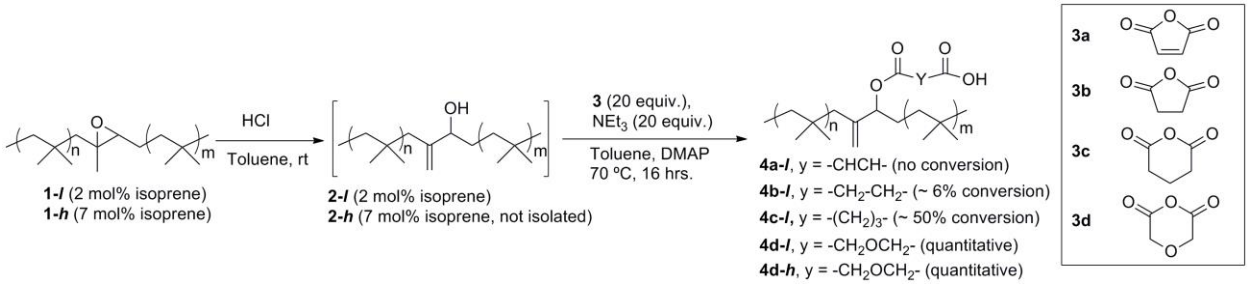

Scheme 2.1. Synthesis of butyl rubber with pendant carboxylic acid moieties.

As shown in Scheme 2.1, the reaction of **2-*l*** with excess maleic anhydride **3a** in the presence of triethylamine (NEt_3) and 4-(dimethylamino)pyridine (DMAP), standard conditions for the reaction of alcohols with anhydrides,[44,45] resulted only in the recovery of the starting material. The saturated, and thus more reactive succinic anhydride, **3b**, under the same conditions, provided only minimal conversion to the desired carboxylic acid, **4b-*l***. The more reactive pentadioic anhydride **3c** provided approximately 50% conversion to acid **4c-*l***, while finally the electron deficient diglycolic anhydride **3d** provided a quantitative conversion of all allylic alcohols to the corresponding acid **4d-*l*** based on ^{1}H NMR spectroscopy (Figure 2.1). Even if the excess of anhydride was dropped to 10 equivalents quantitative conversion was retained. To achieve higher carboxylic acid content, the reaction was also performed on the material derived from the 7 mol% IP rubber. In this case, the epoxide **1-*h*** was directly converted to **4d-*h*** without isolating the alcohol intermediate.

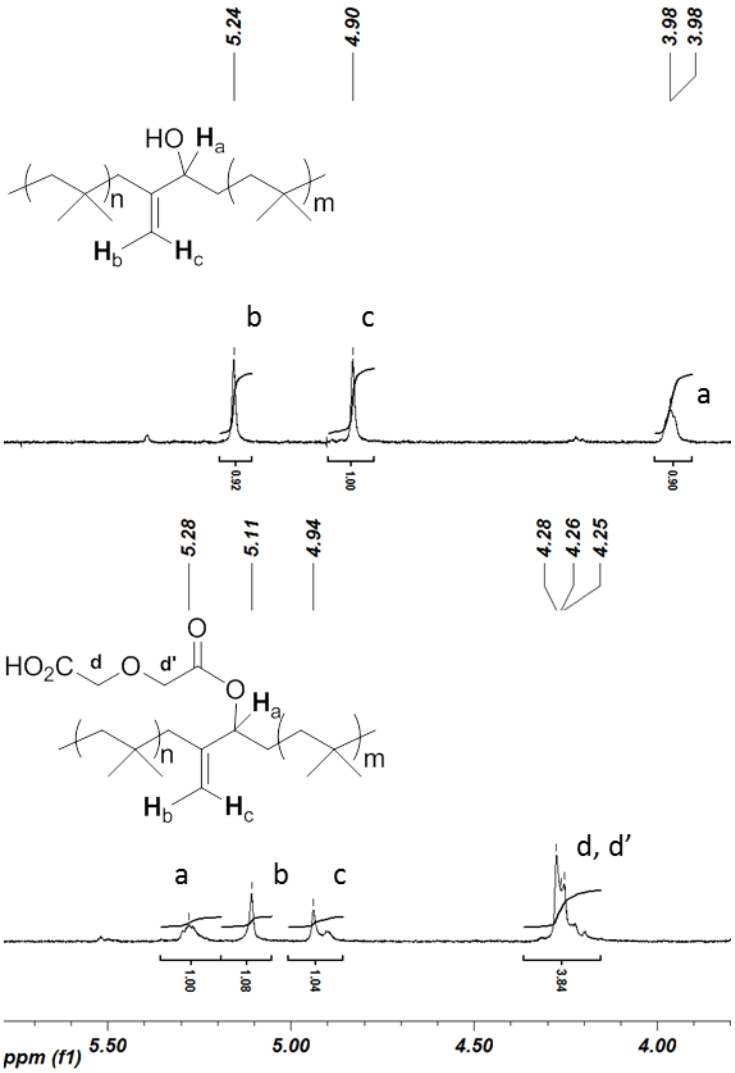

Figure 2.1. The downfield region of the ^{1}H NMR spectra of a) polymer **2-l** and b) polymer **4d-l** showing conversion of the allylic alcohol to the carboxylic acid derivative.

In addition to NMR spectroscopy, the products were also characterized by infrared (IR) spectroscopy. The appearance of two peaks in the carbonyl region at 1728 and 1748 cm^{-1} was consistent with the introduction of carboxylic acid moieties via ester linkages. Chloroform performed better than THF for size exclusion chromatography (SEC) of **4d-*l***, and a weight average molecular weight (M_w) of 309 kg/mol and a polydispersity index (PDI) of 2.5 relative to PS standards was measured under these conditions. This was a modest decrease relative to the starting RB, which had an M_w of 400 kg/mol and a PDI of 2.8. This might be attributable to some interactions of the carboxylic acid moieties with the column rather than due to any degradation of the backbone. Due to column interactions, meaningful SEC results could not be

obtained for **4d-*h***. DSC revealed that polymer **4d-*l*** had a T_g of −61 °C, in comparison to −70 °C to −63 ºC reported for RB.[46,47] A further increase to −53 °C was observed for polymer **4d-*h*** with the higher carboxylic acid content. It is likely that the increase in intermolecular hydrogen-bonding and dipole-dipole interactions due to the introduction of the polar pendant groups restricts the segmental motion of the polymer, resulting in this increase in T_g.

2.3.1 Measurement of adhesion

The adhesion of rubber to stainless steel is critical for its use in vascular stent coatings, as well as a vast array of other potential coating applications, as weak adhesion can lead to coating delamination. The adhesion of the polymer to the metal substrate is result of the van der waals forces acting between the polymer and the metal surface. Unmodified RB is known to show only moderate adhesion to stainless steel.[42] It is therefore of interest to determine whether the introduction of carboxylic acid moieties enhances the rubber's adhesivity. In addition, the adhesivity of the various synthetic intermediates, including the epoxide- and hydroxyl-functionalized rubber derivatives, were also studied.

To measure adhesion, a RB sample was pressed between two stainless steel plates with a contact area of 320 mm^2, and the force required to separate the plates was measured. As shown in Table 2.1, all of the functionalized rubber derivatives exhibited stronger adhesion than the parent RB. As expected, the carboxylic acid functionalized rubber had the highest adhesivity, likely due to the ability of the carboxylic acid moities to undergo specific ligand-metal interactions at the stainless steel surface. The hydroxyl-functionalized rubber also exhibited good adhesivity, likely for similar reasons. Based on the expected interactions with the metal surface, it was anticipated that the materials derived from the RB with the higher IP content (**PIB-*h*,1-*h***, **2-*h***, **4d-*h***) would exhibit higher adhesivity than the analogous materials prepared from the lower IP content rubber (**PIB-*l*,1-*l***, **2-*l***, **4d-*l***). This was not the case, however. The lower apparent adhesion of **2-*h*** and **4d-*h*** can possibly be attributed to the properties of the materials, as the test resulted in the fracture of the material itself during the test, rather than delamination from the metal surface. These properties will be explored further through mechanical and rheological studies described below. For comparision, a comparable experiment on a phosphonium-functionalized rubber prepared from RB with 6.5 % IP content gave a separation force of 30.3 psi, very similar to that of the carboxylic acid functionalized **4d** series.[48] Importantly, our results

indicate that a significantly enhanced adhesivity can be achieved even at very low (2 mol%) carboxylic acid content.

Table 2.1. Adhesive properties of butyl rubber derivatives.

Sample	Separation force (psi)	Sample	Separation force (psi)
PIB-*l*	14.6 ± 0.3	**PIB-*h***	12.1 ± 0.2
1-*l*	22 ± 2	**1-*h***	25 ± 2
2-*l*	29.6 ± 0.6	**2-*h***	20 ± 2
4d-*l*	33 ± 1	**4d-*h***	28 ± 3

2.3.2 Tensile testing

Tensile strength is very important for predicting the structural integrity and strength of the material and determining its performance in load-bearing applications. Tensile testing of samples **1-*l/h***, **2-*l/h***, and **4d-*l/h*** was performed using the standard ASTM D882 – 12 protocol.[43] Representative stress-strain curves are shown in Figure 2.2, and the Young's modulus, ultimate tensile strength, and elongation at break are summarized in Table 2.2. The Young's moduli of the RB with 2 mol% isoprene (**PIB-*l*)** and its derivatives **1-*l***, **2-*l***, and **4d-*l***, were all similar, in the range of 0.3-0.6 MPa. The tensile strength of **1-*l*** was the same as that of the original RB. The tensile strength was slightly higher for the hydroxyl-functionalized polymer **2-*l***, and increased significantly for the carboxylic-acid-functionalized polymer **4d-*l***. The observed increase in strength may result from ionomeric or hydrogen-bond-mediated cross-linking involving the carboxylic acid moieties and, to a lesser extent, the hydroxyl groups. No significant trend was observed in the data for percent elongation at break.

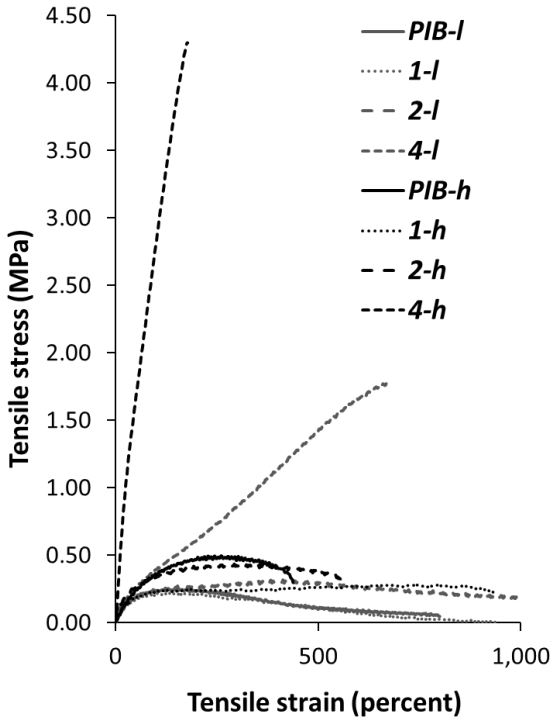

Figure 2.2. Representative stress-strain curves for functionalized rubber derivatives.

Table *2*.2. Tensile properties of the polymers.

Sample	Young's modulus (MPa)	Ultimate tensile strength (MPa)	Elongation at break (%)
PIB-*l*	0.6 ± 0.2	0.23 ± 0.01	770 ± 70
1-*l*	0.4 ± 0.1	0.20 ± 0.03	800 ± 300
2-*l*	0.43 ± 0.07	0.32 ± 0.05	1600 ± 600 *
4d-*l*	0.35 ± 0.08	1.7 ± 0.3	600 ± 100
PIB-*h*	0.59 ± 0.02	0.8 ± 0.2	430 ± 30
1-*h*	0.41 ± 0.07	0.25 ± 0.04	800 ± 100
2-*h*	0.8 ± 0.3	0.42 ± 0.05	600 ± 100
4d-*h*	3.1 ± 0.8	3.5 ± 1	150 ± 30

* Some samples failed to break at the maximum elongation of 2000%. Data presented are the mean of six measurements per polymer, and uncertainties are the standard deviations.

Similar trends were observed for the compounds **1-*h***, **2-*h***, and **4d-*h*,** derived from RB with 7 mol% isoprene (**PIB-*h***), although the effects appeared to be more significant due to the higher density of functional groups. For example, the carboxylic acid derivative **4d-*h***, had a Young's modulus of 3.10 MPa, 5 to 10 times higher than all of the other materials, and an ultimate tensile strength of 3.46 MPa, again higher than the other materials, including **4d-*l***. Elongation at break for **4d-*h*** was significantly smaller than for any of the other materials, indicating that it is more brittle. This increase in brittleness supports the observations made in the adhesion tests. At this increased level of carboxylic acid loading, the brittleness of the material outweighs possible increases in adhesion and interactions with stainless steel surfaces. Overall, these results suggest that the introduction of chemical functionality, and in particular carboxylic acid moieties, along the RB backbone results in significant changes in tensile properties, and that the magnitude of these changes depends on the degree of functionalization. While the carboxylic-acid-functionalized materials do not exhibit the same tensile properties as cross-linked rubber or SIBS,[3,49] their properties are indicative of a physical or supramolecular cross-linking.

2.3.3 Rheological evaluation

Rheological measurements are helpful for determining the processing characteristics of materials. RB itself is an elastomer that exhibits a considerable amount of creep when subjected to stress over a long period.[50,52,53] We hypothesized that the functionalization of PIB with carboxylic acid or other moieties might reduce its susceptibility to creep, making it more useful for applications such as biomedical coatings. With this application in mind, the viscoelastic behavior of the materials was measured under small-amplitude oscillatory shear at 37 ºC.

The viscous and elastic moduli of two representative materials, **PIB-*h*** and **4d-*h***, are plotted as a function of angular frequency ω in Figure 2.3. Both the viscous modulus G" and the elastic modulus G' depend only weakly on frequency, and G' is much larger than G". This behavior is typical of rubbery materials. In Figure 2.4, the elastic and viscous moduli at $\omega = 1$ rad/s are shown for all of our materials. In all cases, G' >> G", but the values of the moduli vary by an order of magnitude, depending on functionalization. At this frequency, both unmodified butyl rubbers, **PIB-*l*** and **PIB-*h*** have elastic moduli slightly less than 10^5 Pa and viscous moduli

about a factor of three smaller. The epoxide derivative **1-*h*** has moduli similar to its parent unmodified rubber at ω = 1 rad/s, and indeed, over the full frequency range studied. The carboxylated and hydroxyl derivatives **4d-*h*** and **2-*h***, which have the ability to form hydrogen bonds, have substantially lower moduli but qualitatively similar frequency dependence. Although the moduli of **PIB-*l*** and **PIB-*h*** are similar, the materials derived from **PIB-*l*** have much lower viscous and elastic moduli than the corresponding derivatives of **PIB-*h*.** In general, the hydrophobic derivatives have higher moduli than the hydrophilic derivatives, with the carboxylated derivative **4d-*l*** having the lowest value over most of the frequency range studied.

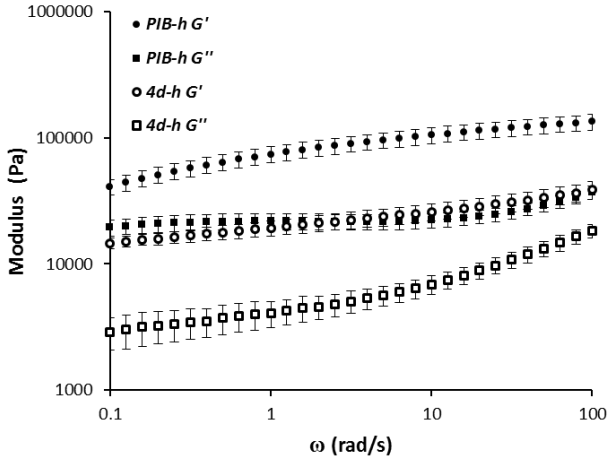

Figure 2.3. Frequency dependence of the elastic and viscous moduli, G' and G" respectively, for two representative materials. The data points are averages over at least three trails, and error bars are standard deviations.

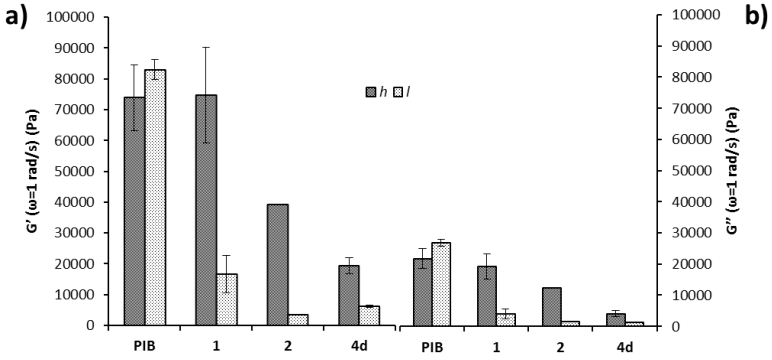

Figure 2.4. a) Elastic moduli of the polymers at ω=1 rad/s; b) Viscous moduli of the polymers at ω=1 rad/s.

The ratio of the viscous and elastic moduli G''/G' = loss tangent (tan α), where α is the phase angle between the applied stress and the measured strain. Loss tangent is less than 1 for predominantly elastic materials, while it is greater than one for viscous materials. Figure 2.5 shows loss tangent for the polymers studied here. Loss tangent is less than 1 in all cases and at all frequencies studied, reflecting the fact that these materials are all primarily elastic. For a given polymer, the moduli are expected to become equal to each other and cross over at some low frequency ω_c, with the reciprocal of the crossover frequency being a measure of the slowest relaxation time in the system. Although ω_c is below the frequency range we investigated, the approach to the crossover is indicated by a rise in loss tangent as the frequency is lowered. Our data suggest that ω_c is highest and, correspondingly, the polymer relaxation time is shortest, for polymer **2-*l***. The relatively high values of loss tangent we observed at low ω for **2-*l*** and **2-*h*** and their fairly low moduli are consistent with our qualitative observation that these materials are softer and behave more like weak gels than like rubbers. On the other hand, the carboxylated polymers **4-*l*** and **4-*h*** show no increase in loss tangent at low ω, suggesting that the relaxation time in these materials is much longer. This suggests that the carboxylic acid groups in these materials do indeed form a significant number of cross-links which restrict the dynamics of the polymer molecules.

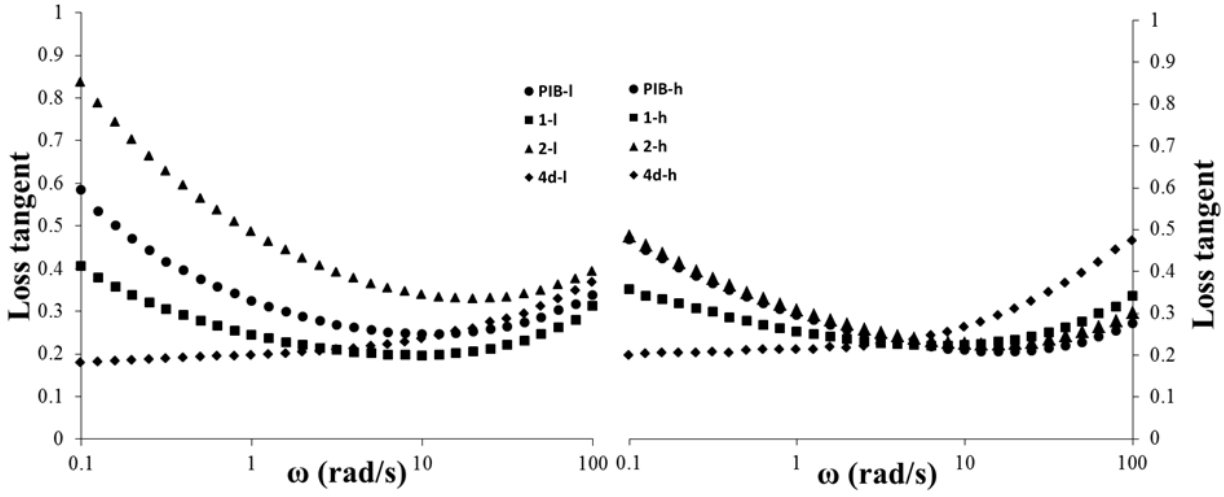

Figure 2.5. Loss tangent as a function of frequency; a) shows behavior of low isoprene content derivatives, b) shows behavior of high isoprene derivatives.

This viscoelastic data, tensile data, and adhesion data is consistent with the physical form of the materials. The epoxides (**1**-***l/h***) and the native rubbers feel very similar, while the hydroxylated derivatives (**2**-***l/h***) appear more like a soft gels than the other materials, and the carboxylic acids (**4**--***l/h***) appear more like rubbers than the **2** series but are qualitatively more brittle than the native rubber.

2.4 Conclusion

The synthesis of a carboxylic acid-functionalized RB was accomplished through the ring opening of diglycolic anhydride from allylic alcohol moieties along the polymer backbone affording pendant carboxylic acids. The degree of functionalization was controlled *via* the IP content of the RB starting material. Epoxide-, hydroxide-, and carboxylic-acid-functionalized polymers were synthesized. All of the functionalized materials showed stronger adhesion to stainless steel than the unfunctionalized PIB, with the 2 mol% carboxylic-acid-functionalized rubber exhibiting the highest adhesivity. Carboxylic acid moieties also significantly increased the ultimate tensile strength of the high- IP -content polymer and the Young's modulus of both the high- and low- IP-content materials. Rheological measurements showed that functionalization of the RB tended to decrease both elastic and viscous moduli. The addition of carboxylic acid significantly decreased the ratio of the viscous to the elastic modulus of the polymer, consistent with the carboxylic acid groups contributing to the formation of a cross-linked network of polymer molecules. Hydroxyl functionalization had the opposite effect. Overall, many of the measured properties of these new materials may prove useful in new applications of RB, potentially including coatings for stents and other biomedical devices.

2.5 References

1. Greve, H.-H.; Threadingham, D. In *Ullmann's Encyclopedia of Industrial Chemistry*; Wiley-VCH Verlag GmbH & Co. KGaA: 2000.
2. Threadingham, D.; Obrecht, W.; Wieder, W.; Wachholz, G.; Engehausen, R. In *Ullmann's Encyclopedia of Industrial Chemistry*; Wiley-VCH Verlag GmbH & Co. KGaA: 2000.
3. Strickler, F.; Richard, R.; McFadden, S.; Lindquist, J.; Schwarz, M. C.; Faust, R.; Wilson, G. J.; Boden, M. *Journal of Biomedical Materials Research Part A.* **2010**, *92A*, 773.
4. Pinchuk, L.; Wilson, G. J.; Barry, J. J.; Schoephoerster, R. T.; Parel, J.-M.; Kennedy, J. P. *Biomaterials* **2008**, *29*, 448-460.
5. Kali, G.; Vavra, S.; Laszlo, K.; Ivan, B. *Macromolecules.* **2013**, *46*, 5337-5344.
6. Haraszti, M.; Toth, E.; Ivan, B. *Chemistry of Materials.* **2006**, *18*, 4952.
7. Ivan, B.; Haraszti, M.; Erdodi, G.; Scherble, J.; Thomann, R.; Mulhaupt, R. *Macromolecular Symposia.* **2005**, *227*, 265.
8. Ivan, B.; Almdal, K.; Mortensen, K.; Johannsen, I.; Kops, J. *Macromolecules* **2001**, *34*, 1579.
9. Groenewolt, M.; Brezesinski, T.; Schlaad, H.; Antonietti, M.; Groh, P. W.; Ivan, B. *Advanced Materials.* **2005**, *17*, 1158.
10. Chen, X.; Ivan, B.; Kops, J.; Batsberg, W. *Macromolecular Rapid Communications.* **1998**, *19*, 585.
11. Jakubowski, W.; Tsarevsky, N. V.; Higashihara, T.; Faust, R.; Matyjaszewski, K. *Macromolecules* **2008**, *41*, 2318.
12. Storey, R. F.; Scheuer, A. D.; Achord, B. C. *Polymer* **2005**, *46*, 2141.
13. Kurian, P.; Zschoche, S.; Kennedy, J. P. Jour*nal of Polymer Science Part A: Polymer Chemistry.* **2000**, *38*, 3200.
14. Kali, G.; Szesztay, M.; Bodor, A.; Ivan, B. *Macromolecular Symposia.* **2013**, *323*, 37.
15. Feldthusen, J.; Ivan, B.; Mueller, A. H. E. *Macromolecules* **1998**, *31*, 578.
16. Keszler, B.; Fenyvesi, G. Y.; Kennedy, J. P. *Journal of Polymer Science Part A: Polymer Chemistry.* **2000**, *38*, 706.
17. Zhu, Y.; Storey, R. F. *Macromolecules* **2012**, *45*, 5347.
18. Breland, L. K.; Storey, R. F. *Polymer* **2008**, *49*, 1154.
19. Binder, W. H.; Sachsenhofer, R. *Macromolecular Rapid Communications.* **2008**, *29*, 1097.

20. Bonduelle, C. V.; Karamdoust, S.; Gillies, E. R. *Macromolecules* **2011**, *44*, 6405.
21. Bonduelle, C. V.; Gillies, E. R. *Macromolecules* **2010**, *43*, 9230.
22. Karamdoust, S.; Bonduelle, C. V.; Amos, R. C.; Turowec, B. A.; Guo, S.; Ferrari, L.; Gillies, E. R. *Journal of Polymer Science Part A: Polymer Chemistry*. **2013**, *51*, 3383.
23. Fonagy, T.; Ivan, B.; Szesztay, M. *Macromolecular Rapid Communications*. **1998**, *19*, 479.
24. Yamashita, S.; Kodama, K.; Ikeda, Y.; Kohjiya, S. *J. P Journal of Polymer Science Part A: Polymer Chemistry*. **1993**, *31*, 2437.
25. Parent, J. S.; Malmberg, S.; McLean, J. K.; Whitney, R. A. *European Polymer Journal*. **2010**, *46*, 702.
26. Isayeva, I. S.; Kasibhatla, B. T.; Rosenthal, K. S.; Kennedy, J. P. *Biomaterials*. **2003**, *24*, 3483.
27. Ivan, B.; Kennedy, J. P.; Mackey, P. W. *ACS Symp. Series* **1991**, *469*, 203.
28. Antony, P.; De, S. K. *J. Macromol. Sci. C* **2001**, *41*, 41.
29. Ozvald, A.; Scott Parent, J.; Whitney, R. A. *Journal of Polymer Science Part A: Polymer Chemistry*. **2013**, *51*, 2438.
30. Parent, J. S.; Penciu, A.; Guillén-Castellanos, S. A.; Liskova, A.; Whitney, R. A. *Macromolecules* **2004**, *37*, 7477.
31. Zosel, A. In *Advances in Pressure Sensitive Adhesive Technology*; Satas, D., Ed.; Satas and Associates: Warwick, RI, 1992; Vol. 1, p 92.
32. Vendamme, R.; Olaerts, K.; Gomes, M.; Degens, M.; Shigematsu, T.; Eevers, W. *Biomacromolecules* **2012**, *13*, 1933.
33. Bellamine, A.; Degrandi, E.; Gerst, M.; Stark, R.; Beyers, C.; Creton, C. *Macromol. Mat. Eng.* **2011**, *296*, 31.
34. Lange, A.; Mach, H.; Rath, H. P.; Ulrich, K.; 20041125, W. A., Ed. 2004.
35. Viktoria, P.; Ivan, B. *PMSE Preprints* **2009**, *101*, 1630.
36. Fang, Z.; Kennedy, J. P. Jour*nal of Polymer Science Part A: Polymer Chemistry*. **2002**, *40*, 3662.
37. McLean, J. K.; Guillen-Castellanos, S. A.; Parent, J. S.; Whitney, R. A.; Resendes, R. *European Polymer Journal*. **2007**, *43*, 4619.
38. Li, L.; Zhang, J.; Chen, Q.; Boonkerd, K.; Kim, J. K. *Polym. Eng. Sci., DOI 10.1002/pen.23720*.

39. Sabaa, M. W.; Younan, A. F.; Mohsen, R. M.; Tawfic, M. L. *J. Appl. Polym. Sci.* **2008**, *108*, 850.
40. Abd Rabo Moustafa, M. M.; Gillies, E. R. *Macromolecules* **2013**, *46*, 6024.
41. Kopchick, J. G.; Storey, R. F.; Beyer, F. L.; Mauritz, K. A. *Polymer* **2007**, *48*, 3739.
42. Kopchick, J. G.; Storey, R. F.; Jarrett, W. L.; Mauritz, K. A. *Polymer* **2008**, *49*, 5045.
43. ASTM, Standard Test Method for Tensile Properties of Thin Plastic Sheeting. ASTM: New York, 2012; Vol. D882-12.
44. Shimizu, T.; Kobayashi, R.; Ohmori, H.; Nakata, T. *Synlett* **1995**, *6*, 650.
45. Deutsch, H. M.; Glinski, J. A.; Hernandez, M.; Haugwitz, R. D.; Narayanan, V. L.; Suffness, M.; Zalkow, L. H. *J. Med. Chem.* **1989**, *32*, 788.
46. Franta, I.; Editor *Studies in Polymer Science, 1: Elastomers and Rubber Compounding Materials*; Elsevier, 1989.
47. Willenbacher, N.; Lebedeva, O. In *Handbook of Pressure Sensitive Adhesives and Products*; Benedek, I., Feldstein, M. M., Eds.; Taylor and Francis Group: Boca Raton, La, 2009.
48. Resendes, R.; Krista, R.; Hickey, J. N.; Office, U. S. P., Ed.; Lanxess Inc.: U.S., 2010.
49. Flory, P. J.; Rabjohn, N.; Shaffer, M. C. *J. Polym. Sci.* **1949**, *4*, 435.
50. Vinogradov, G. V.; Volfson, S. I.; Karp, M. G. *Intl. J. Polym. Mater. Polym. Biomater.* **1982**, *9*, 87.
51. Senyek, M. L. In *Encyclopedia of Polymer Science and Technology*; John Wiley & Sons, Inc.: 2002.
52. Kopchick, J. G.; Storey, R. F.; Jarrett, W. L.; Mauritz, K. A. *Polymer* **2008**, *49*, 5045.

Chapter 3

3 Covalent polyisobutylene-paclitaxel conjugates as potential vascular stent coatings with controlled drug release

3.1 Introduction

Atherosclerosis is a leading cause of cardiac arrest and a growing concern for developed and developing societies worldwide.[1] Many treatments are currently available for mild and moderate cases,[2-6] but surgical intervention is often required for more severe cases.[7] To avoid the more invasive bypass surgery, arterial stents can be introduced into an artery to improve blood flow.[8] Bare-metal stents consist simply of stainless steel meshes, that although initially effective, inevitably lead to severe vessel damage due to the pathological biological cascade.[9] To address this issue, drug eluting stents (DES) were developed. These stents release anti-proliferative agents that greatly reduce cell replication and growth, preventing restenosis, the recurrence of arterial blockage.[10, 11]

Several DES systems have been developed.[12-15] The coatings used in these stents are physical mixtures of a drug and a polymer carrier, and are designed for biocompatibility, controlled-release, and adhesion of the polymer to the stainless steel mesh. Although these stents have been shown to reduce restenosis relative to bare metal stent (BMS),[16, 17] they still suffer from the possibility of post-implantation thrombosis. In addition, restenosis is still possible as the drug-release period is sufficient for the initial healing process, [18] but does not necessarily provide long-term protection because of drug depletion.[19, 20] An additional disadvantage of these coatings is the possibility of delamination from the stainless steel stent, which would cause a burst release of drug, the release of polymeric coating material into the bloodstream, and the exposure of the BMS.[21, 22]

Butyl rubber (RB) is a copolymer of *iso*-butylene and small amounts of isoprene (IP). The IP content provides an olefinic handle for cross-linking. However, the IP units can also be chemically modified to provide a range of functionalities, most commonly through halogenation.[23-25] In previous work, the Gillies group reported an efficient and clean epoxidation/elimination sequence that produces an allylic alcohol functionalized PIB, which in turn was conjugated to amine-terminated PEG to provide access to graft copolymers.[26, 27] In chapter 2, carboxylic-acid-functionalized PIBs were generated by reacting the allylic alcohols with cyclic anhydride derivatives. The pendant carboxylic acid moieties were found to enhance adhesion of the polymer to stainless steel and to modify the rheological and tensile properties of the materials.

In this chapter, these pendant carboxylic acid groups are used as sites for further covalent functionalization of the rubber. Carboxylic acid moieties can act as conjugation sites for a wide array of alcohols and amines, providing ester and amide linkages respectively. PIB is the main component of the thermoplastic elastomer PS -*b*-PIB-*b*- PS (SIBS), which is used in combination with the drug paclitaxel (PTX) as the coating material on the clinical TAXUS™ stent.[29] Here we investigate whether carboxylic acid moieties on PIB can be used to covalently immobilize PTX, and study the drug release and coating properties of the resultant material. There has been limited previous work on the covalent conjugation of drug molecules to polymer coatings,[30] and we are unaware of any reports in the literature on the biomechanical properties of the material or its effectiveness in atherosclerosis treatment. In this paper we describe the preparation, chemical and physical characterization, and preliminary biological evaluation of two PIB-PTX conjugates.

3.2 Experimental

3.2.1 General

Carboxylic-acid-functionalized PIBs **1a** and **1b** were prepared as described in chapter 2 from RB containing 2 mol% IP ($M_w = 4.00 \times 10^5$ g/mol, PDI = 2.8), and 7 mol% IP ($M_w = 1.05 \times 10^6$ g/mol, PDI = 3.3) provided by LANXESS Inc. (London, Canada). Solvents were purchased from Caledon Labs (Caledon, Ontario) and all other chemicals were purchased from either Sigma-Aldrich or Alfa Aesar and were used as received unless otherwise noted. Dry toluene was obtained from a solvent purification system. Dichloromethane and diisopropylethylamine were

freshly distilled from CaH_2 prior to use. ^{1}H NMR spectra were obtained in $CDCl_3$ at 400 MHz or 600 MHz on Varian Inova instruments. NMR chemical shifts (δ) are reported in ppm and are calibrated against residual solvent signals of $CDCl_3$ (δ 7.26). Infrared spectra were obtained as films on NaCl plates using a Bruker Tensor 27 instrument. Size exclusion chromatography (SEC) was performed in THF using a Waters 515 pump, Wyatt Rex differential refractometer, and two PolyPore columns (300 x 7.5 mm^2, Agilent) connected in series. Calibration was performed using PS standards. DSC and thermogravimetric analysis (TGA) were performed on a Mettler Toledo DSC 822e at a heating rate of 10 °C/min. DSC was performed between -120 to +150 °C. Glass transition temperatures (T_g) were obtained from the first heating cycle.

3.2.2 Synthesis of PIBa-cov

An anhydrous sample (dried under vacuum in the presence of P_2O_5) of carboxylic-acid-functionalized PIB (10 g, 3.9 mmol in terms of CO_2H derived from PIB containing 2.2 % IP (m/m), was dissolved over 36 h, with stirring, in anhydrous toluene (400 mL) under a nitrogen atmosphere. A solution of 1-ethyl-3-(3-dimethylaminopropyl) carbodiimide hydrochloride (EDC·HCl, 940 mg, 4.9 mmol), diisopropylethylamine (DIPEA, 1.2 mL, 6.8 mmol) and 4-dimethylaminopyridine (DMAP, 250 mg, 1.95 mmol) were dissolved in anhydrous CH_2Cl_2 (200 mL) and added in one portion to the dissolved polymer. The solution was stirred for 20 minutes prior to the addition, in one portion, of a solution of PTX (3.7 g, 4.3 mmol) in CH_2Cl_2 (200 mL). The reaction mixture was then stirred at ambient temperature for 16 hours. Following NMR determination of conversion, the CH_2Cl_2 was removed under reduced pressure and the toluene solution washed with deionized water, 1M HCl and twice with 1M $NaHCO_3$ successively. After reduction of the solution by 2/3 under reduced pressure, precipitation into absolute ethanol provided **2a** as an off-white solid. Yield = 77 %; ~95 % conversion. ^{1}H NMR (400 MHz, $CDCl_3$) δ_{ppm} 8.15 (d, *J* = 7.4 Hz, 2H, PTX), 7.76 (t, *J* = 7.1 Hz, 2H, PTX), 7.60 (t, *J* = 7.1 Hz, 1H), 7.56-7.45 (m, 3H, PTX), 7.44-7.36 (m, 5 H, PTX), 7.34 (m, 1H, PTX), 7.15-7.10 (m, 1H, PTX), 6.30 (s, 1H, PTX), 6.29-6.20 (m, 1H, PTX), 6.08-6.01 (m, 1H, PTX), 5.69 (t, *J* = 6.1 Hz, 1H, PTX), 5.62-5.57 (m, 1H, PTX), 5.29-5.19 (m, 1.1H, PIB), 5.13-5.06 (m, 1 H, PIB), 4.97 (d, *J* = 9.1 Hz, 1 H, PTX), 4.91 (m, 2H, PIB), 4.44 (m, 1H, PTX), 4.37-4.12 (m, 6H, PIB/PTX(ethyl acetate contamination), 3.82 (*pseudo*-d, *J* = 6.5 Hz, 1H, PTX), 3.68 (t, *J* = 6.4 Hz, 1H, PTX), 2.62-2.52 (m, 1H, PTX), 2.49-2.46 (s, 3H, PTX), 2.41-2.35 (m, 1H, PTX), 2.26 (m, 2H, PTX), 2.22 (s, 3H,

PTX) 1.96-1.92 (m, 4H, PTX), 1.69 (s, 3H, PTX) 1.42 (s, 315H, PIB), 1.26-0.91 (PIB, m, 950H, PIB/PTX). IR (thin film on NaCl, chloroform) 1232, 1367, 1390, 1475, 1670, 1737, 2960 cm^{-1}. SEC: M_w = 337000 g/mol, PDI = 1.47. T_g = -62 °C.

3.2.3 Synthesis of PIBb-cov

The conjugate was prepared by the same procedure described above for **PIBb-cov**, using carboxylic-acid-functionalized PIB (derived from 7 % m/m IP, 1.5 g, 1.9 mmol in terms of CO_2H) in 250 mL of anhydrous toluene; EDC·HCl (540 mg, 2.8 mmol), DIPEA (680 µL, 3.9 mmol), and DMAP (110 mg, 0.93 mmol) in 50 mL CH_2Cl_2; PTX (2.0 g, 2.4 mmol) in 100 mL CH_2Cl_2. Yield = 73 %; ~85 % conversion; ^{1}H NMR (400 MHz, $CDCl_3$) 8.15 (d, *J* = 7.3 Hz, 2H, PTX), 7.74 (d, *J* = 6.4 Hz, 2H, PTX), 7.60 (t, *J* = 7.2 Hz, 1H, PTX), 7.52 (t, *J* = 7.6 Hz, 2H, PTX), 7.49 (t, *J* = 7.6 Hz, 1H, PTX), 7.44-7.31 (m, 8H, PTX), 7.02-6.96 (m, 1H, PTX), 6.29 (s, 1H, PTX), 6.28-6.20 (m, 2H, PTX), 6.08-6.00 (m, 1H, PTX), 5.69 (d, *J* = 6.8 Hz, 1H, PTX), 5.62-5.56 (m, 1H, PTX), 5.28-5.19 (m, 1.4H, PIB), 5.12-5.07 (m, 1.4H, PIB), 4.97 (d, *J* = 9.4 Hz, 1.2H, PTX), 4.91-4.89 (m, 1.6H, PIB), 4.47-4.41 (m, 1H, PTX) 4.40-4.10 (m, 9H, PTX/PIB), 3.82 (d, *J* = 6.5 Hz, 1H, PTX), 3.70-3.64 (m, 1H, PTX), 2.62-2.52 (m, 1H, PTX), 2.52-2.44 (m, 4H, PTX), 2.42-2.34 (m, 2H, PTX), 2.23 (s, 3H, PTX), 1.94 (bs, 4H), 1.68 (bs, 3H, PTX), 1.41 (s, 112H, PIB), 1.29-0.87 (m, 400H, PTX/PIB); IR: 1232, 1367, 1390, 1475, 1670, 1737, 2960 cm^{-1}; SEC: M_w =501400 g/mol, PDI = 2.66. T_g = -56 °C.

3.2.4 Preparation of Films

The surface of a stainless steel plate with dimensions of 31 mm × 11 mm was milled to obtain a smooth surface with a roughness of 420 nm. The films were prepared from a 100 mg/mL solution of the polymers in CH_2Cl_2. For the physically mixed samples, PTX was added to achieve the desired wt%. A 100 µL aliquot of each of the polymer solutions was drop cast onto the stainless steel plate. The sample was dried under reduced pressure prior to the release study. Each sample was prepared and studied in quadruplicate.

3.2.5 Release Study

The release study was performed in 0.01 M phosphate buffer solution with pH = 7.4, containing 0.138 M NaCl and 0.0027 M KCl and 0.05% (m/v) Tween 20 as a surfactant. The stainless steel

plates were submerged in 10 mL of buffered solution in a vial. The solution was maintained at 37 °C. The buffer was removed every seven days for PTX analysis and replaced with fresh medium. Due to the low amounts of PTX released, the release medium was removed via lyophilization and the resulting solid redissolved in 2 mL of 80:20 water:acetonitrile with agitation and filtered through a 2.2 μm syringe filter. A control study demonstrated that PTX was soluble at this concentration.

3.2.6 HPLC protocol

The high performance liquid chromatography (HPLC) instrument comprised a Waters Separations Module 2695, a Photodiode Array Detector (Waters 2998) and a Nova-Pak C18 4um (3.9x150mm) column connected to a C_{18} guard column. The PDA detector was used to monitor the PTX absorbance at 228 nm. PTX separation was obtained using a gradient method with Solvent A (5% acetonitrile in water) and Solvent B (80% acetonitrile, 0.1% H_3PO_4 in water) flowing at 1 mL/min. Gradient: Solvent A was decreased from an initial proportion of 65% to 30% over 10 min, and then increased back to 65% over the next 5 min; the column was then allowed to re-equilibrate over 5 min. The calibration curve was obtained from PTX (LC Laboratories, >99%, P-9600) standard solutions. Stock solutions of 1000 μg/mL, 100 μg/mL and 50 μg/mL PTX in acetonitrile were prepared. The stock solutions were used to make standard solutions of 25, 20, 15, 10, 7.5, 5, 2, 1, 0.5 μg/mL in 20:80 acetonitrile:PBS solution. Standards were filtered and injected at 100 μL using the above instrument method. Samples were prepared in a 20:80 acetonitrile:PBS solution, filtered through 0.2 μm filters and injected at 100 μL using the same conditions. The limit of detection of PTX was determined to be 0.02 μg. The calibration curve and a sample HPLC trace are provided in the appendies.

3.2.7 Atomic Force Microscopy

Surfaces for atomic force microscopy (AFM) analysis were those prepared for the release study. Surfaces were visualized using an XE-100 microscope from Park Systems. Images were obtianed by scanning the surface at three different resolutions: 20 μm × 20 μm, 5 μm × 5 μm, and 1 μm × 1 μm. Scanning was carried out using rectangular-shaped silicon cantilevers (T300, VISTA probes), with a nominal tip radius of 10 nm and spring constant of 40 N/m. Measurements were carried out under atmospheric conditions and ambient temperature. Topographic (height) and

phase (force imaging mode) images were recorded simultaneously in tapping mode. The cantilever was oscillated at its resonance frequency of approximately 300 kHz. All images contained 256 data points per line for 256 lines, and the scan rate was maintained at 1 Hz. Post-imaging analysis was carried out using XEI, version 1.7.0 from Park Systems. Images were flattened to remove curvature in both the x and y axes. Grain size calculations were carried out on the 5 μm x 5 μm images by measuring the areas of 20 largest grains in the field of view using DOMAN3,[31] for at least two images. The mean size of these 40 (two images) or 60 (three images) largest grains is provided as the mean largest grain size (MLGS), and the reported error represents the standard deviation of the measurements. These values should be used for comparative purposes only.

3.2.8 Tensile Testing

Tensile tests were carried out according to ASTM D882 – 12,[32] using an Instron universal testing machine 3300 series. For each sample, 1.5 g of polymer was compressed into 0.3 mm thick flat sheets using a hydraulic hot press (Carver Hydraulic Unit Model # 3851 OC). Samples 60 mm × 5mm in size were cut from this sheet for analysis. The tensile test was performed using a 1-kN load cell and an extension rate of 400 mm/min at ambient temperature (22 ± 1 ºC). Load and extension calibration were preformed prior to the test. To prevent slippage of the samples from the clamps, 10 mm of material was inserted into each clamp giving an effective length of 40 mm. At least six trials were performed for each polymer.

3.2.9 Rheology

Rheological measurements were performed using a TA Instruments AR-1500ex stress-controlled rheometer with a 25 mm-diameter parallel-plate tool. Sandpaper was affixed to both plates to prevent slip. Circular samples 25 mm in diameter were cut from a sheet prepared by compressing 1.5g of polymer into a flat sheet using the hydraulic hot press. The sample thickness was measured at three different places (all samples were approximately 0.5 mm thick). The sample was then placed in the rheometer, the gap between the plates set to the lowest of these measurements, and the sample annealed at 100 ºC for 1 hour. The sample was then compressed to 90% of the original thickness prior to measurement. Small-angle oscillatory shear measurements were performed at angular frequencies between 0.1 and 100 rad/s with the

oscillating stress amplitude controlled at 100 Pa. All rheological measurements were done at 37 ºC. The data were averaged over at least four trials for each polymer.

3.2.10 Toxicity assay

Sample preparation: Test samples were melt-pressed to a thickness of 0.4 mm. The melt-pressed film was then cut into 1 cm × 1 cm squares. Samples were sterilized by washing with 70% ethanol and subsequently dried for 2 hours under UV light. They were placed in Petri dishes and incubated in 2 mL of Dulbecco's Modified Eagle Medium (DMEM, Invitrogen) supplemented with 10% fetal bovine serum (Invitrogen), 1% Glutamax (100x) solution and 1% Penstrep (100x) in an incubator at 37°C for 24 hours. The leachate was then removed and passed through a 0.2 μm filter.

MTT assay: C2C12 mouse myoblast cells were seeded in a Nunclon® 96-well U bottom transparent polystrol plate to obtain 10,000 cells/well in 100 μL of DMEM containing serum, glutamax and antibiotics as described above. The cells were allowed to adhere to the plate in a 5% CO_2 incubator at 37 °C for 24 hours. Next, the growth medium was aspirated and was replaced with either the positive control - sodium dodecyl sulfate (SDS) in the cell culture medium at concentrations of 0.2, 0.15, 0.10, or 0.05 mg/mL, serial two-fold dilutions of the leachate, or just the medium. The cells were then incubated at 37 °C (5% CO_2) for 24 hours. The medium was then aspirated and replaced with 110 μL of fresh medium containing 0.5 mg/mL (3-(4, 5-dimethylthiazol-2-yl)-2, 5-diphenyltetrazolium bromide) (MTT) reagent. After 4 hours of incubation (37 °C, 5% CO_2), the MTT solution was carefully aspirated and the purple crystals were dissolved by addition of 50 μL of spectroscopic grade dimethylsulfoxide (DMSO). After shaking (1 second, 2 mm amp, 654 rpm), the absorbance of the wells at 540 nm was read using an M1000-Pro plate reader (Tecan). The absorbance of wells not containing cells but treated by all of the above steps was subtracted as a background and the cell viability was calculated relative to wells containing cells that were exposed to just culture medium. No (0%) cell viability was detected for the cells exposed to the highest concentrations of the positive control sodium lauryl sulfate, confirming the sensitivity of the assay.

3.2.11 Evaluation of cell growth on films

C2C12 cells were maintained at 37 ºC and 5% CO_2 in Dulbecco's Modified Eagle Medium (Invitrogen) supplemented with 10% fetal bovine serum (Invitrogen) and supplemented with 1% Glutamax (100x) solution and 1% Penstrep (100x). First, microscope glass cover slips (circular, 25 mm diameter) were coated with a minimum layer of polymer by applying a 35 mg/mL solution of polymer in toluene and allowing the solvent to dry completely. The surfaces were sterilized by submersion in 70% ethanol, and were then left to dry completely under reduced pressure for 96 hours. The sterilized samples were placed in the wells of a 6-well plate and 5×10^5 cells in 2 mL of cell culture medium were seeded onto each surface. The samples were incubated for 48 hours, then fixed with 4% paraformaldehyde solution for 10 min. The samples were washed twice with phosphate-buffered saline (PBS) (Invitrogen) at pH 7.2, and then treated with 2 mL of acetone at -20 ºC for 5 minutes to permeabilize the membrane. After that, they were washed again with PBS, stained with Alexa Fluor 568 phalloidin (Invitrogen) and DAPI (Invitrogen) following the manufacturer's directions. The samples were washed again with PBS and placed face down onto glass microscope slides with ProLong® Gold Antifade Reagent (Invitrogen) and sealed. Confocal images were obtained using a confocal laser scanning microscope (LSM 510 Duo Vario, Carl Zeiss) using a 20× objective and excitation wavelengths of 405 (DAPI) and 578 nm (phalloidin). Cell were counted using Image Pro Plus software on 5 different images. Statistical analyses (ANOVA followed by Tukey's test) were performed using the software Excel.

3.3 Results and discussion

3.3.1 Synthesis and characterization of a PIB-PTX conjugate

The first goal of this work was the development of simple and rapid synthesis of a covalent PIB-PTX conjugate. To this end, carboxylic-acid-functionalized PIB (Scheme 3.1) derived from rubber containing either 2 mol% (**1a**) or 7 mol% (**1b**) of carboxylic-acid-functionalized monomer was prepared as described in Chapter 2. PTX, a potent mitotic inhibitor,[33, 34] was selected as the pharmaceutical agent as it is used in the commercial SIBS-based stent. The relationship between SIBS and the PIB system, in that SIBS contains PIB blocks, allows us to

compare the properties of this studied system to a commercial product.[29] Although widely used in anticancer treatment, PTX is also an excellent anti-proliferative for use with cardiovascular stents. From a synthetic perspective, Lataste and coworkers demonstrated that, despite the molecule's complexity, esterification of PTX resulted in a single isomeric monoester, as the C2' hydroxyl group is significantly more nucleophilic than the C7 hydroxyl group.[35] Consequently, a single regioisomeric PTX-PIB conjugate is expected (Scheme 3.1).

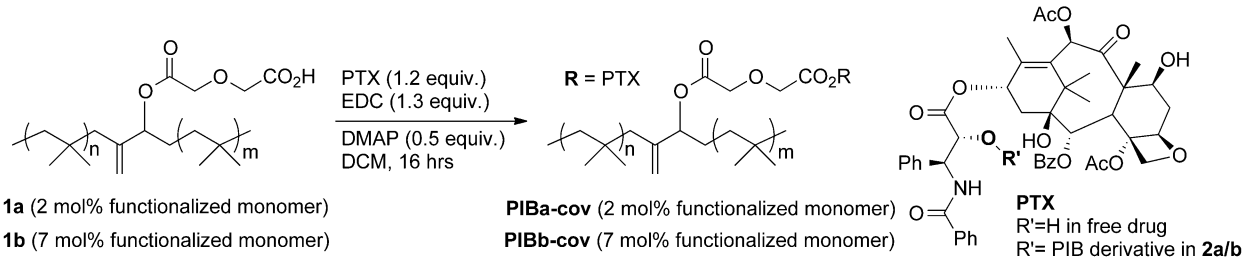

Scheme 3.1. Synthesis of PIB-PTX conjugates

As shown in Scheme 3.1, PTX was coupled to **1a**/**1b** using 1-ethyl-3-(3-dimethylaminopropyl)carbodiimide (EDC) in the presence of 4-(dimethylamino)pyridine (DMAP) in CH_2Cl_2 to afford the conjugates **PIBa-cov/PIBb-cov** with PTX loadings corresponding to the original degree of carboxylic acid functionalization. Proton nuclear magnetic resonance (^{1}H NMR) spectroscopy was used to confirm the chemical structure of the conjugate and to estimate the PTX loading. The spectra shown in Figure 3.1 indicate an up-field shift of the peak corresponding to the allylic proton of the polymer backbone (labeled 3) from 5.30 to 5.23 ppm. This is indicative of reaction near this site. A small amount of uncoupled carboxylic acid results in the small residual peak at 5.30 ppm in Figure 3.1b, but the data indicate that the coupling proceeded to greater than 95% conversion, which is remarkable for the conjugation of a large drug molecule to a polymer backbone. Based on this, the PTX content is approximately 24 wt% for **PIBa-cov**. In the conjugation between **1b** and PTX, the coupling regularly proceeded to greater than 80% conversion, resulting in approximately 48 wt% PTX for **PIBb-cov**. The other peaks corresponding to PTX in Figure 3.1 can be reliably assigned based on previous reports of PTX and PTX 2' ester conjugates.[35, 36] The large downfield shift of the peak corresponding to the 2' proton on PTX (labeled a) undergoes a large downfield shift from 4.81 to 5.60 ppm, and no resonance is observed at 4.81 ppm in the coupled material. In addition the peak corresponding to the adjacent benzyl proton (labeled b) shifts from 5.80 to 6.05 ppm.

These results indicate that the PTX resonances in **PIBa-cov** and **PIBb-cov** are due to conjugated PTX and not to physically entrapped PTX molecules, and the observed chemical shifts are consistent with selective formation of the 2' ester linkage.[36]

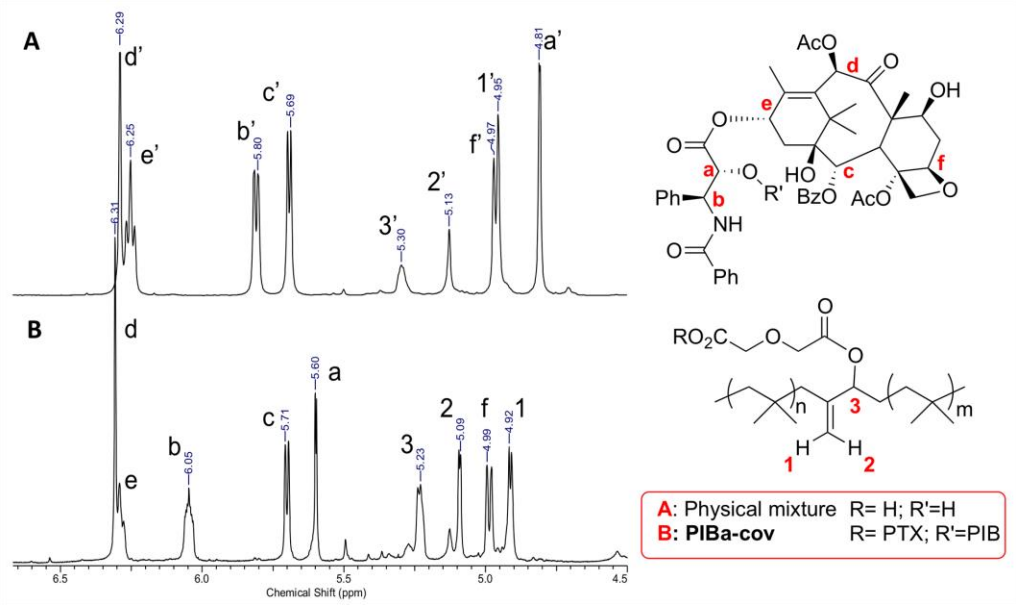

Figure 3.1. Portion of the ^{1}H NMR spectrum used to determine the success and extent of PTX coupling in **PIBb-cov**. A) Physical mixture of PTX and **1a**; B) Conjugate **PIBb-cov**. Letter and number resonance labels refer to the corresponding protons on PTX and PIB respectively.

Size exclusion chromatography (SEC) analysis of **PIBa-cov** suggested a slight increase in molecular weight over the carboxylic-acid-functionalized rubber and confirmed that no main-chain degradation had occurred during the synthesis. The compounds were also characterized by TGA and DSC (Appendix 3). The TGA traces for both materials demonstrated negligible mass loss below 200 °C, with 5 % mass loss at 312 ºC for **PIBa-cov**, and 240 ºC for **PIBb-cov**. The reported temperature of decomposition for free PTX is approximately 216 ºC, although the material does not decompose to gaseous byproducts at this low temperature.[28] DSC traces for the materials suggest that the introduction of even a large quantity of PTX has only a very limited effect on the T_g of the materials. The T_g of **1a** was previously reported to be -61 ºC (Chapter 2), and the introduction of 24 wt% PTX in **PIBa-cov** results in a similar T_g of -62 ºC. Similarly, the T_g of **1b** was reported to be -54 °C (Chapter 2), while that of **PIBb-cov** was measured to be -56 °C. While PTX is known to be a crystalline solid in its pure form with a melting point similar to

its degradation temperature, only trace peaks corresponding to melting transitions were observed in the range 100-150 ºC for both **PIBa-cov** and **PIBb-cov** (appendix). As the thermal degradation of **PIBb-cov** prevented the DSC analysis above 200 °C, the presence of a melting transition above 200 °C for this material cannot be fully excluded.

3.3.2 Preparation of polymer-PTX films for the PTX release study

The drug-release properties of films of the PIB-PTX conjugates **PIBa-cov** and **PIBb-cov** were studied, and compared with those of films of several other materials, as listed in Table 3.1. Physical mixtures of PTX and the carboxylic-acid-functionalized rubbers **1a** and **1b** were prepared with the same drug content as in **PIBa-cov** and **PIBb-cov**. In addition, samples of SIBS containing 10 and 20 wt% styrene, referred to as SIBS1 and SIBS2 respectively, physically combined with 24 wt% PTX as in the covalent conjugate **PIBa-cov** or 8.8 wt% PTX, as used in a commercial stent coating were also prepared.[13] Films were prepared by dissolving a fixed quantity of the polymer-drug material in toluene, filtering the solution, and drop casting it on a stainless steel surface.

Table 3.1. Composition, PTX loading, and thickness measurements of films used for the PTX release study. Uncertainties are standard deviations.

Sample Name	Polymer Composition	PTx wt.%	PTx immobilization	Film thickness before release (µm)	Film thickness after release (µm)[a]
PIBa-cov	**PIBa-cov**	~24	Covalent	50 ± 10	39 ± 9
PIBb-cov	**PIBb-cov**	~48	Covalent	52 ± 7	67 ± 2
PIBa-phy	**1a**	24	Physical	51 ± 4	65 ± 5
PIBb-phy	**1b**	48	Physical	25 ± 4	42 ± 9
SIBS1-24	SIBS (10% styrene)	24	Physical	58 ± 5	70 ± 4
SIBS2-24	SIBS (20% styrene)	24	Physical	60 ± 7	78 ± 2
SIBS1-9	SIBS (10% styrene)	8.8	Physical	52 ± 2	65 ± 3
SIBS2-9	SIBS (20% styrene)	8.8	Physical	54 ± 4	89 ± 2

[a]*Due to the destructive nature of the AFM thickness measurement, different films were used for the measurements before and after release*

The thickness of each film was measured by AFM prior to the drug release study. As shown in Table 3.1, most samples had thicknesses of 50-60 nm, with the exception of the mixture of **1b** and PTX, which was considerably thinner than the other samples. This difference likely results from the very different physical properties and intermolecular interactions in this material resulting from its high carboxylic acid content.

3.3.3 Release of PTX from polymer-PTX coatings

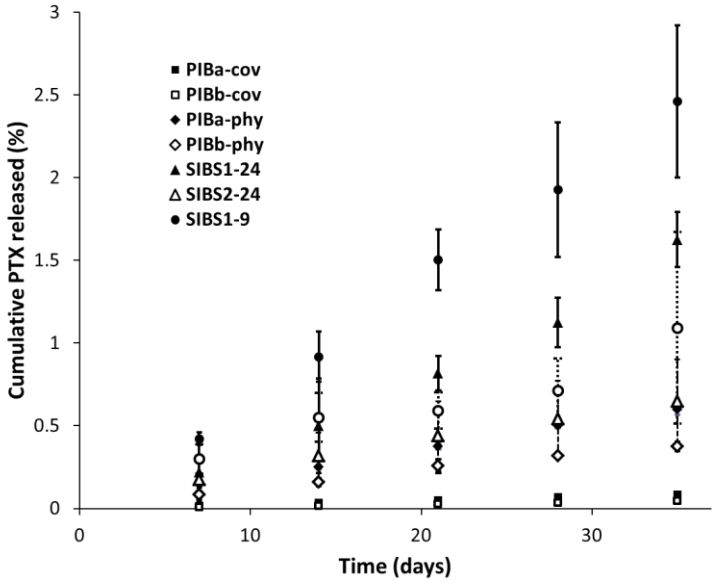

Figure 3.2. Cumulative fraction of PTX released from the polymeric films listed in Table 3.1 in aqueous solution at pH =7.4. Data points are the mean of three trials and error bars are standard deviations. Data points for **PIBa-cov** and **PIBb-cov** overlap, as do those for **SIBS2-24** and **PIBa-phy**.

The release of PTX from the polymer-PTX films was studied according to previously published protocols.[29, 37, 38] PTX release was measured weekly over a period of 35 days. The results are shown in Figure 3.2. All SIBS samples exhibited more rapid drug release than the PIB-based samples. SIBS1, which had the lower PS content, released the drug more rapidly than SIBS2, with a higher PS content. The PTX covalently bound to the modified PIB materials was released far more slowly than the physically-bound PTX at both PTX loadings. In addition, the rubbers with 7 mol% carboxylic acid released the drug more slowly than those with 2 mol% carboxylic acid loading in both the physically mixed and covalently bonded cases. Overall, these results

suggest that the PIB materials containing covalently bound PTX should exhibit a longer drug-release life-time than the SIBS materials. In the context of vascular stents, this may provide added protection against restenosis.

3.3.4 AFM imaging of films

To gain further insight into the release of PTX from the polymer-PTX films, AFM was used to image the surfaces before and after release. Representative phase and topography images are shown in Figure 3.3. Additional images of the other films are included in the appendix. As shown in Figure 3.3a, phase images **SIBS2-24** showed the presence of regions within the film having different physical properties. This may be indicative of phase separation of the film components such as PTX as well as the different blocks of the copolymer. The topography image in Figure 3.3b showed many hill-like features about 30 nm in height on the film surface. These features were not observed in AFM images of SIBS films without PTX.[39] This suggests that they are due to PTX, and that the PTX forms aggregates rather than being dispersed evenly throughout the films. Figure 3.3c showed that after 35 days of PTX release these features had disappeared and been replaced by holes in the film surface, indicating that the aggregates had been released over the course of the study. Similar results were observed for the other SIBS-based films (Appendices).

Similar behavior was observed for samples consisting of a physical mixture of PTX and carboxylic-acid-functionalized PIB. The phase image for these films (Figure 3.3d) showed two distinct phases which we suggest correspond to the rubber and PTX. The topography image (Figure 3.3e) is consistent with this interpretation, showing a series of small hills about 10 nm high rising from a relatively flat background. Following PTX release, a surface of rolling hills was exposed (Figure 3.3f) that were both higher and much larger in lateral extent. The phase image of this surface showed only a single phase (considering the large differences in vertical height, appendix 3) which we suggest is the remaining carboxylic-acid-functionalized rubber. The observed topography may result from the tendency of PIB to shrink during extended exposure to water.

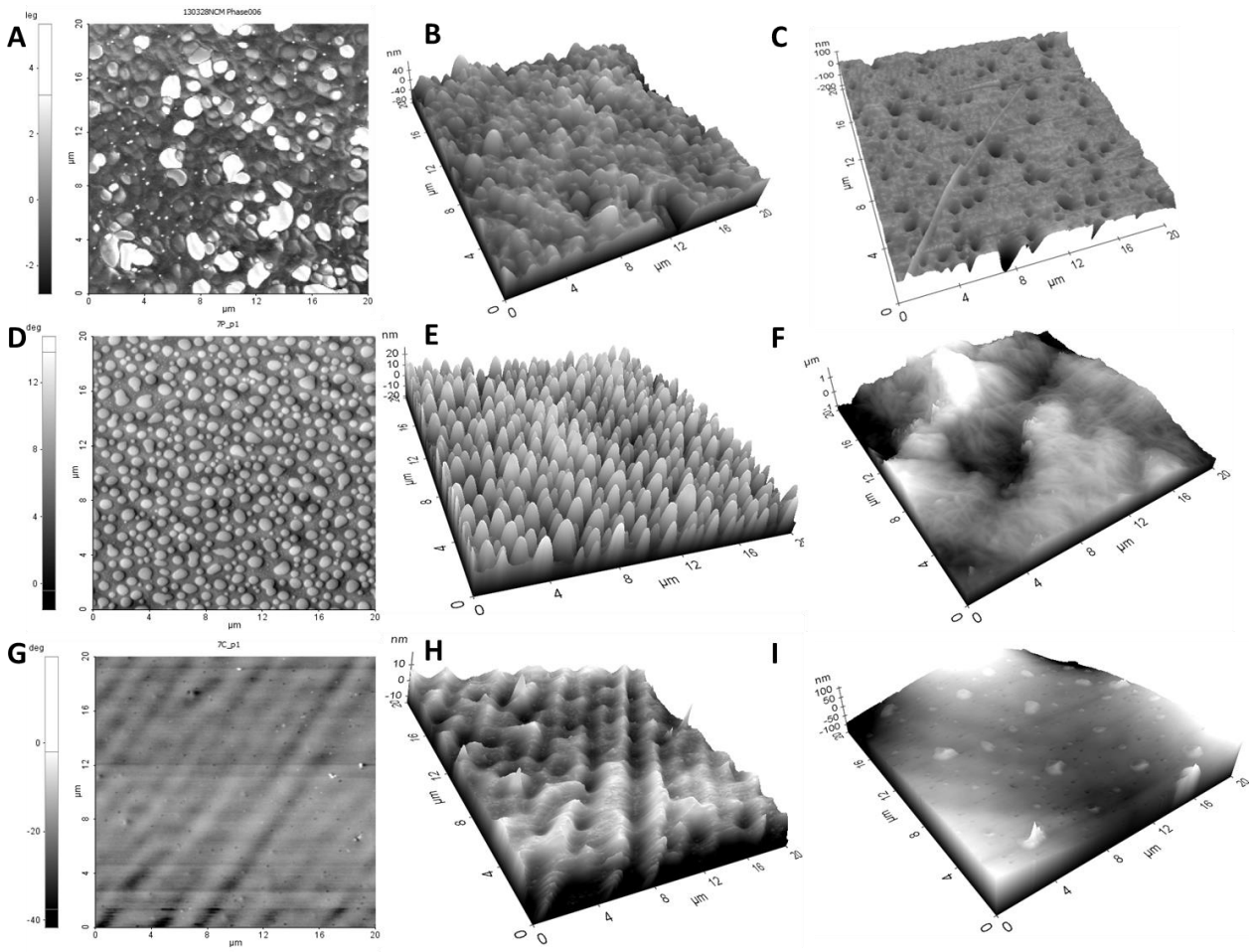

Figure 3.3 AFM images showing the polymer surface before and after the release study: A-C) **SIBS2-24**; D-F) **PIBb-Phy**; G-H) **PIBb-cov**. Phase images: A, D, G; topography images before PTX release: B, E, H; topography images after 35 days of PTX release: C, F, I. **The vertical axes of the topography images have different magnitudes.*

The AFM images of films of the covalent PIB-PTX conjugates appeared quite different from those of the physical mixtures. As shown in Figure 3.3g, the phase image suggested that the surface consisted mostly of a single phase. This is consistent with the covalent conjugation of PTX to the PIB backbone by the short diglycolic acid linker, which would favour a uniform distribution of the drug throughout the rubber. It is also consistent with the thermal properties of the materials described above. The topography image (Figure 3.3h) showed some surface roughness on the order of 2-3 nm, but did not exhibit the distinct hill-like features of the physical mixtures. After PTX release, the remaining surface was did not exhibit any topographical features. The large vertical range in Figure 3.3h is due to a few small sharp peaks which we

believe to be salt deposits from the release study that were not removed despite repeated water washes of the surface.

The root mean square (RMS) roughness of the surfaces before and after PTX release and the mean largest grain size (MLGS) [31] of the PTX aggregates were also measured by AFM. The results are provided in Table 3.2. In general, the two covalent PIB-PTX films show much lower roughness than any of the physical mixtures due to the absence of PTX aggregates on their surfaces. The surfaces of the physical mixtures of carboxylic-acid-functionalized rubber and PTX were intermediate in roughness. For a given PTX content, the SIBS films were considerably rougher. Even with only 8.8 wt% PTX, the surface of **SIBS2-9** was rougher than that of **PIBa-phy**, which contained 24 wt% PTX. At 24 wt% PTX, the **SIBS1-24** and **SIBS2-24** films were approximately 10 times rougher than **PIBa-phy**. These differences in roughness between the different physical mixtures can be partially accounted for by differences in the surface roughness of PIB and SIBS themselves,[39] but may also be influenced by differences in how PTX is physically incorporated into the two materials. As shown in Table 3.2, the diameter of the PTX aggregates on the surface of **PIBa-phy** was smaller than on SIBS, for the same PTX content, suggesting that the PTX may be dispersed more effectively in the carboxylic-acid-functionalized rubber.

Table 3.2. Surface characteristics of polymer-PTX films before and after drug release.

Sample	Roughness prior to release (nm)	Roughness after release (nm)	MLGS paclitaxel aggregates (μm^2)
PIBa-cov	1.1	2.5	N/A
PIBb-cov	2.9	4.9	N/A
PIBa-phy	0.9	630	0.2±0.2
PIBb-phy	8.2	430	0.5±0.2
SIBS1-24	48	38	1.7±0.5
SIBS2-24	28	24	1.1±0.8
SIBS1-9	3.9	4.0	0.013±0.009
SIBS2-9	5.0	3.5	0.11±0.07
Substrate	420	420	N/A

The roughnesses of the SIBS films did not change significantly after 35 days of exposure to aqueous buffer. All of the PTX originally on the film surface appeared to have been released from the films, and the peaks in the AFM images that were attributed to PTX were replaced by pits, resulting in a similar surface roughness. In constrast, films of the physical mixtures **PIBa-phy** and **PIBb-phy** showed a 100-fold increase in roughness resulting from exposure to the aqueous environment coupled with the loss of material from the surface. The roughness of the covalent conjugates **PIBa-cov** and **PIBb-cov** did not change appreicably after 35 days of release, consistent with the qualitative observation that AFM images of the surfaces appeared very similar before and after release.

Partial to complete delamination of the SIBS films from the 316L stainless steel substrate over the 35-day PTX release study was observed (appendix). This is likely related at least in part to the film damage that was observed by SEM. In contrast, most films prepared from the carboxylic-acid-functionalized PIB did not delaminate. The exception was **PIBb-phy**, which contained a very high (48 wt%) loading of PTX and partially delaminated. These results suggest that the carboxylic-acid-functionalized PIB materials may have some advantages over SIBS in terms of coating properties. Indeed, we have observed that the carboxylic-acid-functionalized rubbers **1a** and **1b** show enhanced adhesion to stainless steel over the parent RBs, and the covalent PTX conjugates of these materials may retain this advantageous property.

3.3.5 Mechanical and rheological properties

The above results suggest that the covalent PIB-PTX conjugates exhibit slow drug release and form smooth, stable films. The mechanical and rheological properties of the materials are also critical to their potential application in vascular stent coatings, as they must survive the process of stent expansion and the shear forces due to blood flow. The tensile properties of the materials are provided in Table 3.3, and are compared with the those of the unfunctionalized RBs, SIBS1 and SIBS2, as well as the carboxylic acid functionalized rubber derivatives **1a** and **1b**. Representative stress-strain curves are shown in Figure 3.4. Compared to the parent RBs, as well as the corresponding carboxylic-acid-functionalized derivatives, the PTX conjugates exhibit greatly increased ultimate tensile strength (UTS) and Young's modulus and a corresponding decrease in the maximum elongation, indicative of more brittle elastic behaviour. **PIBb-cov** has a higher Young's modulus and UTS than the **PIBa-cov**. This trend is similar to what was seen

with acid functionalized rubbers **1a** and **1b**, where greater changes in properties relative to the parent rubbers were observed with increased degrees of functionalization. In comparison with SIBS, the strength and modulus of the new conjugates are comparable to those of SIBS1 and SIBS2. However, they are much more brittle, and this limitation should be considered in their optimization and application.

Table 3.3. Tensile properties of polymers.

Material[a]	Young's modulus (MPa)	Ultimate tensile strength (MPa)	Elongation at break (%)
PIBa-cov	3.7 ± 0.8	3.9 ± 0.6	150 ± 20
PIBb-cov	6.6 ± 0.1	5 ± 2	110 ± 50
SIBS1	2.1 ± 0 .4	7 ± 2	800 ± 100
SIBS2	3.7 ± 0.4	11 ± 2	530 ± 30
1a	0.35 ± 0.08	1.7 ± 0.3	600 ± 100
1b	3.1 ± 0.8	4 ± 1	140 ± 30
PIBa	0.6 ± 0.1	0.23 ± 0.01	770 ± 70
PIBb	0.59 ± 0.02	0.8 ± 0.2	430 ± 30

[a] *Data for **1a**, **1b**, **PIBa**, and **PIBb** from McEachran et al.*

As stent coatings are designed to be used at physiological temperatures, the rheological behaviour of the materials was studied at 37 ºC. Figure 3.5 shows the storage and loss moduli, G' and G" respectively, of the PTX conjugates as a function of frequency ω, measured in small-amplitude oscillatory shear. Both moduli are only weakly dependent on frequency, and for both materials G' >> G". This behavior is typical of rubber-based materials. The moduli of **PIBa-cov** and **PIBb-cov** at ω=1 rad/s are compared with those of the parent carboxylic-acid-functionalized RBs and with SIBS in Figure 3.6. In both cases, the storage and loss moduli of the PIB were substantially increased by the introduction of the PTX, and the material with the higher PTX content had larger moduli than the lower PTX content material.

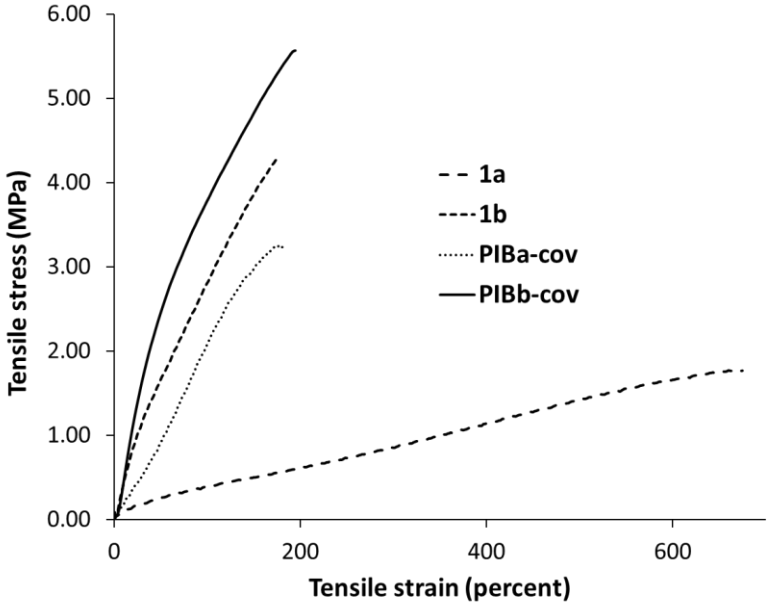

Figure 3.4. Representative tensile behaviour of covalent PTX conjugates and carboxylic-acid-functionalized rubbers.

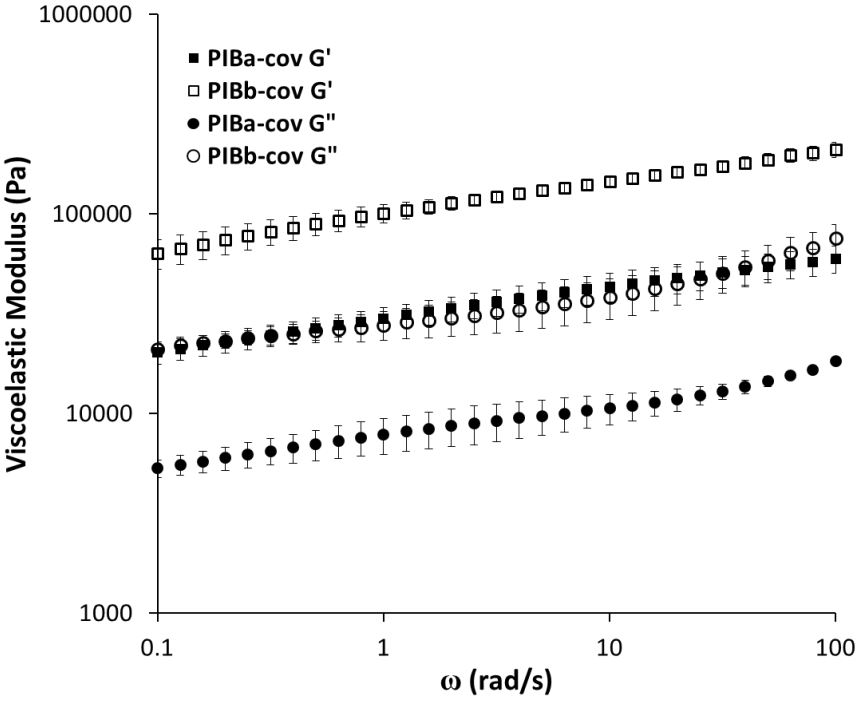

Figure 3.5. Storage and loss moduli G' and G" of the PTX-conjugated polymers **PIBa-cov** and **PIBb-cov**. The data have been averaged over at least three trials, and error bars show the standard deviation.

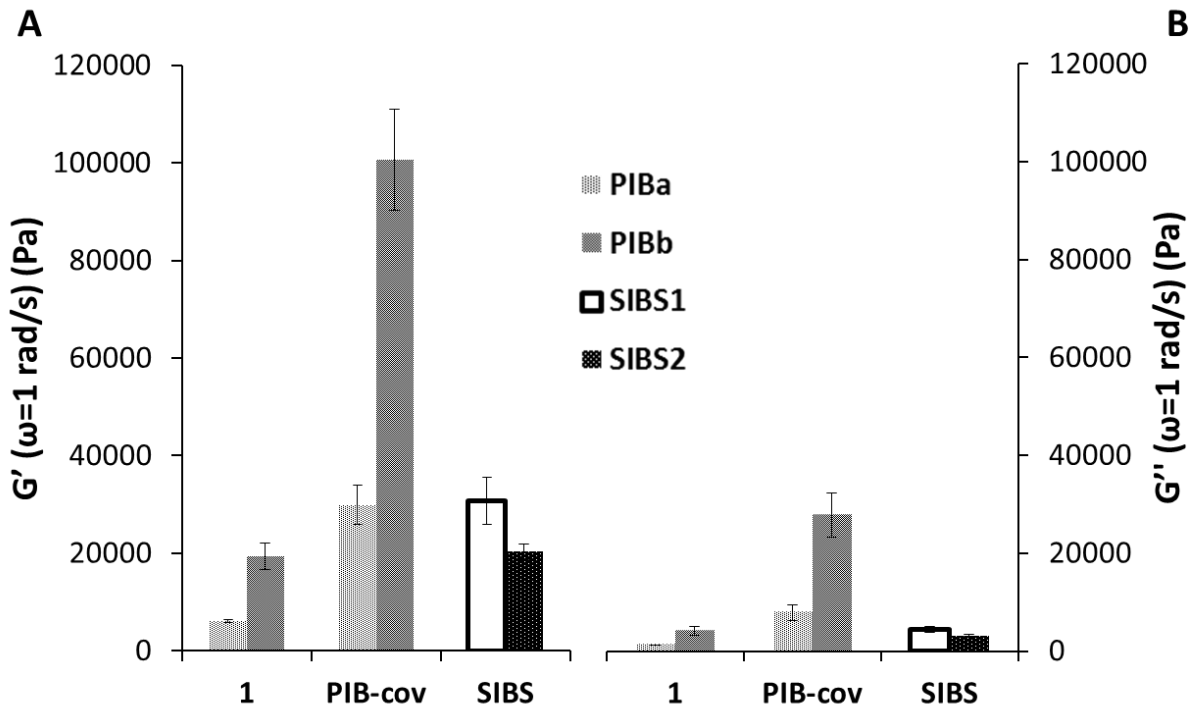

Figure 3.6. A) Storage modulus G' and B) loss modulus G'' of the polymers at ω=1 rad/s, of the carboxylic acid (**1**) and PTX-conjugated (**PIB-cov)** derivatives of both the low isoprene (**PIBa**) and high isoprene (**PIBb**) butyl rubber along with commercial **SIBS1** and **SIBS2** for comparison. The data have been averaged over at least three trails and error bars represent standard deviations.

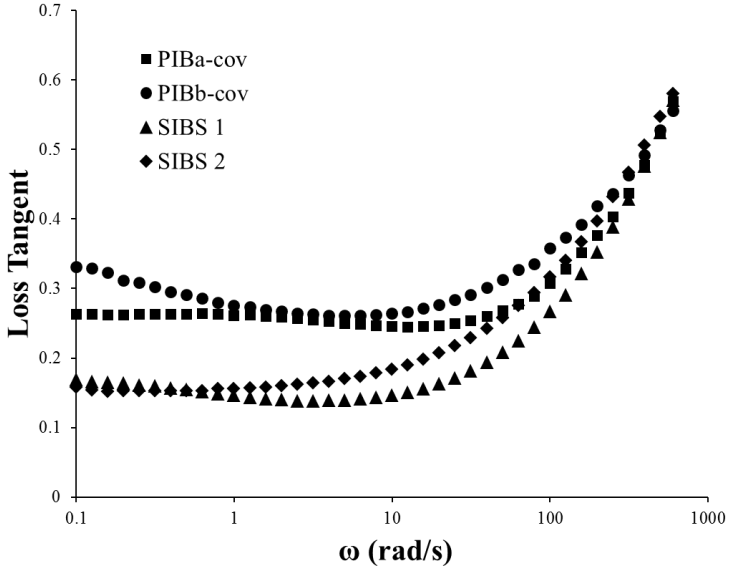

Figure 3.7. Loss tangent as a function of frequency.

Figure 3.7 shows loss tangent, the ratio of the loss modulus to the storage modulus. A value of loss tangent less than one is indicative of solid-like behavior. The behavior of the PTX-conjugated PIB and the SIBS materials is very similar as loss tangent is relatively insensitive to frequency at low frequencies, but begins to increase as the frequency rises. This increase in the ratio reflects the slight upturn in G" that is visible at high ω in Figure 3.5 and indicates that dissipation due to the motion of the polymer molecules on the scale of the distance between cross-links is becoming important at high frequencies. Similar behavior was observed for other RB derivatives in chapter 2. These results suggest that the RB derivatives behave similarly to the SIBS materials in terms of rheology.

3.3.6 Preliminary biological evaluation

The toxicity of the polymers and their effectiveness as anti-proliferative coatings is critical to their potential application in vascular stents. The polymers themselves are all insoluble in aqueous solution, but we investigated the possibility that they could be leaching toxic materials. Consequently, an MTT assay was performed using various concentrations of polymer leachate to assess cytotoxicity to C2C12 mouse myoblasts, a model cell line. High-density polyethylene (HDPE) was used as a negative control and sodium dodecyl sulfate was used as a positive control (toxicity detected at 0.2 μg/mL, results not shown). According to the ISO standard 10993-5,[40] a cell viability of greater than 70% is indicative of a non-toxic material. The results of the study are shown in Figure 3.8, and demonstrate that all materials tested are non-toxic by this measure. Importantly, no toxic leachates were detected in any of the PTX-free materials. However, PTX is highly cytotoxic, and the leachates of materials containg PTX did lead to modest reductions in cell viability. These modest reductions in cell viability likely result from the small quantities of PTX released during this assay.

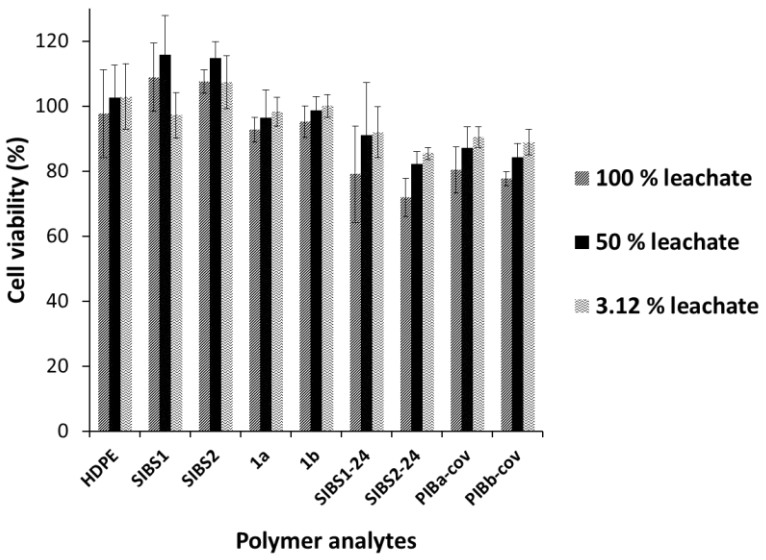

Figure 3.8. Viability of C2C12 mouse myoblast cells grown in various dilutions of leachate (cell culture medium that was incubated in the presence of polymer materials), as measured by an MTT assay.

The slow release of PTX from the covalent PIB-PTX conjugates and the lack of toxicity seen in the MTT assay raise the concern that the level of bioactive PTX in the coatings may not be sufficient to impart the desired anti-proliferative effects required for DES applications. To investigate this further, the growth of C2C12 cells on the coatings was investigated. Coatings of the polymeric material were seeded with C2C12 cells, incubated for 48 hours, then washed to remove cells that had not adhered to the polymer. The cells were fixed and stained with 4',6-diamidino-2-phenylindole (DAPI, light grey, cell nulcei) and Alexa Fluor 568 phalloidin (cytoskeletons, grey), then imaged by fluorescence confocal microscopy. As shown in Figure 3.9, both RB (2 mol% IP) (Figure 3.9a) and carboxylic-acid-functionalized rubber **1a** (Figure 3.9b) were very good substrates for cell growth. The cells appeared healthy, the cytoskeletons normal, and the cells well spread over the polymer surface.

The introduction of PTX resulted in significant changes. Most of the **PIBa-cov** surface was free from cells, although a few cells were able to adhere to isolated regions, as shown in Figure 3.9c. In these cases, the cells tended to stack rather then spread out on the surface, possibly taking advantage of a region of the rubber that has a low PTX content. Most of the

surface was free from intact cellular structures and only dead or dying cells and some cellular debris was observed (Figure 3.9d). On **PIBb-cov**, which had a higher PTX loading, no clusters of cells were detected (Figure 3.9e). A few isolated nuclei were observed, but no associated intact and healthy cytoskeletons. These results were quantified by counting the cells adhered to the surfaces. As shown in Figure 3.9f, there were on average, 17 times fewer cells on **PIBa-cov** and 65 times fewer on **PIBb-cov** than on the surface of **1a**. These results indicate that even though these materials release PTX very slowly , the release rate or the presence of the covelently-bound drug is sufficient to prevent cell adhesion and growth on the coatings. This is a promising indicator that these materials may be able to inhibit restenosis in an implanted stent.

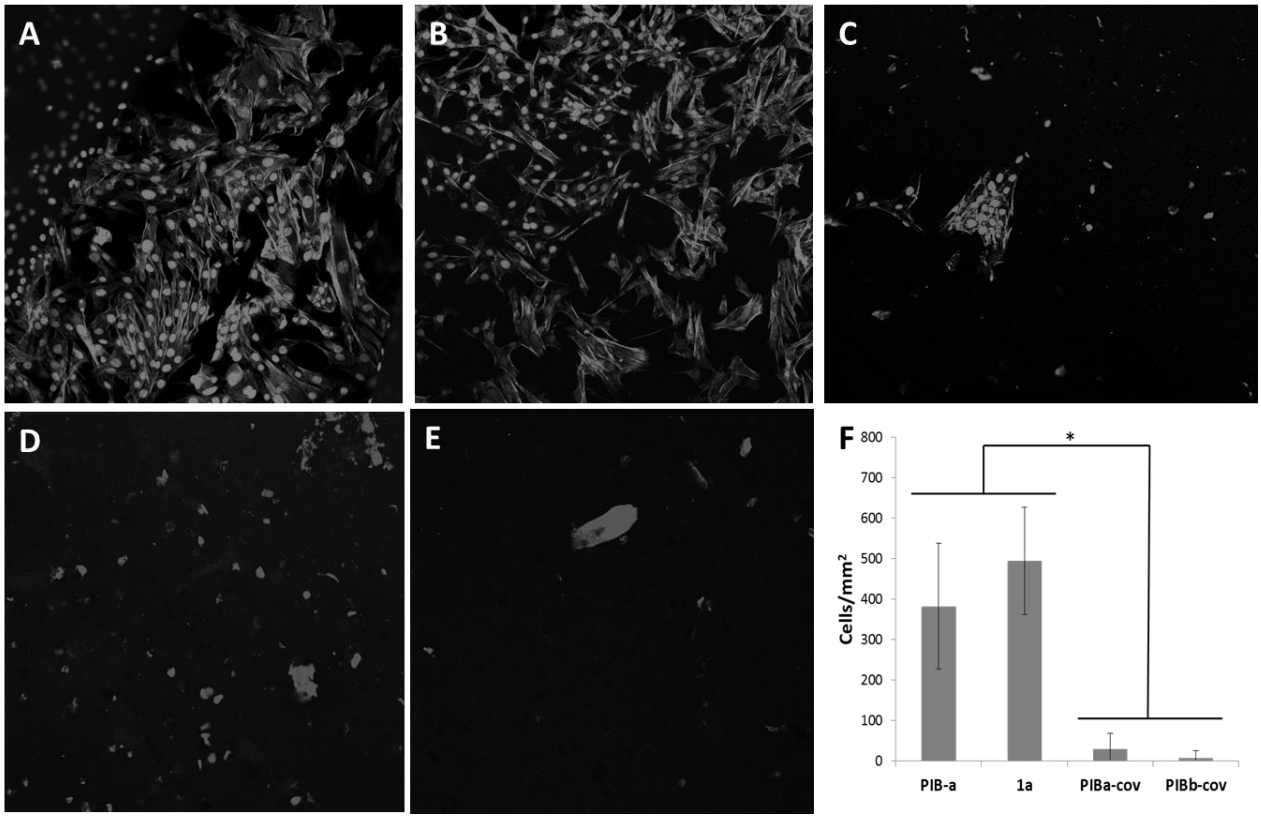

Figure 3.9. Confocal microscopy images of the results of the adhesion tests using C2C12 cells on: A) butyl rubber (2.2 % IP); B) **1a**; C) **PIBa-cov**, showing a rare region with cell adhesion; D) **PIBa-cov**, showing a more typical region of the surface; E) **PIBb-cov**; F) Cell counts for the polymers examined. (*P < 0.05). All images are the same magnification and each image represents an area of 0.4 x 0.4 mm

3.4 Conclusions

A simple, scalable synthesis of covalent PIB-PTX conjugates was developed. The PTX content of these novel materials was tuned to either 24 to 48 wt% by varying the content of pendant carboxylic acid moieties on the PIB derivatives. The release of PTX from coatings of the PIB-PTX conjugates was studied and compared to that from physical mixtures of PTX with the carboxylic-acid-functionalized PIB and with SIBS. It was found that the distribution of the PTX in the films was more uniform and the release of the PTX significantly slower for the covalent PIB-PTX conjugates. In contrast, physical mixtures of PTX with carboxylic-acid-functionalized PIB or SIBS displayed what is proposed to be PTX aggregates on the film surfaces, which were eroded over the course of the PTX release study. AFM showed that films of the PIB-PTX conjugates remained relatively intact throughout the study and exhibited enhanced adhesion to the stainless steel surface. The introduction of PTX into the polymer matrix changed the tensile and rheological properties of the material, increasing their elasticity and tensile strength. An MTT assay revealed that none of the covalent or physically mixed PTX systems released toxic levels of PTX. Despite this, the levels of PTX released or on the surface of the covalently conjugated PIB-PTX coatings were sufficient to prevent the adhesion and growth of C2C12 cells, suggesting that they show the desired anti-proliferative effect. Overall, the results of this study demonstrate that covalent PIB-PTX conjugates have promise as vascular stent coatings. Future work will involve further tuning of the biological and mechanical properties of these novel biomaterials.

3.5 References

1. Harris, R. E., Epidemiology of cardiovascular disease. In *Epidemiology of Chronic Disease: Global Perspectives*, Jones & Bartlett Learning: Burlington, Mass, 2013.
2. Libby, P.; Ridker, P. M.; Hansson, G. K., *Nature* **2011**, *473*, 317.
3. Moller, D. E.; Kaufman, K. D., *Ann. Rev. Med.* **2005**, *56*, 45.
4. Michos, E. D.; Sibley, C. T.; Baer, J. T.; Blaha, M. J.; Blumenthal, R. S., *J. Am. Coll. Cardiol.* **2012**, *59*, 2058.
5. Chyu, K.-Y.; Peter, A.; Shah, P., *Curr. Atheroscler. Rep.* **2011**, *13*, 405.
6. Kaliora, A. C.; Dedoussis, G. V. Z.; Schmidt, H., *Atheroscler.* **2006**, *187*, 1.
7. Christian Weber, Oliver Soehnlein.;Editor *Atherosclerosis : Treatment and Prevention*. Pan Stanford Pub, Singapore, 2013.
8. Iqbal, J.; Gunn, J.; Serruys, P. W., *Brit. Med. Bull.* **2013**, *106*, 193.
9. Scott, N. A., *Adv. Drug Deliv. Rev.* **2006**, *58*, 358.
10. Stettler, C.; Wandel, S.; Allemann, S.; Kastrati, A.; Morice, M. C.; Schömig, A.; Pfisterer, M. E.; Stone, G. W.; Leon, M. B.; de Lezo, J. S.; Goy, J.-J.; Park, S.-J.; Sabaté, M.; Suttorp, M. J.; Kelbaek, H.; Spaulding, C.; Menichelli, M.; Vermeersch, P.; Dirksen, M. T.; Cervinka, P.; Petronio, A. S.; Nordmann, A. J.; Diem, P.; Meier, B.; Zwahlen, M.; Reichenbach, S.; Trelle, S.; Windecker, S.; Jüni, P., *Lancet* **2007,** *370*, 937.
11. Stone, G. W.; Moses, J. W.; Ellis, S. G.; Schofer, J.; Dawkins, K. D.; Morice, M.-C.; Colombo, A.; Schampaert, E.; Grube, E.; Kirtane, A. J.; Cutlip, D. E.; Fahy, M.; Pocock, S. J.; Mehran, R.; Leon, M. B., *The New England Journal of Medicine.* **2007**, *356*, 998.
12. Cordis, *CYPHER Sirolimus-Eluting Coronary Stent of RAPTOR Over-The-Wire Delivery System*; 2011.
13. Boston Scientific Corporation. *The Element™ Stent Series*; Boston, 2009.
14. Kandzari, D. E., *Exp. Rev. Med. Dev.* **2010**, *7*, 449.
15. Kukreja, N.; Onuma, Y.; Serruys, P. W., *Exp. Rev. Med. Dev.* **2009**, *6*, 219.
16. Lemos, P. A.; Serruys, P. W.; van Domburg, R. T.; Saia, F.; Arampatzis, C. A.; Hoye, A.; Degertekin, M.; Tanabe, K.; Daemen, J.; Liu, T. K. K.; McFadden, E.; Sianos, G.; Hofma, S. H.; Smits, P. C.; van der Giessen, W. J.; de Feyter, P. J., *Circulation* **2004**, *109*, 190.
17. Serruys, P. W.; Kutryk, M. J. B.; Ong, A. T. L., *The New England Journal of Medicine.* **2006**, *354*, 483.

18. Ren, P.; Wu, Y.; Guo, W.; Li, S.; Chen, Y., *Tanxingti* **2013**, *23*, 13-17.
19. James, S. K.; Stenestrand, U.; Lindbäck, J.; Carlsson, J.; Scherstén, F.; Nilsson, T.; Wallentin, L.; Lagerqvist, B., *The New England Journal of Medicine.* **2009**, *360*, 1933.
20. Inoue, T.; Node, K., *Circ. J.* **2009**, *73*, 615.
21. Levy, Y.; Mandler, D.; Weinberger, J.; Domb, A. J., *Journal of Biomedical Materials Research Part B: Applied Biomaterials.* **2009**, *91B*, 441.
22. Ormiston, J. A.; Currie, E.; Webster, M. W. I.; Kay, P.; Ruygrok, P. N.; Stewart, J. T.; Padgett, R. C.; Panther, M. J., *Catheterization and Cardiovascular Interventions.* **2004**, *63*, 332.
23. Baldwin, F. P., *Rubber Chemistry and Technology*. **1979**, *52*, 77.
24. Jones, G. E.; Tracey, D. S.; Tisler, A. L., *Rubber Technology.* **2001**, 178.
25. Malmberg, S. M.; Parent, J. S.; Pratt, D. A.; Whitney, R. A., *Macromolecules* **2010**, *43*, 8456.
26. Bonduelle, C. V.; Gillies, E. R., *Macromolecules* **2010**, *43*, 9230.
27. Bonduelle, C. V.; Karamdoust, S.; Gillies, E. R., *Macromolecules* **2011**, *44* , 6405.
28. Priyadarshini K, Aparajitha U. K. *Paclitaxel Against Cancer: A Short Review. 2012.*
29. Strickler, F.; Richard, R.; McFadden, S.; Lindquist, J.; Schwarz, M. C.; Faust, R.; Wilson, G. J.; Boden, M. *Journal of Biomedical Materials Research Part A.* **2010**, *92A*, 773.
30. Michal, E. T.; Ding, N.; Buchko, C. J. *Methods for Covalently Immobilizing Anti-thrombogenic Material into a Coating on a Medical Device*. 2010.
31. Jackman, J.; Noestheden, M.; Moffat, D.; Pezacki, J. P.; Findlay, S.; Ben, R. N., *Biochem. Biophys. Res. Commun.* **2007**, *354*, 340.
32. ASTM, S*tandard Test Method for Tensile Properties of Thin Plastic Sheeting.* ASTM: New York, 2012; Vol. D882-12.
33. Schiff, P. B.; Fant, J.; Horwitz, S. B., *Nature* **1979**, *277*, 665.
34. Jordan, M. A.; Wilson, L., *Nat. Rev. Canc.* **2004**, *4*, 253.
35. Lataste, H.; Senilh, V.; Wright, M.; Guénard, D.; Potier, P., *Proc. Natl. Acad. Sci. (USA)* **1984**, *81*, 4090.
36. Deutsch, H. M.; Glinski, J. A.; Hernandez, M.; Haugwitz, R. D.; Narayanan, V. L.; Suffness, M.; Zalkow, L. H., *J. Med. Chem.* **1989**, *32*, 788.

37. Sirianni, R. W.; Jang, E.-H.; Miller, K. M.; Saltzman, W. M., *J. Control. Release* **2010**, *142*, 474-482.
38. Sipos, L.; Som, A.; Faust, R.; Richard, R.; Schwarz, M.; Ranade, S.; Boden, M.; Chan, K., *Biomacromolecules* **2005**, *6*, 2570.
39. Puskas, J. E.; Antony, P.; Kwon, Y.; Kovar, M.; Norton, P. R., *Macromolecular Symposia*. **2002**, *183*, 191.
40. ISO, *Tests for in vitro Cytotoxicity*. In *Biological Evaluation of Medical Devices*, ISO: Geneva, Switzerland, 2009; Vol. 10993-5.

Chapter 4

4 Synthesis and properties of covalent paclitaxel-arborescent polyisobutylene conjugates

4.1 Introduction

Polyisobutylene (PIB) and its copolymers with isoprene (IP), commonly referred to as butyl rubber (RB), exhibit many advantageous properties such as high chemical stability, elasticity, biocompatibility, and low permeability to gases and solvents.[1, 2] This rather unique set of properties has enabled the use of PIB materials in wide range commercial products including the bladders of sporting equipment, sealants, automobile tires, and even chewing gum. More recently, linear PS-PIB-PS (SIBS) triblock copolymers have been developed as the drug-eluting coating on the Taxus™ vascular stent.[3, 4] Over the past couple of decades, there have been many reports describing the derivatization of PIB at its terminus.[5-12] There are also many examples of the grafting of small molecules or linear polymer chains to the IP units randomly distributed throughout the RB backbone.[13-21] However, because of the chemical inertness of the PIB backbone and the relatively low IP content in RB, the scope of chemical structures accessible from linear PIB is still relatively limited.

Pioneering work by Puskas and coworkers demonstrated that the cationic polymerization of IB in the presence of an initiator-monomer ("inimer") such as 4-(2-methoxyisopropyl)styrene,[22, 23] or 4-(1,2-oxirane-isopropyl)styrene,[24] leads to arborescent (arb-PIB) or hyperbranched PIB. This technology opens many possibilities for PIB-based materials with new properties and functions. For example, Puskas and coworkers have prepared arb-PIB with terminal PS domains and found that the arborescent analogues retain the biocompatibility of SIBS, yet exhibit different mechanical and rheological properties, including improved fatigue life and lower creep.[25-28] In addition, arb-PIB with terminal IP-rich sequences (arb-PIB-*co*-IP) exhibits thermoplastic elastomer properties unlike RB.[29] The Gillies group has recently prepared arb-PIB grafted with PEG chains and compared them with the linear PIB-PEG graft

copolymers.[30] It was found that the arborescent materials exhibited similar resistance to protein adsorption as the linear analogues when cast as films, but different tensile properties and self-assembly behaviour in aqueous solution and in the solid state. Overall, this work reinforces the importance in polymer architecture in imparting specific properties to materials.

The Gillies group has also recently reported a chemical derivatization approach for the introduction of epoxides and allylic alcohols to RB, and in Chapter 2 this was extended to carboxylic acid moieties. It was found that the introduction of the carboxylic acid moieties in particular imparted increased tensile strength and rheological properties characteristic of ionic or hydrogen-bond mediated physical cross-linking. In addition, in Chapter 3 it was demonstrated that PTX could be conjugated to the carboxylic acid derivatives prepared from RB containing 2 or 7 mol% IP. This was of interest because PTX serves as an antiproliferative agent in the Taxus™ vascular stent, where its local delivery to the wall of the coronary artery prevents restenosis.[31] In proof of principle studies, it was found that covalent immobilization significantly slowed PTX release from the coating, while still inhibiting cell proliferation on the coating surface, thereby potentially enhancing the life-time of the stent coating.

With the aim of developing new functional materials and investigating the effect of polymer architecture on properties and function, we describe here the application of the IP derivatization sequence to provide epoxide, allylic alcohol, carboxylic acid, and PTX conjugate derivatives of arb-PIB-*co*-IP. The new materials are thoroughly studied to investigate their thermal, tensile and rheological properties. Coatings are prepared from the PTX conjugate and the rate of drug release and coating degradation is studied and compared to a control with physically incorporated PTX, and to a coating similar to that on the Taxus™ stent. Preliminary *in vitro* studies are also performed to probe the release of toxic molecules from the coatings and the adhesion and proliferation of mouse myoblast cells on these coatings.

4.2 Experimental

4.2.1 General procedures and materials

Arb-PIB-*co*-IP with 6 mol% IP (M_w = 216 kDa, PDI = 1.4) was prepared as previously reported[29] and provided by LANXESS Inc. (London, Canada). Solvents were purchased from Caledon Labs (Caledon, Ontario). PTX was purchased from LC laboratories (Woburn, Ma). All other chemicals were purchased from either Sigma-Aldrich or Alfa Aesar and were used without further purification unless otherwise noted. Dry toluene was obtained from an Innovative Technology (Newburyport, USA) solvent purification system based on aluminium oxide columns. CH_2Cl_2, pyridine, triethylamine and diisopropylethylamine (DIPEA) were freshly distilled from CaH_2 prior to use. ^{1}H NMR spectra were obtained in $CDCl_3$ at 600 MHz on a Varian Inova instrument. NMR chemical shifts (δ) are reported in ppm and are calibrated against residual solvent signals of $CDCl_3$ (δ 7.26). Infrared spectra were obtained of films from CH_2Cl_2 on NaCl plates or as KBr pellets using a Bruker Tensor 27 instrument. SEC was performed in tetrahydrofuran (THF) with a flow rate of 1 mL/min at 25 °C using an SEC instrument equipped with a Viscotek Max VE2001 solvent module and a Viscotek VE3580 RI detector operating at 30 °C. The separation technique employed two Agilent Polypore (300 mm × 7.5 mm) columns connected in series to a Polypore guard column (50 mm × 7.5 mm). The calibration was performed using PS standards. DSC and TGA were performed on a Mettler Toledo DSC 822e. For DSC, the heating/cooling rate was 10 °C/min between -120 to +150 °C. Glass transition temperatures (T_g) and melting temperatures (T_m) were obtained from the second heating cycle.

4.2.2 Synthesis of epoxide functionalized polymer 2.

Polymer **1** (10 g, 11 mmol of IP), cut into small pieces (<100 mg each), was dissolved in anhydrous $CHCl_3$ (400 mL) over a period of 8 h. To this solution was added a freshly dried solution of *m*-chloroperoxybenzoic acid (mCPBA) (5.5 g, 32 mmol) prepared by washing a CH_2Cl_2 solution (50 mL) of commercially available mCPBA (7.1 g, 77 % purity) using phosphate buffer, pH =7.2, followed by drying the organic phase with magnesium sulfate. The reaction was stirred for 16 h, and then diluted with CH_2Cl_2, and washed 3 times with 4 M NaOH, then 2 times with H_2O. The combined organic layers were then concentrated to ~200 mL, and precipitated into acetone (1 L) to provide polymer **2** (10 g, > 99%) as a white rubbery solid. T_g =

-66 ºC; ^{1}H NMR[1] (600 MHz, $CDCl_3$) δ 2.75-2.65 (m, 0.3H), 1.40 (s, 29H), 1.10 (s, 88H); IR (thin film on NaCl, chloroform): 923, 950, 1230, 1263, 1366, 1389, 1473, 2979 cm^{-1}. SEC: M_w = 194 kDa, PDI = 1.5.

4.2.3 Synthesis of allylic alcohol functionalized polymer 3

Epoxidized polymer **2** (9.0 g, 9.4 mmol of epoxide) was dissolved in $CHCl_3$ (400 mL). Concentrated HCl (2.5 mL, 30 mmol) was added and the reaction was stirred for 20 min, at which point NMR analysis suggested reaction completion. The reaction mixture was then neutralized using triethylamine (10 mL, 71 mmol), concentrated to 150 mL, and precipitated into acetone (500 mL) to provide polymer **4** (8.9 g, >99%) as a white rubbery solid. T_g = -65 ºC; ^{1}H NMR* (600 MHz, $CDCl_3$) δ 5.22 (s, 0.07H), 4.88 (s, 0.06H), 4.00-3.94 (m, 0.07H), 1.41 (s, 29H), 1.10 (s, 88H); IR (thin film on NaCl, chloroform): 923, 950, 1230, 1365, 1389, 1472, 2979, 3436 cm^{-1}. SEC: M_w = 200 kDa, PDI = 1.6.

4.2.4 Synthesis of carboxylic acid-functionalized polymer 4

Allylic alcohol functionalized polymer **3** (7.0 g, 7.3 mmol of alcohol) was dissolved in toluene (300 mL). The toluene and any residual water were then removed by azeotropic evaporation and replaced with fresh anhydrous toluene (300 mL). Diglycolic anhydride (17 g, 150 mmol) was added along with freshly distilled triethylamine (21 mL, 150 mmol) and 4-(dimethylamino)aminopyridine (DMAP) (1.8 g, 15 mmol). The reaction mixture was heated at 70 ºC for 36 h, and then was cooled to ambient temperature. It was then washed with 1 M HCl, saturated $NaHCO_3$, and water. The reaction was then precipitated into acetone (1 L), redissolved in toluene (250 mL) and reprecipitated into acetone (1L) to provide polymer **4** (7.0 g, > 98%) as an off-white rubbery solid. The material was immediately redissolved in toluene and stored as a solution as it physically crosslinks in its solid form on standing, resulting in an insoluble gel. T_g = -66 ºC; ^{1}H NMR* (600 MHz, $CDCl_3$) δ 5.29-5.21 (m, 0.02H), 5.13-5.10 (m, 0.02H), 4.97-4.85 (m, 0.04H), 4.32-4.16 (m, 0.53H), 1.41 (s, 29H), 1.10 (s, 88H); IR (thin film on NaCl, chloroform): 923, 950, 1228, 1367, 1390, 1486, 1742, 1756, 3006 cm^{-1}. SEC: M_w = 228 kDa, PDI = 1.6.

[1]H NMR integrations are provided for comparison purposes only. Due to the branched nature of the polymer, the relaxation times are much higher (>10 s) for the signals associated with the isoprene molecules and thus are significantly less than the expected value.

4.2.5 Synthesis of PTX-conjugated polymer 5

A solution of acid-functionalized polymer **5** (1.5 g, 1.6 mmol of acid) in toluene (15 mL) was diluted with anhydrous toluene (100 mL) under argon. In a separate flame-dried flask, 1-ethyl-3-(3-dimethylaminopropyl)carbodiimide hydrochloride (EDC·HCl, 400 mg, 2.1 mmol) was dissolved in dry CH_2Cl_2 (10 mL) along with DIPEA (600 µL, 3.3 mmol) and DMAP (100 mg, 0.8 mmol). This solution was cannulated into the toluene solution and the resulting reaction mixture was warmed to 40 ºC with stirring under an argon atmosphere for 20 min. At this point, a solution of PTX (2.2 g, 2.5 mmol) in CH_2Cl_2 (10 mL) was added at once, and the reaction mixture was stirred at 40 ºC for 48 h. After reaction completion (determined by NMR) the reaction mixture was cooled to ambient temperature, decanted from some gelled material present, and precipitated into acetone. The resulting solid was redissolved in $CHCl_3$ and reprecipitated into acetone to provide polymer **5** (2.1 g, 40%) as an off-white solid. A reaction conversion of 50% was determined by ^{1}H NMR spectroscopy using peak assignments based on those of the linear analogues. The analysis was based on a comparison of the PTX peak integration (average value = 0.03 H/proton) with those of the IP units (δ= 5.29-5.20, 5.15-5.08 which include signals corresponding to both the PTX conjugated and unconjugated IP derivatives on the backbone, 0.06 H/proton). This implies ~35 wt % PTX content. TGA mass loss analysis on two separate synthetic batches of **5** (each showing approximately 50 % NMR conversion) suggested PTX content of 35 and 40 % respectively, averaging to 37.5 wt% PTX in the conjugate prepared by this method. T_g = -65 ºC; ^{1}H NMR* (600 MHz, $CDCl_3$) δ 8.14 (bd, J = 6.4 Hz, 0.055H), 7.75 (bd, J = 6.9 Hz, 0.051H), 7.63-7.58 (m, 0.027H), 7.53-7.47 (m, 0.17H), 7.45-7.33 (m, 0.19H), 7.22-7.19 (m, 0.062H), 7.10-7.05 (m, 0.027H), 6.31-6.20 (m, 0.057H), 6.07-5.97 (m, 0.026H) 5.70-5.65 (m, 0.028H), 5.64-5.56 (m, 0.032H), 5.29-5.17 (m, 0.067H), 5.15-5.08 (m, 0.061H), 4.99-4.87 (m, 0.16H), 4.49-4.04 (m, 0.53H), 3.83-3.78 (m, 0.15H), 2.69-2.51 (m, 0.034H), 2.50-2.42 (m, 0.099H), 2.41-2.38 (m, 0.036H), 2.25-2.23 (m, 0.22H), 1.97-1.80 (m, 0.18H), 1.69 (s, 0.29H), 1.47-1.33 (m, 29.7H), 1.11 (s, 92H); IR (thin film on NaCl, chloroform): 923, 949, 1231, 1366, 1389, 1472, 1645, 1743, 2952 cm^{-1}. SEC: M_w = 234 kDa, PDI = 1.82.

4.2.6 Thermogravimetric analysis of PTX content

TGA was performed as described above in the general procedures and materials section for **4**, **5** (two different synthetic batches) and PTX itself. Arborescent rubber **4** lost 5.5 % of its mass between 170 ºC and 350 ºC, a result consistent with the other arborescent materials **1-3**. Arborescent PIB-PTX conjugate **5** lost 12.2 % of its mass over the same range. PTX lost 19 % of its mass over the same range. The difference in mass loss between **4** and **5** was attributed to PTX. This corresponded to a PTX content of 35 wt%, in agreement with the NMR evidence.

4.2.7 Tensile testing

1.5 g of polymer was compressed into a 0.3 mm thick flat sheet using a hydraulic hot press (Carver Hydraulic Unit Model # 3851 OC). Samples 60 mm x 5 mm in size were cut from this sheet. The tensile test was performed at ambient (22 ± 1 ºC) temperature using an Instron Universal Testing Machine (Model 5943) and Bluehill 2 software. 1-kN load cell at an extension rate of 400 mm/min was used, in accordance with ASTM D882 – 12.[32] Load and extension were calibrated prior to the test. To prevent slippage of the samples from the clamps of the testing machine, 10 mm of material were inserted into each clamp, leaving an effective sample length of 40 mm. At least six trials were performed for each polymer.

4.2.8 Rheology

Rheological measurements were performed using a TA Instruments AR-1500ex stress-controlled rheometer with a 25 mm-diameter parallel-plate tool. Sandpaper was glued to both plates to prevent slip. Circular samples 25 mm in diameter were cut from a sheet prepared by compressing 1.5 g of polymer into a flat sheet using the hydraulic hot press. The sample thickness was measured at three different places in each sample and was approximately 0.5 mm for all samples. The sample was then placed in the rheometer, the gap between the plates set to the lowest of the thickness measurements, and the sample annealed at 100 ºC for 1 h. Small-angle oscillatory shear and creep-recovery measurements were carried out on each sample. Oscillatory tests were performed at angular frequencies between 0.1 and 100 rad/s with the oscillating stress amplitude controlled at 100 Pa, which we confirmed was in the linear viscoelastic regime for our materials. Creep measurements were performed by applying a fixed shear stress of 100 Pa at time t = 0 and monitoring the deformation (strain) of the sample over time. At t = 10 min, the stress was reduced to zero and the relaxation of the strain monitored for a further 10 min. All rheological

measurements were done at 37 ºC. The data were averaged over at least four trials for each polymer.

4.2.9 Preparation of films on stainless steel

The surface of a stainless steel plate with dimensions of 31 mm × 11 mm was milled to obtain a smooth surface with a roughness of 420 nm. The films were prepared from a 100 mg/mL solution of the polymer in CH_2Cl_2. For the physically mixed samples, PTX was added to achieve the desired wt%. A 100 µL aliquot of polymer solution was drop cast onto the stainless steel plate. The sample was dried under reduced pressure prior to the release study. Each sample was prepared and studied in quadruplicate.

4.2.10 PTX release from polymer films

The release study was performed in 0.01 M phosphate buffer solution with pH = 7.4, containing 0.14 M NaCl, 2.7 mM KCl, and 0.05% (mass/vol) Tween 20 as a surfactant. The stainless steel plates were submerged in 10 mL of buffered solution in a vial. The solution was maintained at 37 °C. The buffer was removed every seven days for PTX analysis and replaced with fresh medium. Due to the low amounts of PTX released, the 10 mL of release medium was concentrated by lyophilization, followed by redissolution of the resulting solid in 2 mL of 80:20 water:acetonitrile with agitation. Samples were filtered through a 2.2 µm syringe filter prior to HPLC analysis, which was performed as previously reported in Chapter 3.

4.2.11 Atomic force microscopy

Surfaces for AFM analysis were those prepared for the release study. Surfaces were visualized using an XE-100 microscope from Park Systems. Images were obtained by scanning the surface at three different magnifications with fields of view of 20 µm × 20 µm, 5 µm × 5 µm, and 1 µm × 1 µm respectively. Scanning was performed using rectangular-shaped silicon cantilevers (T300, VISTA probes), with a nominal tip radius of 10 nm and spring constant of 40 N/m. Measurements were carried out under atmospheric conditions at ambient temperature. Topographic (height) and phase (force imaging mode) images were recorded simultaneously in tapping mode. The cantilever was oscillated at its resonance frequency of approximately 300 kHz. All images contained 256 data points per line for 256 lines, and the scan rate was

maintained at 1 Hz. Post-imaging analysis was carried out using XEI, version 1.7.0 from Park Systems. Images were flattened to remove curvature in both the x and y axes.

4.2.12 Toxicity assay

Test samples were melt-pressed to a thickness of 0.4 mm. The melt-pressed film was then cut into 1 cm × 1 cm squares. Samples were sterilized by washing with 70% ethanol and subsequently dried for 2 h under UV light. They were placed in Petri dishes and incubated in 2 mL of Dulbecco's Modified Eagle Medium (DMEM, Invitrogen) supplemented with 10% fetal bovine serum (Invitrogen), 1% Glutamax (100×) solution and 1% Penstrep (100×) in an incubator at 37°C for 24 h. The leachate was then removed and passed through a 0.2 µm filter. C2C12 mouse myoblast cells were seeded in a Nunclon 96-well U bottom transparent polystrol plate to obtain 10,000 cells/well in 100 µL of DMEM containing serum, glutamax and antibiotics as described above. The cells were allowed to adhere to the plate in an incubator at 37 °C (5% CO_2) for 24 h. Next, the growth medium was aspirated and was replaced with either the positive control (sodium dodecyl sulfate (SDS) in the cell culture medium at concentrations of 0.2, 0.15, 0.10, or 0.05 mg/mL), serial two-fold dilutions of the leachate, or just the medium. The cells were then incubated at 37 °C (5% CO_2) for 24 h. The medium was then aspirated and replaced with 110 µL of fresh medium containing 0.5 mg/mL (3-(4,5-dimethylthiazol-2-yl)-2,5-diphenyltetrazolium bromide) (MTT) reagent. After 4 h of incubation (37 °C, 5% CO_2), the MTT solution was carefully aspirated and the resulting purple crystals were dissolved by addition of 50 µL of spectroscopic grade dimethylsulfoxide (DMSO). After shaking (1 second, 2 mm amp, 654 rpm), the absorbance of the wells at 540 nm was read using an M1000-Pro plate reader (Tecan). The absorbance of wells not containing cells but treated by all of the above steps was subtracted as a background and the cell viability was calculated relative to wells containing cells that were exposed to just culture medium. No (0%) cell viability was detected for the cells exposed to the highest concentrations of the positive control SDS, confirming the sensitivity of the assay.

4.2.13 Evaluation of cell growth on films

C2C12 cells were maintained at 37 ºC and 5% CO_2 in Dulbecco's Modified Eagle Medium (Invitrogen) supplemented with 10% fetal bovine serum (Invitrogen), 1% Glutamax (100×) solution and 1% Penstrep (100×). Glass microscope cover slips (circular, 25 mm diameter) were

coated with polymer by drop casting 0.25 mL of a 35 mg/mL solution of polymer in toluene and allowing the solvent to dry completely. In addition to the polymer samples, an uncoated glass slide was used as a positive control. The surfaces were disinfected by submersion in 70% ethanol and then left to dry completely under reduced pressure for 96 h. The sterilized samples were placed in the wells of a 6-well plate and 5×10^5 cells in 2 mL of cell culture medium were seeded onto each surface. The samples were incubated for 48 h, then fixed with 4% paraformaldehyde solution for 10 min. They were washed twice with phosphate-buffered saline (PBS) (Invitrogen) at pH 7.2, and then treated with 2 mL of acetone at -20 ºC for 5 min to permeabilize the membrane. They were then washed again with phosphate buffered saline (PBS), then stained with Alexa Fluor 568 phalloidin (Invitrogen) and 4',6-diamidino-2-phenylindole (DAPI, Invitrogen) following the manufacturer's directions. The samples were washed again with PBS and placed face down onto glass microscope slides with ProLong Gold Antifade Reagent (Invitrogen) and sealed. Confocal images were obtained using a confocal laser scanning microscope (LSM 510 Duo Vario, Carl Zeiss) using a 20× objective and excitation wavelengths of 405 (DAPI) and 578 nm (phalloidin). Cells were counted using Image Pro Plus software from 3 different random regions on each of 3 surfaces per polymer. Statistical analyses (ANOVA followed by Tukey's test) were performed using the software Microsoft Excel.

4.3 Results and discussion

4.3.1 Synthesis

Arb-PIB-*co*-IP was prepared as previously reported, by the synthesis of arb-PIB using cationic polymerization of IB in the presence of the 4-(2-methoxyisopropyl)styrene inimer,[29] followed by the addition of IP, leading to short terminal blocks of isoprene-rich PIB-*co*-IP (Figure 4.1). Overall, the copolymer contained 6 mol% of IP relative to IB. As shown in Scheme 4.1, following the chemistry previously developed for linear RB, arb-PIB-*co*-IP **1** was epoxidized using mCPBA in $CHCl_3$ to provide the epoxide **2**. The epoxide was subsequently converted to the allylic alcohol **3** using HCl in $CHCl_3$. Reaction with diglycolic anhydride in the presence of DMAP as a nucleophilic catalysist provided the carboxylic acid functionalized polymer **4**. The PTX conjugate **5** was prepared by coupling of polymer **4** to PTX (**6**) using EDC in the presence of DMAP and DIPEA.

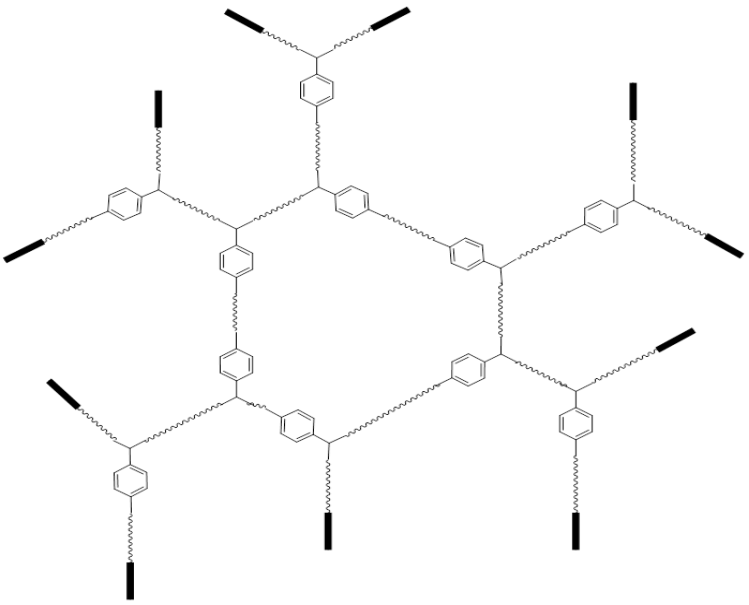

Figure 4.1. Schematic structure of arb-PIB-co-IP. The wavy lines represent the PIB. The inimer is represented by the branching styrenic moieties, and the thick black blocks represent IP-rich outer arms.

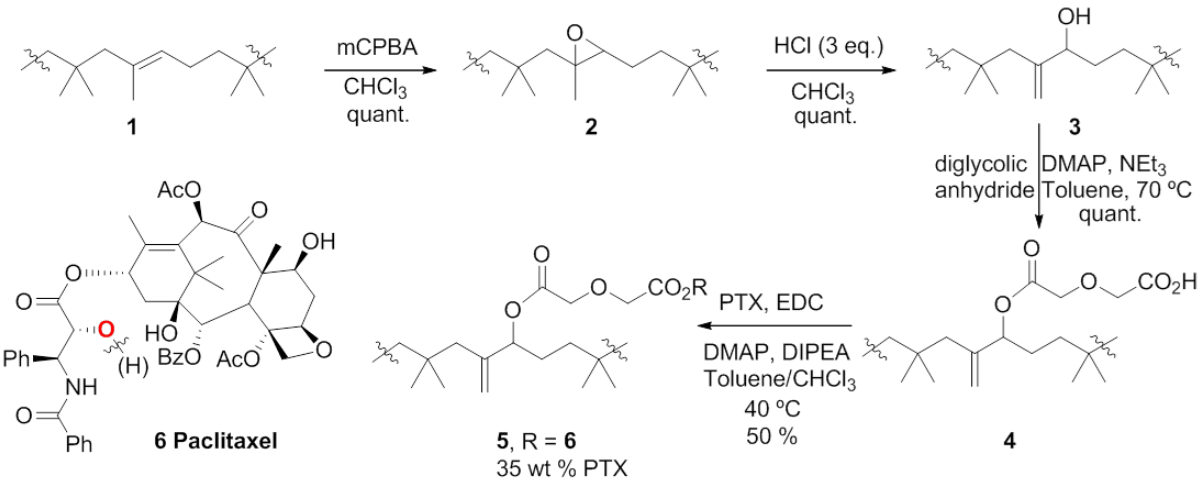

Scheme 4.1. Functionalization of arb-PIB-co-IP and conjugation with PTX (for simplicity, only the IP moiety, flanked by two isobutylene groups is shown).

This sequence is identical to that previously used for the preparation of linear analogues as described in Chapters 2 and 3 except that the final PTX functionalization was found to be slower for this arborescent derivative, and was consequently carried out at 40 ºC rather than at ambient temperature. This can likely be attributed to steric hindrance due to the close proximity of the IP moieties in these materials. The same issue was encountered in the preparation of PEG graft copolymers of arb-PIB-*co*-IP.[30]

SEC in THF was used to confirm that the functionalization chemistry did not result in degradation of the polymer backbone. Small fluctuations in the molar mass and polydispersity were observed throughout the functionalization process, likely resulting from the varying hydrodynamic volumes of the different functionalized materials and possible interactions of the more polar derivatives **3** and **4** with the column. However, the SEC traces and overall molecular weight characteristics remained relatively unchanged throughout the process, suggesting that the backbone remains intact (appendix).

IR spectroscopy confirmed the presence of the expected functional groups at each step. For example, a strong OH stretch was observed for the allylic alcohol **3** at 3436 cm^{-1}, which was not present for the epoxide derivative **2** and which significantly weakened for the carboxylic acid derivative **4**. Two carbonyl stretches were also observed in the spectrum of **4** at 1743 and 1756 cm^{-1}, corresponding to the expected ester and carboxylic acid functionalities of the conjugated diglycolic acid. Upon conjugation of PTX the carbonyl stretch appeared to shift to 1743 cm^{-1}, consistent with the conversion of the acid to an ester. However, the large numbers of ester and amide functionalities present on PTX complicate this analysis.

^{1}H NMR spectroscopy was used to monitor the reactions and the peaks were assigned based on those of the previously prepared linear analogues. The spectra showed that a clean conversion of functional groups was achieved for polymers **2** to **4**. However, peaks corresponding to the functionalized IP moieties, particularly those on the more polar derivatives **3** and **4**, exhibited integrations considerably lower than expected relative. This is presumably because they exhibit long relaxation times due to the branched structure and possibly some intra- and intermolecular aggregation. Based on a comparison of the integration of the PTX peaks in **5** relative to the functionalized IP moieties, approximately 50% conversion of the carboxylic acids to PTX esters was obtained, corresponding to ~35 wt% PTX in polymer **5**. This coupling yield is lower than those previously obtained for the linear analogues and may be attributed to the close proximity of the pendant carboxylic acid moieties, which results in steric hindrance to coupling.

Attempts to quantify the PTX content using ultraviolet-visible spectroscopy failed to provide any meaningful results as the conjugation of PTX to arb-PIB-*co*-IP results in a substantial change in its absorption properties and all attempts to hydrolyze the PTX from the polymer for subsequent quantification resulted in the precipitation of the polymer conjugate,

even at combinations of very low polymer concentrations (50 µg/ mL) and low (< 4 vol%) water content. To corroborate the NMR quantification, quantitative TGA was performed as PTX begins to thermally decompose at a lower temperature than the PIB itself.[33] Through comparison of the mass loss results for polymer **4**, **5**, and PTX, it was determined that the PTX conjugate **5** contained approximately 37.5 wt% PTX, in agreement with the NMR data.

4.3.2 Thermal properties

Thermogravimetric analysis (TGA) showed that polymers **1 - 4** exhibit onset degradation temperatures (T_o) of 381 - 392 ºC and peak degradation temperatures (T_p) of 399 - 411 ºC (Table 4.1). In contrast, the PTX conjugate **5** exhibits a two phase degradation profile with T_o of 239 ºC and 388 ºC, and T_p of 274 ºC and 403 ºC. As described above, the ~13% mass loss between 170 and 350 ºC can be attributed to degradation of the PTX, which is known to start degrading around 216 ºC.[33] The remaining polymeric material decomposes at a temperature similar to derivatives **1 - 4**. As shown in Table 4.1, all of the polymers **1** to **5** exhibit very similar glass transition temperatures (T_g), in the range -62 to -66 ºC. The PTX conjugate **5** exhibits a melting temperature (T_m) of 40 ºC, probably corresponding to the melting of PTX domains, as PTX is known to be a crystalline solid. The formation of small domains of PTX may be obtained with this arborescent material as the PTX is concentrated in the terminal blocks of the polymer. In contrast, no T_m was observed for linear conjugates where the PTX was randomly distributed along the polymer backbone.

Table 4.1. Thermal behavior of polymers **1 - 5** as measured by TGA and DSC.

Polymer	T_o (ºC)	T_p (ºC)	T_g (ºC)	T_m (ºC)
1	381	399	-62	--
2	384	400	-66.5	--
3	392	411	-65	--
4	389	406	-66	--
5	239, 388	274, 403	-65	40

4.3.3 Mechanical and rheological properties

As the mechanical properties of these materials will be critical for their use in all applications, the tensile and rheological properties of polymers **1** - **5** were investigated. Tensile testing was performed using the standard ASTM D882 – 12 protocol[32] and 6 samples of each material were evaluated. Representative stress-strain curves are plotted in Figure 4.2 and the Young's modulus (E), ultimate tensile strength (UTS), and elongation at break (El_t) are provided in Table 4.2. The tensile properties of the starting arb-PIB-*co*-IP **1**, epoxy derivative **2**, and allylic alcohol derivative **3** were similar to one another. E, UTS and El_t of **1** and **3** were similar to those of the linear analogues prepared, while E for **2** was two-fold higher than its linear analogues. The introduction of carboxylic acid moieties in polymer **4** resulted in an increase in E to 0.66 MPa from 0.39 MPa for polymer **3**. A significant increase in UTS and a decrease in El_t were also observed. These results are consistent with those of the linear analogue with similar carboxylic acid content, and may be attributed to the ability of the carboxylic acid moieties to form ionomeric or hydrogen-bonded domains within the material, which leads to a reinforcing effect. Introduction of PTX in polymer **5** resulted in an increase in E and UTS, and a further decrease in the El_t. These changes may result from a mechanical reinforcement effect imparted by the crystalline domains of PTX suggested by the thermal properties of **5** discussed above. However, the linear analogues also exhibited comparable mechanical properties despite no observable T_m.

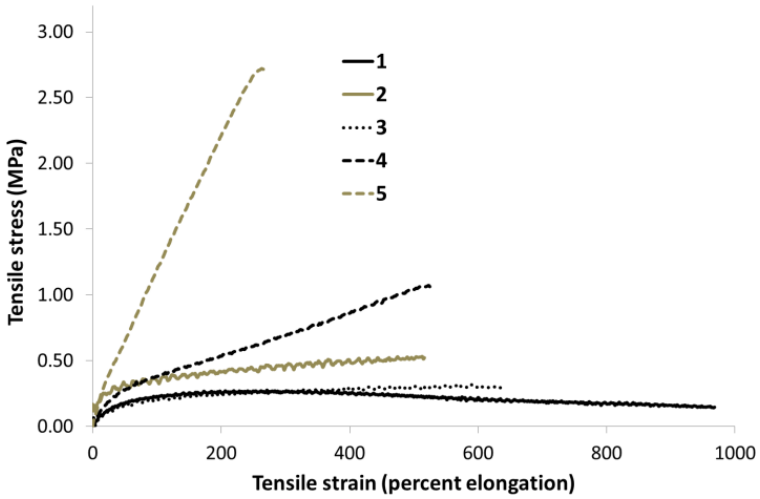

Figure 4.2. Representative results of tensile tests on polymers **1** to **5**.

Table 4.2. Tensile properties of polymers **1** to **5**.

Polymer	Young's modulus (E) (MPa)	Ultimate tensile strength (UTS) (MPa)	Elongation at break (El_t) (%)
1	0.47 ± 0.2	0.3 ± 0.2	900 ± 300
2	1.1 ± 0.4	0.58 ± 0.09	600 ± 100
3	0.39 ± 0.04	0.37 ± 0.03	600 ± 200
4	0.66 ± 0.06	1.2 ± 0.1	560 ± 30
5	1.4 ± 0.1	2.5 ± 0.6	240 ± 30

The rheological properties of the materials were measured as a function of frequency using small-amplitude oscillatory shear. Figure 4.3 shows the results of this study for the carboxylic acid functionalized polymer **4** and the PTX conjugate **5**. These serve as representative examples as all of the materials behaved similarly. Additional data are included in the appendix. Figure 4.3a shows the frequency dependence of the elastic and viscous moduli, G' and G" respectively, and Figure 4.3b shows loss tangent, the ratio of the loss and storage moduli, as a function of frequency. In all cases, the materials are strongly elastic: G' is greater than G" (loss tangent < 1) over the full frequency range and both moduli are only weakly dependent on frequency. The increase in loss tangent at high frequencies hints at an eventual crossover to glassy behavior. This behavior is typical of rubbery materials.[34]

Figure 4.4 shows G' and G'' at an angular frequency of $\omega = 1$ rad/s for all the arborescent materials. As noted above, G' is substantially greater than G'', as expected for a strongly elastic material. The moduli of polymers **1** to **4** are the same within experimental uncertainties. This result differs from that for the linear analogues (chapter 2), in which case G' and G" decreased significantly on introduction of allylic alcohols or carboxylic acid moieties. Both G' and G" increase by a factor of approximately ten relative to **4** when PTX is introduced, roughly twice as large as the increase in the moduli observed for the linear PTX conjugates. Furthermore, in the case of the linear analogue, the PTX conjugate had similar G' and G'' values as the parent rubber. For the arborescent material, the increase is almost an order of magnitude relative to the parent arborescent rubber. This difference in behavior between linear and arborescent materials may result from the presence of crystalline domains of PTX in polymer **5**, as suggested above.

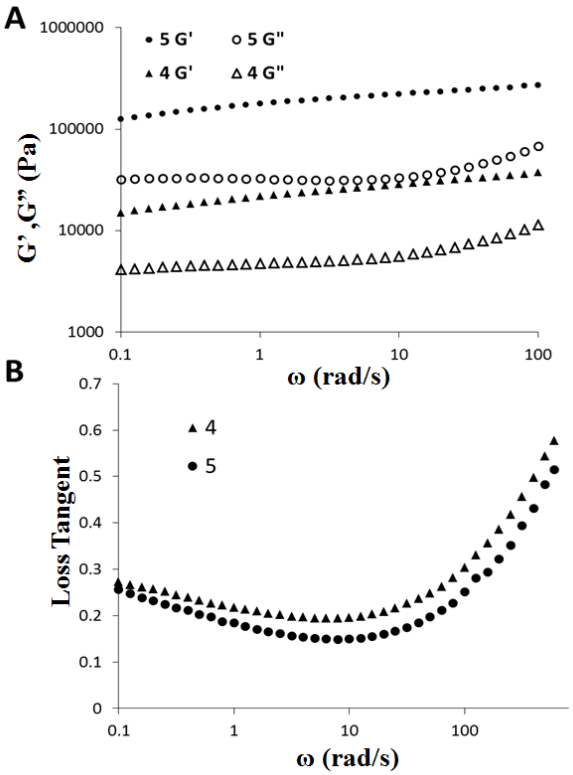

Figure 4.3. **A**: Frequency dependence of the elastic and viscous moduli, G' and G'', of the carboxylic acid functionalized polymer **4** and the PTX conjugated polymer **5**. Error bars are roughly the size of the plotted symbols and are omitted for clarity. B: loss tangent = G''/G' as a function of frequency for polymers **4** and **5**. Polymers **2** and **3** behave in a similar fashion.

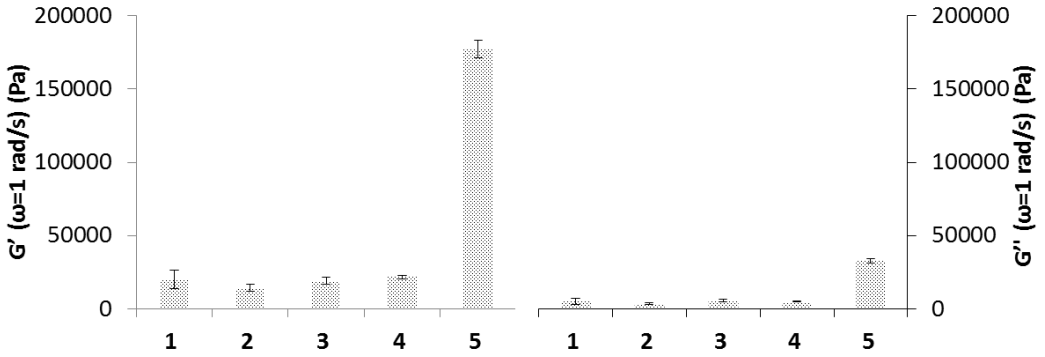

Figure 4.4. Elastic (G') and viscous (G'') moduli at 1 rad/s for polymers **1** to **5**. Error bars represent the standard deviation of at least three measurements.

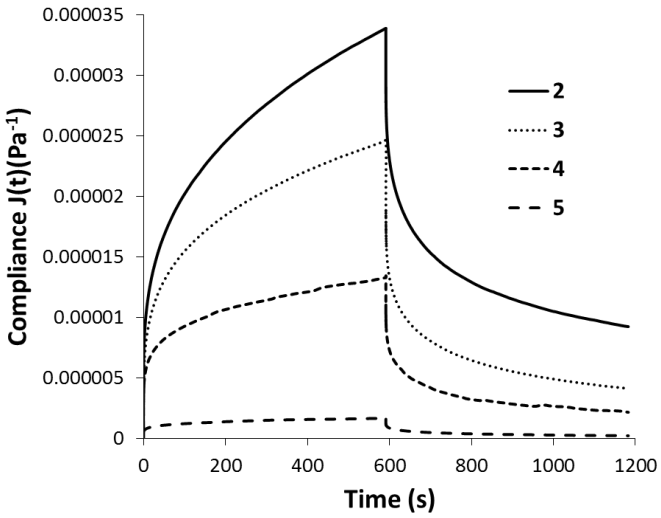

Figure 4.5. Creep and relaxation curves for polymers **2** to **5**. A constant shear stress of 100 Pa was applied at time t = 0, then removed at t = 600 s. The creep compliance J is plotted as a function of time.

The results of creep experiments are shown in Figure 4.5, in which the creep compliance J (strain divided by shear stress) is plotted for polymers **2-5** (abnormal slippage behavior was observed for arborescent rubber **1**, rendering the data from the creep analysis of this polymer meaningless). The hydrogen-bond forming derivatives **3** and **4** have a much lower compliance, and so are much more resistant to flow, than the epoxidized version **2**. The PTX conjugated polymer **5** is even more resistant to flow, and the almost complete recovery of the deformation when the applied stress is released indicates the strongly elastic behavior of the material. These results suggest that the PTX conjugated arborescent polymer has mechanical and rheological properties that are compatible with those required for a stent coating.

4.3.4 Preparation of films and release of PTX from polymer 5

To investigate the potential of the PTX conjugate **5** to provide controlled release of PTX, the rate of PTX release from polymer films was measured, and the physical changes in the films after drug release were investigated. For comparison, we also investigated a physical mixture of **4** and PTX at the same drug loading (**4 + PTX)** to determine the effect of covalent drug conjugation on the film's properties and release rate. A SIBS composed of 80:20 (wt:wt) PS:PIB containing 8.8 wt% of PTX (**SIBS + PTX**), similar to the material used in the TAXUS clinical stent coatings, was also studied. Films were prepared by drop casting solutions of the materials in CH_2Cl_2 onto stainless steel slides.

Table 4.3. Film thickness and roughness measurements before and after the PTX release study.

Sample	Film thickness before release (μm)	RMS roughness prior to release (nm)	Film thickness after release (μm)[1]	RMS roughness after release (nm)[1]
4 + PTX	21 ± 1	51	40 ± 10	55
5	20 ± 8	48	9 ± 1	60
SIBS + PTX	54 ± 4	5.0	89 ± 2	3.5

[1] Due to the destructive nature of the measurement, it was not possible to use exactly the same film for measurements before and after release.

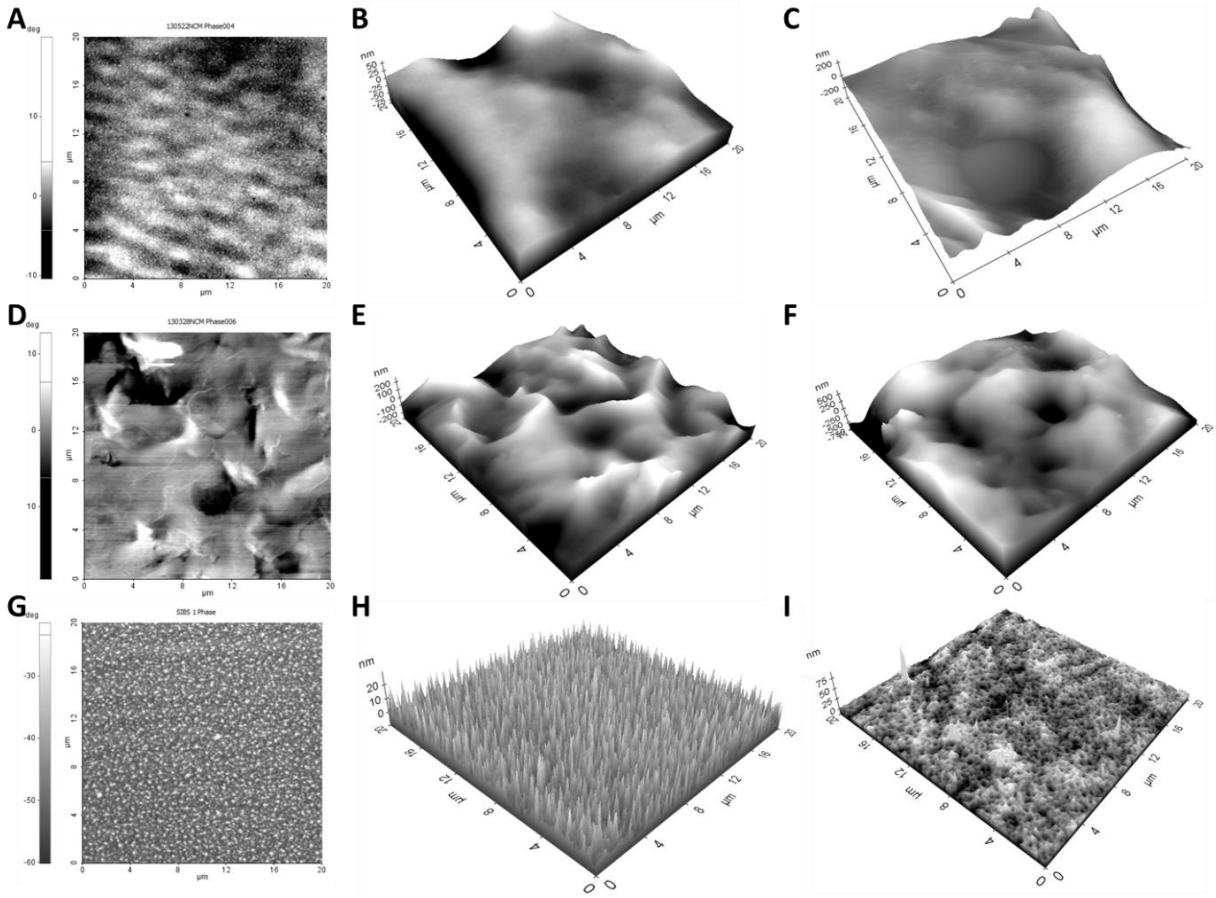

Figure 4.6. Representative AFM images showing the polymer surface before and after the release study. a-c) **4 + PTX;** d-f) **5**; g-i) **SIBS + PTX**. Phase images before release: a, d, g; Topography images before PTX release: b, e, h; Topography images after 35 days of PTX release: c, f, i. **The vertical axes of the topography images have different magnitudes.*

Prior to the release study, AFM was used to determine the film thickness and root mean square (RMS) roughness of one representative film of each material, and to image the surface topography. Phase images prior to PTX release, and topography images before and after release, are shown in Figure 4.6. Phase images after release are available in the appendies. As shown in Table 4.3, the film thicknesses ranged from 20 to 54 μm prior to the release of PTX. The surfaces of the films prepared from **5** and from **4 + PTX** were approximately 10 times rougher than the **SIBS + PTX** film. The high roughness of the **5** and **4 + PTX** films masked any phase separation. However, in the case of **SIBS + PTX**, roughly spherical domains with diameters on the order of 100 nm and that protrude from the surface by approximately 10 nm were observed in both phase and topography images. These features were not observed in AFM images of SIBS films without PTX,[35] which suggests that they may be due to aggregates of PTX. Similar features were also observed on the surface of the linear analogues of **4 + PTX**, which were considerably less rough than their arborescent analogues (and were not visible on the chemically conjugated linear analogue of **5**).

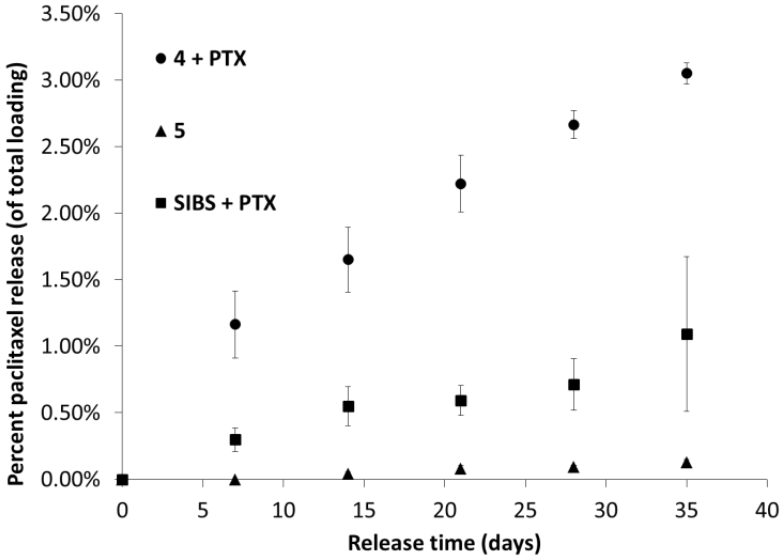

Figure 4.7. PTX release over 35 days from films of **4 + PTX**, **5**, and **SIBS + PTX** into phosphate buffer containing Tween 20 at 37 °C. Error bars represent the standard deviation of three measurements, error bars for **5** are the same size as or smaller than the data markers.

The release of PTX from the polymer films was measured using a previously reported protocol.[22, 23] The films were incubated in phosphate buffer containing Tween 20 at 37 °C, and measurement of the PTX concentration in the release media was measured at various times by HPLC. [36, 37] The results are provided in Figure 4.7. **4 + PTX** exhibits the most rapid PTX release, which may be facilitated by the polar carboxylic acid moieties on the polymer backbone that enhance water penetration into the film. Polymer **5** exhibits the slowest release of PTX. This can likely be attributed to the fact that hydrolysis of the ester linkage between PTX and the polymer backbone must occur before the PTX can be released from the film. The release rate from **SIBS + PTX** is intermediate. The same trends were observed for the linear analogues, and the overall release rate of PTX from the covalent arborescent conjugate **5** being very similar to that of the linear analogue. As shown in Table 4.3, the film roughness did not change appreciably during the release study. No significant changes in surface topography were observed for the films of **4 + PTX** (Figure 4.6c) or **5** (Figure 4.6f). However, the **SIBS + PTX** (Figure 4.6i) film became pitted with holes, presumably due to the erosion of PTX domains on the surface.

4.3.5 Preliminary biological evaluation

Preliminary biological studies were performed to investigate the cytotoxicity of the materials and their ability to support cell growth. C2C12 mouse myoblasts were used as a model cell line. To determine if toxic molecules were released from the polymer, the films were incubated in cell culture medium for 24 h. This medium was then added to the C2C12 cells at different dilutions. An MTT assay was performed to assess cell viability after 48 h. As shown in Figure 4.8, no significant toxicity was observed for any of the materials, with cell viabilities above 70 %.[38] This suggests that no toxic chemical intermediates leach from the functional polymer derivatives **1** - **4**. In addition, the lack of significant toxicity for the PTX conjugate **5** indicates that the concentration of PTX released in this study was not sufficient to kill the cells.

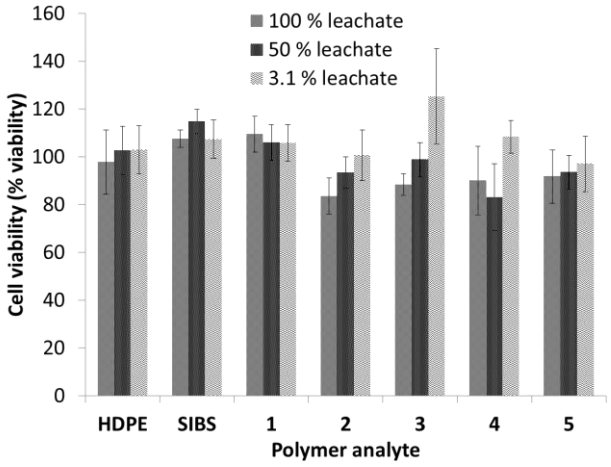

Figure 4.8. Viability of C2C12 mouse myoblast cells grown in various dilutions of cell culture medium that was incubated in the presence of polymer materials, as measured by an MTT assay. Only **5** contains PTX (chemically conjugated). High density polyethylene (HDPE) was used as a negative control and sodium dodecyl sulfate (SDS) was used as a positive control (not shown).

To be useful as DES coatings, the materials must release PTX in a manner that allows the drug to exhibit its desired anti-proliferative activity, while remaining non-toxic. To investigate this, we studied the growth of C2C12 cells grown directly on the films of the PTX conjugate **5**, the carboxylic acid-functionalized polymer **4** without PTX, and control glass cover slips, which is known to be a good substrate for cell growth. Cells were seeded on the surfaces. After 48 h, the cells were fixed and their nuclei were stained with DAPI, while their cytoskeletons were stained with Alexa Fluor 568 phalloidin. Figure 4.9 shows confocal microscope images of the cells on each of the three surfaces studied. Figures 4.9a and b show that cells formed well-spread, confluent monolayers on both the glass slide and polymer **4**. In contrast, there were far fewer cells on the PTX conjugate **5** (Figure 4.9c,d), and the cells that were present did not appear to have healthy cytoskeletons as can be seen in Figure 4.9c. This is consistent with our previous observations for linear PIB-PTX conjugates and with the action of PTX as a microtubule dissociation inhibitor that prevents the cell from reorganizing its cytoskeleton.[39] These results suggest that although the release of PTX is very slow, it is still sufficient for the drug to exhibit its desired anti-proliferative activity.

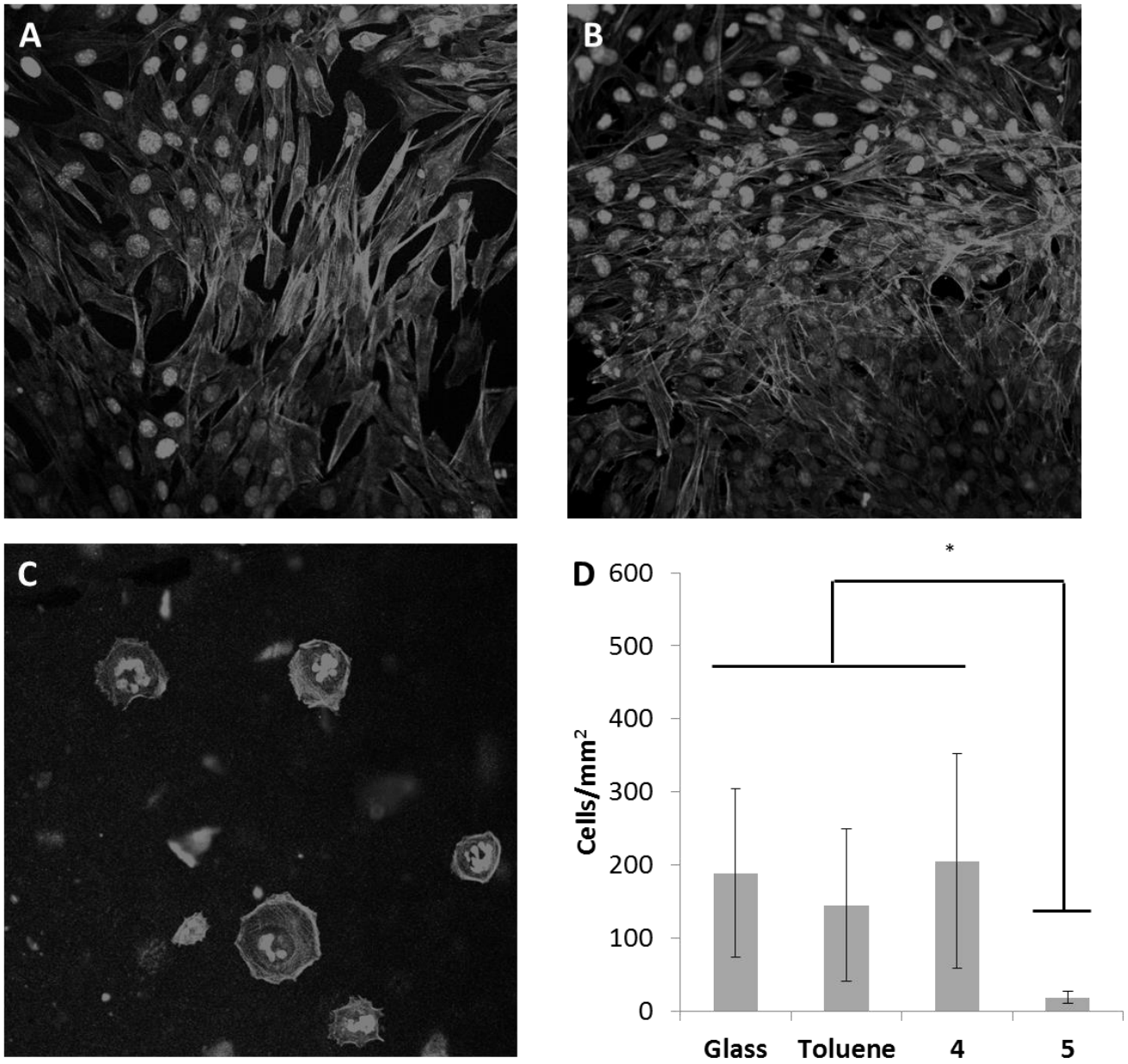

Figure 4.9. Confocal microscopy images of C2C12 cells on: A) glass slide; B) carboxylic acid-functionalized polymer **4**; C) PTX conjugate **5**; D) cell counts for the polymers examined. (*P < 0.05 by one-way ANOVA test followed by Tukey's test). The cell nuclei are stained with DAPI (light grey) and the cytoskeletons are stained with Alexa Fluor 568 phalloidin (grey). All images are the same magnification and each image represents an area of 0.4 x 0.4 mm^2.

4.4 Conclusions

The chemistry previously developed for the functionalization of linear RB was successfully used to prepare epoxide, allylic alcohol, carboxylic acid, and PTX derivatives of arb-PIB-co-IP and the properties of these materials were compared to those of their linear analogues. Thermally these materials exhibited similar properties to the linear analogues; however, a T_m was observed for the arborescent PTX conjugate **5** that was not apparent in the linear analogue. This suggests that the introduction of the PTX at high density in the outer blocks of the arborescent material allows it to phase separate to a degree, which was not possible for the randomly distributed PTX molecules in the linear material. In examining the different derivatives through tensile and rheological testing, it was found that the differences in properties between the epoxide, allylic alcohol, and carboxylic acid were generally smaller for the arborescent polymer than for the analogous linear materials. However, the introduction of PTX imparted significant changes in the tensile and rheological properties of both the linear and arborescent materials. The arborescent PTX conjugate exhibits slow PTX release relative to physical mixtures of PTX with either SIBS or polymer **4**, which can be attributed to the requirement for ester bond hydrolysis to occur prior to drug release rather than simple diffusion. The PTX release rate from the arborescent conjugate was very similar to that of the linear analogue. None of the studied materials released toxic concentrations of PTX or other impurities as measured by an MTT assay on C2C12 cells. However, the PTX present in and/or released from films of the covalent PTX conjugate was sufficient to prevent the growth of C2C12 cells on the material, a promising property suggesting that the immobilized drug retains properties characteristic of those required in DES applications. These results, coupled with their release profile and acceptable mechanical properties make this arborescent PTX conjugate a promising candidate for further evaluation as a DES coating.

4.5 References

1. Greve, H.-H., Threadingham, D. In *Ullmann's Encyclopedia of Industrial Chemistry*, Wiley-VCH Verlag GmbH & Co. KGaA: 2000.
2. Threadingham, D.; Obrecht, W.; Wieder, W.; Wachholz, G.; Engehausen, R. In *Ullmann's Encyclopedia of Industrial Chemistry*; Wiley-VCH Verlag GmbH & Co. KGaA: 2000.
3. Pinchuk, L.; Wilson, G. J.; Barry, J. J.; Schoephoerster, R. T.; Parel, J.-M.; Kennedy, J. P., *Biomaterials* **2008**, *29*, 448.
4. Puskas, J. E.; Muñoz-Robledo, L. G.; Hoerr, R. A.; Foley, J.; Schmidt, S. P.; Evancho-Chapman, M.; Dong, J.; Frethem, C.; Haugstad, G., *Wiley Interdiscip. Rev. Nanomed. Nanobiotechnol.* **2009**, *1*, 451.
5. Percec, V.; Guhaniyogi, S.; Kennedy, J.; Ivan, B., *Polym. Bull.* **1982**, *8*, 25.
6. Gao, B.; Kops, J., *Polym. Bull.* **1995**, *34*, 279.
7. Kurian, P.; Zschoche, S.; Kennedy, J. P., *Journal of Polymer Science Part A: Polymer Chemistry.* **2000**, *38* , 3200.
8. Groenewolt, M.; Brezesinski, T.; Schlaad, H.; Antonietti, M.; Groh, P. W.; Iván, B., *Advanced Materials.* **2005**, *17*, 1158.
9. Storey, R. F.; Scheuer, A. D.; Achord, B. C., *Polymer* **2005**, *46*, 2141.
10. Haraszti, M.; Tóth, E.; Iván, B., *Chemistry of Materials.* **2006**, *18*, 4952.
11. Jakubowski, W.; Tsarevsky, N. V.; Higashihara, T.; Faust, R.; Matyjaszewski, K., *Macromolecules* **2008**, *41*, 2318.
12. Kali, G.; Vavra, S.; László, K.; Iván, B., *Macromolecules* **2013**, *46* , 5337.
13. Parent, J. S.; White, G. D. F.; Whitney, R. A.; Hopkins, W., *Macromolecules* **2002**, *35*, 3374.
14. Guillén-Castellanos, S. A.; Parent, J. S.; Whitney, R. A., *Journal of Polymer Science Part A: Polymer Chemistry.* **2006**, *44*, 983.
15. Guillén-Castellanos, S. A.; Parent, J. S.; Whitney, R. A., *Macromolecules* **2006**, *39*, 2514.
16. McLean, J. K.; Guillen-Castellanos, S. A.; Parent, J. S.; Whitney, R. A.; Resendes, R., *European Polymer Journal.* **2007**, *43*, 4619.
17. McLean, J. K.; Guillén-Castellanos, S. A.; Parent, J. S.; Whitney, R. A.; Kulbaba, K.; Osman, A., *Ind. Eng. Chem. Res.* **2009**, *48*, 10759.
18. Bonduelle, C. V.; Gillies, E. R., *Macromolecules* **2010**, *43*, 9230.
19. Bonduelle, C. V.; Karamdoust, S.; Gillies, E. R., *Macromolecules* **2011**, *44*, 6405.

20. Karamdoust, S.; Bonduelle, C. V.; Amos, R. C.; Turowec, B. A.; Guo, S.; Ferrari, L.; Gillies, E. R., *Journal of Polymer Science Part A: Polymer Chemistry*. **2013**, *51*, 3383.
21. Abd Rabo Moustafa, M. M.; Gillies, E. R., *Macromolecules* **2013**, *46*, 6024.
22. Puskas, J. E.; Grasmüller, M., *Macromolecular Symposia*. **1998**, *132*, 117.
23. Paulo, C.; Puskas, J. E., *Macromolecules* **2001**, *34*, 734.
24. Foreman, E. A.; Puskas, J. E.; Kaszas, G., *Journal of Polymer Science Part A: Polymer Chemistry*. **2007**, *45*, 5847.
25. Puskas, J. E.; Antony, P.; El Fray, M.; Altstädt, V., *European Polymer Journal*. **2003**, *39*, 2041.
26. Puskas, J. E.; Kwon, Y.; Antony, P.; Bhowmick, A. K., *Journal of Polymer Science Part A: Polymer Chemistry*. **2005**, *43*, 1811.
27. Puskas, J. E.; Kwon, Y., *Polymers for Advanced Technologies*. **2006**, *17*, 615.
28. El Fray, M.; Prowans, P.; Puskas, J. E.; Altstädt, V., *Biomacromolecules* **2006**, *7*, 844.
29. Puskas, J. E.; Dos Santos, L. M.; Kaszas, G.; Kulbaba, K., *Journal of Polymer Science Part A: Polymer Chemistry*. **2009**, *47*, 1148.
30. Karamdoust, S.; Crewdson, P.; Ingratta, M.; Gillies, E. R., *Submitted* **2014**.
31. Heldman, A. W.; Cheng, L.; Jenkins, G. M.; Heller, P. F.; Kim, D.-W.; Ware, M.; Nater, C.; Hruban, R. H.; Rezai, B.; Abella, B. S.; Bunge, K. E.; Kinsella, J. L.; Sollott, S. J.; Lakatta, E. G.; Brinker, J. A.; Hunter, W. L.; Froehlich, J. P., *Circulation* **2001**, *103*, 2289.
32. ASTM, Standard Test Method for Tensile Properties of Thin Plastic Sheeting. ASTM: New York, 2012; Vol. D882-12.
33. Liggins, R. T.; Hunter, W. L.; Burt, H. M., *J. Pharm. Sci.* **1997**, *86*, 1458.
34. Vinogradov, G. V.; Volfson, S. I.; Karp, M. G., *Intl. J. Polym. Mater. Polym. Biomater.* **1982**, *9*, 87.
35. Puskas, J. E.; Antony, P.; Kwon, Y.; Kovar, M.; Norton, P. R., *Macromolecular Symposia*. **2002**, *183*, 191.
36. Strickler, F.; Richard, R.; McFadden, S.; Lindquist, J.; Schwarz, M. C.; Faust, R.; Wilson, G. J.; Boden, M. *Journal of Biomedical Materials Research Part A*. **2010**, *92A*, 773.
37. Sirianni, R. W.; Jang, E.-H.; Miller, K. M.; Saltzman, W. M., *J.Control Release*. **2010**, *142*, 474.

38. ISO, *Tests for in vitro cytotoxicity*. In *Biological Evaluation of Medical Devices*, ISO: Geneva, Switzerland, 2009; Vol. 10993.
39. Jordan, M. A.; Wilson, L., *Nature Rev. Cancer* **2004**, *4*, 253.

Chapter 5

5 Conclusions

5.1 Concluding remarks and future directions

Cardiovascular diseases are one of the top causes of death in western society. The current treatment for cardiovascular disease may require the insertion of a stent into the artery. However current stents on the market have some limitations that can potentially be addressed by optimization of the drug-eluting coating. With the aim of achieving this, this thesis described the development and study of both linear RB and arb-PIB derivatives and their application to the preparation of covalent PTX conjugates to control drug release.

In Chapter 2, the synthesis of carboxylic acid functionalized RB was described. The functionalization was achieved through ring opening of diglycolic anhydride from allylic alcohol moieties on the polymer backbone. The introduction of carboxylic acids improved the tensile properties of the rubber. The ultimate tensile strength and Young's modulus were increased for both the high- and low- IP-content RB. Rheological studies showed that introduction of carboxylic acids made the material more elastic, which is believed to result from the formation of a physical cross-linked network of polymer molecules. This improvement in physical properties of RB can make it more useful for biomedical applications including coatings for stents and other devices.

In Chapter 3, the synthesis of PTX conjugates of RB was accomplished via a carbodiimide coupling. The introduction of PTX into RB changed the tensile and rheological properties of the material, increasing their elasticity and tensile strength. Films of the PTX conjugates were prepared to explore the potential application of these new polymers in drug eluting stents. The polymers were compared with several controls that contained physical mixtures of PTX and SIBS or the carboxylic acid functionalized rubber. The covalent conjugate had a more uniform distribution of PTX and exhibited a very slow, sustained release in contrast to the control films. The films of the PTX conjugate also exhibited enhanced adhesion to the stainless steel surface and remained intact throughout the study. The preliminary biological assays showed that none of the covalent or physically systems released toxic levels of PTX.

However, the level of PTX on the surface of the covalently conjugated samples was sufficient to prevent the adhesion and growth of C2C12 cells. Therefore they still appear to have the desired anti-proliferative properties. The results from these studies suggest the potential of these PTX conjugates as vascular stent coatings.

In Chapter 4, the chemistry developed in chapter 2 and 3 was successfully used to prepare epoxide, allylic alcohol, carboxylic acid, and PTX derivatives of arb-PIB-co-IP. The properties of the arborescent materials were compared to the linear analogues. These materials show similar thermal properties to the linear analogues; however a melting point was seen for arborescent PTX derivative that was not visible in the linear analogue. This suggests that introduction of PTX to the arborescent material allows it to phase separate to a degree. The differences in tensile and rheological properties of the various arborescent derivatives were found to be generally smaller than for the analogous linear materials. The PTX conjugate with the arborescent polymer had a lower ultimate tensile strength and higher elongation at break compared to its linear analogue. The PTX release rate from the arborescent conjugate was very similar to that of the linear analogue. The arborescent materials also showed no toxicity in the MTT assay on C2C12 cells. However, the level of PTX on the surface of the film was still sufficient to inhibit the adhesion and development of C2C12 cells, as for the linear materials. Combined these results suggest that the arborescent PIB is also a promising candidate for further evaluation as a DES coating.

With respect to future direction of this work, there are several aspects that can be investigated. Films of the drug conjugates were prepared and studied on stainless steel plates. It would be beneficial to apply them to actual stents and study their properties and drug release rates in this context. In addition, the mechanical properties of the polymers described in this thesis are still not as ideal as SIBS. It is not yet clear whether this would prevent their application as stent coatings, and this requires further investigation. A means of covalently cross-linking these PIBs may still need to be investigated. Finally, all testing was performed *in vitro* using the modal cell line C2C12. It will be important in the future to extend these studies to more relevant cells such as human coronary artery smooth muscle cells, and to also perform testing *in vivo* in animal models.

Appendices

Appendix 1: Supporting Information of Chapter 2

- ^{1}H NMR spectra of copolymers **4d-l**, and **4d-h.**
- Tensile stress vs strain of **PIB-l, 1-l, 2-l, 4d-l, PIB-h, 1-h, 2-h and 4d-h.**
- G’ and G” of **PIB-l, 1-l, 2-l, 4d-l, PIB-h, 1-h, 2-h and 4d-h.**

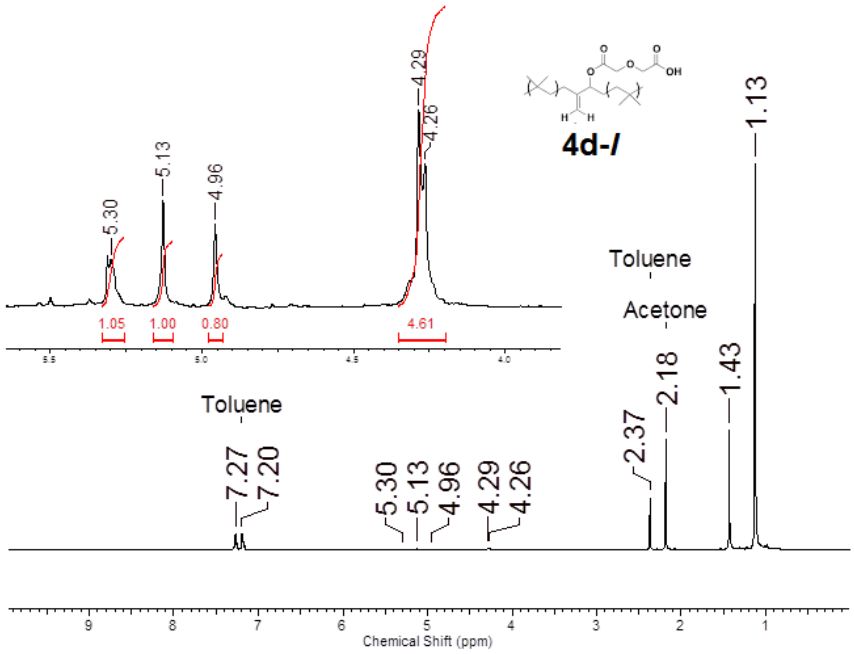

Figure A2.1. ^{1}H NMR spectrum of **4d-l**

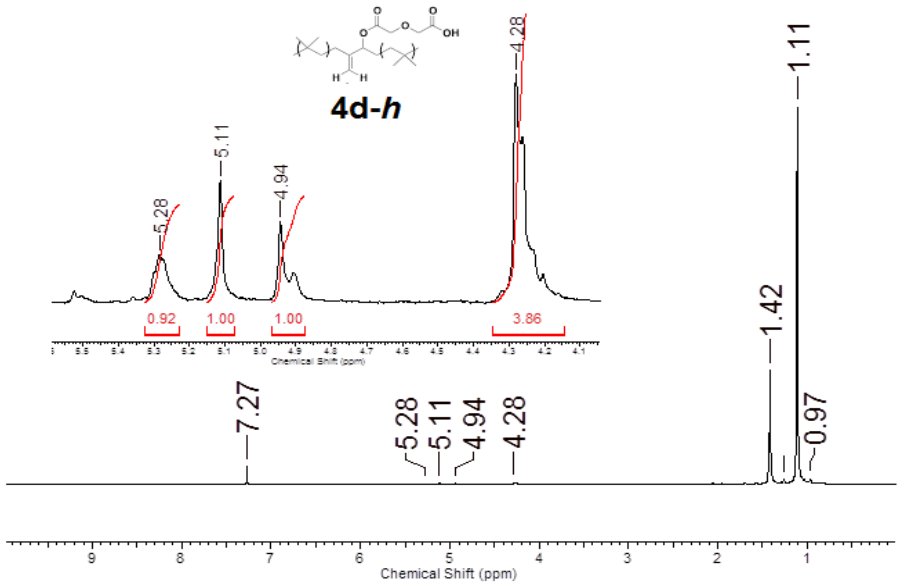

Figure A2.2. ^{1}H NMR spectrum of **4d-h**

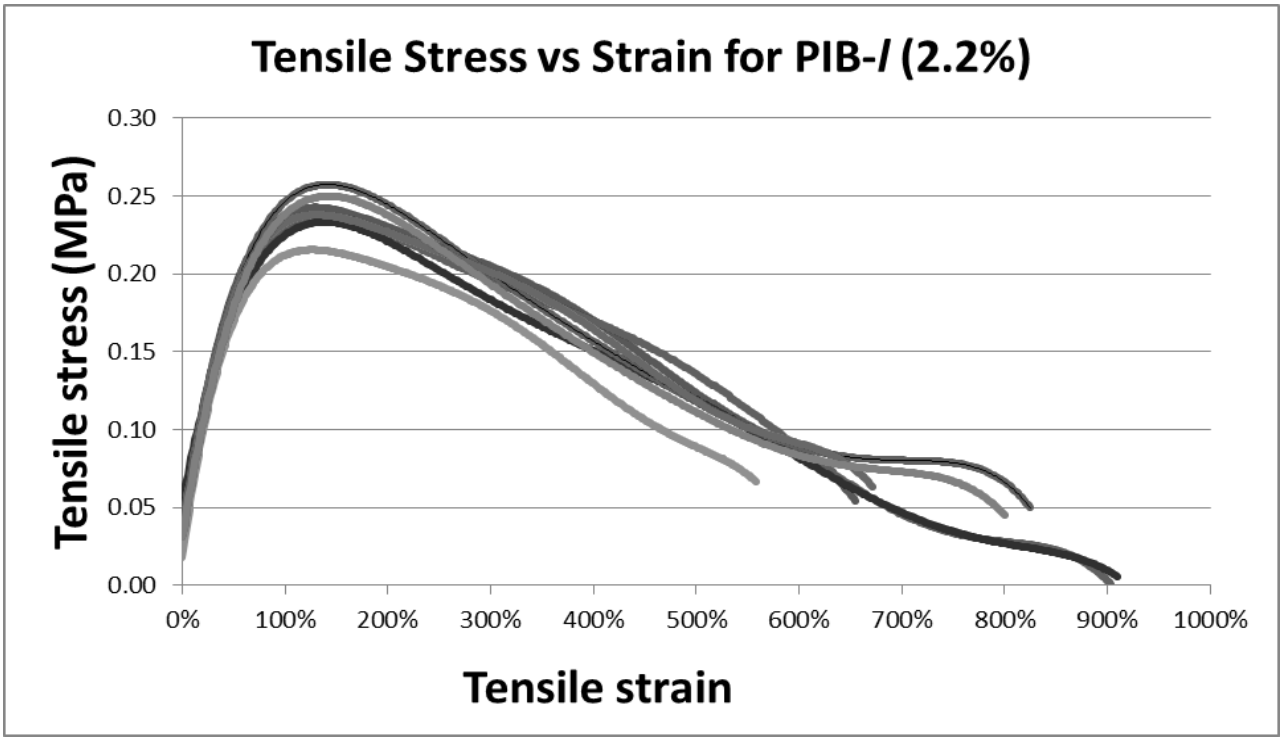

Figure A2.3. Tensile stress vs strain of **PIB-l**

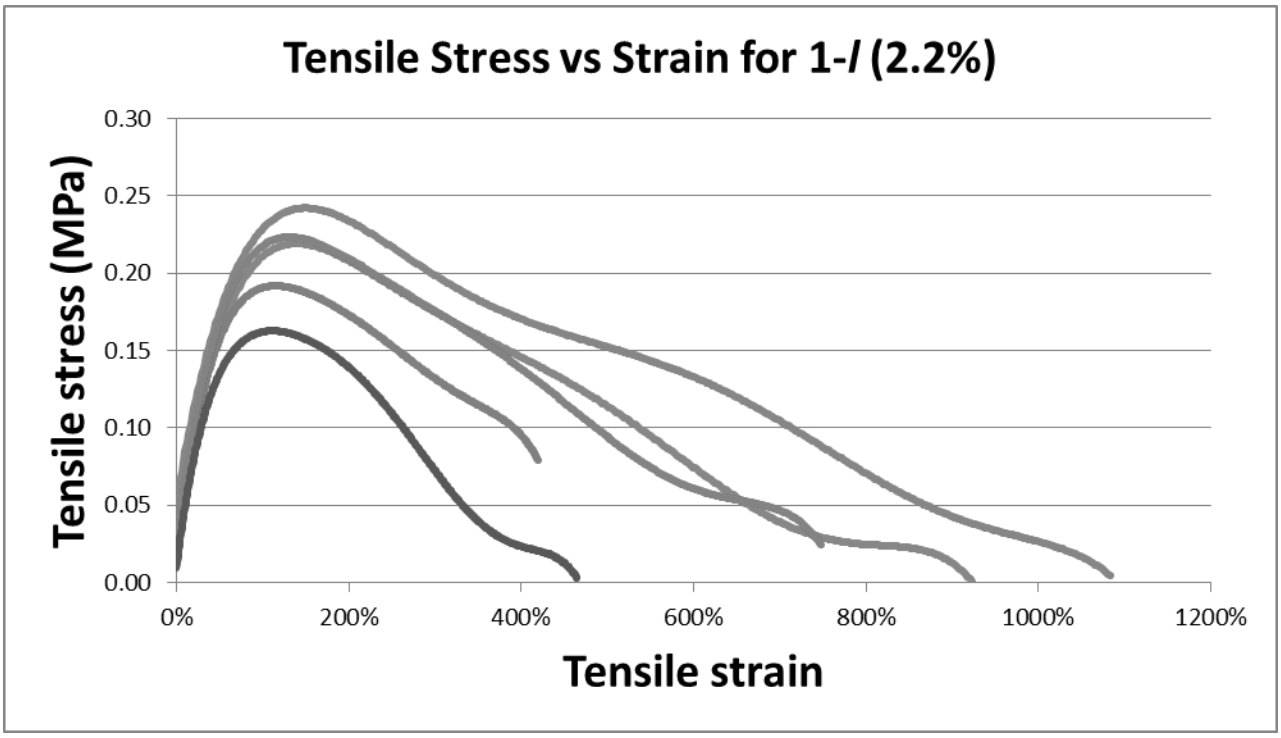

Figure A2.4. Tensile stress vs strain of **1-l**

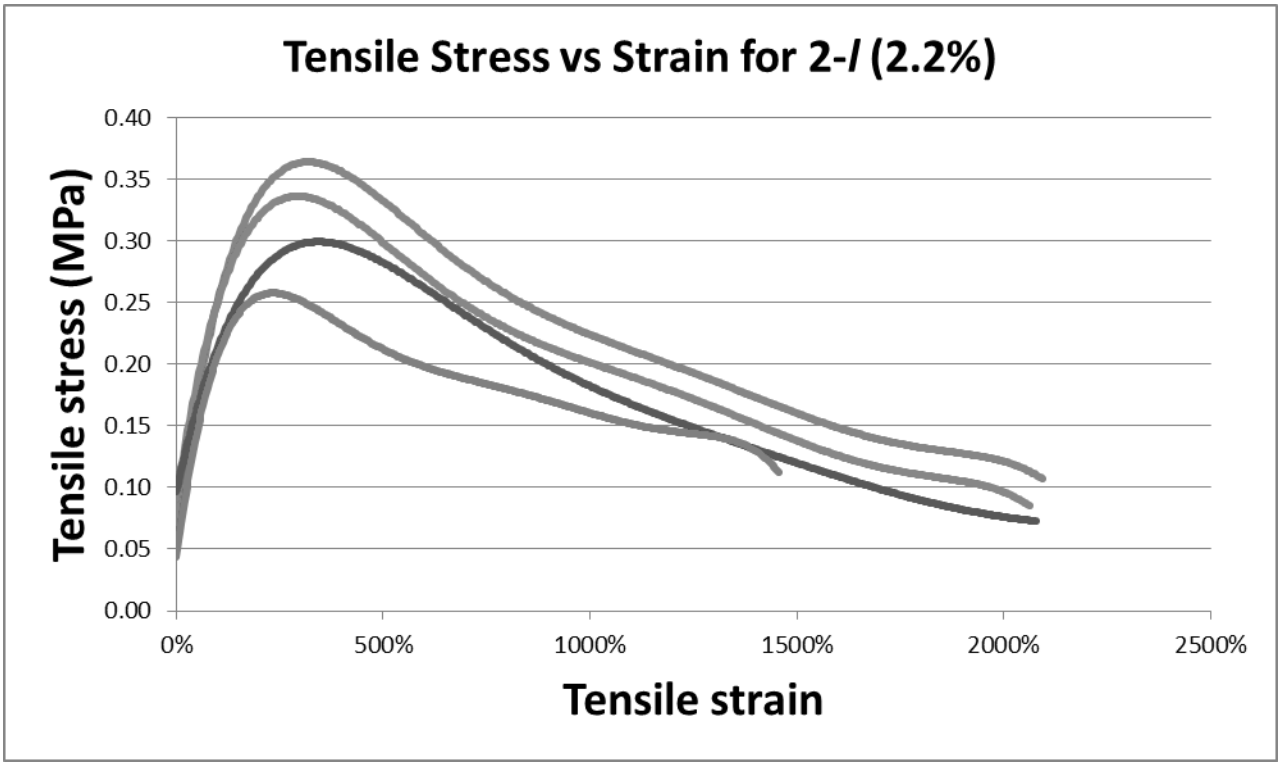

Figure A2.5. Tensile stress vs strain of **2-l**

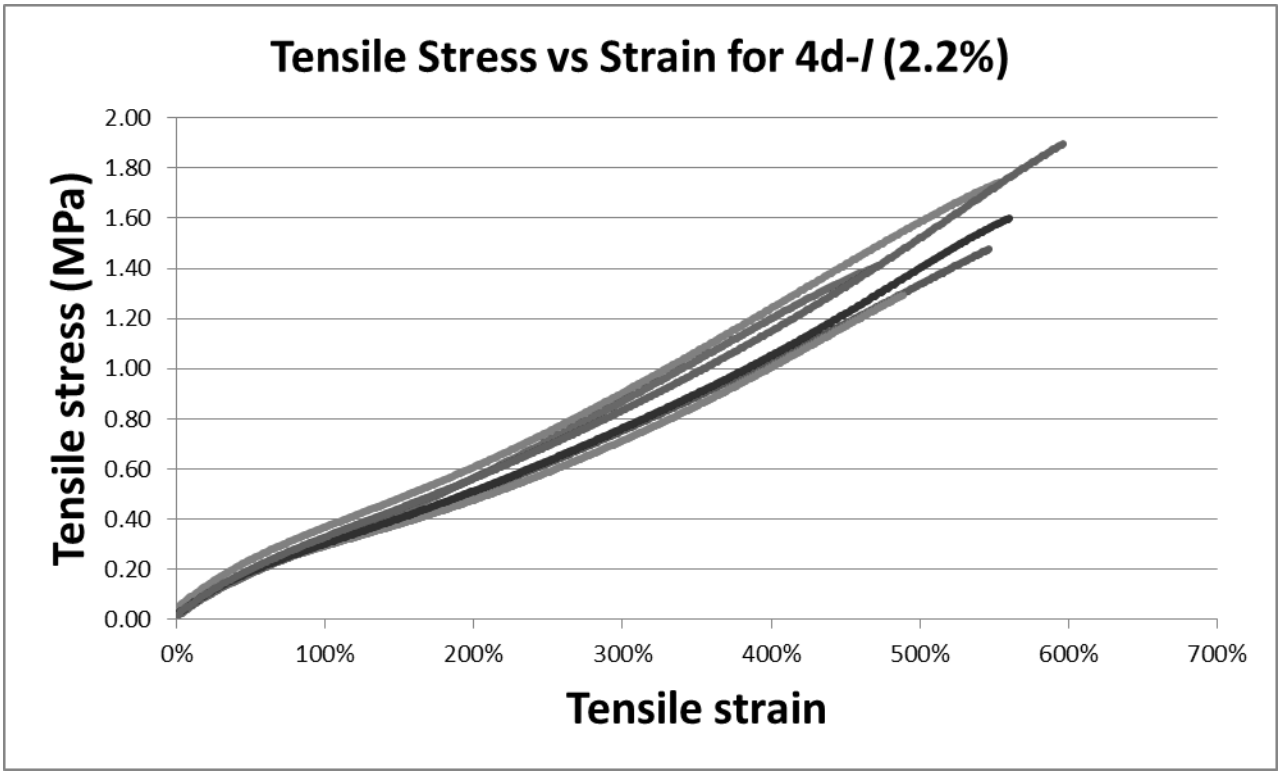

Figure A2.6. Tensile stress vs strain of **4d-l**

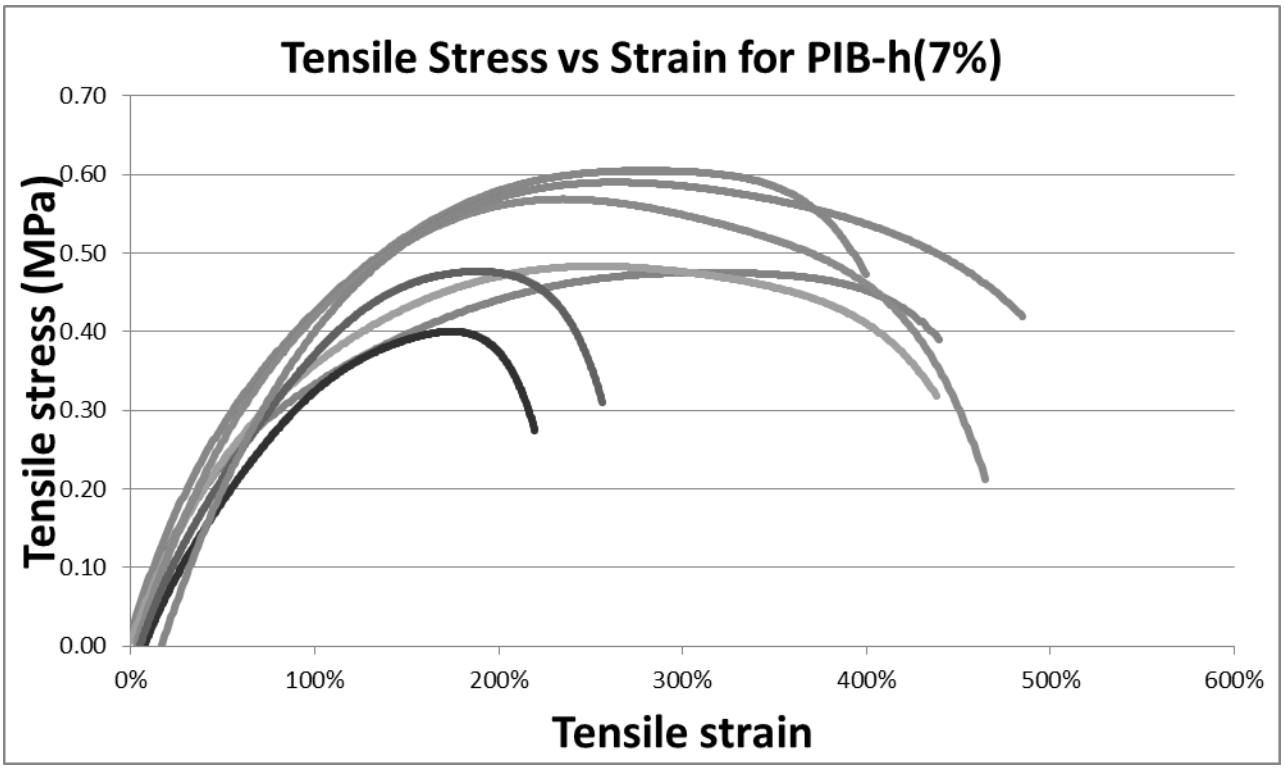

Figure A2.7. Tensile stress vs strain of **PIB-h**

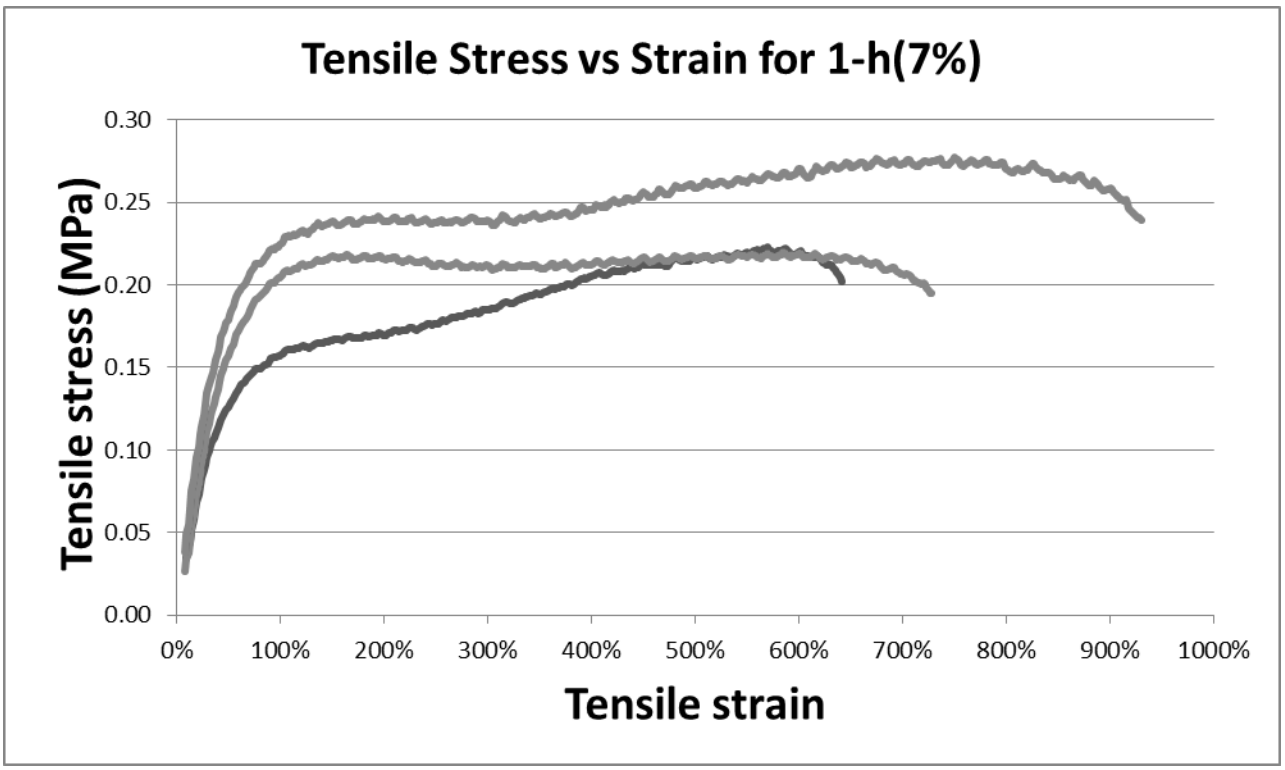

Figure A2.8. Tensile stress vs strain of **1-h**

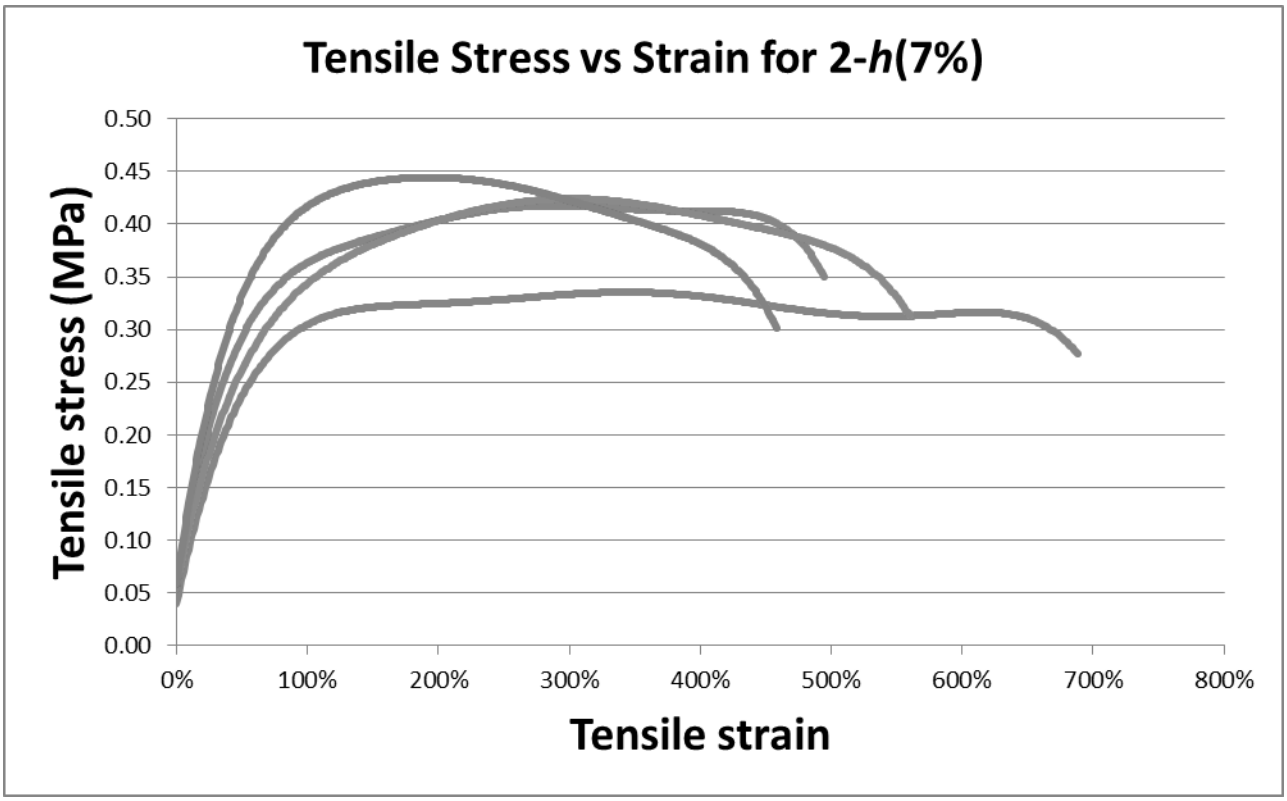

Figure A2.9. Tensile stress vs strain of **2-h**

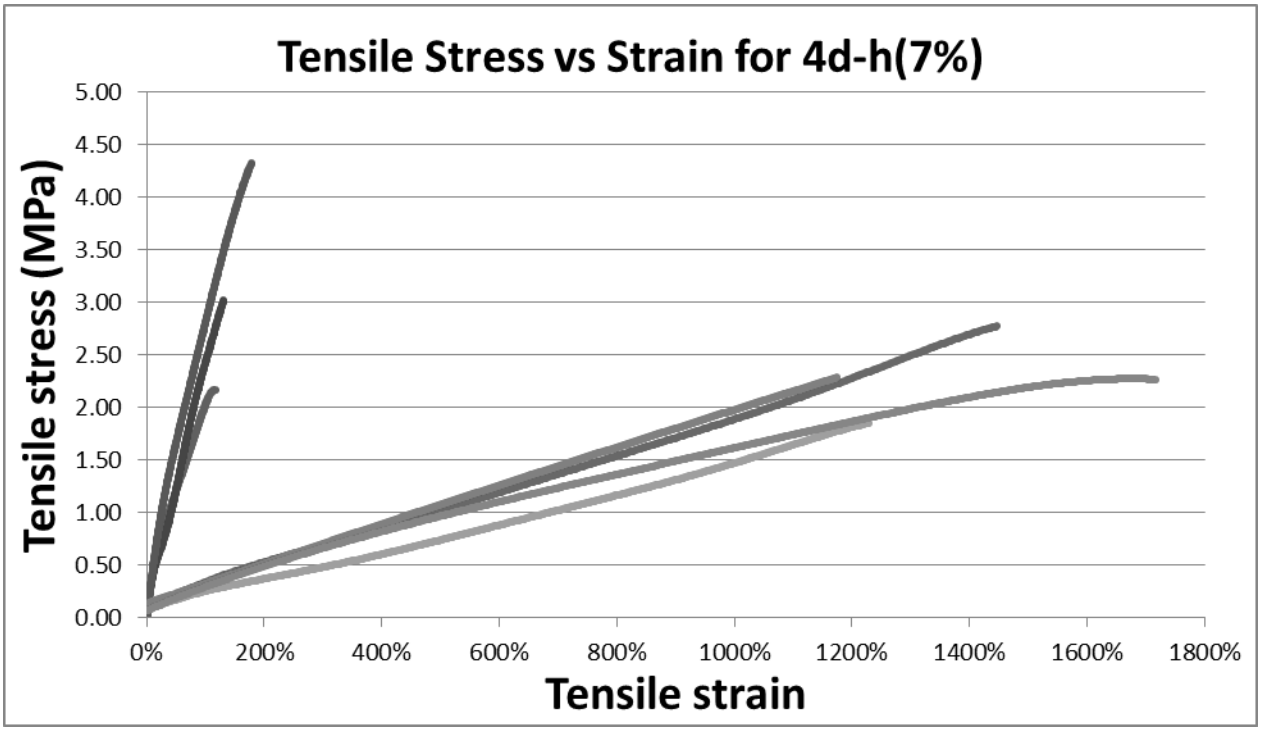

Figure A2.10. Tensile stress vs strain of **4d-h**

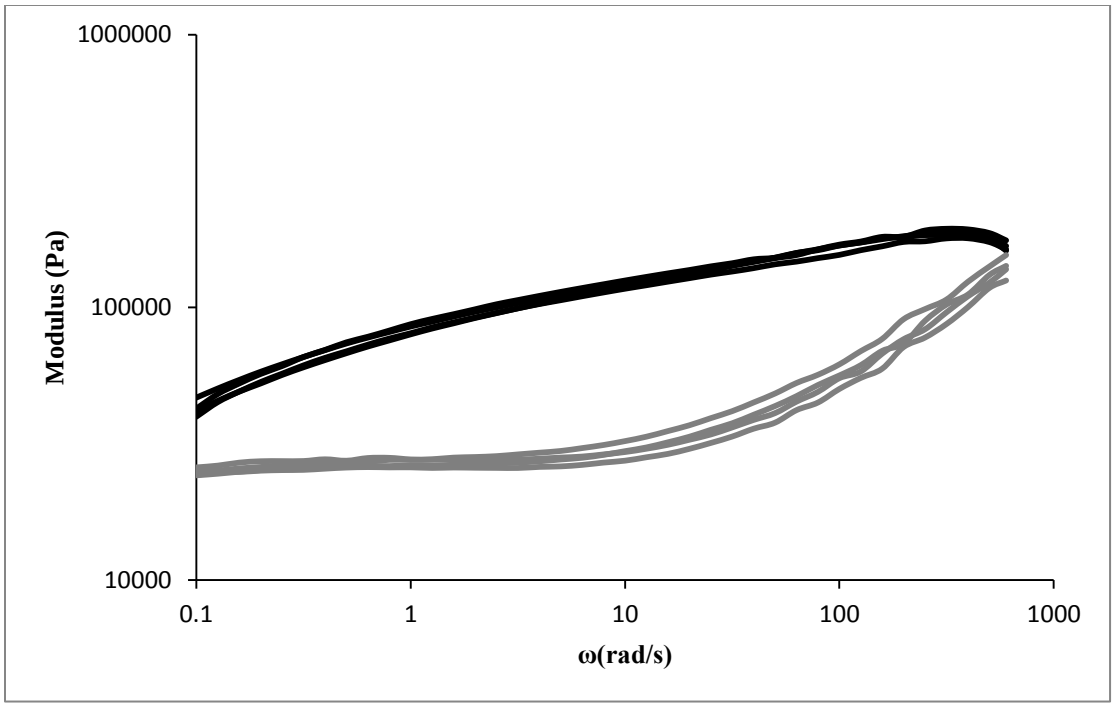

Figure A2.11. Frequency dependence of the elastic (G', black) and viscous (G", grey) moduli for **PIB-*l***.

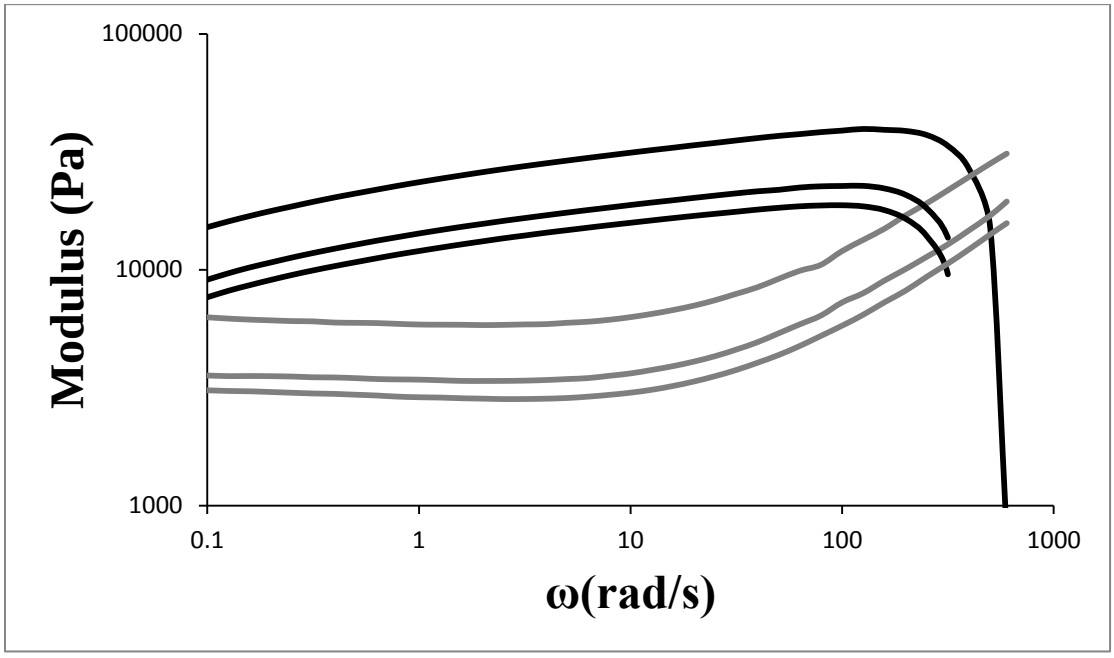

Figure A2.12. Frequency dependence of the elastic (G', black) and viscous (G", grey) moduli for **1-*l***.

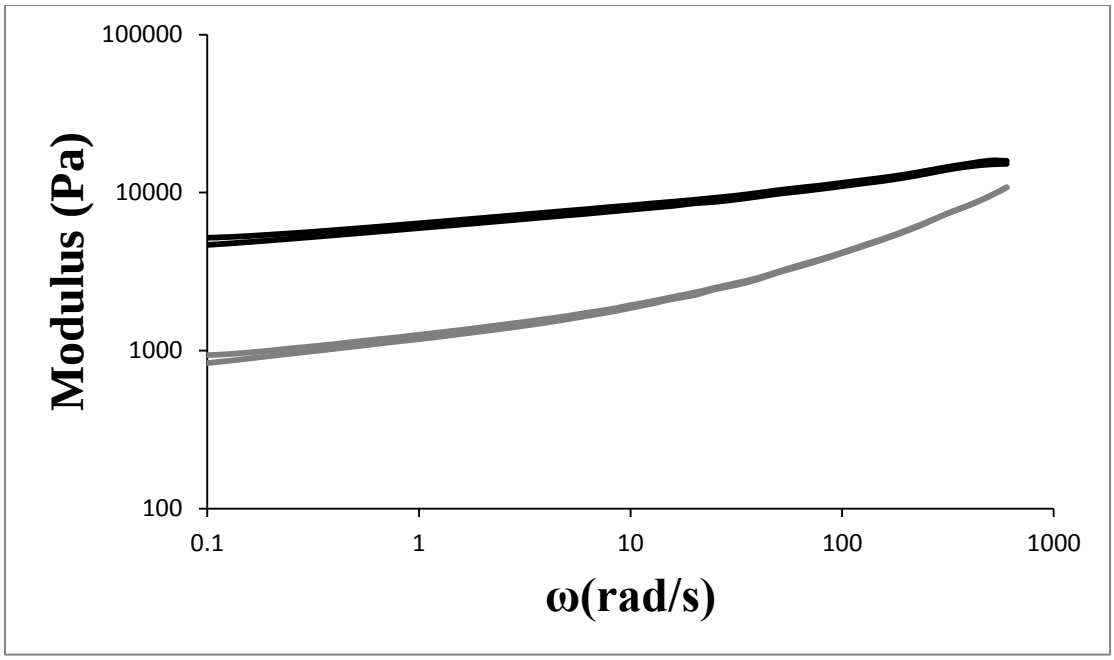

Figure A2.13. Frequency dependence of the elastic (G', black) and viscous (G", grey) moduli for **2-*l***.

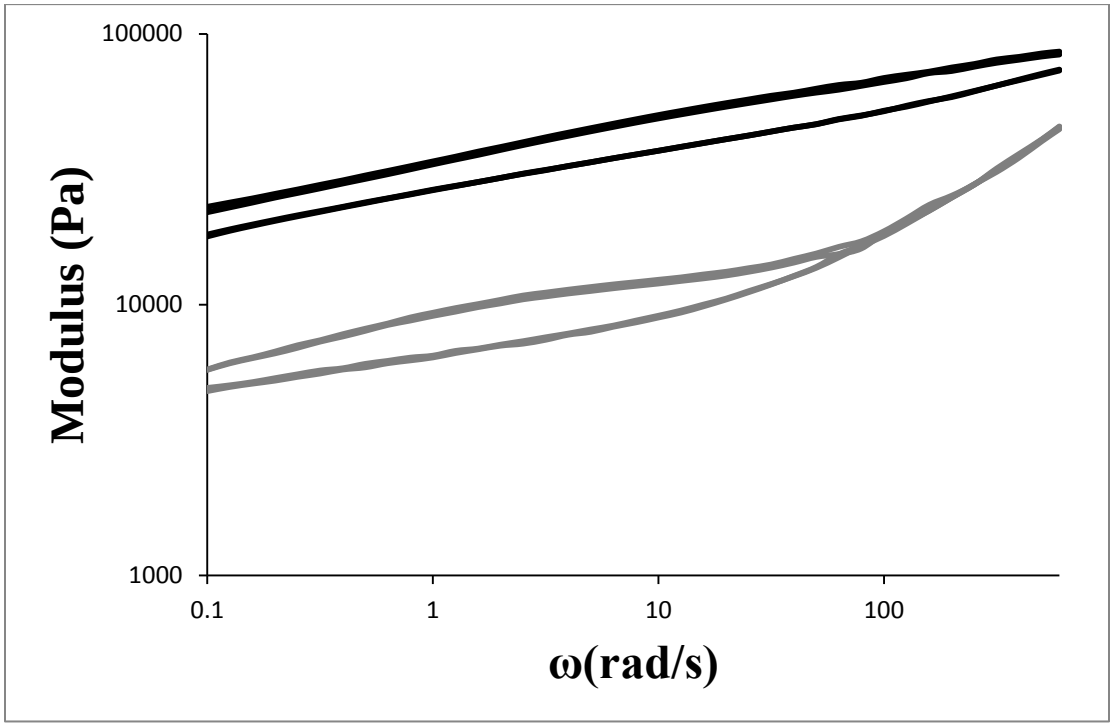

Figure A2.14. Frequency dependence of the elastic (G', black) and viscous (G", grey) moduli for **4d-*l***.

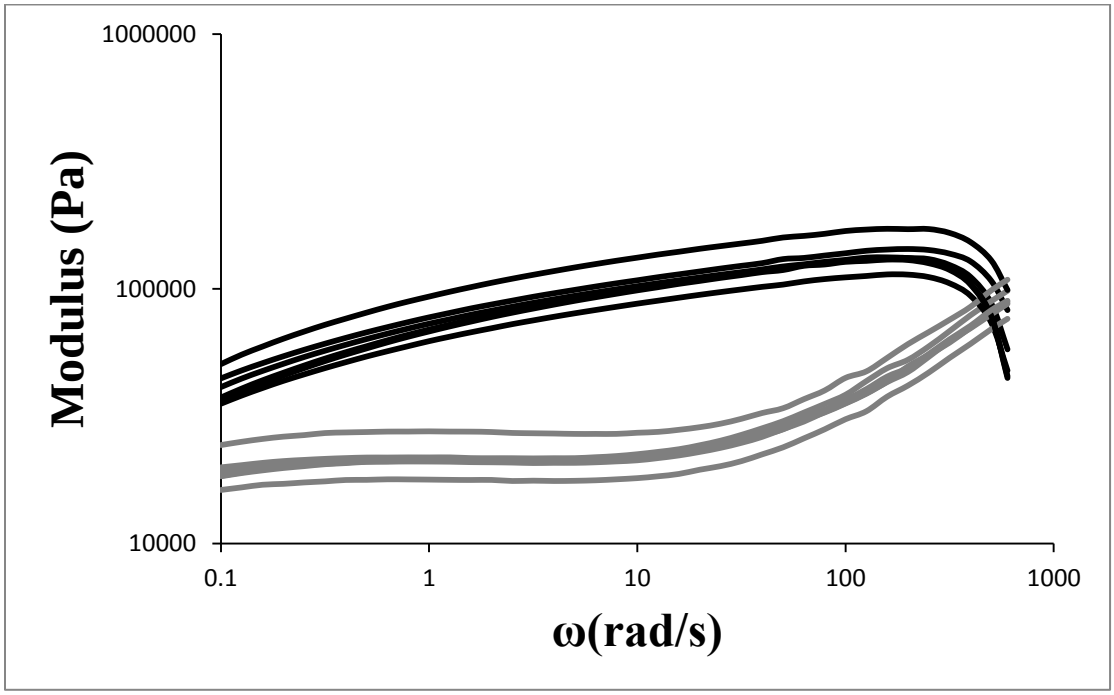

Figure A2.15. Frequency dependence of the elastic (G', black) and viscous (G", grey) moduli for **PIB-*h***.

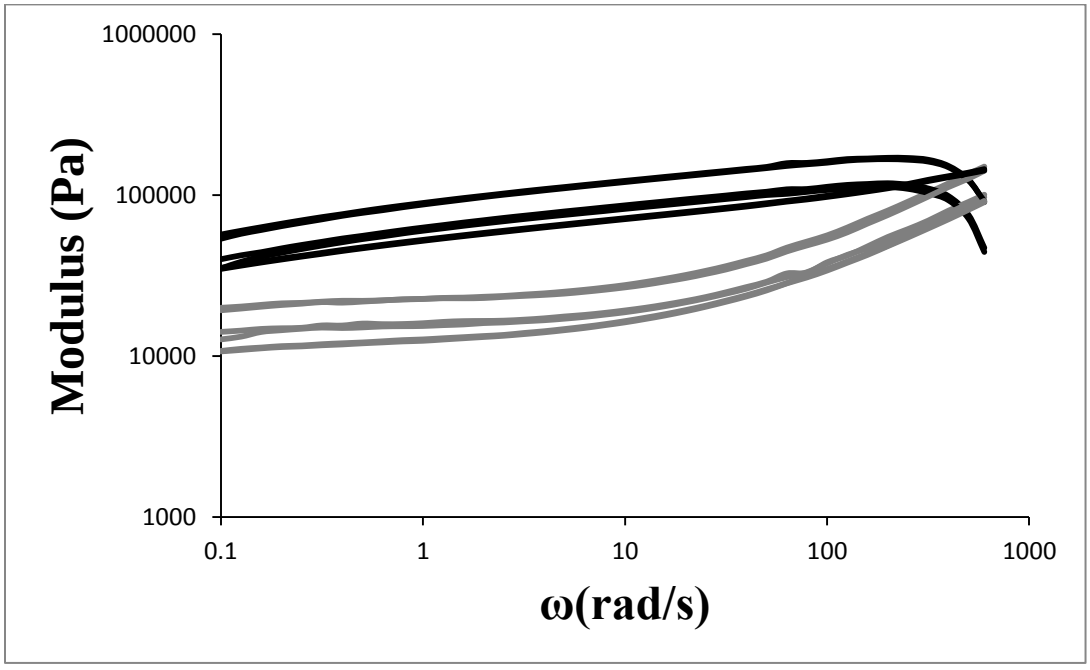

Figure A2.16. Frequency dependence of the elastic (G', black) and viscous (G", grey) moduli for **1-*h***.

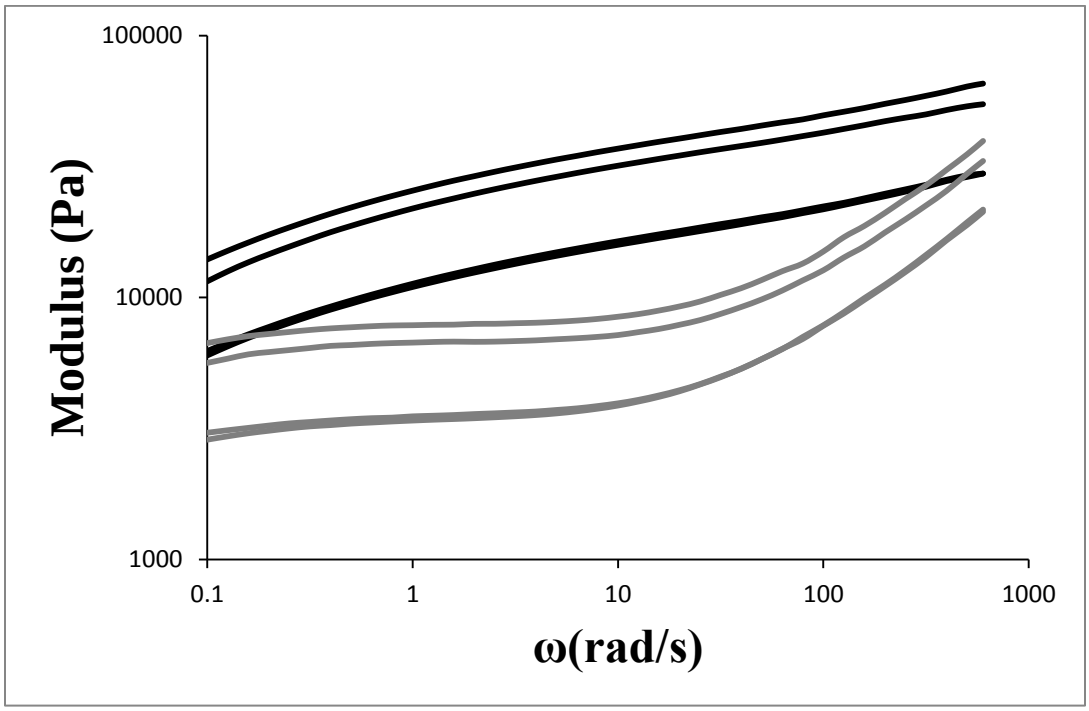

Figure A2.17. Frequency dependence of the elastic (G', black) and viscous (G", grey) moduli for **2-*h***.

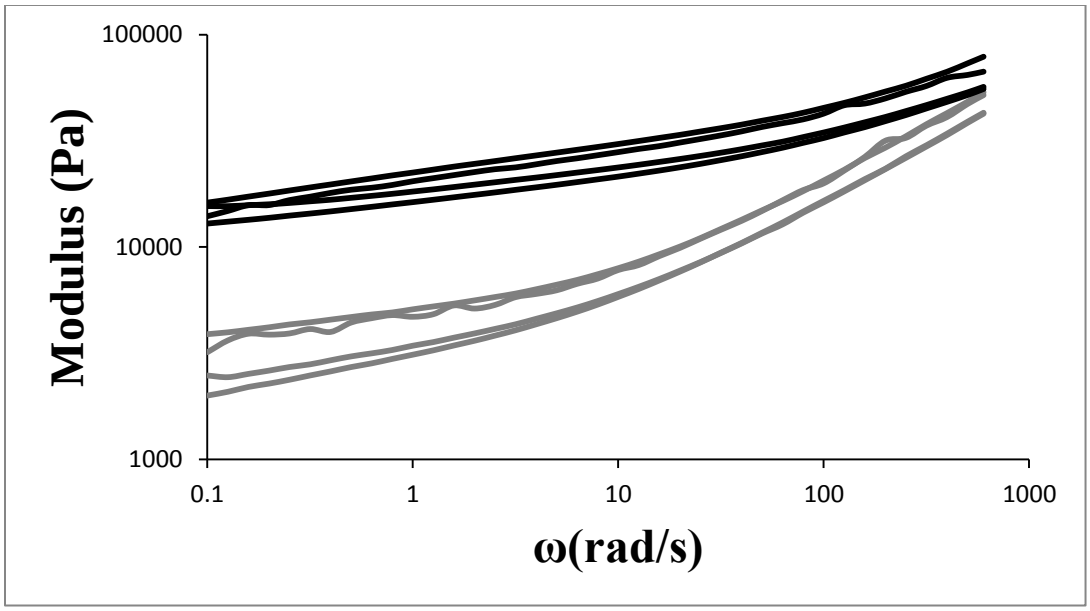

Figure A2.18. Frequency dependence of the elastic (G', black) and viscous (G", grey) moduli for **4d-*h***.

Appendix 2: Supporting Information of Chapter 3

- ^{1}H NMR spectra of copolymers **PIBa-cov**, and **PIBa-cov.**
- Thermal analysis of **PIBa-cov** and **PIBb-cov**
- Additional AFM images for surfaces
- Representative tensile curves of **SIBS1** and **SIBS2** and **PIBa/PIBb-cov** for comparison
- Rheological data for **PIBa-cov**, **PIBb-cov**, **SIBS1** and **SIBS2**

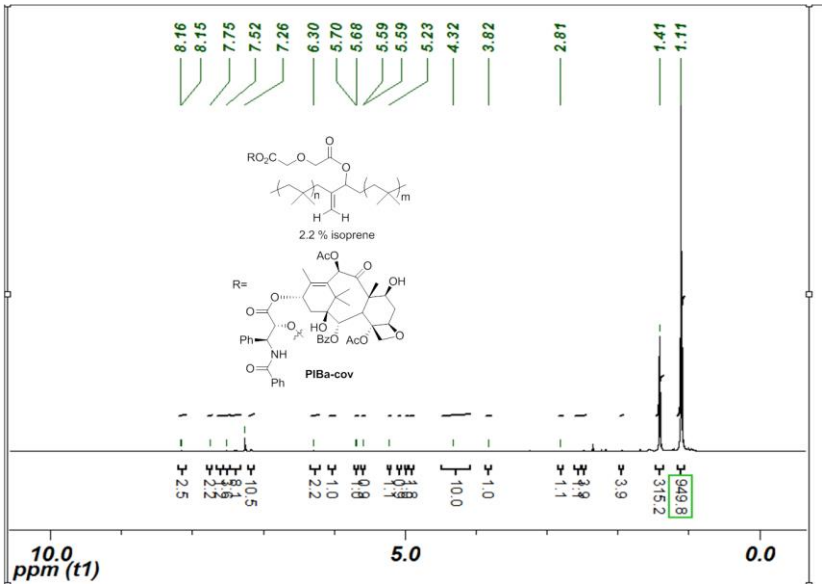

Figure A3.1. [1]H NMR spectrum of covalent PIB-PTX conjugate **PIBa-cov** showing the PIB peaks.

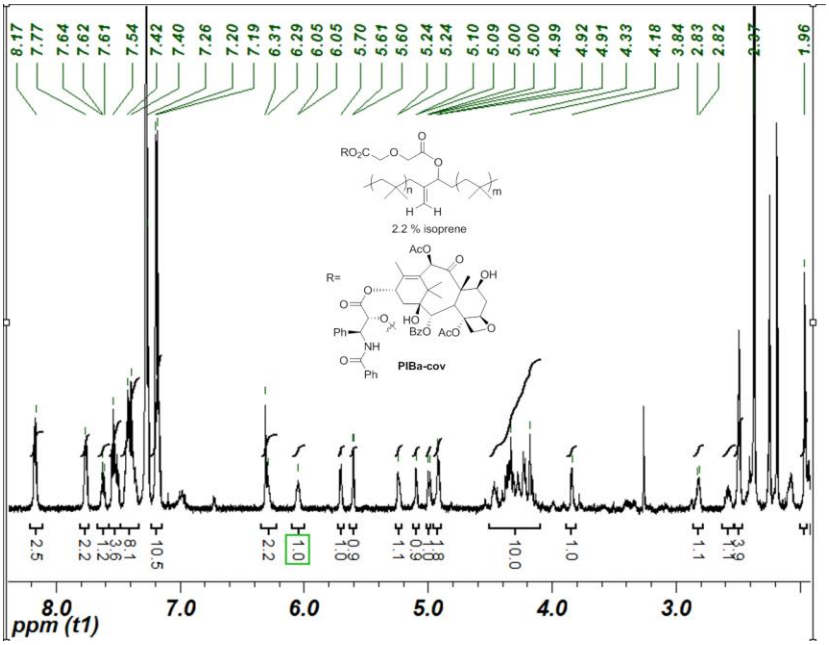

Figure A3.2. [1]H NMR spectrum of covalent PIB-PTX conjugate **PIBa-cov** showing the IP-related and PTX related peaks as an expansion of Figure **A3.1**, with toluene contamination**.**

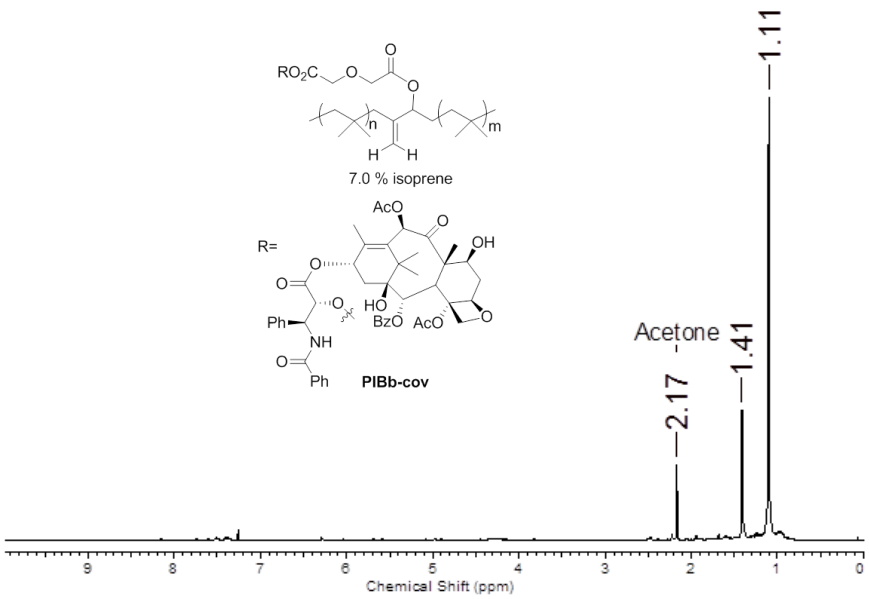

Figure A3.3. ^{1}H NMR spectrum of covalent PIB-PTX conjugate **PIBb-cov** showing the PIB peaks.

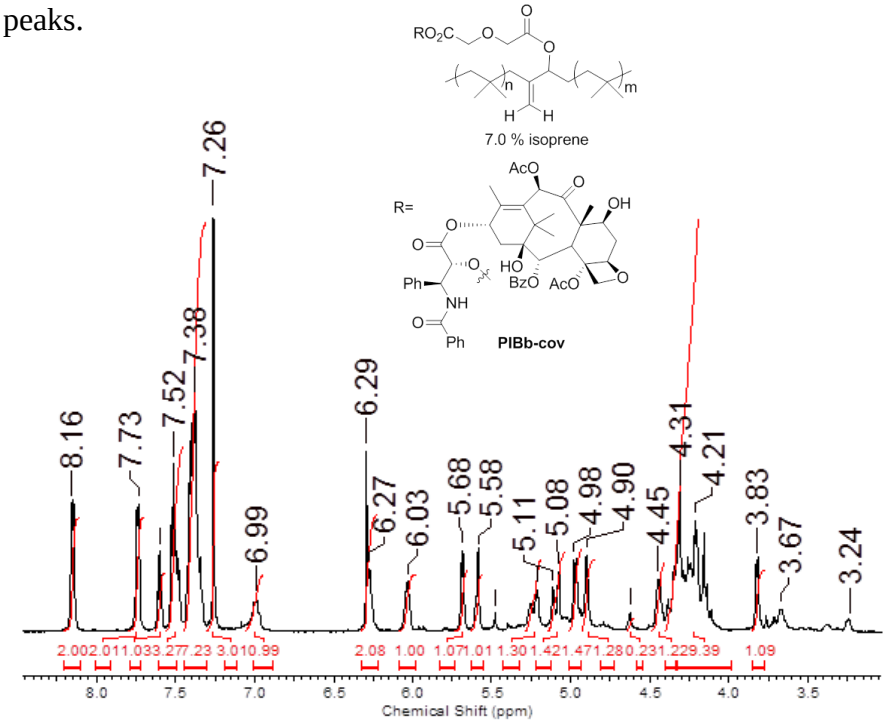

Figure A3.4. ^{1}H NMR spectrum of covalent PIB-PTX conjugate **PIBb-cov** showing the IP-related and PTX related peaks as an expansion of Figure **A3.3.**

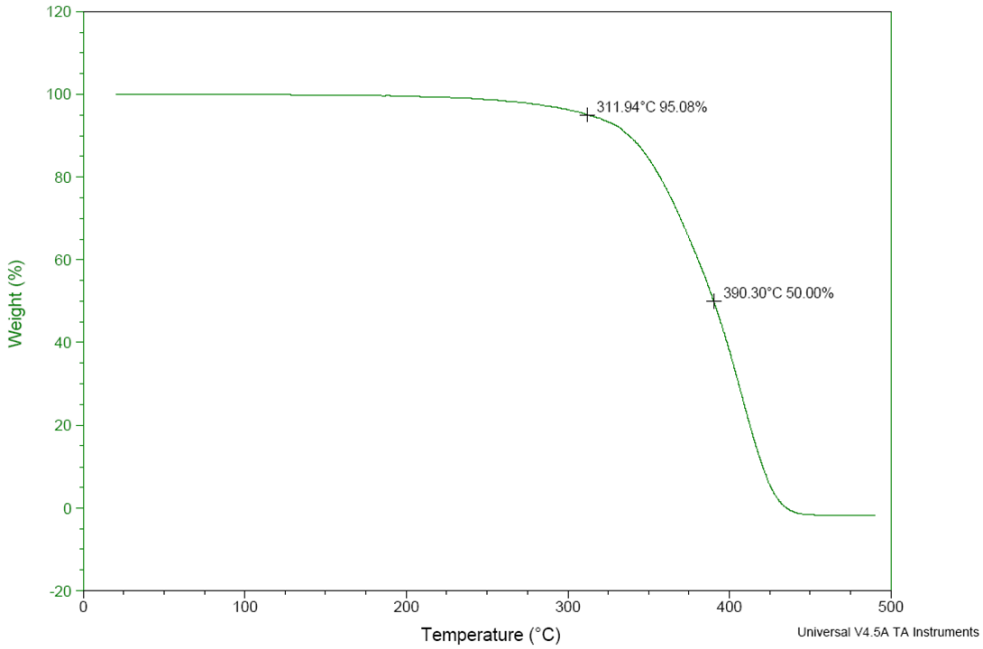

Figure A3.5. TGA trace for PIBa-cov.

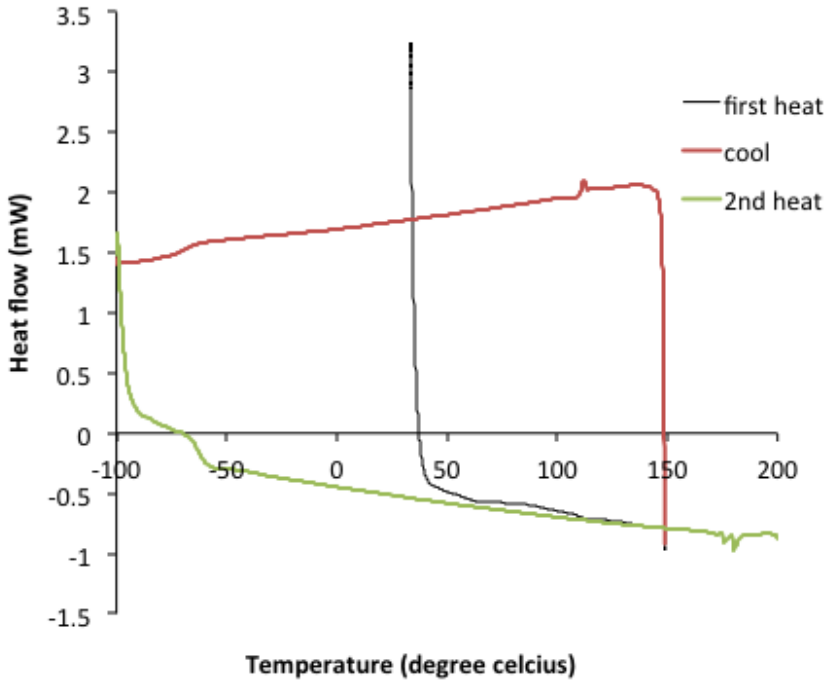

Figure A3.6. DSC trace for PIBa-cov. Note that the first heating cycle was only performed to 150 °C to ensure that the sample did not degrade thermally. In the second heating cycle, heating was performed to 300 °C but no further thermal transitions were observed.

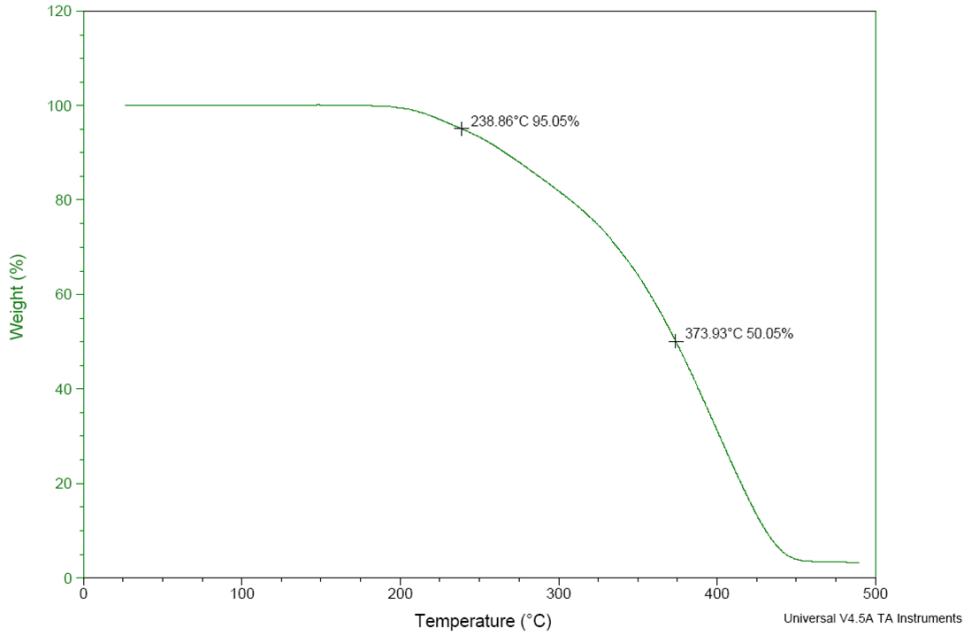

Figure A3.7. TGA trace for PIBb-cov.

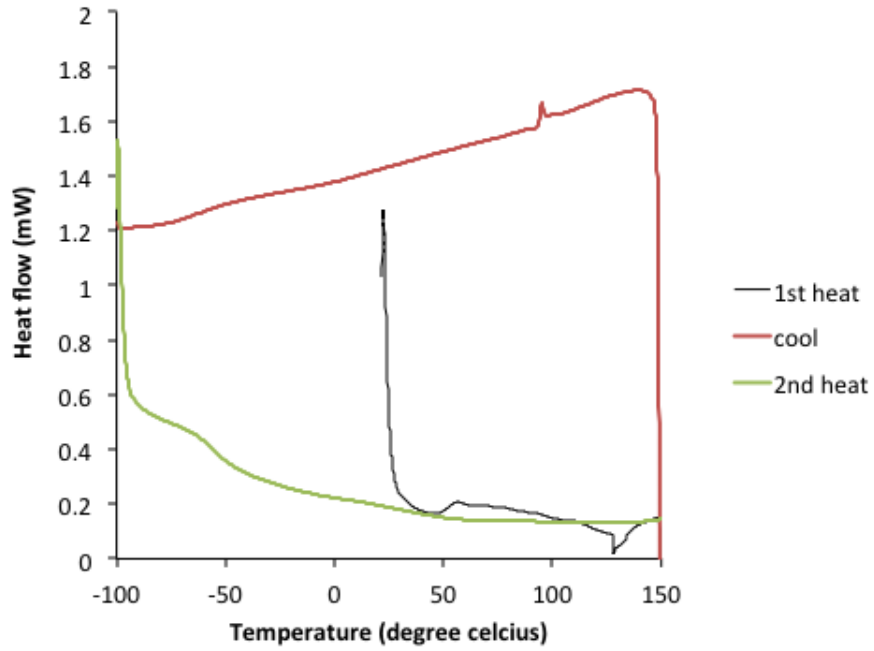

Figure A3.8. DSC trace for PIBb-cov. Note that the first heating cycle was only performed to 150 °C to ensure that the sample did not degrade thermally. In the second heating cycle, heating was performed to 250 °C but sample degradation was observed above 150 °C**.**

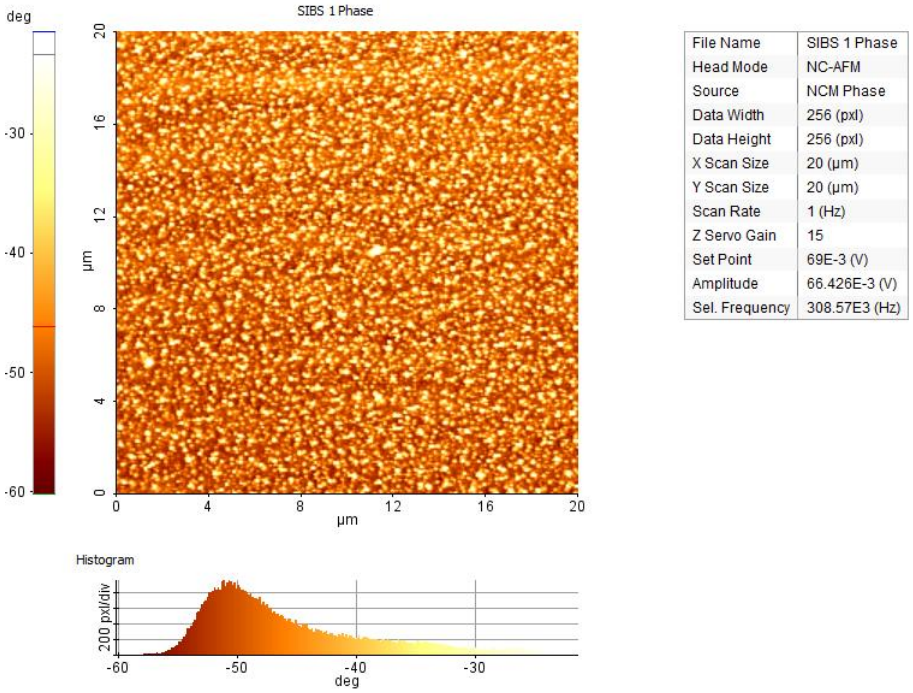

Figure A3.9. Representative phase image of **SIBS1-9** prior to release.

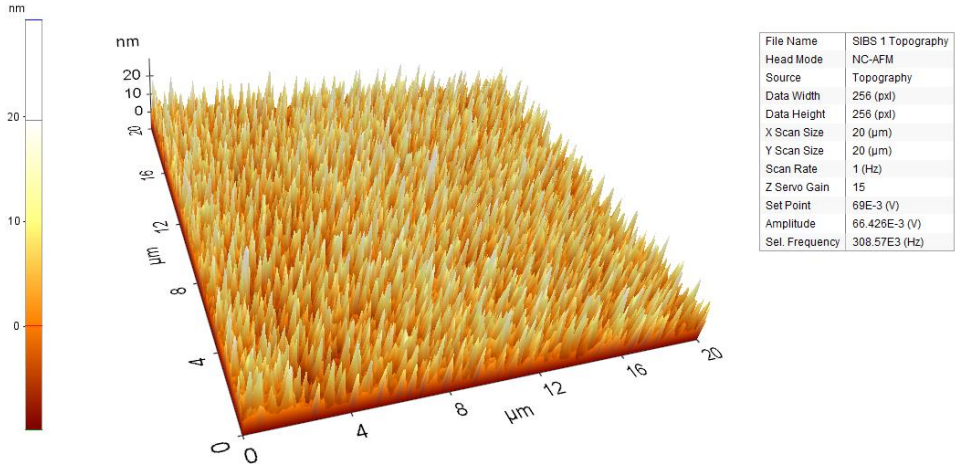

Figure A3.10. Representative topographic image of **SIBS1-9** prior to release. Note peaks due to PTX aggregates.

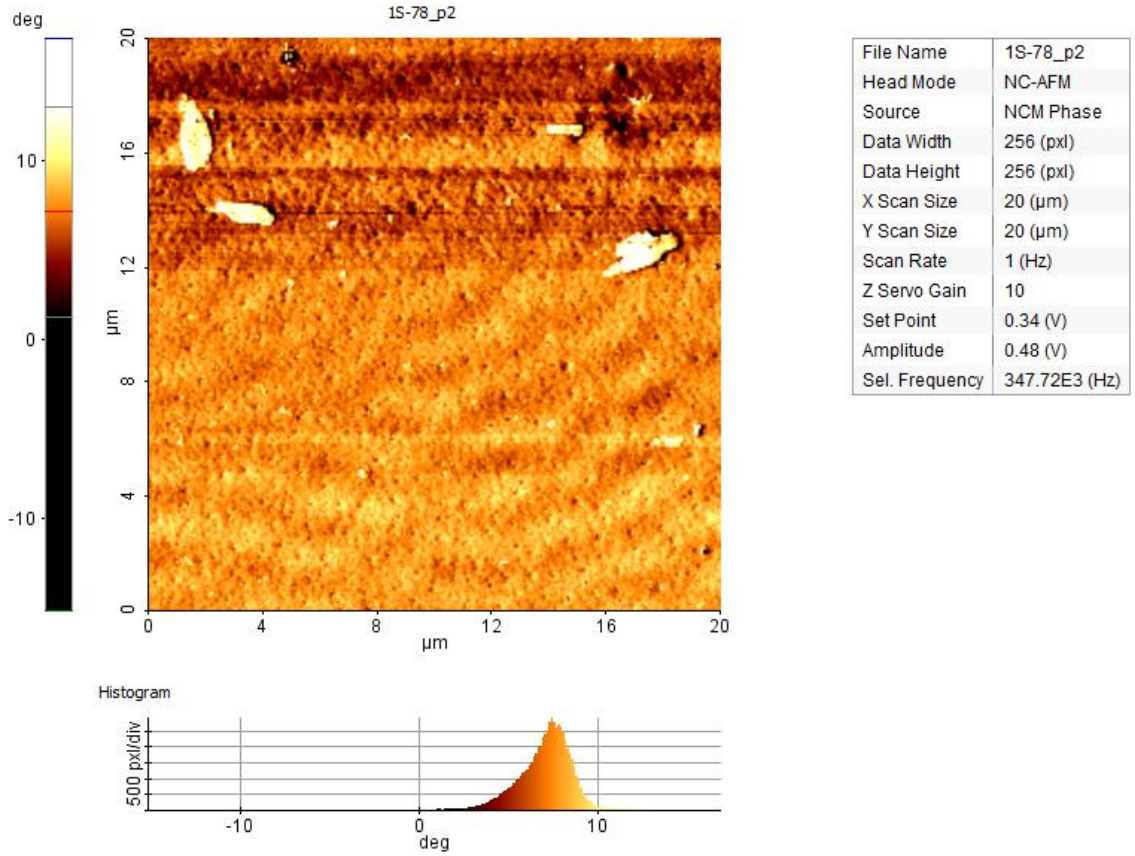

Figure A3.11. Representative phase image of **SIBS1-9** after release.

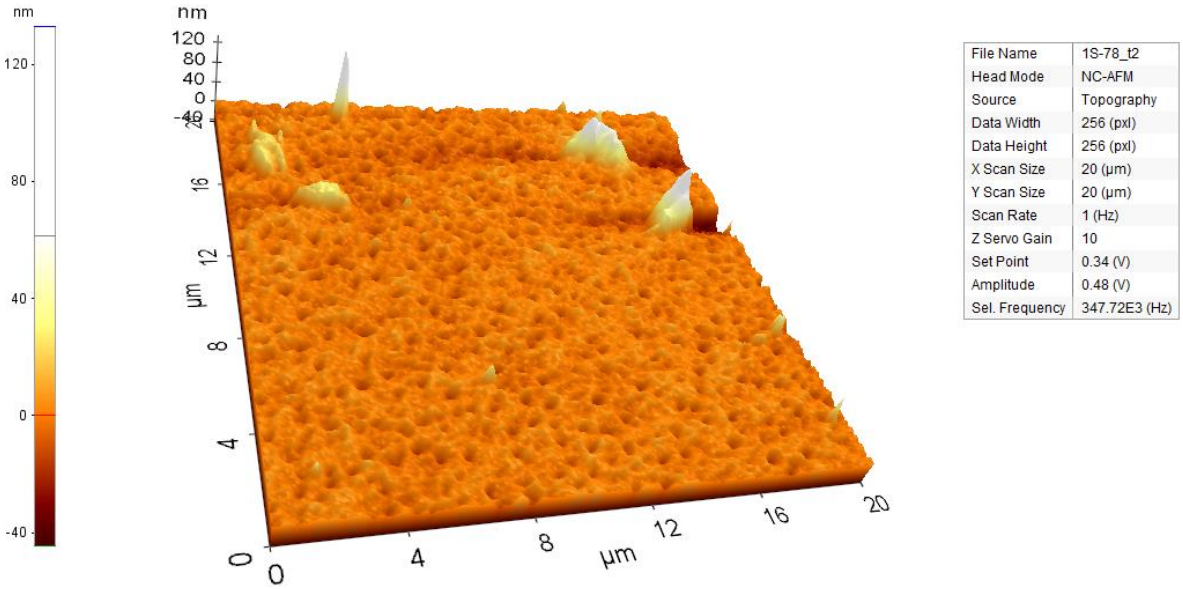

Figure A3.12. Representative topographic image of **SIBS1-9** after release. Note the salt deposits (peaks, not removed after repeated washes with deionized water) and valleys left by released PTX.

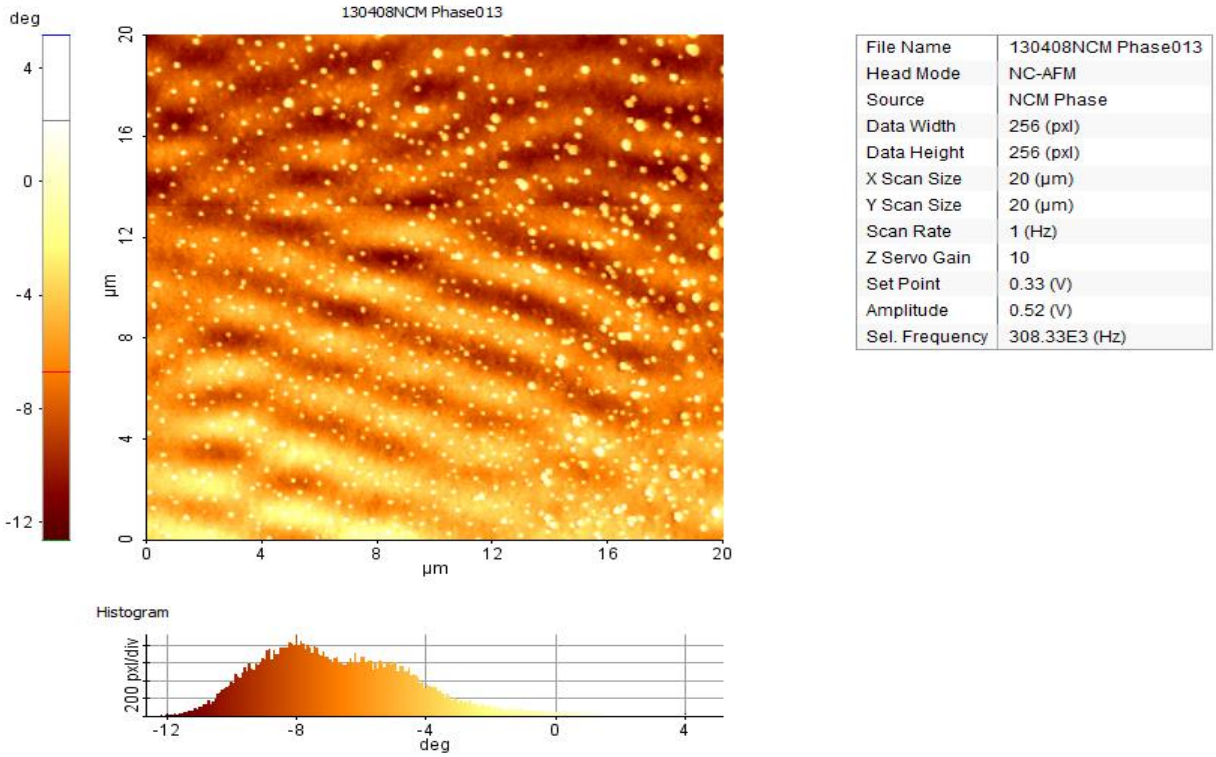

Figure A3.13. Representative phase image of **SIBS2-9** prior to release.

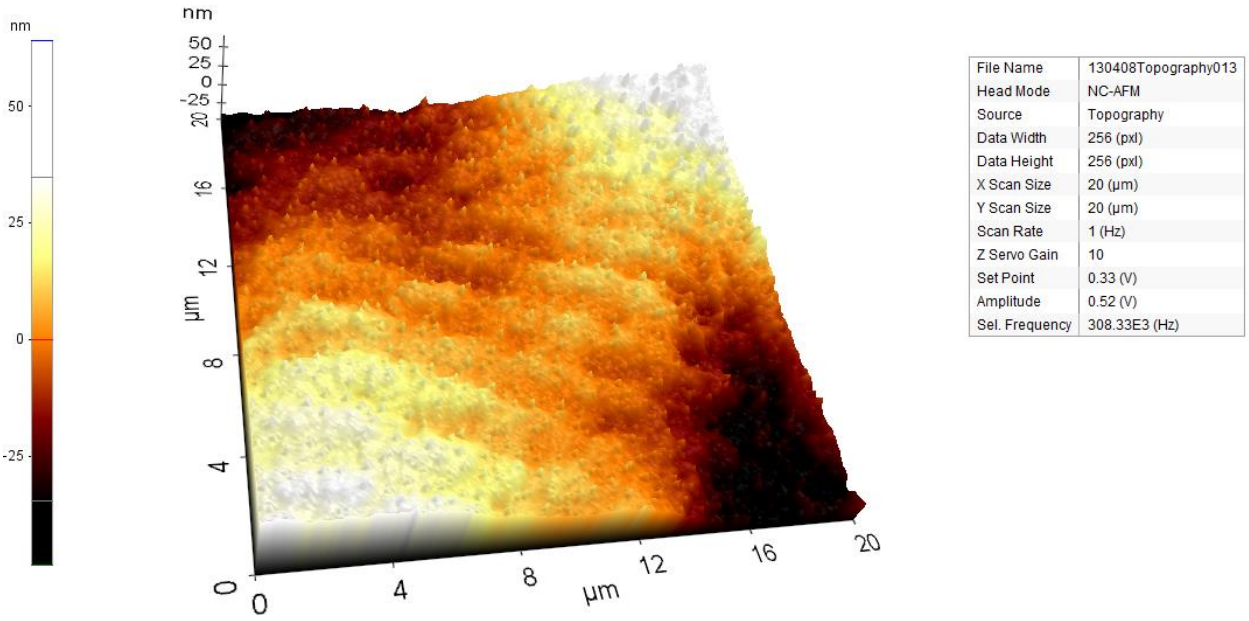

Figure A3.14. Representative topographic image of **SIBS2-9** prior to release. Note peaks due to PTX aggregates.

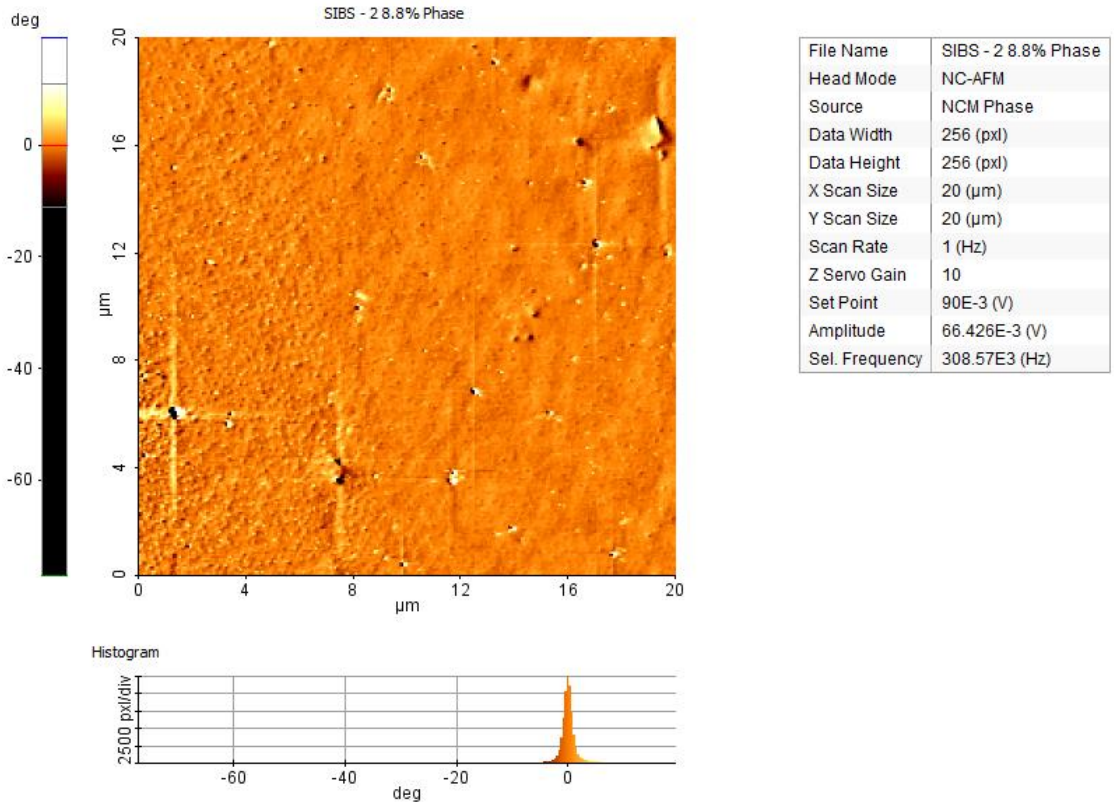

Figure A3.15.. Representative phase image of **SIBS2-9** after release.

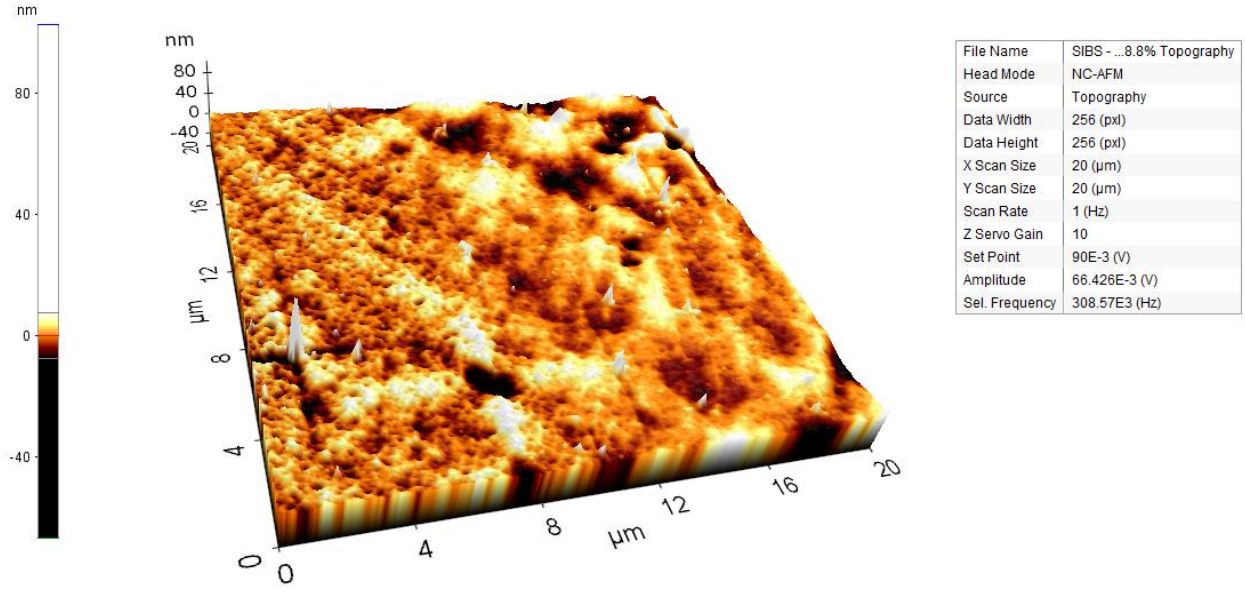

Figure A3.16. Representative topographic image of **SIBS2-9** after release. Note the salt deposits (peaks, not removed after repeated washes with deionized water) and valleys left by released PTX.

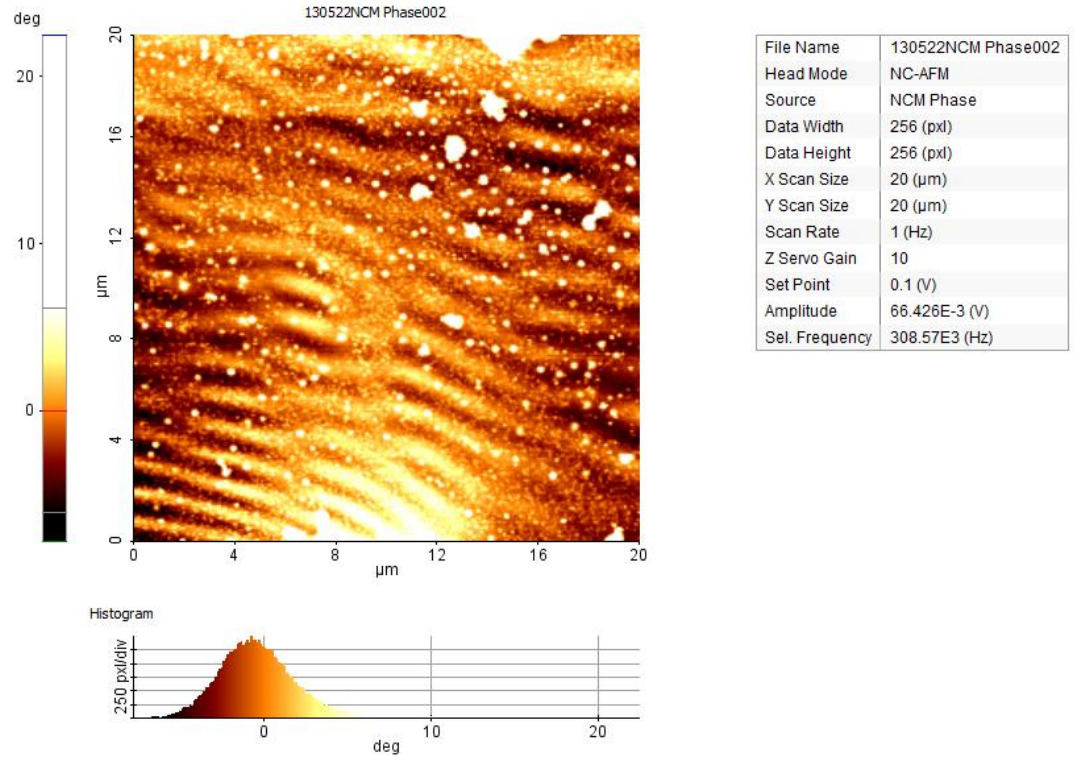

Figure A3.17. Representative phase image of **PIBa-phy** prior to release.

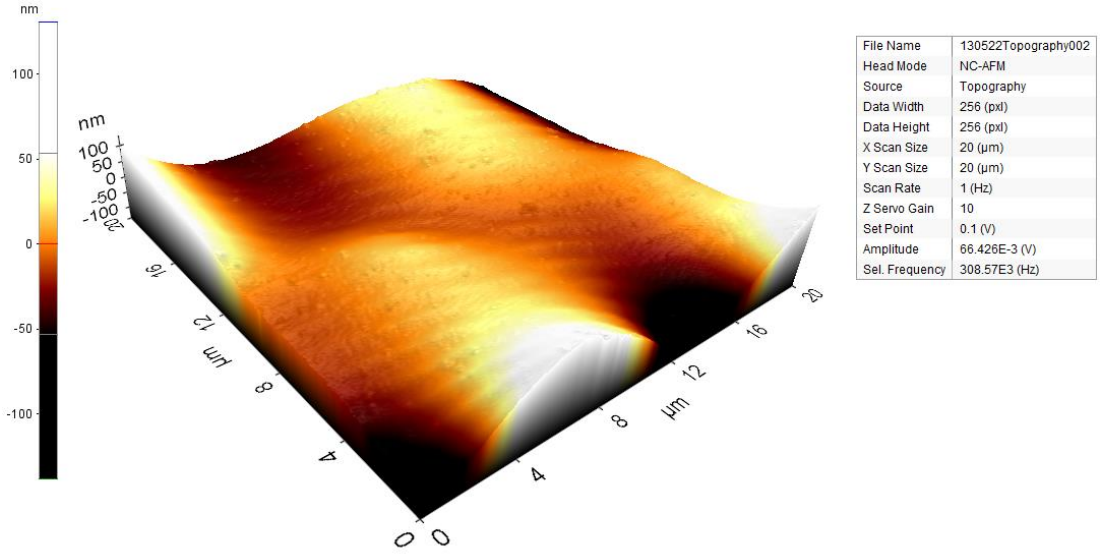

Figure A3.18. Representative topographic image of **SIBS1-9** prior to release. Note minor peaks (relative to surface undulations) due to PTX aggregates.

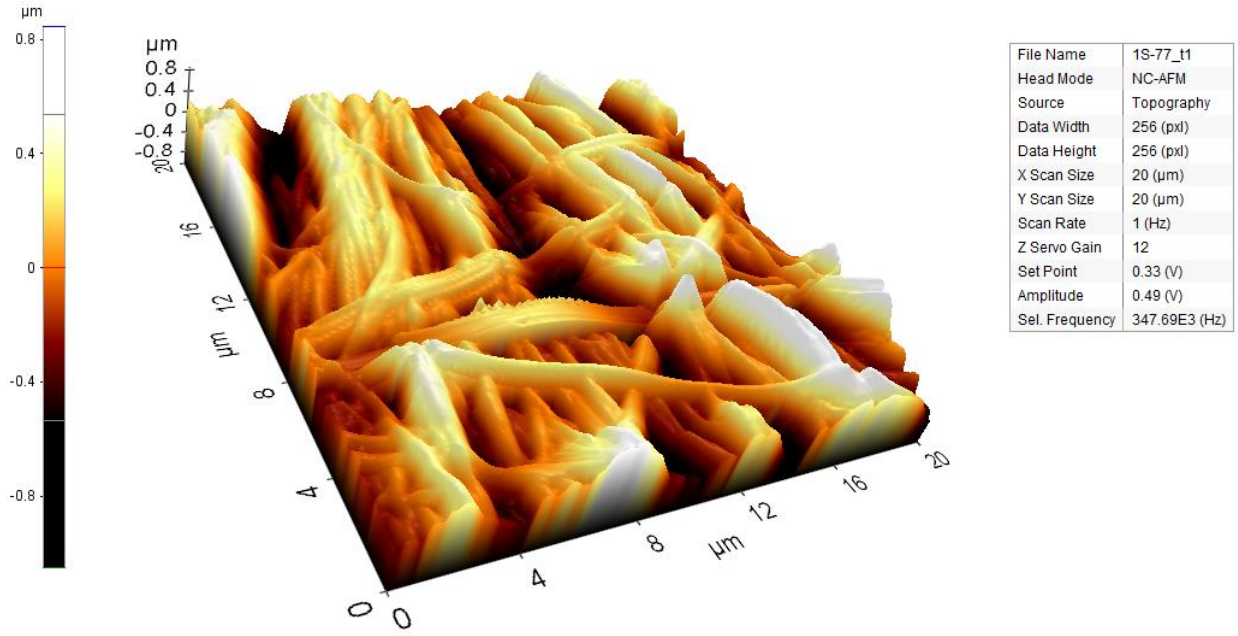

Figure A3.19. Representative topographic image of **PIBa-phy** after release. Note the large increase in surface roughness, appearance of distinctive ridges after release.

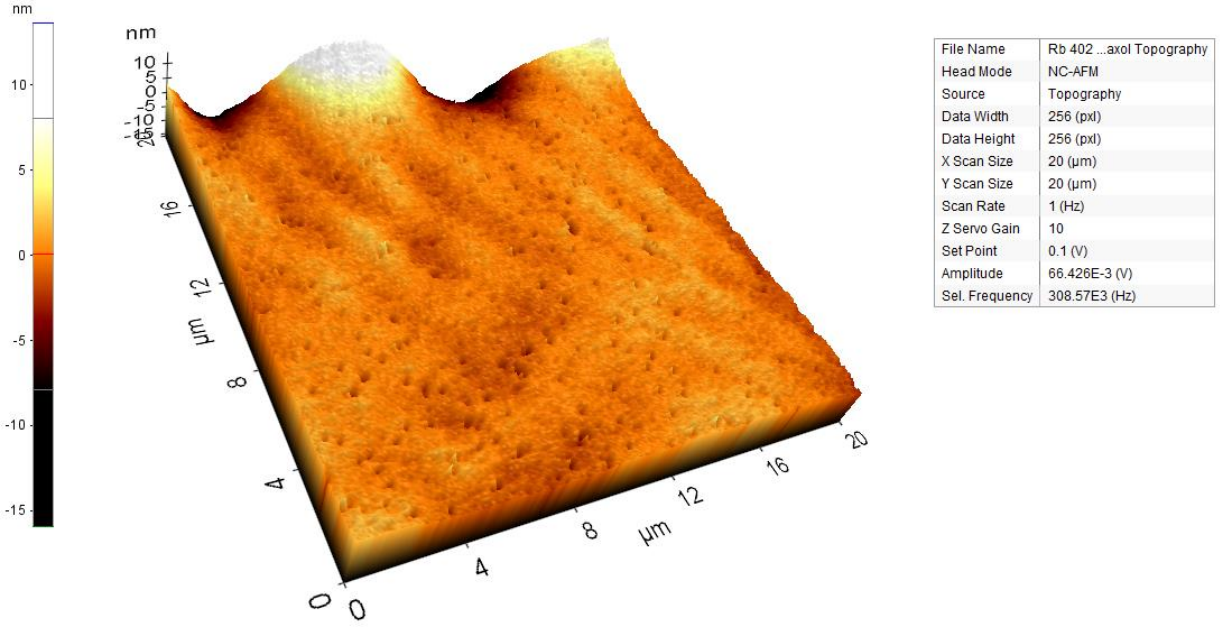

Figure A3.20. Alternative topographic image of **PIBa-phy** after release. Note the holes in the surface left after release.

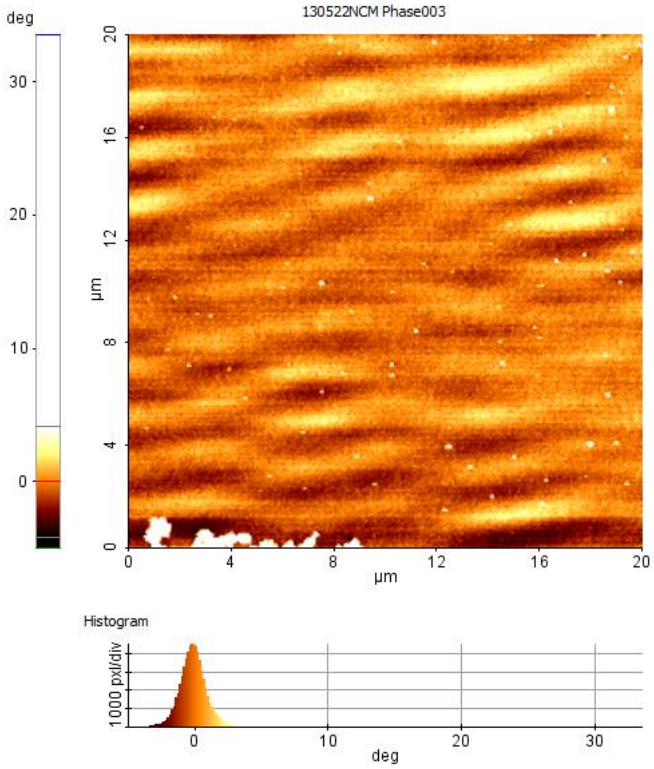

File Name	130522NCM Phase003
Head Mode	NC-AFM
Source	NCM Phase
Data Width	256 (pxl)
Data Height	256 (pxl)
X Scan Size	20 (µm)
Y Scan Size	20 (µm)
Scan Rate	1 (Hz)
Z Servo Gain	15
Set Point	69E-3 (V)
Amplitude	66.426E-3 (V)
Sel. Frequency	308.57E3 (Hz)

Figure A3.21. Representative phase image of **PIBa-cov** prior to release. Note minor "peaks" due to instrument noise at the bottom of the image.

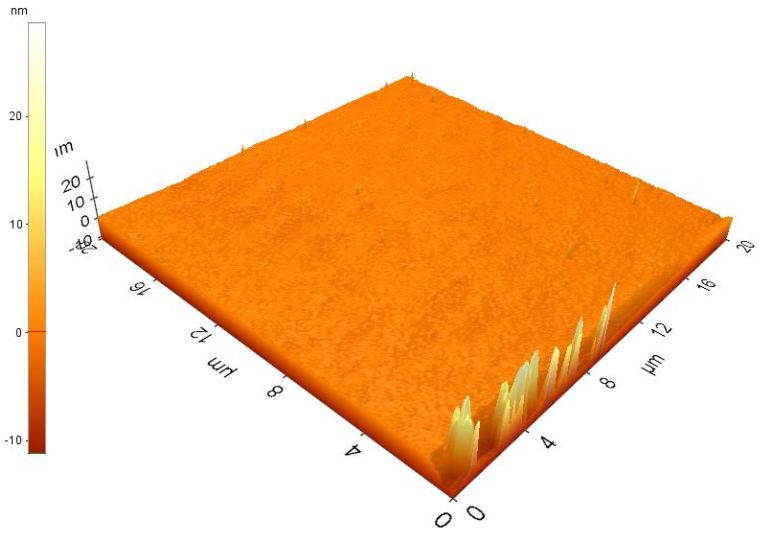

File Name	130522Topography003
Head Mode	NC-AFM
Source	Topography
Data Width	256 (pxl)
Data Height	256 (pxl)
X Scan Size	20 (µm)
Y Scan Size	20 (µm)
Scan Rate	1 (Hz)
Z Servo Gain	15
Set Point	69E-3 (V)
Amplitude	66.426E-3 (V)
Sel. Frequency	308.57E3 (Hz)

Figure A3.22. Representative topographic image of **PIBa-cov** prior to release. Note minor "peaks" due to instrument noise at the bottom of the image.

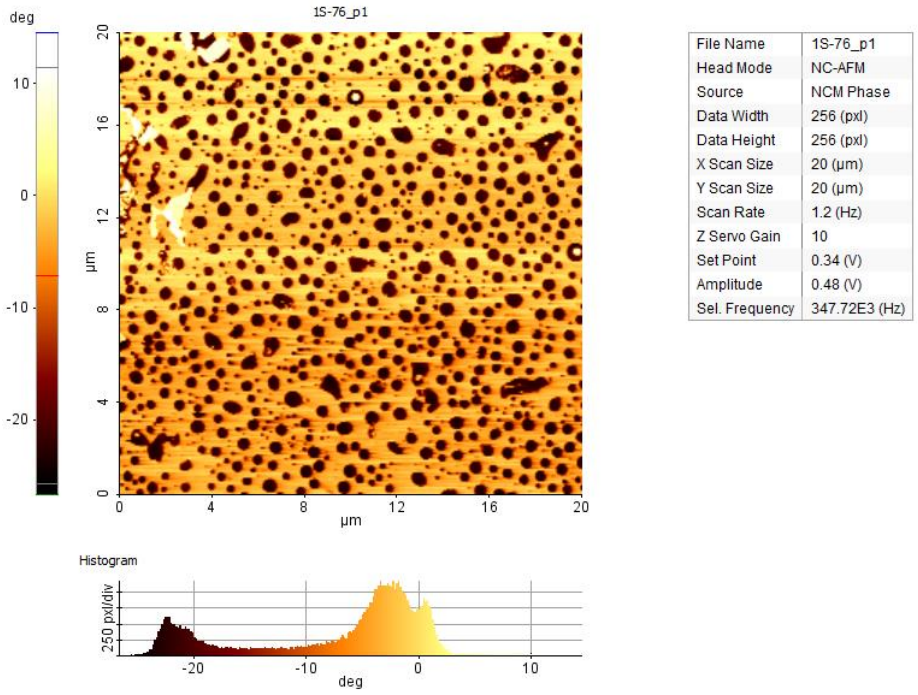

Figure A3.23. Representative phase image of **PIBa-cov** after release. Note the "negative" phase of the surface deposits (relative to the "positive" phase observed from PTX in all other samples) indicating they are perhaps salts that failed to wash off despite repeated washes with deionized water.

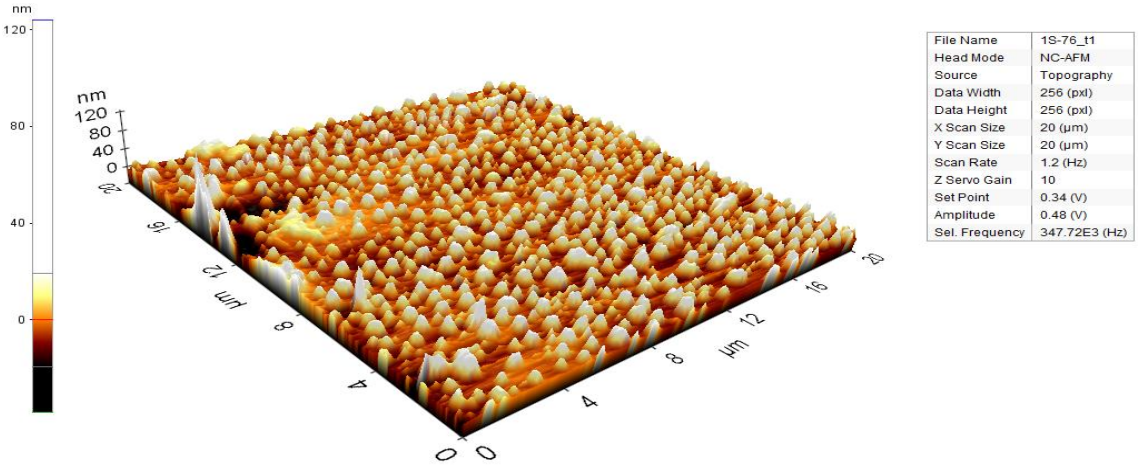

Figure A3.24. Typical topographic image of **PIBa-cov** after release. Note the peaks (potentially salt deposits). The salts could not be removed from the surface despite extensive washing with deionized water.

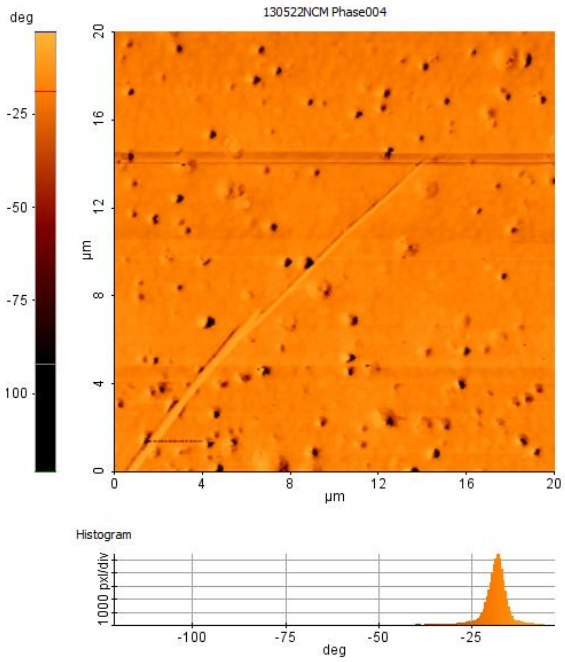

File Name	130522NCM Phase004
Head Mode	NC-AFM
Source	NCM Phase
Data Width	256 (pxl)
Data Height	256 (pxl)
X Scan Size	20 (µm)
Y Scan Size	20 (µm)
Scan Rate	1 (Hz)
Z Servo Gain	12
Set Point	0.1 (V)
Amplitude	0.14 (V)
Sel. Frequency	307.33E3 (Hz)

Figure A3.25. Representative phase image of **SIBS2-24** after release. The negative phase corresponds to the physical holes observed in the topographic image (manuscript, **Figure 3C**).

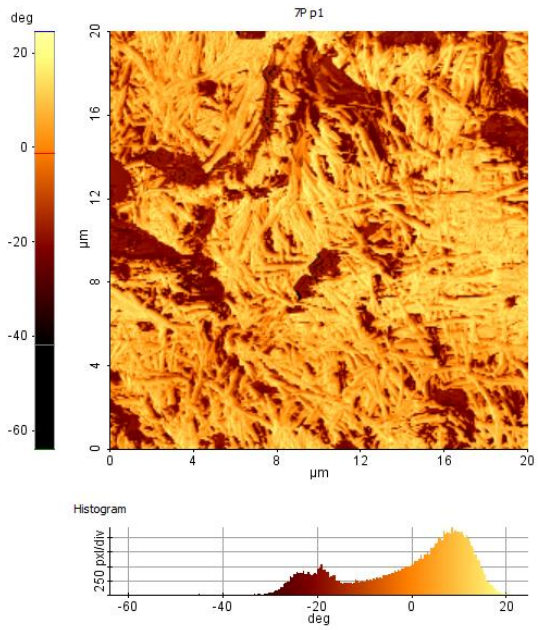

File Name	7P p1
Head Mode	NC-AFM
Source	NCM Phase
Data Width	256 (pxl)
Data Height	256 (pxl)
X Scan Size	20 (µm)
Y Scan Size	20 (µm)
Scan Rate	0.75 (Hz)
Z Servo Gain	20
Set Point	0.35 (V)
Amplitude	0.5 (V)
Sel. Frequency	335.81E3 (Hz)

Figure A3.26. Representative phase image of **PIBb-phy** after release. The large differences in vertical height observed on the topographic image are represented by the large apparent difference in phase (manuscript, **Figure 3F**).

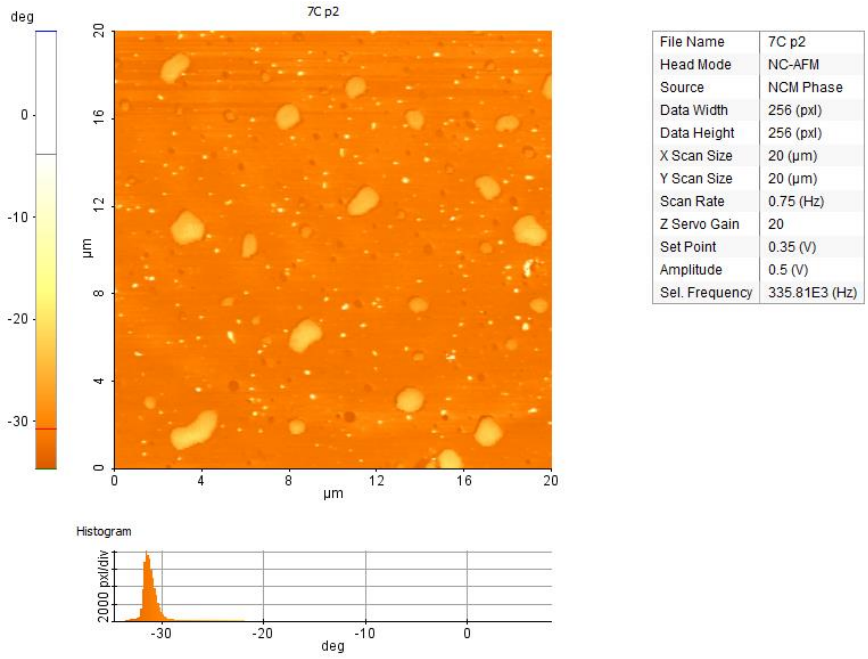

File Name	7C p2
Head Mode	NC-AFM
Source	NCM Phase
Data Width	256 (pxl)
Data Height	256 (pxl)
X Scan Size	20 (µm)
Y Scan Size	20 (µm)
Scan Rate	0.75 (Hz)
Z Servo Gain	20
Set Point	0.35 (V)
Amplitude	0.5 (V)
Sel. Frequency	335.81E3 (Hz)

Figure A3.27. Representative phase image of **PIBb-cov** after release. The white spots correspond to the irremovable salt deposits observed for the corresponding topographic image (manuscript, **Figure 3I**).

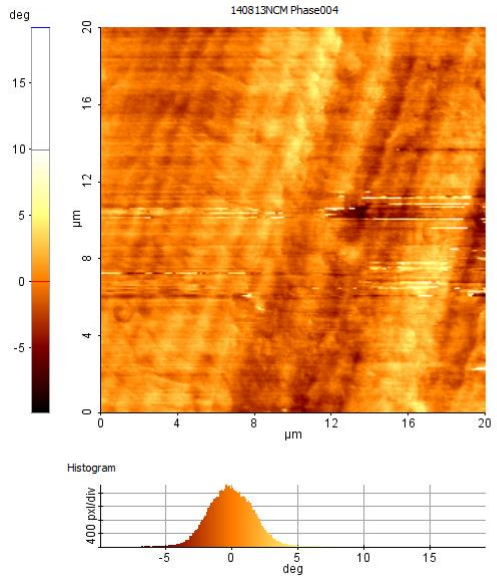

File Name	140813NCM Phase004
Head Mode	NC-AFM
Source	NCM Phase
Data Width	256 (pxl)
Data Height	256 (pxl)
X Scan Size	20 (µm)
Y Scan Size	20 (µm)
Scan Rate	0.5 (Hz)
Z Servo Gain	20
Set Point	0.35 (V)
Amplitude	0.78 (V)
Sel. Frequency	337.62E3 (Hz)

Figure A3.28. Representative phase image of stainless steel substrate.

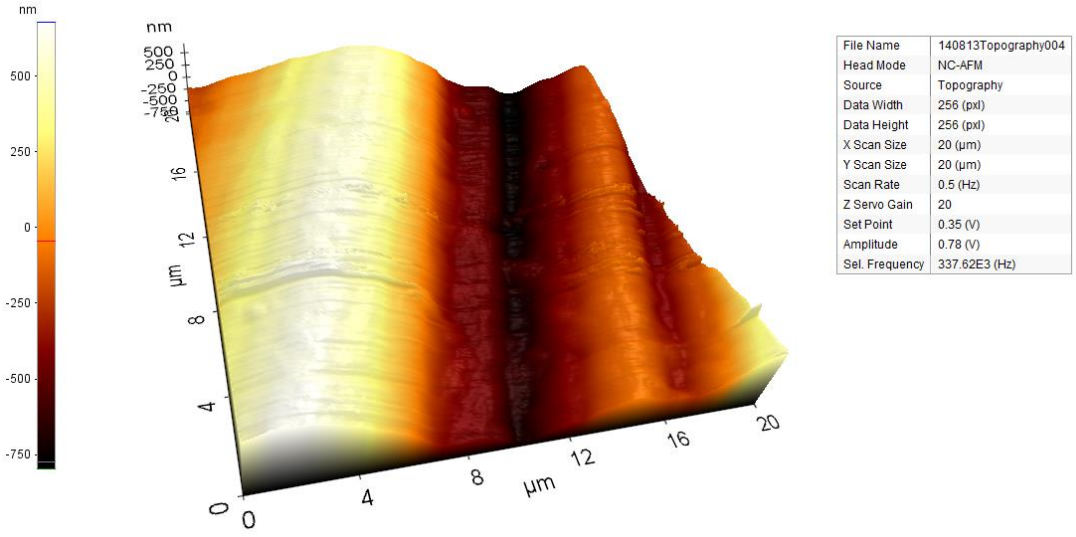

Figure A3.29. Representative topographic image of stainless steel substrate.

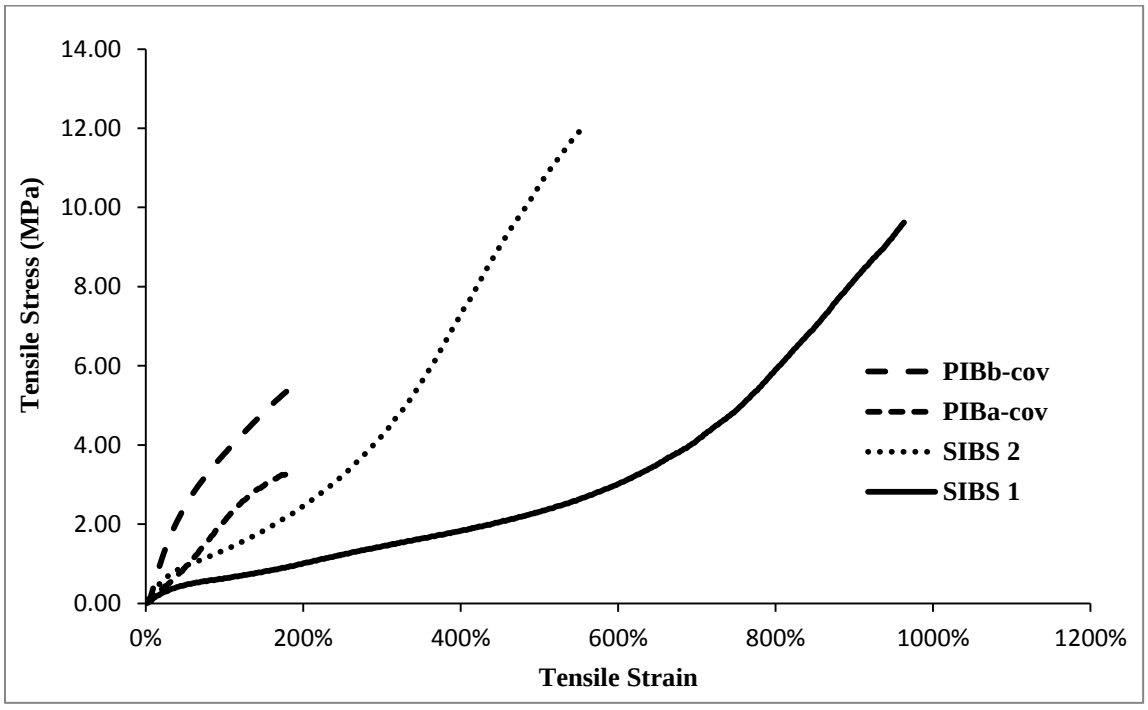

Figure A3.28. Representative tensile-behavior profiles of the examined rubbers.

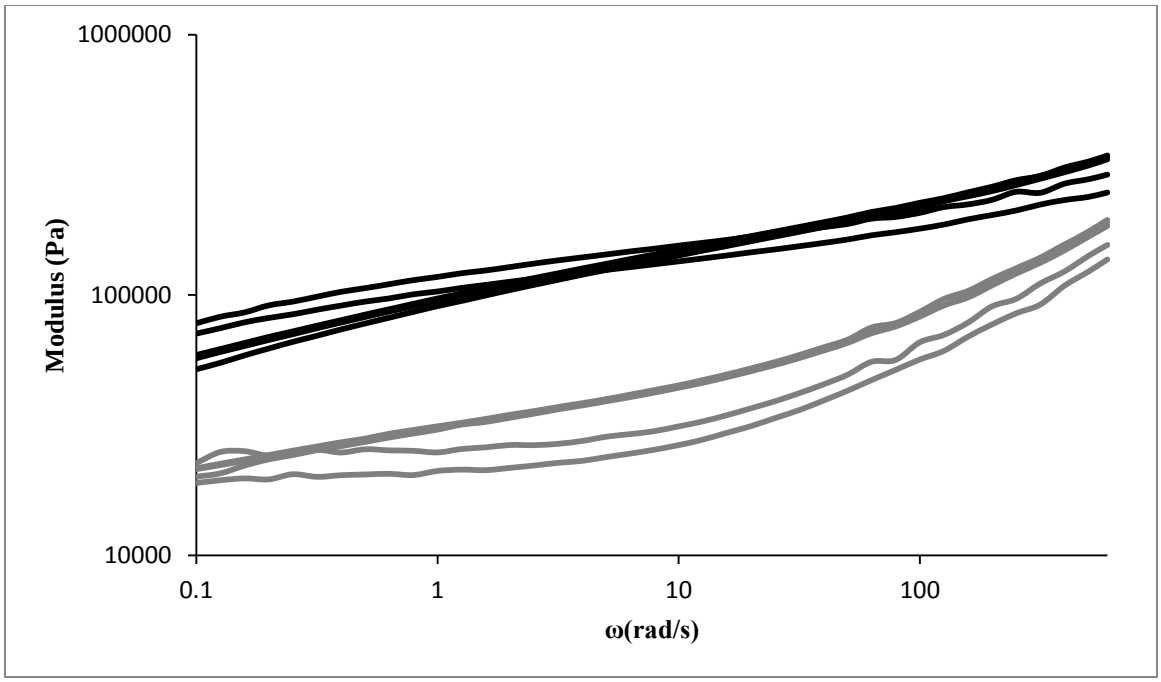

Figure A3.29. Frequency dependence of the elastic (G', black) and viscous (G", grey) moduli for **PIBb-cov.**

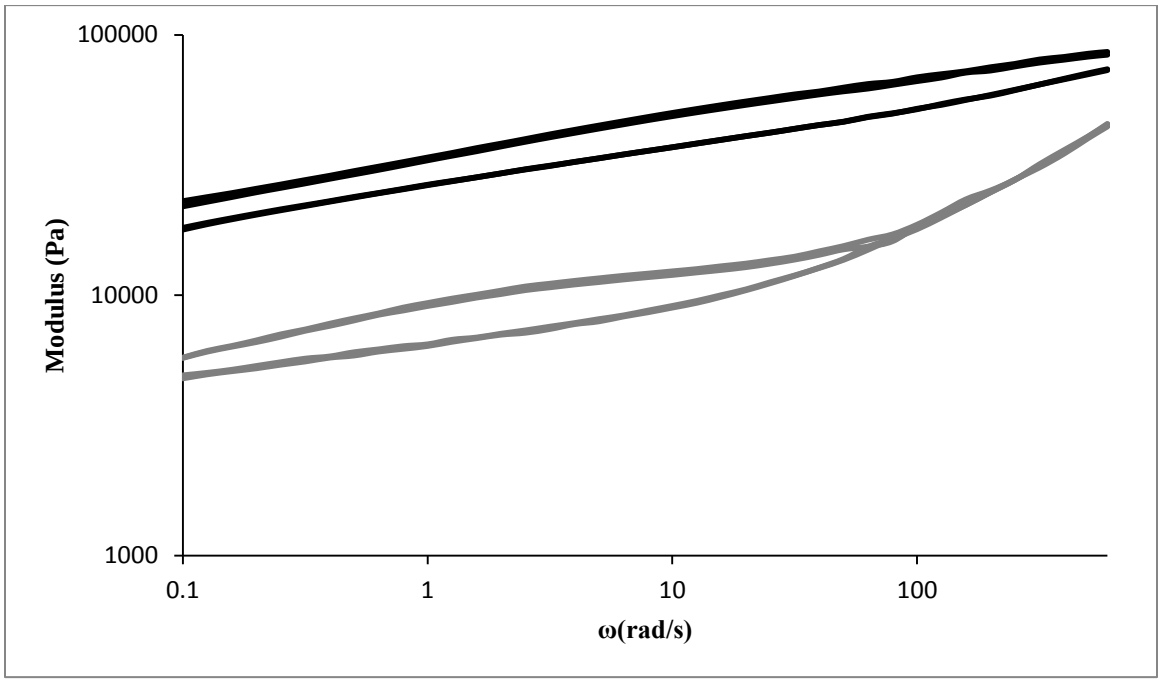

Figure A3.30. Frequency dependence of the elastic (G', black) and viscous (G", grey) moduli for **PIBa-cov**.

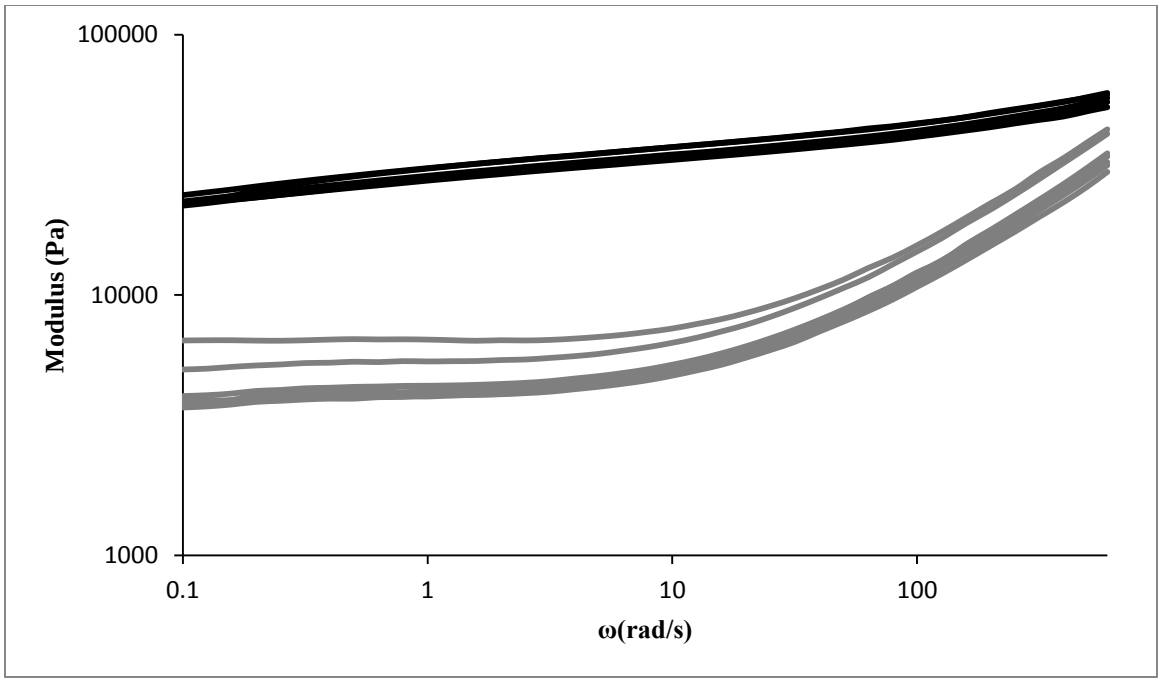

Figure A3.31. Frequency dependence of the elastic (G', black) and viscous (G", grey) moduli for **SIBS1**.

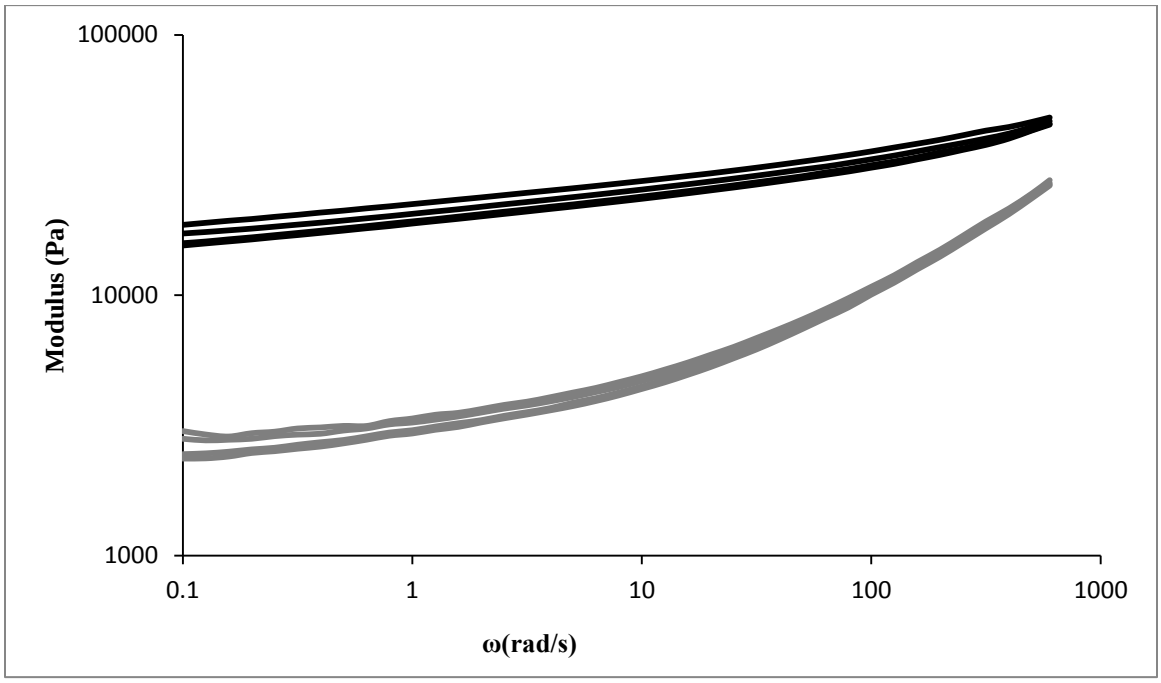

Figure A3.32. Frequency dependence of the elastic (G', black) and viscous (G", grey) moduli for **SIBS2**.

Appendix 3: Supporting Information for Chapter 4

- ^{1}H NMR spectra of copolymers **1**, **2**, **3**, **4** and **5**.
- SEC Traces of copolymers **1**, **2**, **3**, **4** and **5**.
- Additional AFM images for surfaces
- Thermal analysis of **1**, **2**, **3**, **4** and **5**.
- Rheological data for of copolymers **1**, **2**, **3**, **4** and **5**.

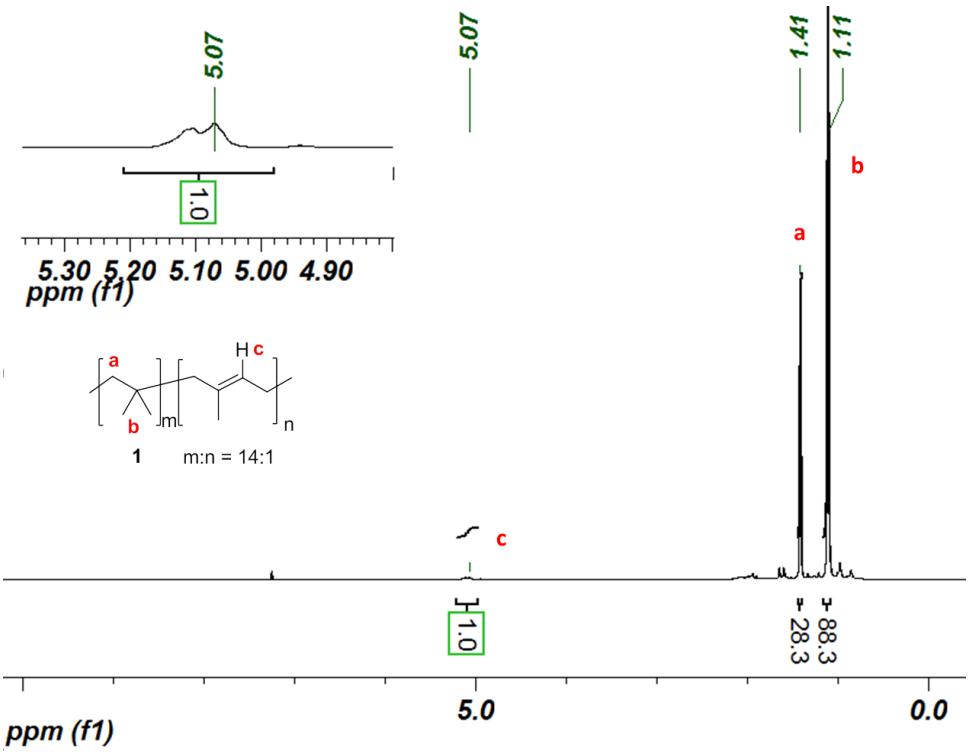

Figure A4.1. ^{1}H NMR spectrum of arb-PIB-*co*-IP **1** ($CHCl_3$, 600 MHz).

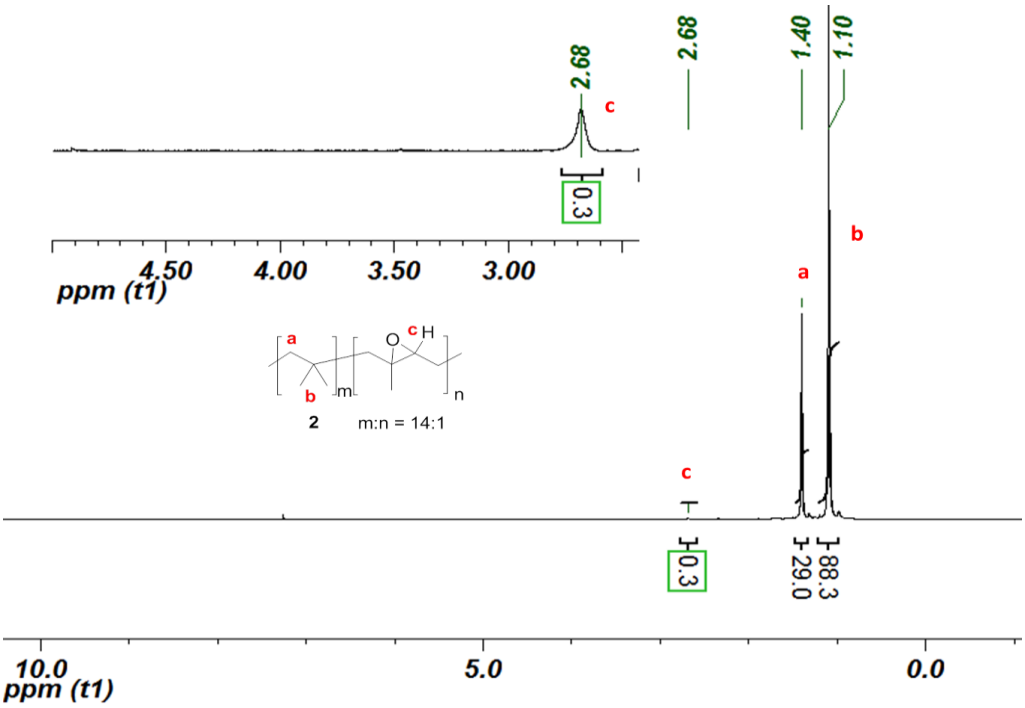

Figure A4.2. ^{1}H NMR spectrum of polymer **2** ($CHCl_3$, 600 MHz).

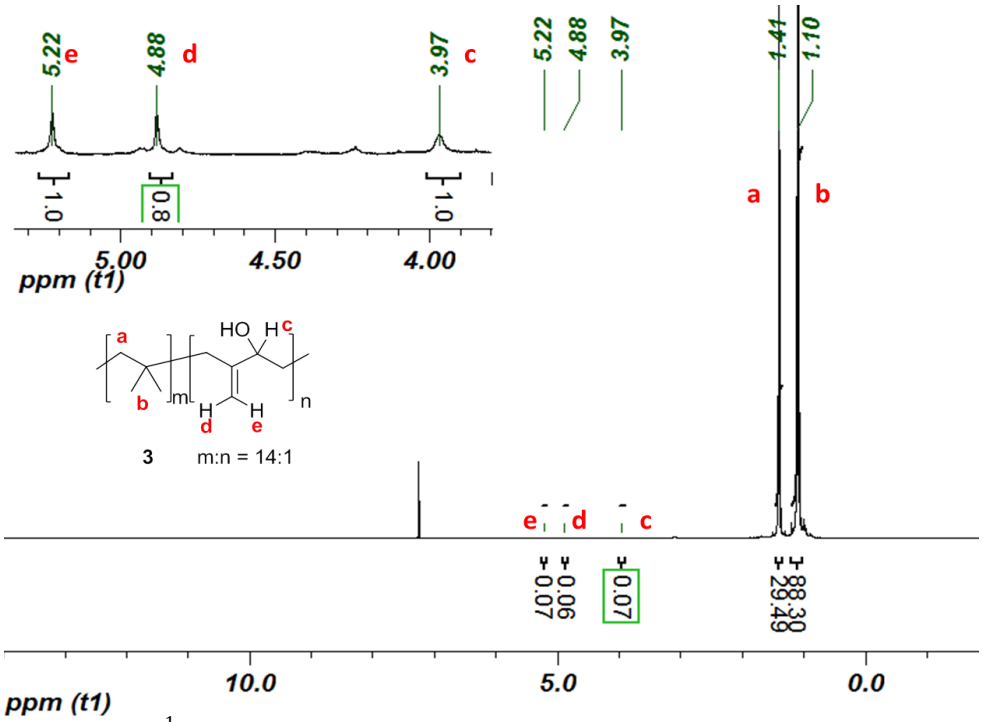

Figure A4.3. ^{1}H NMR spectrum of polymer **3** ($CHCl_3$, 600 MHz).

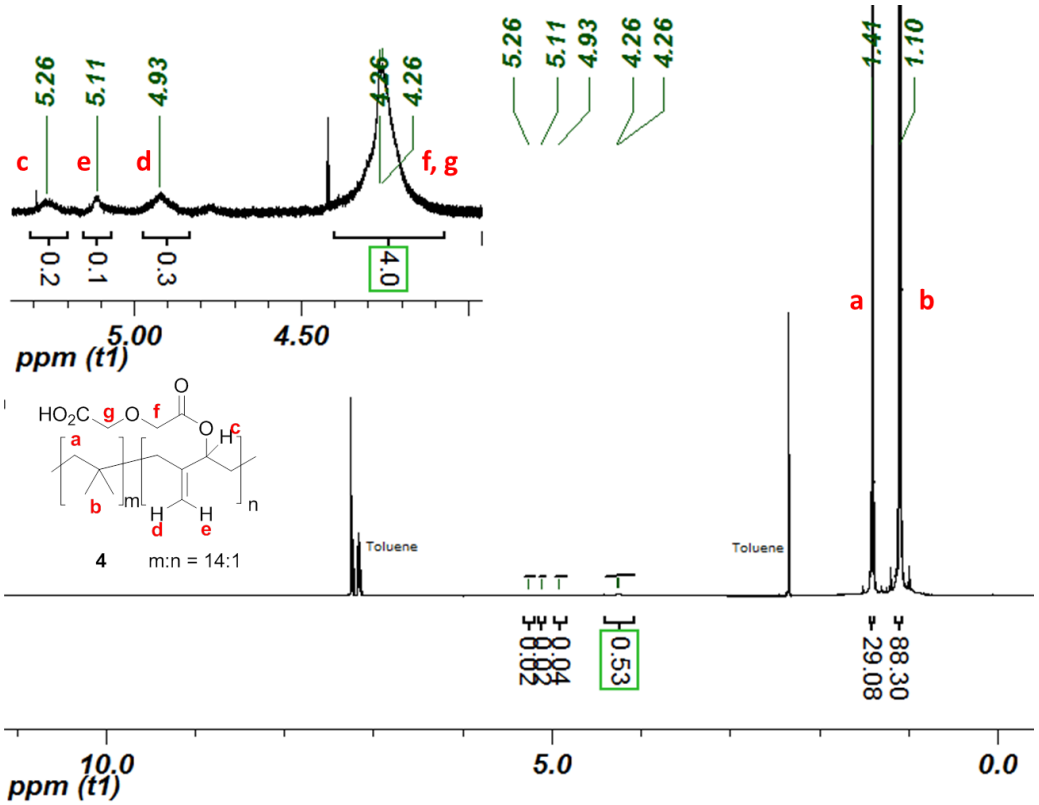

Figure A4.4. ^{1}H NMR spectrum of polymer **4** ($CHCl_3$, 600 MHz (d1 = 10 s)).

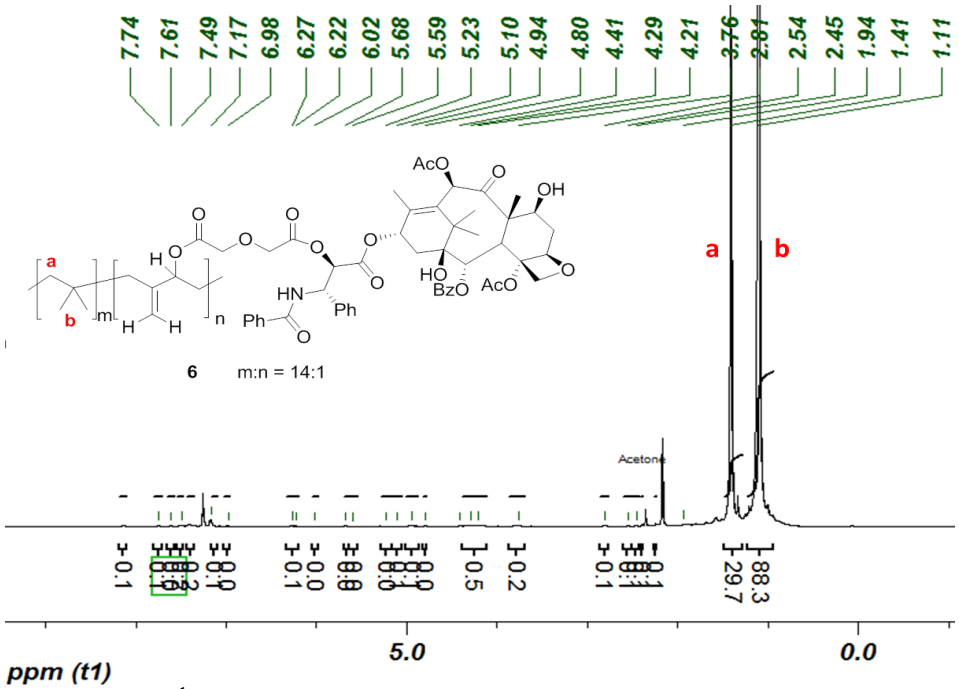

Figure A4.5. ^{1}H NMR spectrum of polymer **5** ($CHCl_3$, 600 MHz).

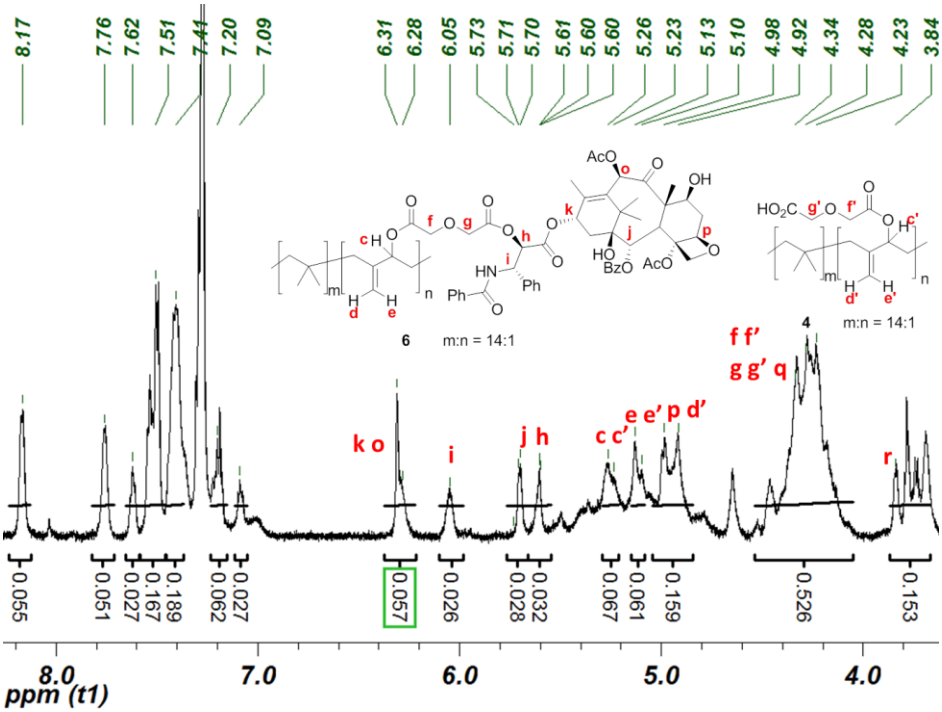

Figure A4.6. Expansion of the ^{1}H NMR spectrum of polymer **5** ($CHCl_3$, 600 MHz). Key resonances are assigned. Ratio of PTX associated peaks to rubber peaks (i.e. c,c' at 5.23 to i or h at 6.02 and 5.59) suggest 50% conversion. PTX and polymer peaks were assigned based on previous linear analogues as well as Deutsch et al.[1,1]

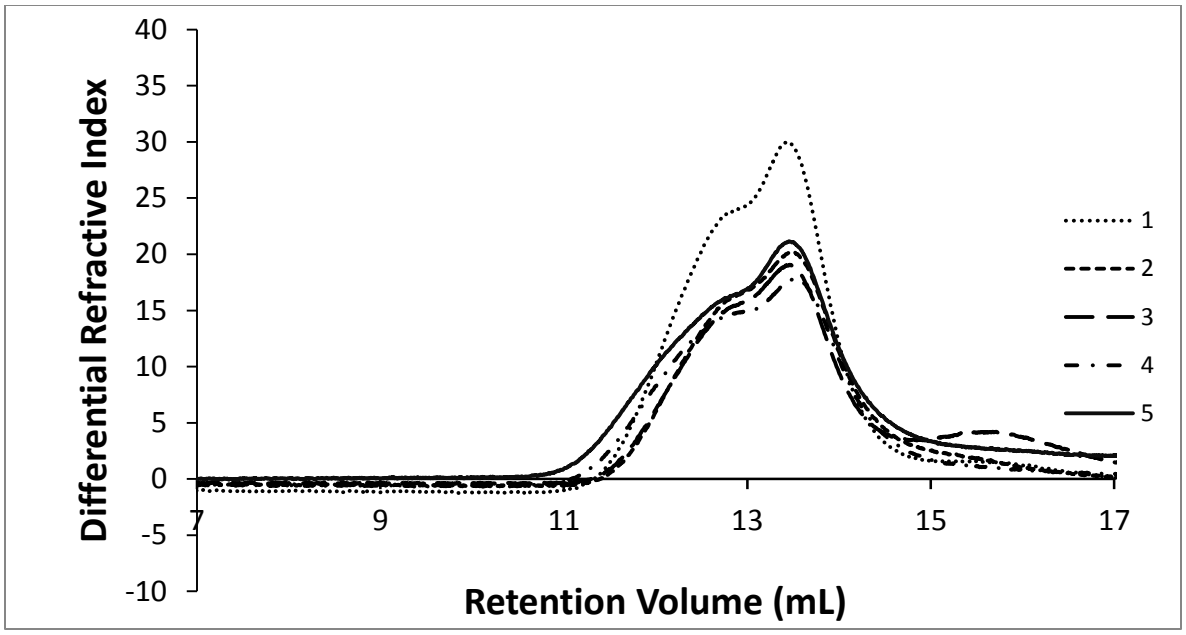

Figure A4.7. SEC traces for polymers **1**-**5** (THF).

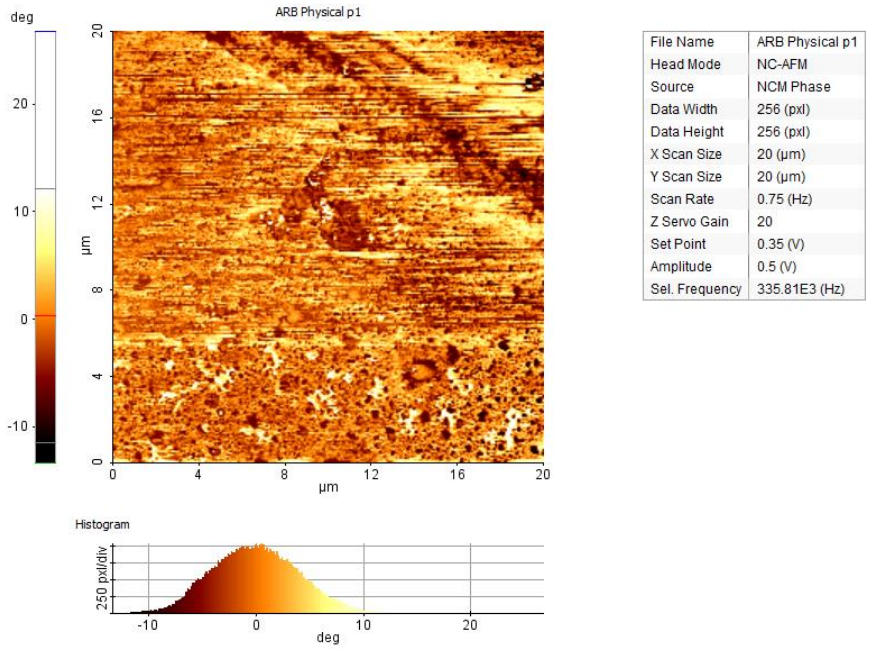

Figure A4.8. Representative AFM phase image of **4 + PTX** after release study.

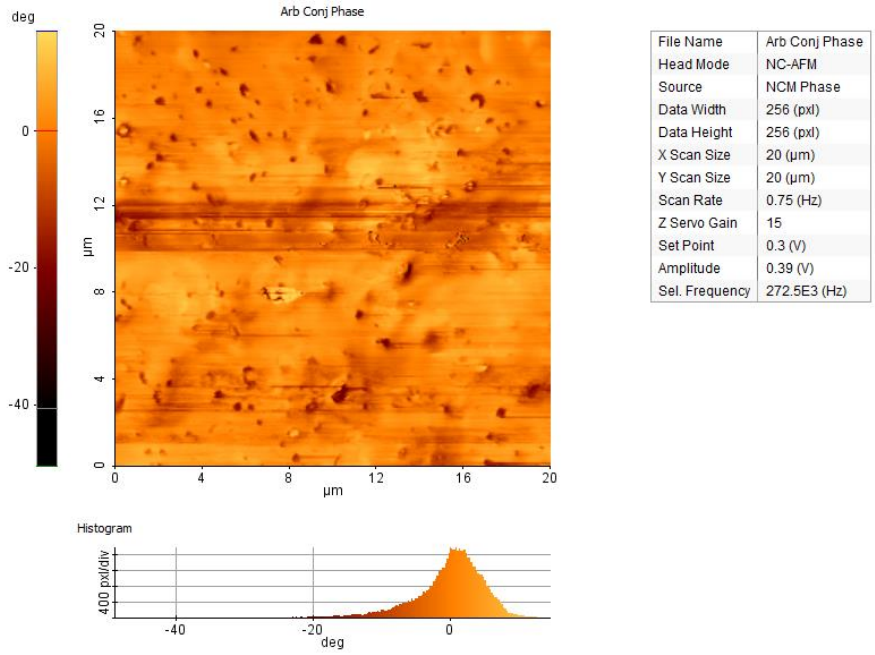

Figure A4.9. Representative AFM phase image of **5** after the release study. Differences in phase correspond to stark differences in topography.

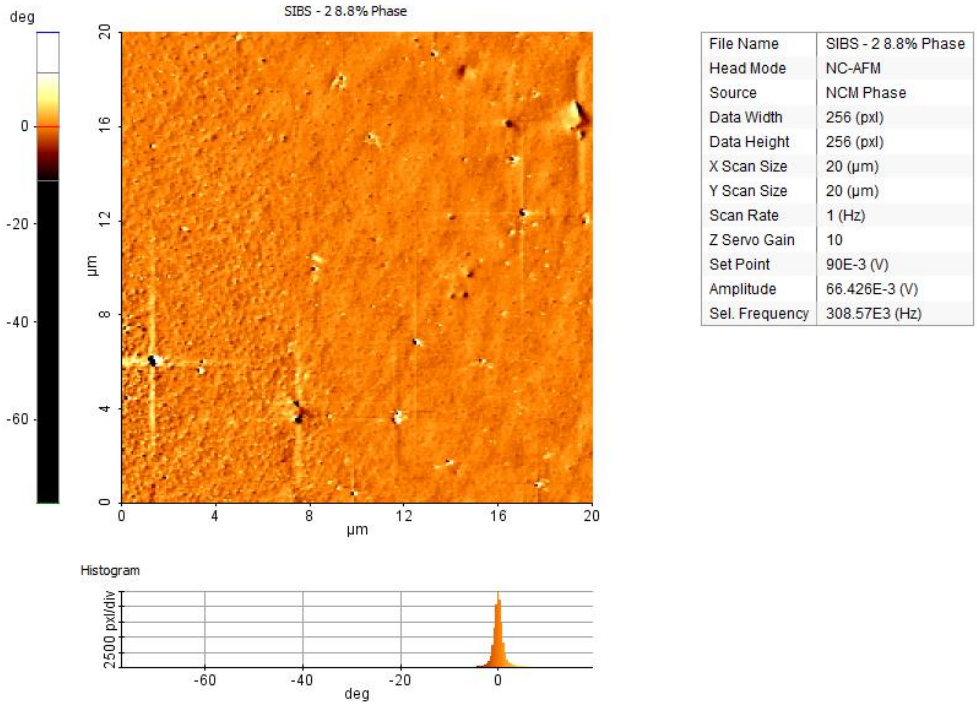

Figure A4.10. Representative phase image of **SIBS + PTX** after release (Reproduced from reference [2]).

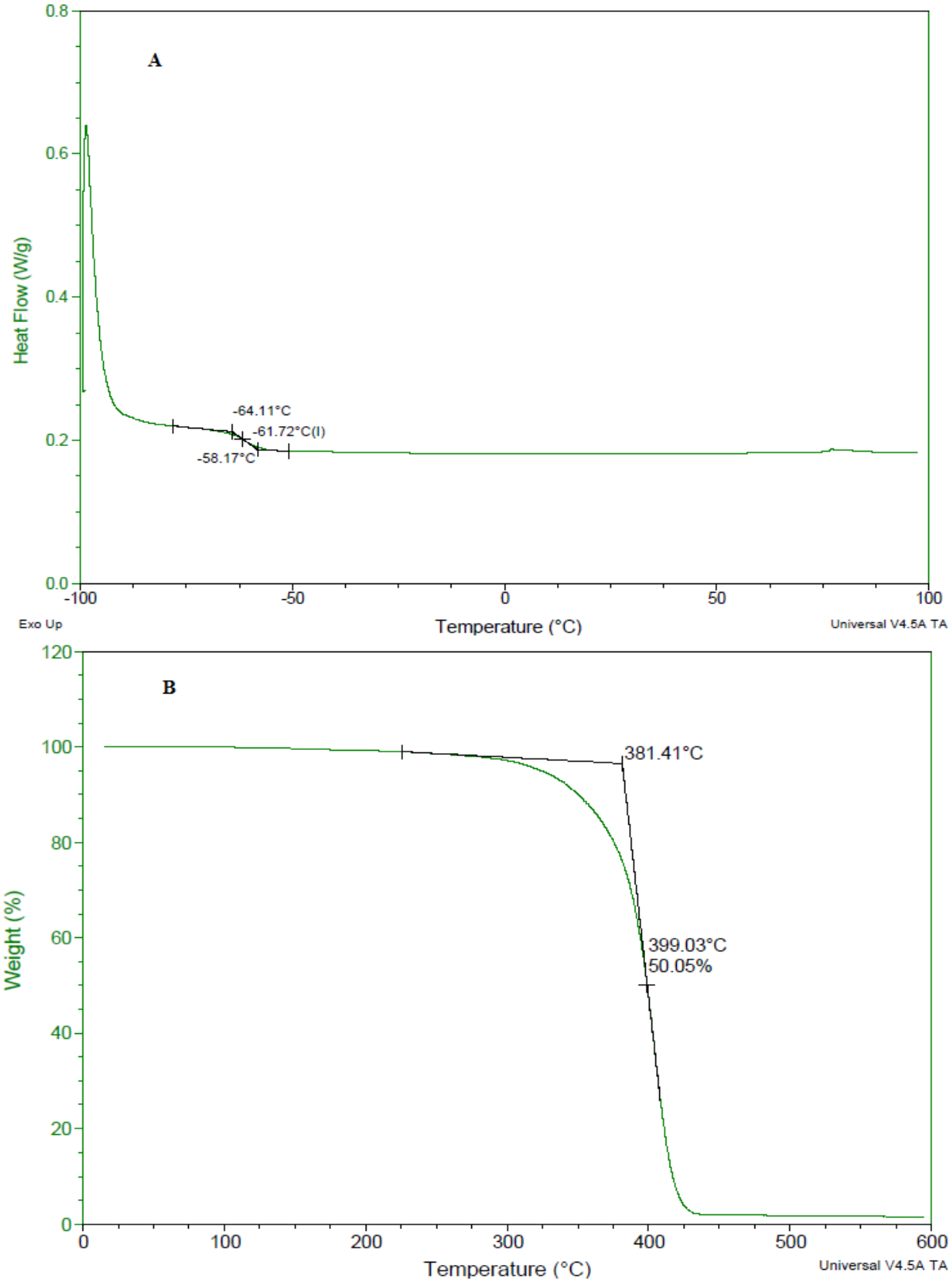

Figure A4.11. Thermal analysis data for polymer **1:** A) DSC, B) TGA.

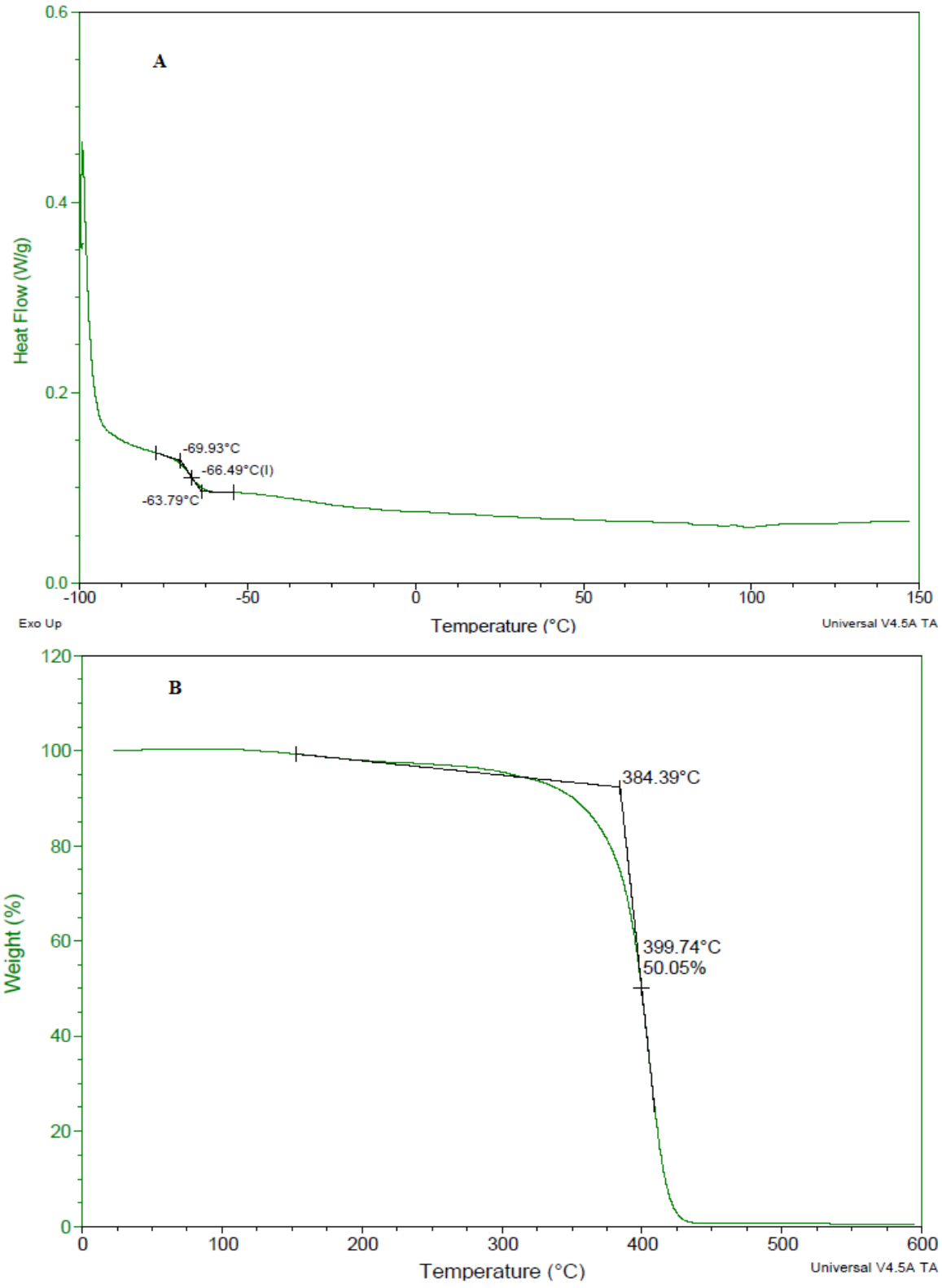

Figure A4.12. Thermal analysis data for polymer **2**: A) DSC, B) TGA.

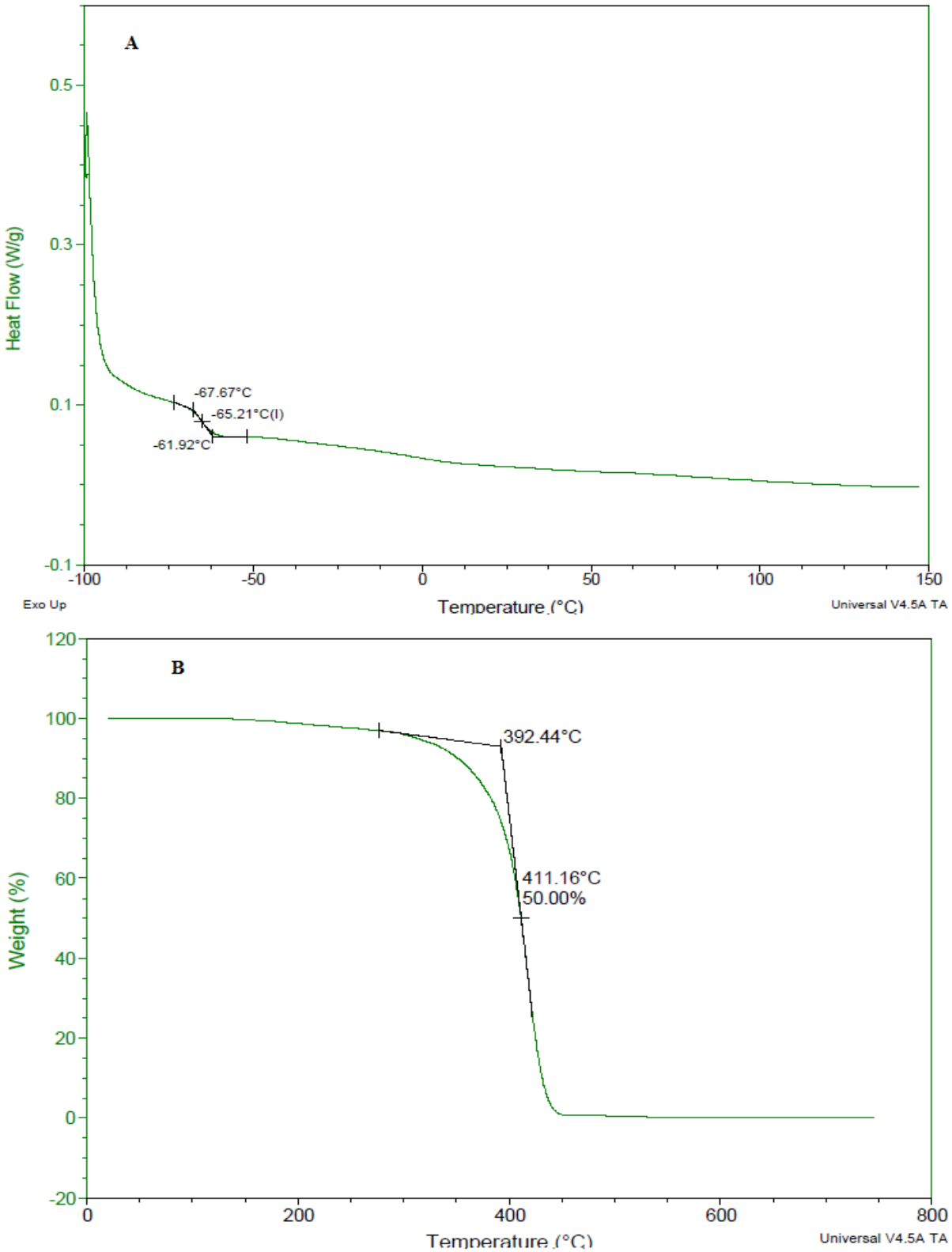

Figure A4.13. Thermal analysis data for polymer **3**: A) DSC, B) TGA.

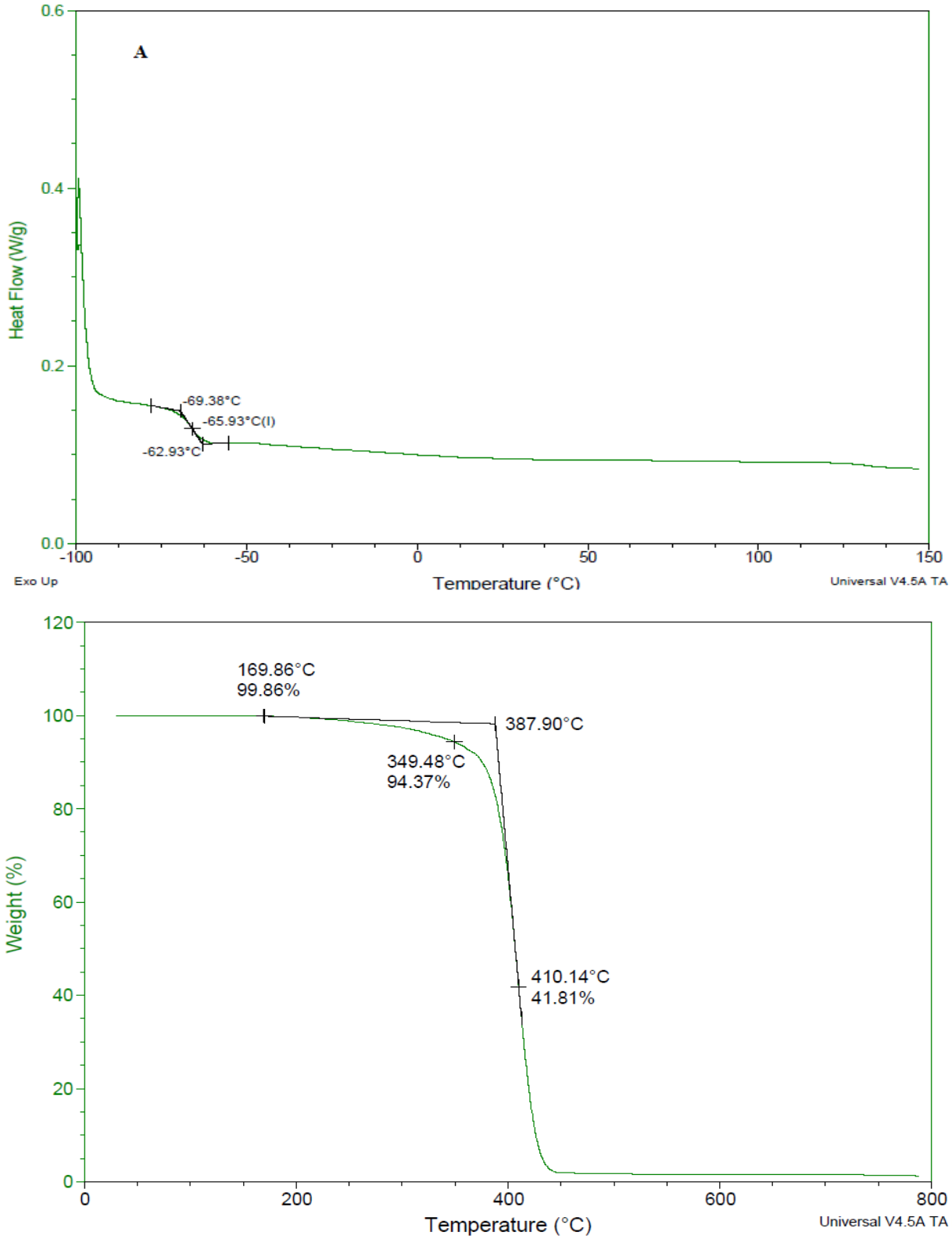

Figure A4.14. Thermal analysis data for polymer **4**: A) DSC, B) TGA.

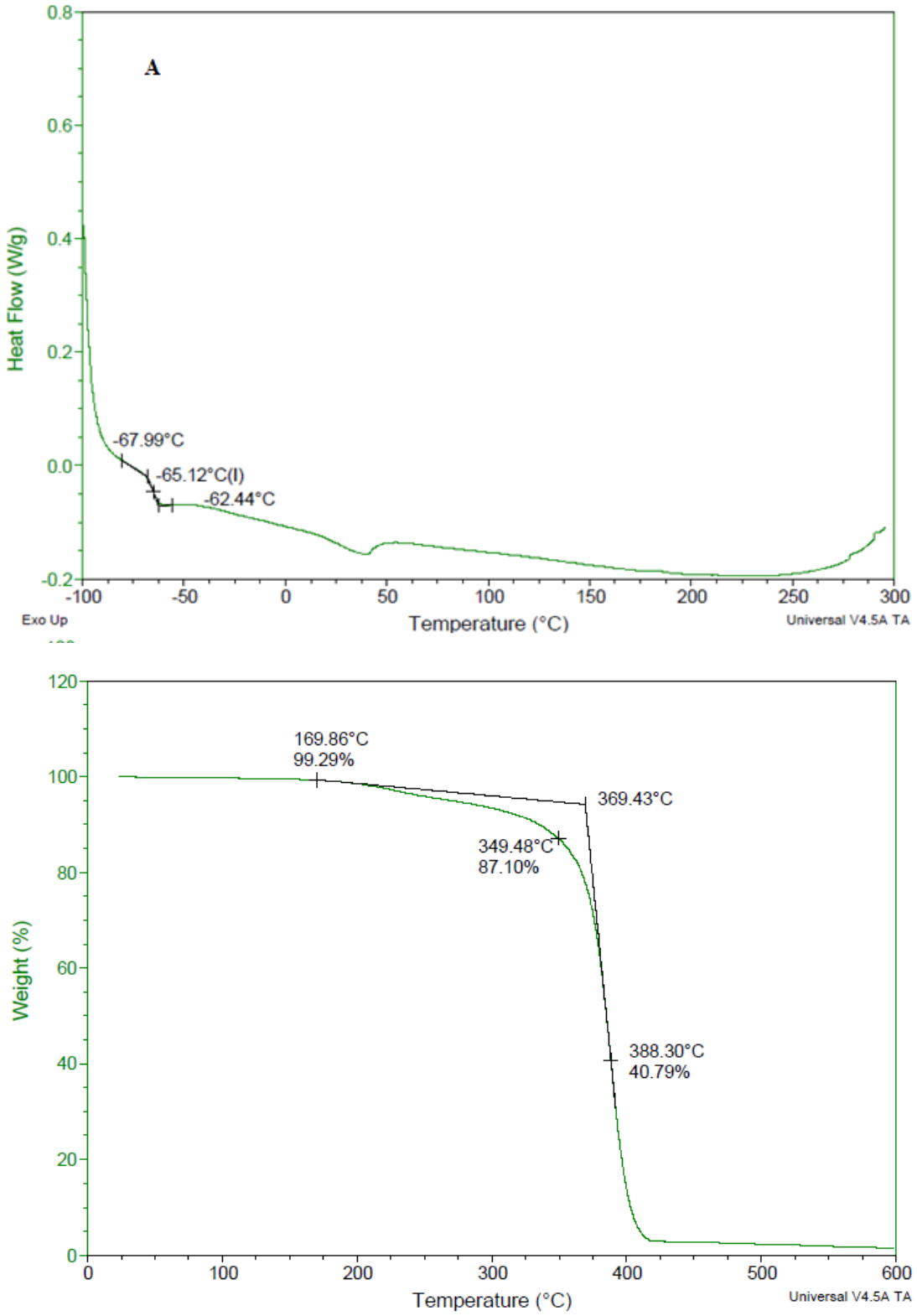

Figure A4.15. Thermal analysis data for polymer **5**: A) DSC, B) TGA.

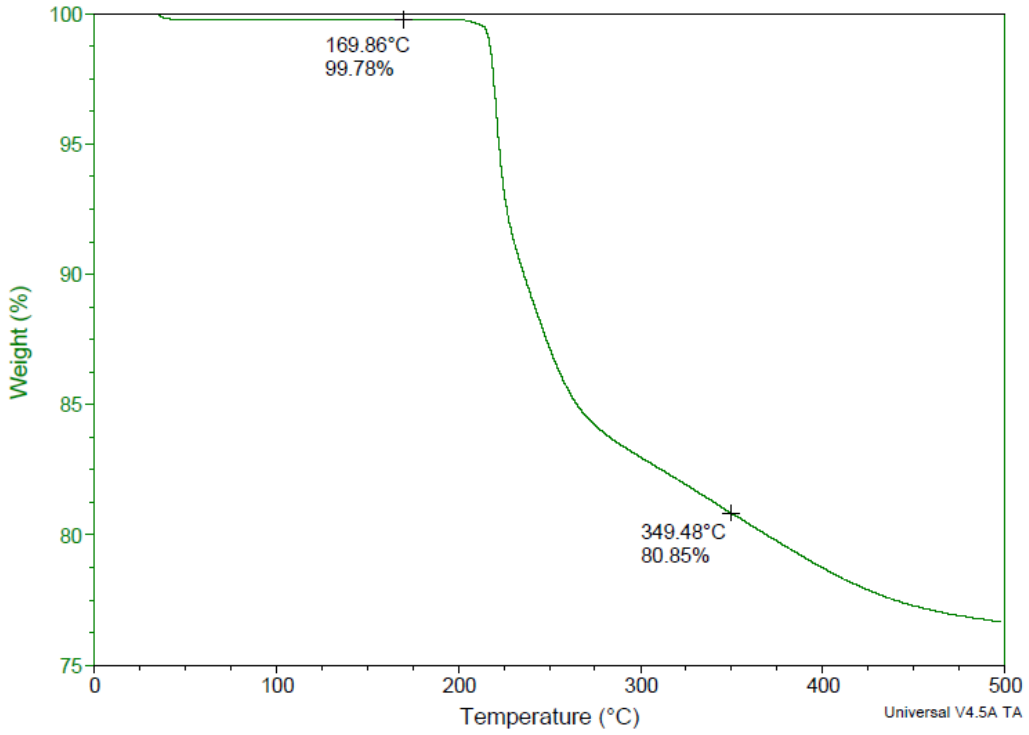

Figure A4.16. TGA of Paclitaxel.

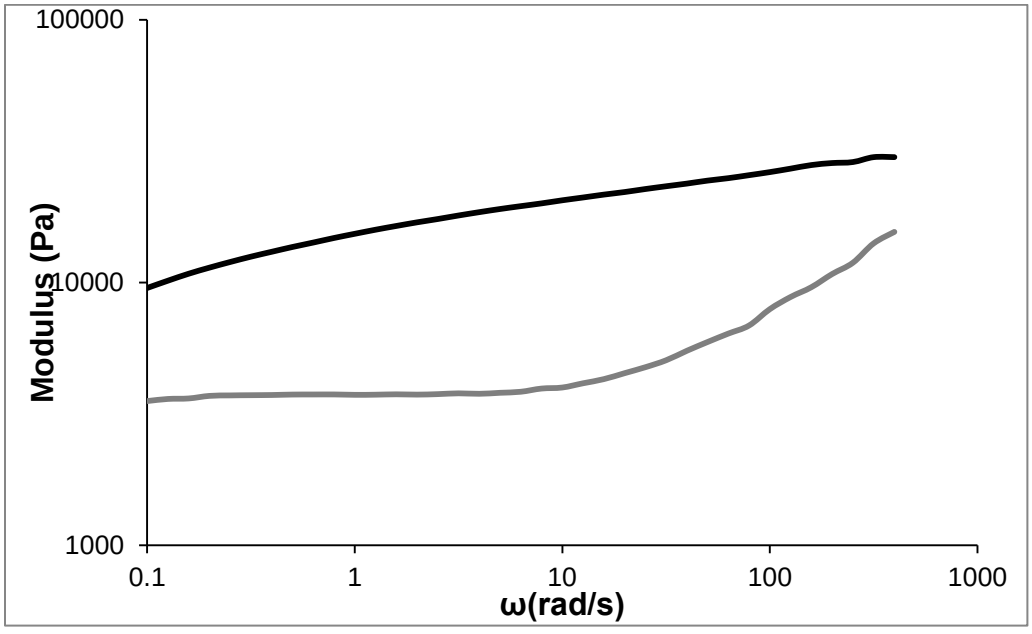

Figure A4.17. Frequency dependence of the elastic (G', black) and viscous (G", grey) moduli for polymer **2** (representative trace shown).

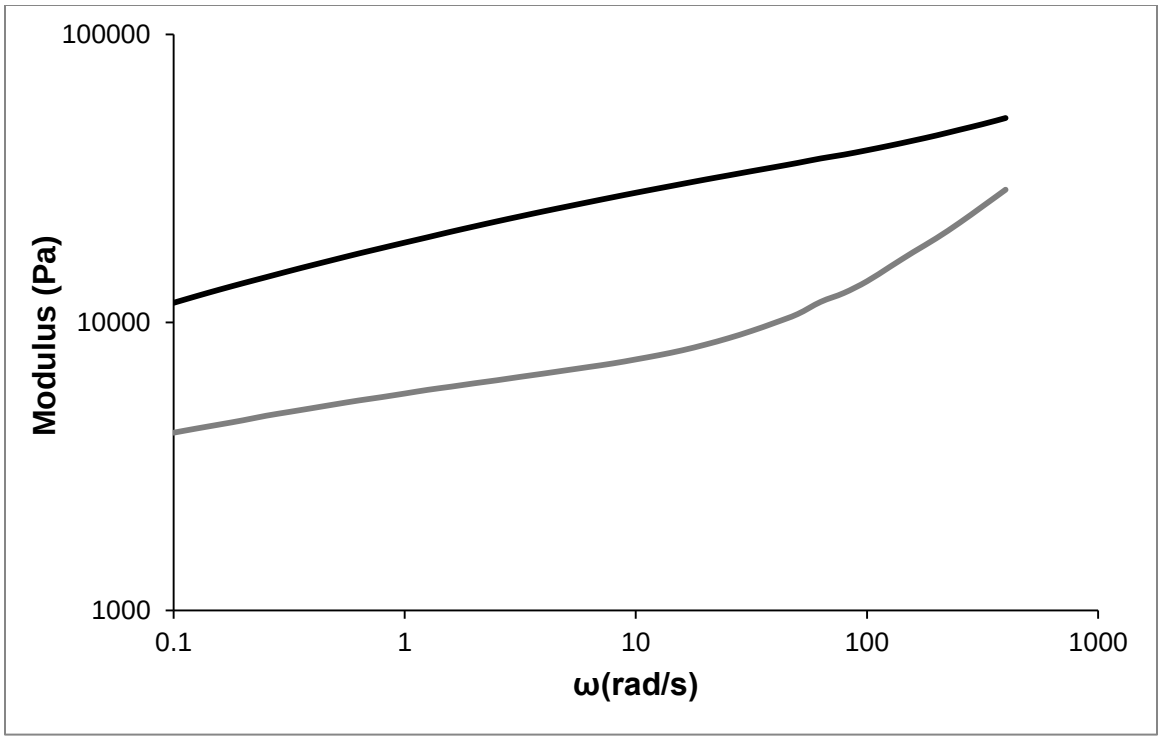

Figure A4.18. Frequency dependence of the elastic (G', black) and viscous (G", grey) moduli for **3** (representative trace shown).

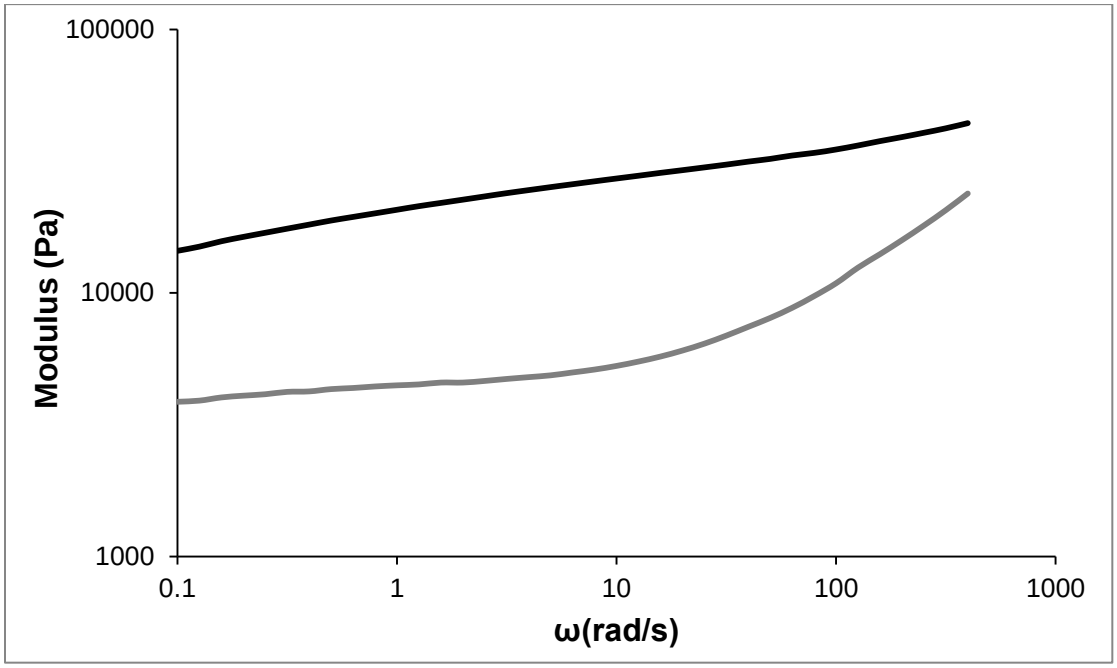

Figure A4.19. Frequency dependence of the elastic (G', black) and viscous (G", grey) moduli for **4** (representative trace shown).

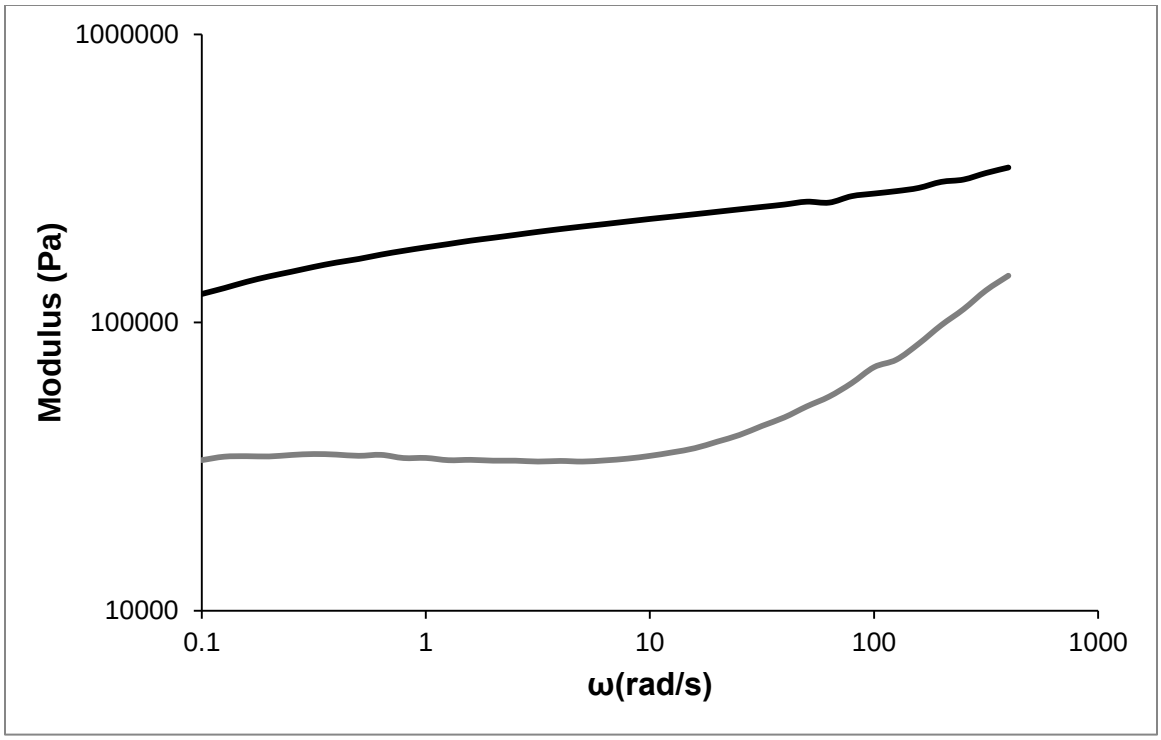

Figure A4.20. Frequency dependence of the elastic (G', black) and viscous (G", grey) moduli for **5** (representative trace shown).

Curriculum Vitae

Name: Inderpreet Sran

EDUCATION

09/2012 – 08/2014, University of Western Ontario, London, Ontario, Canada, Master of Engineering Science, Chemical and Biochemical Engineering Graduate Program

01/2009 – 04/2012, Laurentian University, Sudbury, Ontario, Canada, Bachelor of Engineering in Chemical Engineering

TEACHING EXPERIENCE

Teaching Assistant – to Dr. Lars Rehmann in "Computational Methods for Engineers" Jan – Apr 2013

Teaching Assistant – to Dr. Anand Prakash in "Staged Operations" Sept – Dec 2013

PUBLICATIONS and PATENTS

McEachran, M., Trant, J. F., **Sran, I.**, Bruyn, J.R., Gillies, E. R. Carboxylic acid functionalized butyl rubber: synthesis, characterization and physical properties. submitted to LANXESS Inc. for their approval to publish, Nov. 1, 2013

Trant, J. F., **Sran, I.**, McEachran, M., Bruyn, J.R., Turowec, B., and Gillies, E. R. Covalent polyisobutylene-paclitaxel conjugates as potential vascular stent coatings with controlled drug release submitted to LANXESS Inc. for their approval to publish, May 12, 2014.

Trant, J. F., **Sran, I.**, Bruyn, J.R., Ingratta, M., Borecki, A., and Gillies, E. R. Synthesis and properties of covalent paclitaxel-arborescent polyisobutylene conjugates, submitted to LANXESS Inc. for their approval to publish, May 12, 2014